Involvement of *N*^{1}-Methyladenosine (m^{1}A) in the mitochondrial ND5 mRNA and the corresponding writer enzyme TRMT10C in Alzheimer's disease

Dissertation

to obtain the degree "Doctor of natural sciences (Dr. rer. nat.)"

in Pharmacology and Toxicology

submitted to the Faculty of Chemistry, Pharmaceutical Sciences, Geography and Geosciences of the Johannes Gutenberg University Mainz

by Johanna Eleonore Plehn

born on January 24th, 1993 in Brackenheim

Mainz, June 2023

The present dissertation was composed at the Institute of Pharmaceutical and Biomedical Sciences at the Johannes Gutenberg-University of Mainz under supervision of Prof. Dr. _____ in the time between March, 2018 and June, 2023.

I hereby declare that I wrote this dissertation entitled “Involvement of N^1-Methyladenosine (m^1A) in the mitochondrial ND5 mRNA and the corresponding writer enzyme TRMT10C in Alzheimer’s disease” without any unauthorized external help and that I used only the sources clearly indicated in this work. All text passages that were taken verbatim or paraphrased from publications, websites or other published texts are duly marked and cited. If certain parts of this work were done in collaboration with others, I clearly specified what others did and what I contributed myself.

_____ _____

Place, Date Johanna E. Plehn

“I am among those who think that science has great beauty.” – Marie Curie

Abstract

Involvement of *N*^{1}-Methyladenosine (m^{1}A) in the mitochondrial ND5 mRNA and the corresponding writer enzyme TRMT10C in Alzheimer's disease

Alzheimer's disease (AD) is a progressive neurodegenerative disease and the most common form of dementia. Even though the U.S. Food and Drug Administration (FDA) this year approved a new antibody that may moderately decelerate cognitive decline, there is still no treatment that can halt or even reverse the symptoms of AD. Apart from the prime suspects (amyloid β and phosphorylated tau), growing body of evidence suggests mitochondrial dysfunction to be an early and possibly causative event in AD. For the function of mitochondria, Complex I (Cpx I) is of particular importance, as it represents the primary entry point of the electron transport chain required for cellular ATP generation. Although an impairment of Cpx I has been reported multiple times in AD, the underlying mechanism is so far unlcear. However, in 2017, a *N*^{1}-methyladenosine (m^{1}A) modification site has been discovered at position 1374 in the mRNA of ND5, an essential core subunit of Cpx I. Although this m^{1}A^{1374} site has been unanimously reported, its impact on ND5 protein levels, Cpx I and the mitochondrial respiration is so far unknown. As m^{1}A is known to block Watson-Crick base pairing, this work aimed to investigate whether m^{1}A^{1374} in the mRNA of ND5 could disrupt the mitochondrial translation of ND5, thus leading to a reduced activity of Cpx I in AD. For this purpose, the tRNA methyltransferase 10 homolog C (TRMT10C) was also examined, as it installs m^{1}A^{1374} in the mRNA of ND5 (as a so-called writer enzyme). Strikingly, the protein expression of TRMT10C was consistently increased in AD model cells, mice and frontal cortex samples of human AD patients. As revealed by the evaluation of TRMT10C mRNA in single-cell RNA-Seq data from AD patients, this upregulation was cell type-specific for neurons. Besides, m^{1}A^{1374} methylation was significantly increased in AD model cells, which was determined with a site-specific analysis based on m^{1}A-induced mismatch during reverse transcription and subsequent Illumina sequencing. This result was confirmed in RNA-Seq data generated from the primary visual cortex of AD patients. In line with this, ND5 protein levels were significantly reduced in AD model cells, mice and human AD patients with high Braak stages. The results of this work demonstrate in manifold ways that TRMT10C is involved in the pathology of AD and show for the first time that m^{1}A^{1374} levels are altered in AD patients. Moreover, the selective overexpression of TRMT10C in HEK cells provides evidence that m^{1}A^{1374} methylation lowers ND5 protein levels and induces severe mitochondrial deficits. This newly discovered mechanism, along with further research, may provide a basis for the development of new drugs to treat or even cure mitochondrial dysfunction in AD.

Zusammenfassung

Beteiligung von *N*^{1}-Methyladenosin (m^{1}A) in der mitochondrialen ND5 mRNA und dem dazugehörenden Schreiber-Enzym TRMT10C bei der Alzheimer-Krankheit

Die Alzheimer-Krankheit (AK) ist eine neurodegenerative Erkrankung und die häufigste Form von Demenz. Auch wenn die US-amerikanische Arzneimittelzulassungsbehörde (FDA) in diesem Jahr einen neuen Antikörper zugelassen hat, der den kognitiven Verfall in einer Studie geringfügig verlangsamen konnte, gibt es noch immer kein Medikament, das die AK aufhalten oder sogar umkehren kann. Neben den Hauptverdächtigen (Amyloid β und phosphoryliertem Tau) gibt es immer mehr Hinweise darauf, dass die mitochondriale Dysfuntion ein frühes und möglicherweise ursächliches Ereignis bei der AK sein könnte. Für die Funktion der Mitochondrien ist besonders Komplex I (Cpx I) von Bedeutung, da dieser den primären Eintrittspunkt der Elektronentransportkette darstellt, welche für die zelluläre ATP Produktion benötigt wird. Obwohl eine Beeinträchtigung von Cpx I bei der AK mehrfach berichtet wurde, ist der zugrundeliegende Mechanismus bisher unklar. Im Jahr 2017 wurde jedoch eine *N*^{1}-Methyladenosin (m^{1}A) Stelle an Position 1374 in der mRNA von ND5, einer Kernuntereinheit von Cpx I, entdeckt. Allerdings ist die Auswirkung dieser m^{1}A-Stelle auf die ND5 Proteinspiegel, Cpx I und die mitochondriale Funktion bisher unbekannt. Deshalb sollte in dieser Arbeit untersucht werden, ob m^{1}A^{1374} die mitochondriale Translation von ND5 stören und somit zu einer verminderten Aktivität von Cpx I im Rahmen der AK führen könnte. Zu diesem Zweck wurde auch die tRNA-Methyltransferase 10 Homolog C (TRMT10C) untersucht, welche die m^{1}A^{1374} Methylierung in die mRNA von ND5 einbringt (als sogenanntes Schreiber-Enzym). Bemerkenswerterweise war die Proteinexpression der TRMT10C sowohl in Zell- und Mausmodellen als auch in Kortexproben von Alzheimer-Patienten konsequent erhöht. Diese Hochregulation war zelltypenspezifisch für Neurone. Außerdem war die Methylierung von m^{1}A^{1374} in AK-Modellzellen und in RNA-Seq Daten aus dem primären, visuellen Cortex von AK-Patienten deutlich erhöht, was anhand einer stellenspezifischen Analyse festgestellt wurde. Zusätzlich waren die ND5-Proteinspiegel in AK-Modellzellen, -mäusen und Patienten mit hohem Braak-Stadium deutlich vermindert. Die Ergebnisse dieser Arbeit belegen auf vielfältige Art und Weise, dass die TRMT10C in der Pathologie der AK involviert ist und zeigen zum ersten Mal, dass die Methylierungsspiegel von m^{1}A^{1374} im Rahmen der AK verändert sind. Darüber hinaus lieferte die selektive Überexpression der TRMT10C in HEK-Zellen den Beweis, dass die m^{1}A^{1374} Methylierung die ND5 Proteinspiegel senkt und dadurch schwere mitochondriale Defizite verursacht. Dieser neu entdeckte Mechanismus könnte zusammen mit weiteren Forschungen eine Grundlage für die Entwicklung neuer Medikamente zur Behandlung oder gar der Heilung von mitochondrialer Dysfunktion im Rahmen der AK bilden.

Acknowledgements / Danksagung

Contents

1 Introduction

1.1 Alzheimer's Disease

1.1.1 History

In 1906, the physician Alois Alzheimer reported for the first time "a peculiar illness of the cerebral cortex" at the University of Tübingen. One year later, he published a detailed symptomatic characterization [1] of his patient, Auguste Deter, who was under his care at the municipal madhouse in Frankfurt, Germany. He mentioned an abnormal behavior, speech difficulties and memory impairments, which were unusual for her age (early 50s). When Auguste died, Alzheimer used the then-new silver staining histological technique to examine her brain microscopically [2]. Next to a pronounced brain atrophy in the cerebral cortex, he observed the neurofibrillary tangles and amyloid plaques that were to become the hallmarks of the this disease [3]. In 1910, his mentor Dr. Emil Kraepelin included the disease description in his educational book and created the term "Alzheimer's disease" (AD). After that, the disease fell into oblivion for several decades. However, in the late 1960s numerous researchers started to further characterize the neuropsychological symptoms and histological changes. Since then, now more than 60 years ago, thousands of scientists have studied the mechanisms underlying AD and attempted to unravel the cause of non-familial AD cases. Although great progress has been made, several aspects of this complex disease are still unknown and an effective therapy is missing until today.

1.1.2 Epidemiology

According to the World Health Organization (WHO) more than 55 million people worldwide are living with dementia and due to population growth and improved longevity the number is estimated to rise to 78 million by 2030 and to 139 million by 2050[1] (Figure 1.1). AD is the most common form of dementia, accouting for 50-70% of dementia cases [4]. In Germany, the number of people with dementia was reported to be 1.8 million at the end of 2021 and is expected to reach 2.8 million by 2050[2]. Since a definite diagnosis of AD can only be confirmed after a post-mortem histopathological investigation and many patients worldwide remain undiagnosed, it is difficult to state a precise number of AD patients. However, according to estimations, 5.8 million U.S. citizen (age 65 and older) were affected by AD in 2020 [5].

[1] WHO, "Global status report on the public health response to dementia", September 2021
[2] Deutsche Alzheimer Gesellschaft e.V, "Selbsthilfe Demenz Informationsblatt", December 2021

Besides, the german federal agency “Statistisches Bundesamt” recently announced the number of people who had to be hospitalized due to AD. In 2020, this applied to 19 356 people in Germany, of whom 41.5% were male and 58.5% female[3]. Compared to 2020, the number of hospitalization due to AD more than doubled within 20 years (+135%)[3]. This illustrates the dramatic strain on our health care system and points to the enormous financial and social load of providing care to these patients. In 2019, the global cost of dementia was estimated to be 1.3 trillion US$ and gobal costs will increase to a projected 2.8 trillion US$ by 2030[4] (Figure 1.1). These numbers place an enormous burden on health care systems that will exacerbate with each passing year. Therefore, it is tremendously important to draw attention to this issue.

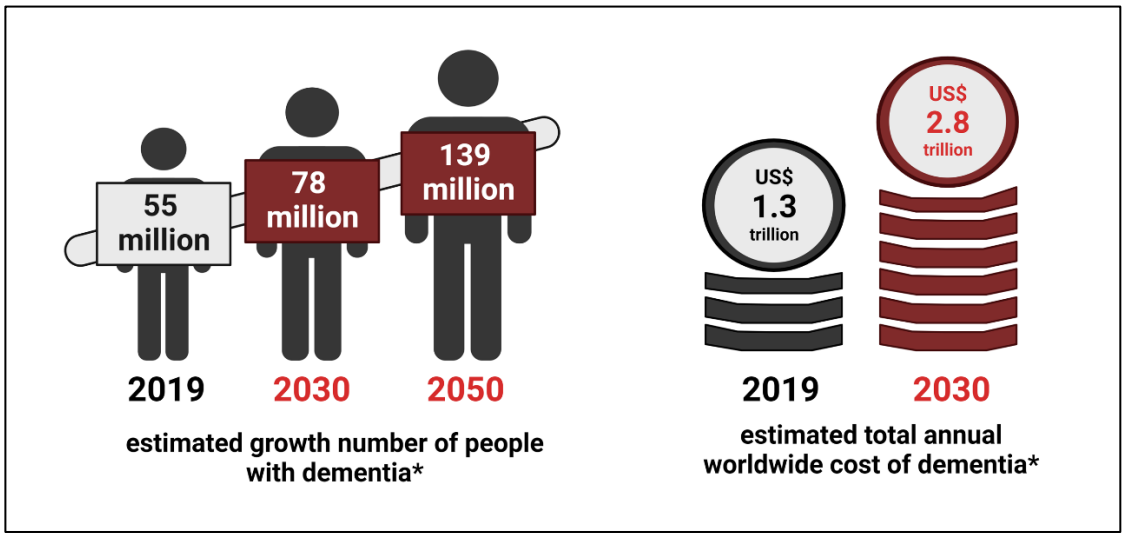

Figure 1.1: Estimated growth number of people with dementia and estimated annual cost of dementia worldwide. *Estimation and forecast of 2030 and 2050 according to the WHO’s Global status report 2021[4], illustration adapted from World Alzheimer Report 2021[5] released by Alzheimer’s disease International (ADI).

Interestingly, several studies suggest that the prevalence and incidence of AD and other dementia types may have declined in higher-income countries (USA and Europe) over the past 25 years [6]–[11]. This decrease has been attributed to the prevention of important risk factors, such as an increased level of education and improved control of cardiovascular risk factors [6], [11]–[14]. Although these findings indicate that a person’s risk of developing AD at any given age may slightly decrease, the total number of AD patients and other dementias is expected to increase continuously due to the growing number of people living in higher-income countries and the growing proportion of people at high ages (>75 years) (as for example in the U.S. population Figure 1.2). Besides, worldwide potential risk factors of AD (such as diabetes and obesity) are increasing and especially in low- and middle-income countries the numbers of AD

[3] https://www.destatis.de/DE/Presse/Pressemitteilungen/Zahl-der-Woche/2022/PD22_38_p002.html, published Septemer 2022
[4] WHO, “Global status report on the public health response to dementia”, September 2021
[5] https://www.alzint.org/resource/world-alzheimer-report-2021/, published September 2021

will continue to grow [15], [16]. According to projections 68% of the estimated increase of the global burden of dementia by 2050 will take place in low- and middle-income countries [5]. Therefore, it is also important to expand the health care system in these countries and prepare for the expected increase of AD cases.

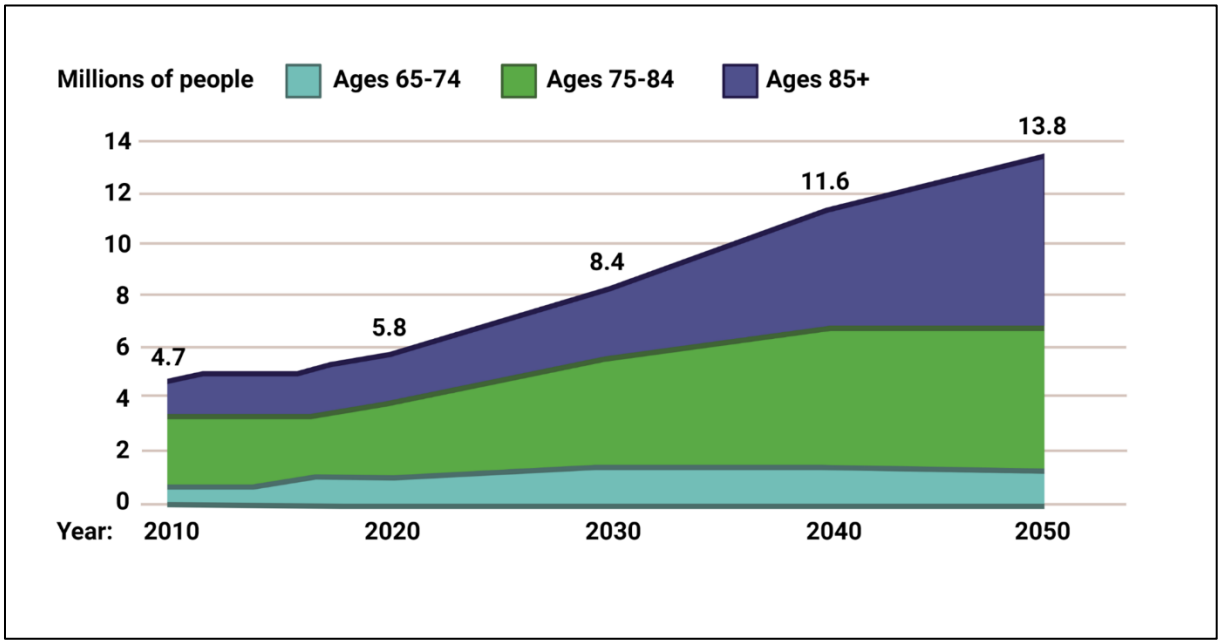

Figure 1.2: Projected number of people older than 65 years in the U.S. population with AD from 2010 to 2050 (overall numbers and proportion of three age groups). The numbers of AD patients will increase, particularly in the older age groups, as more and more people reach advanced ages due to the extended life expectancy. Data from [17], illustration adapted from [5].

As already indicated by the statistics above, aging represents the greatest risk factor for developing AD. This is also evidenced by the fact that the prevalence of AD dramatically increases with age. For example in the U.S., 3% of people age 65-74, 17% of people age 75-84 and 31% of people age 85+ suffer from dementia [17]. The second greatest risk factor is genetics. Researchers have found several genes that increase the risk for developing AD. The strongest impact was found for the *Apolipoprotein E-ε4 (APOE-ε4)* gene. This gene encodes a protein that transports cholesterol in the bloodstream. Those people that inherit one copy of the ε4 allele have a three times higher risk of developing AD and those who inherit two copies have an 8-12 fold risk compared to ε3 allele carriers [18], [19]. The importance of APOE-ε4 is particularly evident considering that 67% of people diagnosed with AD in the U.S. possess at least one APOE-ε4 allele [20]. Besides, individuals who have a parent or sibling with AD are more likely to develop the disease than individuals without AD cases in their family history [21], [22]. Interestingly, this observation was independent of the known risk factor APOE-ε4 [23]. This fact suggests that either additional hereditary factors (genetics) or non-genetic factors (e.g. healthy lifestyle and cognitive engagement) play a role and modulate the risk for AD. Furthermore, it is known that woman are more frequently affected by dementia than men. For

example, WHO estimates that 8.1% of women and 5.4% of men over 65 years are living with dementia worldwide[4]. This difference is likely due to the sudden drop in estrogen levels after the menopause [24], [25], but also due to the higher life expectancy of women[6]. Although age, sex and genetics cannot be changed, other risk factors can be modified to reduce the risk of AD and dementia. According to recommendations[7] published by the WHO in 2019 several lifestyle factors can reduce the risk of cognitive decline and dementia. These are physical activity, quitting smoking, and managing hypertension and diabetes. Along with this, a healthy diet, lifelong learning, social engagement and cognitive training seem to reduce the risk of developing AD [26], [27].

1.1.3 Characteristics

AD is the leading cause of dementia, accounting for 50-70% of cases [4]. The disease can be further divided into early-onset AD (EOAD), defined by age of onset younger than 65 years and late-onset AD (LOAD) with symptoms developing at age 65 or older. Two synonymous terms are familial AD (FAD) and sporadic AD (SAD) [28]. FAD is caused by homozygotic risk genes, namely PSEN1, PSEN2 or APP, and is a very rare form (less than 1%) [29], [30]. The exact etiology of the sporadic LOAD form is so far unknown, however, it seems to be a complex, multifactorial disease and several risk factors, such as aging were identified (see section 1.1.2). Both LOAD and FAD show the same clinical symptoms and neuropathology, as memory loss, amyloid deposits in the brain and neurofibrillary tangles, but FAD is marked by a more rapid disease progression and occurs at younger ages [31], [32].

The progression of AD as a consequence of brain changes that are unnoticeable to the affected person and cause memory and eventually physical disability is called the Alzheimer's disease continuum [33]–[36]. This model was postulated by the National Institute on Aging-Alzheimer's Association (NIA-AA) and provides recommended guidelines for the diagnosis of different AD stages. This continuum separates the disease progression into three broad phases: preclinial AD, mild cognitive impairment (MCI) due to AD, and dementia due to AD (see Figure 1.3). How long individuals spend in each phase of the continuum varies and the length of each part is influenced by age, genetics, gender and other factors [37]. In the first phase, the preclinical phase, individuals have not yet developed symptoms such as memory loss, but they do have measurable brain changes, e.g. abnormal levels of Aβ in the cerebrospinal fluid (CSF) and a decreased glucose metabolism in PET scans [33]. Besides tau tangles can be found in the entorhinal and transentorhinal cortex [38]. Of note, not all

[6] https://www.who.int/data/gho/data/indicators/indicator-details/GHO/life-expectancy-at-birth-(years), Global life expectancy at birth for females and males retrieved for the year 2015

[7] WHO Guideline "Risk reduction of cognitive decline and dementia", released January 2019

individuals that show AD-related brain changes develop MCI or AD afterwards. For example, it frequently happens that amyloid plaques are found in post-mortem brains of cognitively normal people [39]. In the second stage, the MCI due to AD phase, individuals show subtle problems with memory and thinking, as the hippocampus and amygdala are affected [40], [41]. These symptoms are noticeable to close relatives, but not to outsiders and do not interfere with everyday activities. One study showed that 15% of people with MCI developed AD after 2 years and a meta-analysis stated a MCI to AD conversion rate of 38% after 5 years [40], [42]. Interestingly, some individuals with MCI reverted to normal cognition.

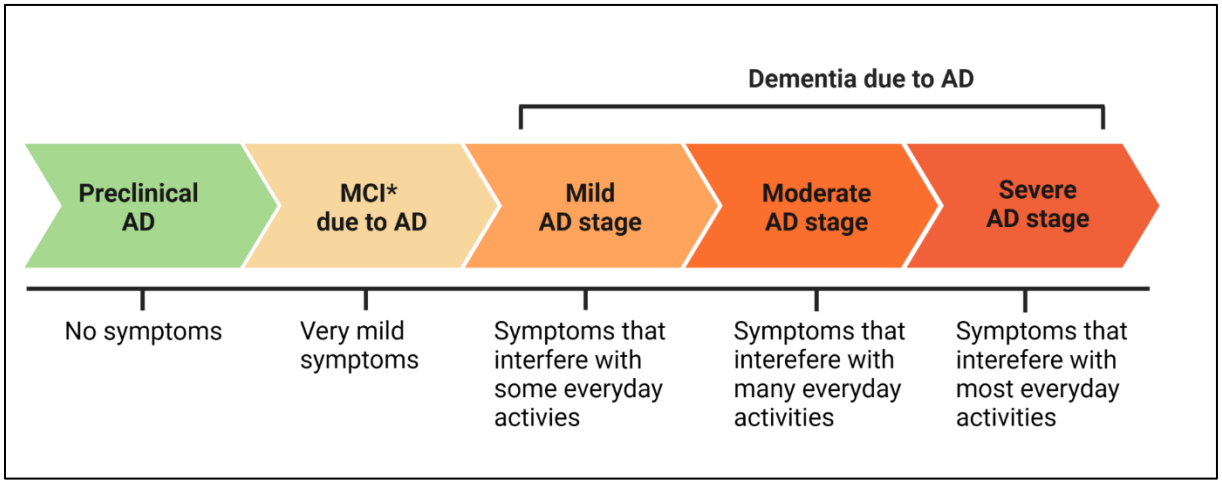

Figure 1.3: Alzheimer's disease continuum defined by the National Institute on Aging-Alzheimer's Association (NIA-AA). *MCI= Mild Cognitive Impairment. Graph adapted from [43].

The subsequent AD stage is characterized by noticeable symptoms concerning memory, thinking and behavior. These impair a person's ability to function in daily life, aggravate over time and reflect the degree of damaged neurons in different parts of the brain. At this point, more and more brain areas are affected by pathologic alterations and tau tangles occur in the whole neocortex [38], [44]. Depending on the severity of symptoms, dementia due to AD is classified as mild, moderate and severe. In the mild stage, patients need help for some everyday activities, but are usually still able to drive, work and participate in social events [35]. The moderate stage is often the longest stage. Here patients have difficulties in communicating and performing routine tasks. Activities that are necessary for the everyday life, such as dressing, brushing teeth or showering, can only be performed with difficulty or no longer at all. In this stage, patients often become incontinent and start showing personal and behavioral changes. In the severe AD stage, patients need help with all activities of daily living and frequently need around-the-clock care, as the physical symptoms become more and more apparent [35]. Due to damage of brain areas that are involved in movement, the patients usually get bed-bound. Being bedridden makes them vulnerable to diseases such as blood clots, skin infections and sepsis, which triggers the body's own inflammation that can lead to organ failure. Swallowing becomes difficult, due to damage in the corresponding brain area,

and may result in food particles entering the lungs (aspiration pneumonia). The failure of vital bodily functions is the ultimate the reason why AD can directly lead to death.

1.1.4 APP and APP processing

The two major histopathologic hallmarks of AD are amyloid plaques composed of Aβ peptides which are generated by the proteolytic cleavage of the Amyloid precursor protein (APP) and neurofibrillary tangles that result from hyperphosphorylation of the microtubule-associated tau proteins. APP belongs to the type-I transmembrane proteins and is a ubiquitously occurring polypeptide with a long N-terminal extracellular, a single trans-membrane and a short C-terminal cytoplasmic domain [45]. The APP family proteins are evolutionary highly conserved and consequently show great functional and structural similarities between mammalian species [45]. In humans, APP is encoded on chromosome 21 and via alternative splicing 8 isoforms are generated with a length of 677 to 770 amino acid residues [46]. These can be post-translationally modified by glycosylation, phosphorylation, or sulfation and reach a molecular weight of 110-140 kDa [47]. All of these forms share the same Aβ sequence, transmembrane and intracellular domains and are found in the cell membrane and its endocytotic parts, as well as in the membranes of the endoplasmic reticulum (ER), the trans-golgi network (TGN) and mitochondria [48], [49]. In neurons, mainly APP-695 is produced, whereas in glia cells APP-751 and APP-770 have also been identified [50]. APP family members are multimodal proteins that regulate biological processes ranging from transcriptional regulation to synaptic functions, such as synaptogenesis and synaptic plasticity [45], [51]. In doing so they can function as receptor-like proteins or ligands.

Numerous physiological functions are attributed not only to the APP holoprotein, but also to its cleavage products, which can be formed via proteolytic cleavage in two alternative canonical pathways (see Figure 1.4). The so-called non-amyloidogenic pathway is physiologically predominant and initiated by the cleavage of the α-secretase [52]. Thereby, an APP ectodomain fragment (sAPPα) and the C-terminal fragment α (CTFα) are released [45]. The latter can be further processed by the γ-secretase resulting in a fragment termed p3 and the APP-intracellular domaine (AICD). Importantly, the α-secretase cleaves APP within the Aβ sequence thereby preventing the formation of the neurotoxic Aβ peptide. Along the amyloidogenic pathway, the β-secretase releases the alternative APP ectodomain fragment sAPPβ and the C-terminal fragment β (CTFβ) [45]. When CTFβ is further cleaved by the γ-secretase, the neurotoxic Aβ peptide is liberated in addition to the AICD. Aβ and its variants ranging from 37-49 amino acid residues are all generated via endo- and exoproteolytic cleavage of the y-secretase. Next to $Aβ_{40}$, especially $Aβ_{42}$ is very prone to aggregation due to its lipophilic β-sheet entity [53]. That means Aβ monomers can form dimers, tetramers,

oligomers and fibrils, which constitute the main component of Amyloid plaques found in post-mortem brains of AD patients.

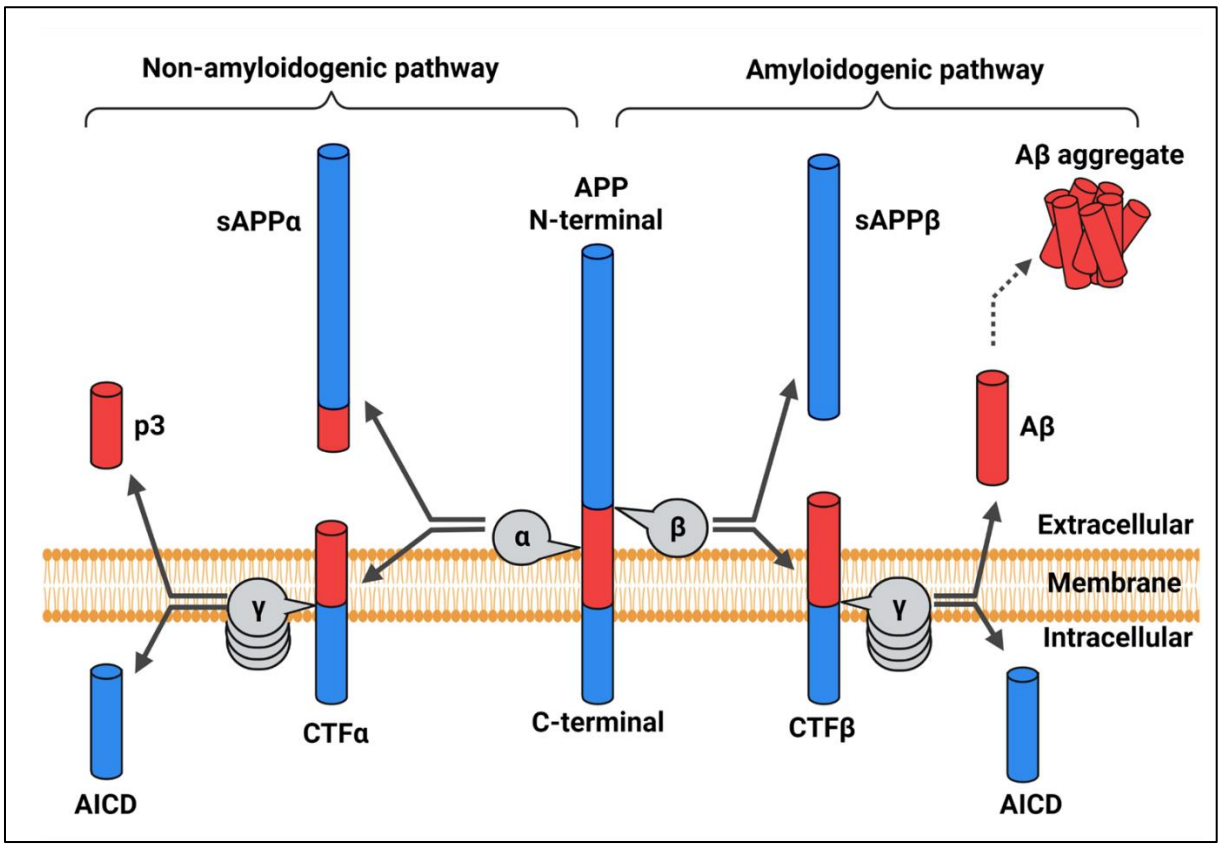

Figure 1.4: Schematic overview of the canonical APP-processing pathways. The schematic shows the amyloidogenic and non-amyloidogenic APP processing pathway including the released fragments and involved cleavage enzymes. APP= Amyloid-Precursor-Protein, sAPPα= α-secretase generated APP ectodomain fragment, sAPPβ= β-secretase generated APP fragment, CTFα= C-terminal fragment α, CTFβ= C-terminal fragment β, AICD= APP intracellular domain, Aβ= Amyloid β, α= α-secretase, β= β-secretease, γ= γ-secretase, α-, β- and γ-secretase are indicated as grey spheres pointing to their cleavage site. The accumulation of grey spheres represents multiple protein subunits. Figure adapted from [54]

The above mentioned fragments of APP exert various cellular effects and must be considered individually. For example, sAPPα is known to be neuroprotective as it acts like a growth factor for cells and promotes neuritogenesis is post-mitotic neurons [51]. Besides, products of the non-amyloidogenic pathway were shown to increase neurite outgrowth and enhance learning and memory [55], [56]. The most abundant forms of APP in the brain are sAPPα and sAPPβ [57]. This pathway can be stimulated by neuronal and synaptic activity [54], [58]. In contrast, Aβ peptides were shown to exert numerous adverse effects in cells, which are described in detail in section 1.1.5. The three mentioned catalyzing enzymes, α-, β- and γ-secretase are all membrane-bound, but built up differently. The major physiological α-secretase in the brain is the desintegrin and metalloproteinase domain-containing protein 10 (ADAM10) [59]. Next to APP this enzyme is known to cleave 20 additional substrates, e.g. Notch1 [60]. As for the β-secretase, there are two different homologs, BACE1 and 2, whereby

mainly BACE1 is expressed in neurons and BACE2 is thought to be more active in the peripheral tissue [61]. In contrast, the γ-secretase is a multicomponent complex composed of a Presenilin 1 or 2 homodimer, the presenilin-enhancer (PEN), Nicastrin, a stabilization factor APH1 and the Presenilin enhancer 2 (PEN-2) [62].

For the sake of completeness, it must be mentioned, that APP can also be cleaved in other non-canonical pathways. So in addition to the aforementioned secretases, APP can also be processed by the δ- and η-secretases, meperin-β and different caspases [45]. This pathways can lead to the generation of Aβ, but additionally various other fragments are produced, e.g. CTFδ, Aη-β and C31 (for more information see [45]). The discovery of these additional cleavage products is relatively recent, and the study of their effects and involvement in AD is subject of current research.

1.1.5 Pathology

Until today, the exact etiology of LOAD is unknown. Though it is known that LOAD is a complex, multifactorial disease and that AD symptoms arise as a consequence of synaptic and neuronal loss, the exact cause that sets pathological cascades in motion has not been conclusively clarified. However, there are numerous hypotheses and hints.

The amyloid cascade hypothesis

Most popular is the amyloid cascade hypothesis which states that “the amyloid β protein, the main component of amyloid plaques, is the causative agent of Alzheimer’s pathology and that neurofibrillary tangles, cell loss, vascular damage, and dementia follows as a direct result of this deposition” [63]. This hypothesis was postulated for the first time in 1992 by J. Hardy and G. Higgins. Certainly, there is ample evidence to support this hypothesis. First of all, the occurance of FAD in individuals carrying autosomal-dominant mutations in genes encoding APP or subunits of the γ-secretase (PSEN1 and 2) [64]. Second, a dramatic portion of patients with Down syndrome manifest AD early in life (97% of patients with a mean age of 55 years at diagnosis) [65]. This fact is apparently attributed to the overexpression of the APP due to the triplication of chromosome 21 in these patients. Besides, a huge body of evidence has accumulated over the last 30 years showing that different forms of Aβ can cause synaptotoxic effects and neuronal death [66], [67]. Importantly, these effects have been shown for different states of Aβ ranging from dimers to oligomers, which are highly heterogeneous in their size, structure and cytotoxicity. Adverse effects of these peptides have been evidenced in numerous *in vitro* and *in vivo* models, whereby it has been established that especially soluble Aβ peptides, rather than their insoluble fribrillar aggregates, seem to be the main responsible of

neurodegeneration in AD [67] (see Figure 1.5). Aβ oligomers cause different types of synaptic defects, such as alteration of neurotransmitter uptake and release, cytoskeletal abnormalities, changes in receptor cellular localization and the disruption of synaptic plasticity (inhibition of long term potentiation (LTP) and enhancement of long term depression (LTD)) [68], [69]. Next to synaptic loss, Aβ and Aβ oligomers were shown to cause neuronal cell death, tau hyperphosphorylation, oxidative stress and neuroinflammation [68], [70]–[72], and according to the amyloid cascade hypothesis, the concurrence of all these effects are the reason for memory and cognitive defecits in AD.

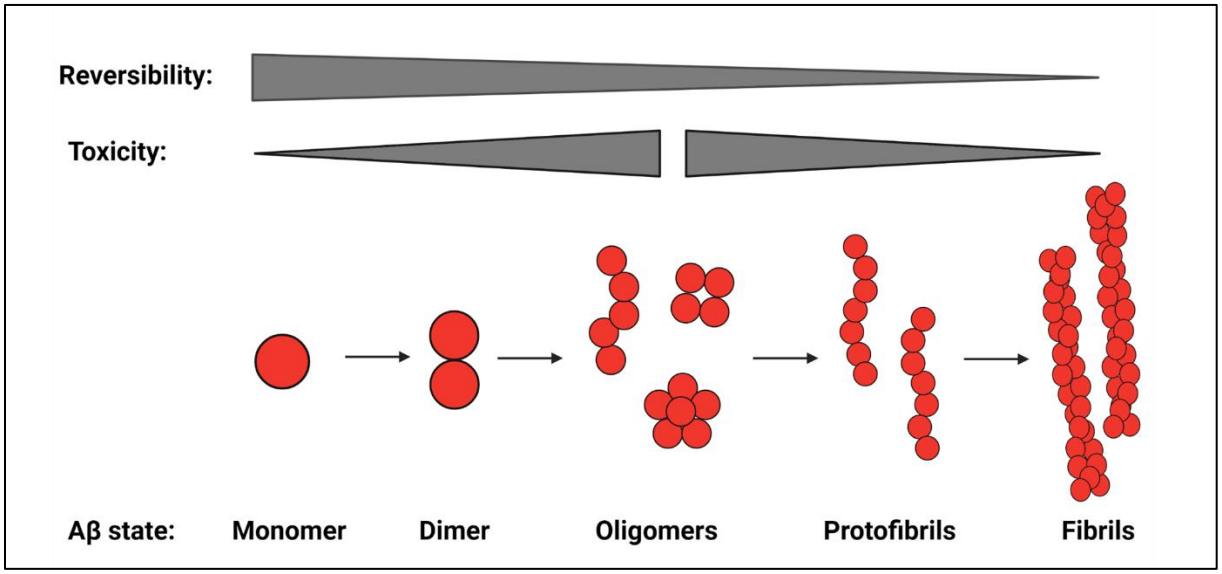

Figure 1.5: Simplified schematic of the Aβ aggregation process. Aβ monomers can form dimers and oligomers of heterogeneous states (fibrillar and non-fibrillar forms). These may further aggregate into protofibrils and mature fibrils en route to the deposition of amyloid plaques. Oligomeric Aβ species represent the most cytotoxic form of Aβ. Figure adapted from [73] and [74].

The amyloid cascade hypothesis has received additional support by the generation of several APP or APP/PSEN1 transgenic mouse models that represent the main histopathological and behavioral characteristics of AD, such as deposition of amyloid plaques, synaptic loss, alterations in synaptic plasticity and memory impairment [75], [76]. Moreover, several pharmacological, genetic and immunological approaches that aimed to reduce the cerebral Aβ load in AD mouse models, showed positive results [77], [78]. As a final point in support of the amyloid cascade hypothesis, it should be mentioned that recent results of the "Clarity AD" study strongly support this hypothesis. This phase 3 study performed by Biogen and Eisai tested the monoclonal antibody Lecanemab (BAN2401). Lecanemab selectively binds to soluble, toxic Aβ aggregates (protofibrils) and is thought to initate their elimination. Investigation of 1795 individuals with MCI due to AD or mild AD for 18 months revealed a highly statistically significant reduction of 27% in the Clinical Dementia Rating-Sum of Boxes

(CDR-SB), the primary endpoint in comparison to placebo[8]. CDR-SB is a numeric scale to assess severity of dementia symptoms covering cognitive and functional performance in areas such as memory, orientation, judgment, etc. The participiants were included from Japan, U.S., Europe and China, and 10 mg/kg of Lecanemab was administered every two weeks. As inclusion criterion, amyloid pathology had to be detected before in the brain. All key secondary endpoints (e.g. amyloid-PET and ADAS-cog14) also met with highly statistically significant results, however, as expected amyloid-related imaging abnormalities (ARIA) E and H occurred in 12% and 17% of all patients[8]. Just recently (January 2023) Biogen received the accelerated approval from the U.S. FDA amid safety concerns. Besides Biogen and Eisai aim to submit marketing authorization applications in Japan and Europe. Whether this drug really represents a breakthrough in Alzheimer's therapy will become clear in the next years, when further data for efficacy and safety will be generated and analyzed by external independent experts. In any case, the drug will only slow down cognitive decline, but won't be able to stop the disease progession. Promising results were also obtained with a similar antibody called Donanemab in a recent phase 3 clinical trial[9].

Limitations of the amyloid cascade hypothesis

Though Aβ indisputably plays a signiticant role in the pathogenesis of AD, a huge amount of evidence suggests that this peptide is not the central disease-causing event. First, even though FAD and LOAD share the same histopathological and clinical features, that does not necessarily mean that they result from the same trigger. In LOAD other factors (e.g. aging-associated mechanisms) could initate a cascade that results in the same pathological final pathway as in FAD, which there is activated by gene mutations. Second, it has been consistently shown multiple times that Aβ accumulation and deposition do not correlate with neuronal loss and cognitive decline [79]–[82] and many cognitively unimpaired individuals also display a significant amyloid plaque burden in PET scans [81], [83]. Hence Aβ itself appears to be a normal peptide which is generated throughout life, even if its physiological role is not fully elucidated so far [84]. In addition, there are several points to consider when evaluating studys using oligomeric Aβ. For example, extraction and purification of soluble oligomers from AD patients and model mice represents an intricate task. Therefore it is not clear whether the different isolated oligomeric species are really endogenously produced or artificially arise during the experimental procedure. Besides, though Aβ oligomers were shown to damage neurons in vitro, neuronal cell death is almost absent in APP and APP/PS1 transgenic mice [85], [86]. This demonstrates that high levels of Aβ peptides, do not trigger neurodegeneration

[8]https://investors.biogen.com/news-releases/news-release-details/lecanemab-confirmatory-phase-3-clarity-ad-study-met-primary
[9]https://investor.lilly.com/news-releases/news-release-details/lillys-donanemab-significantly-slowed-cognitive-and-functional

per se. This discrepancy has brought the tau protein back into focus. In particular, because it has been shown that the reduction of tau in AD mouse models protects from Aβ-induced synaptotoxicity and memory deficits [87]–[89]. Conversely, it was observed that tau mutations lead to accelerated tangle formation and neuronal cell death [90], [91]. Therefore, several lines of evidence suggest that the amyloid peptide drives tau hyperphosphorlyation and that these two proteins may act synergistically to provoke neuronal death [92], [93]. Nevertheless, this hypothesis also provides inconsistencies, because both the temporal and the regional distribution of neurofibrillary tangles and Aβ plaques do not correlate in AD patients. There are some hints that tau tangles even precede plaque formation and the distribution of neurofibrillary tangles correlates much better with clinical symptoms than Aβ plaques [38], [94], [95]. Furthermore, it must be noted that a large proportion of the mentioned findings is based on transgenic AD model mice. These APP and APP/PS1 mice carry mutations found in FAD patients, which raises the question of whether they are appropriate to model LOAD, especially as they don't show neurofibrillary tangles [85]. Even if triple transgenic mice (APP/PS1/tau) reproduce the pathological features of human AD, the issue remains that tau mutations do not cause AD. Furthermore, experiments in the mouse species always entail the question of the extent to which they can be transferred to humans. Lastly, it should be mentioned that the follow up of some AD patients after Aβ-immunization showed that amyloid plaques were reduced, but the disease continued until the death of the patients with all symptoms and histopathological alterations of AD [96]. Whether this fact would be fixed by an application earlier in the pathogenesis of AD is unclear.

In conclusion, despite the positive outcome of Lecanemab and Donanemab, the amyloid cascade hypothesis leaves many questions unanswered. It also misses the point that aging is the main risk factor for LOAD. Since mitochondrial dysfunction -next to extracellular amyloid plaques and intracellular tau tangles- plays a major role in AD and mitochondrial function has been shown to decline with age, the mitochondrial cascade hypothesis provides an interesting link. This hypothesis and the role of mitochondria in the pathogenesis of AD are described in detail in section 1.2.5. Besides, many scientists believe that not all LOAD cases should be lumped together, as both pathology and clinical presentation display a heterogeneity within AD patients [97]. On the one hand, a robust classification into 4 subtypes based on tau spread was made in 2021 by artificial intelligence and on the other hand, a classification based on the most significant risk component, e.g. APOE-ε4 allele or older age, was proposed [98], [99]. Interestingly, there is also a small but notable group of dementia patients displaying the typical AD symptoms and neurodegeneration, but no amyloid deposition [100], [101]. It is controversial whether this variant should be counted as AD or not, however, in these patients mitochondrial dysfunction seems to be one of the first pathological signs on the way to the development of dementia [100], [102].

1.2 Mitochondria

1.2.1 Structure and composition

Mitochondria are double membraned organelles that are present in almost all mammalian cells [103]. They are classically recognized as key regulators of cellular energy in form of adenosine triphosphate (ATP) [104]. Today, it is known that these organelles are also involved in a large variety of physiological processes including redox signaling, cell death execution and maintaining cellular calcium homeostasis [105]. A more detailed description of all mitochondrial functions is provided in section 1.2.3.

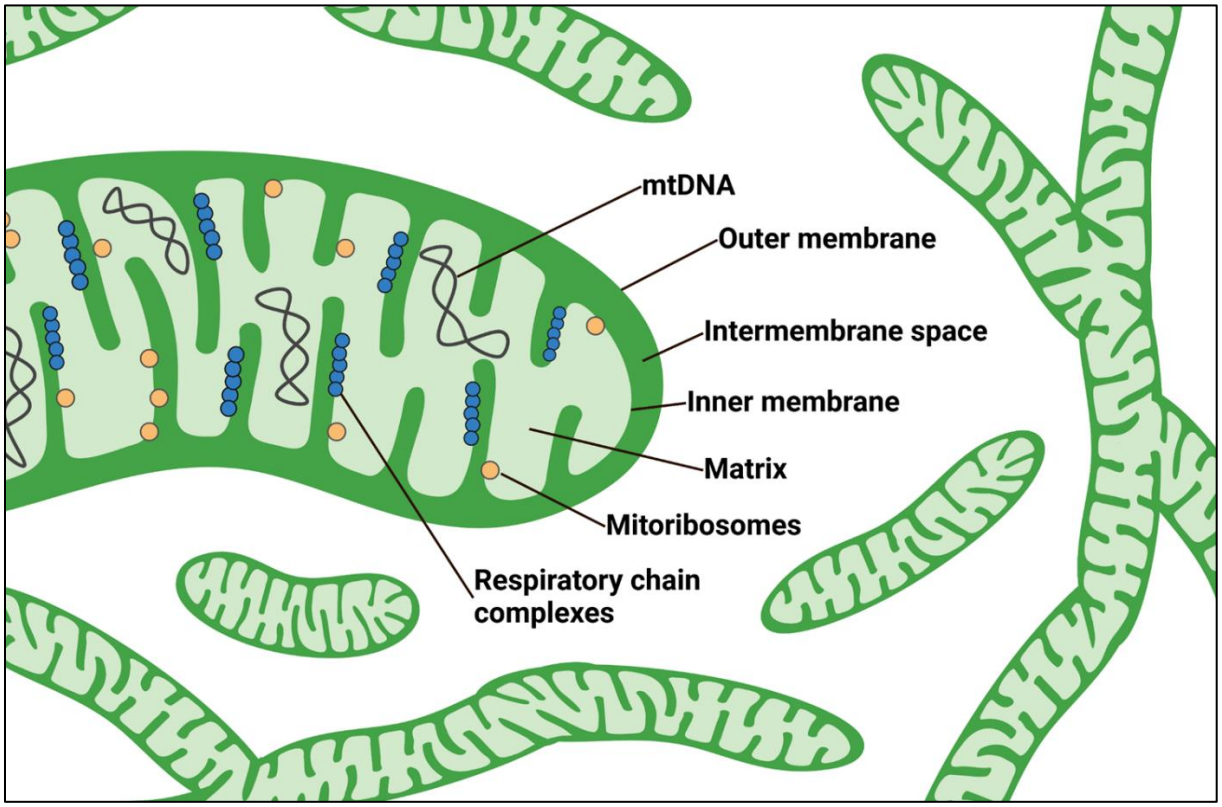

Figure 1.6: Schematic illustration of mitochondria and mitochondrial components. Thin mitochondria represent the tubular mitochondrial network in a cell. The one large mitochondrion demonstrates that mitochondria consist of an outer and an inner membrane, which results in two separated regions: the matrix and the intermembrane space. Mitochondria possess their own DNA (mtDNA) and mitoribosomes (brown dots). The complexes of the respiratory chain (blue dots) which are required for the synthesis of ATP, are located in the inner mitochondrial membrane.

Mitochondria are mainly organized in a continuous tubular network that extends through the cell along a cytoskeletal scaffold. Thereby, it surrounds the nucleus and other organelles and stretches towards the plasma membrane. Due to mitochondrial fission and fusion, as well as the distribution of mitochondria along the cytoskeletal tracks, this network is dynamic and enables the adaptation to changing cellular functions. Therefore, the number, shape and size of mitochondria varies considerably depending on cell type and cell condition. For example, in energy-demanding cardiac muscle cells mitochondria are very abundant and constitute

20-40% of the cellular volume [106], whereas in other cell types mitochondria account for <35% of the cellular volume [107]. Likewise, the size of an individual mitochondrion varies in dependence of cell type and cell conditions, but it is commonly between 0.75 and 3 μm^2 [108].

The entire tubular network (simplified depicted in Figure 1.6) is delimited from the cytosol by the outer mitochondrial membrane (OMM). The OMM has a protein-to-phospholipid ratio similar to that of the cell membrane, is porous and freely traversable by ions, metabolites, nucleotides and other uncharged molecules via pore-forming membrane proteins, such as the voltage-dependent anion chanel (VDAC) [105]. Larger molecules, such as proteins, can enter the mitochondrion through translocases, in case they provide a specific mitochondrial target sequence (MTS). In contrast, the inner mitochondrial membrane (IMM) separates the matrix from the intermembrane space and is a tight diffusion barrier to all ions and molecules, resulting in an electrochemical membrane potential of about -180 mV [105]. It forms numerous invaginations called cristae, that protrude far into the matrix. Here, the enzymes of the respiratory chain are located and mitochondrial ribosomes (mitoribosomes) are also membrane-associated. The protein-to-phospholipid ratio of the IMM is more than 3:1 and it does not contain porins, therefore all proteins require specific transport proteins to enter or leave the matrix [105]. This inner compartment has a high protein density and a relatively high pH of 7.9 - 8.0 (the pH of the intermembrane space is 7.2 - 7.4) [109]. In the matrix, the mitochondrial DNA (mtDNA) is located and replicated. Besides, transcription, protein biosynthesis of mitochondrial encoded genes and numerous enzymatic reactions take place in the matrix. The mtDNA is bound to the transcription factor A (TFAM) and condensed into supramolecular assemblies called nucleoids [110]. In general, each human cell contains several hundred to thousand mitochondria and each mitochondrion containes 2 to 10 copies of mtDNA [111].

It is proposed that all mitochondria derive from a common ancestral organelle that originated from the integration of an endosymbiotic α-proteobacterium into an Archaea host cell [112]. This transition is reflected, for example, in the different protein-to-phospholipid ratio between IMM and OMM. This further implies that mitochondria require a fine regulation in terms of nuclear protein synthesis and import.

1.2.2 mtDNA, transcription and translation

As mentioned above, mitochondria contain an extrachromosomal genome which is differently organized from the nuclear one. The mtDNA is a histone-free circular double-stranded DNA molecule with around 16 000 base-pairs (bp) and encodes 37 genes [113]. Both mtDNA strands, the heavy and the light strand, encode different genes, with the heavy strand

containing most information. It carries the complementary sequence for 14 tRNAs, 2 rRNAs (12S and 16S) and 12 mRNAs. In comparison, the light strand encodes 8 tRNAs and 1 mRNA [114]. Together, this results in 13 mRNAs that all code for proteins of the respiratory chain, including subunits of Cpx I, III, IV and V. The other subunits of these complexes are nuclear encoded, translated in the cytosol, and then imported into the mitochondrion (more information about the respiratory chain in section 1.2.3).

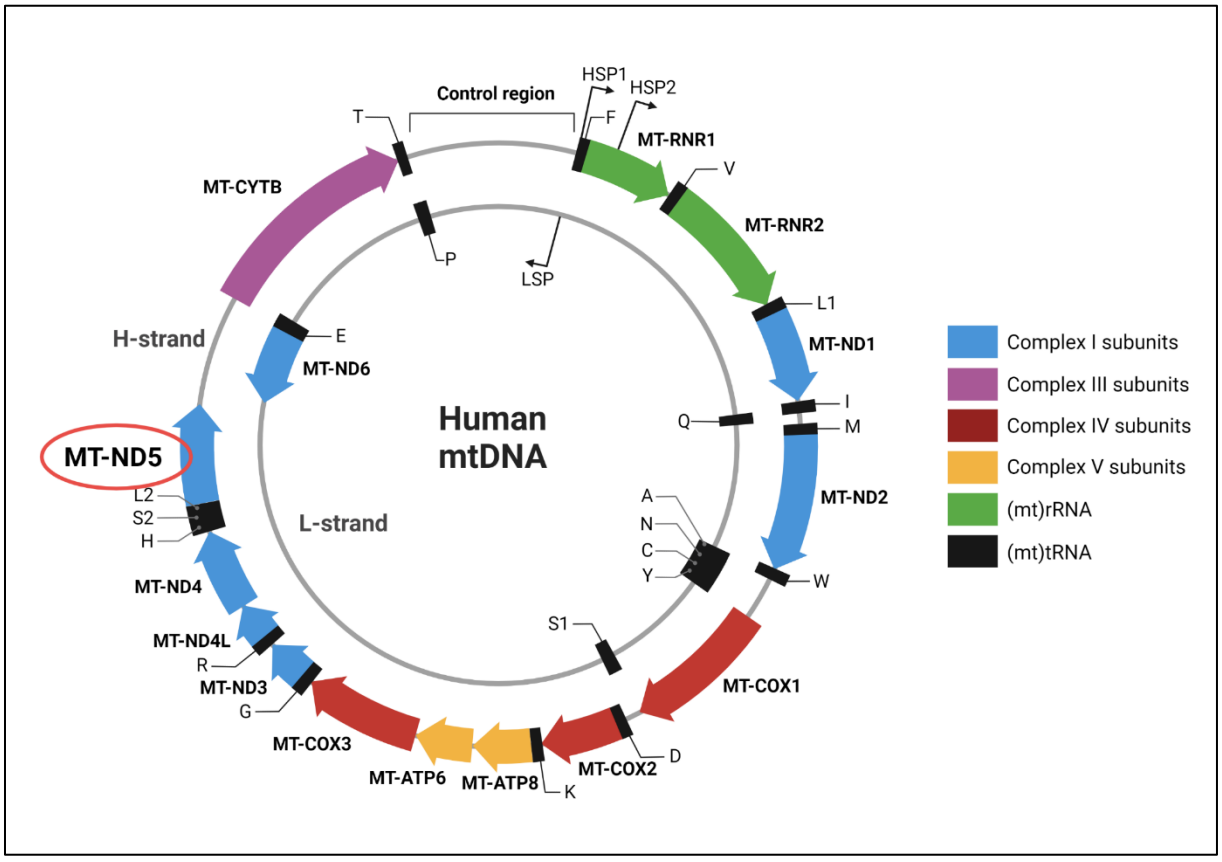

Figure 1.7: Human mtDNA sequence map. The mtDNA consists of one heavy (H-strand) and one light strand (L-strand) coding together for 22 tRNAs, 2 rRNAs and 13 polypetides. Sequences coding for Cpx I, III, IV and V subunits are labeled in blue, purle, red and yellow respectively. In context of this thesis, the Cpx I subunit ND5 encoded in the *MT-ND5* gene is of particular importance (circled in red). The complementary sequences for rRNA are labeled in green and those for (mt)tRNAs in black. The letters associated with tRNA represent the one-letter code of the corresponding amino acid for each tRNA. L1&2 and S1&2 represent two tRNA isoacceptors. Besides mtDNA contains three promoters: Heavy strand promotor 1 and 2 (HSP1, HSP2) and one light strand promotor (LSP). Grey lines are non-coding regions. Figure adapted from [115].

Unlike nulear-encoded genes, mitochondrial genes are devoid of introns and tRNAs are interspersed between protein and rRNA coding genes with no intervening sequences [116]. The largest non-coding sequence is the control region that contains signals to control both RNA and DNA synthesis. This region can also be called D-loop, relating to a structure that is formed when the mtDNA is replicated [117]. Importantly, the mtDNA polymerase has a low fidelity and there is no own mtDNA repair mechanism, which leads to a significant higher mutation rate in the mitochondrial genome compared to nuclear DNA [114]. Besides, mtDNA

contains three promoter regions that are located adjacent to each other near the control region. Transcription of the L-strand is initated by the light strand promoter 1 (LSP1), whereas the heavy strand contains two promoter sequences (HSP1 and HSP2). It is under debate whether both transcription units are necessary for the expression of H strand genes, although today HSP1 is assumed to be the main promoter [115], [118], [119]. The basal mitochondrial transcription machinery contains three proteins: The mitochondrial RNA polymerase (POLRMT), the mitochondrial transcription factor B2 (TFB2M) and TFAM, which was already mentioned in section 1.2.1, as in enables the condensed form of the mtDNA. The transcription by POLRMT results in two long polycistronic transcripts, one that is derived from the LSP and one from the HSP. These two transcripts are processed by the mitochondrial RNA-processing machinery comprising mtRNase P (described in detail in section 1.4.2) and mtRNase Z, which cleaves in a subsequent step [120]. According to the ‘‘tRNA punctuation model of RNA processing in human mitochondria” (mt)tRNAs act like a cleavage signals for these enzymes and through the endonucleolytic cleavage of these tRNA sequences rRNAs and mRNAs are released [121]. This model is generally accepted, but it is unclear how mRNAs are liberated that are not immediately adjacent to a tRNA.

In contrast to nuclear mRNAs, mitochondrial mRNAs contain no or a relatively short 5’-UTRs and lack 3’-UTRs [122]. Besides, the 7-Methylguanosine cap that is essential for nuclear encoded mRNAs is lacking in (mt)mRNAs. However, all (mt)mRNAs, except of ND6, contain polyadenylation tails with ~45-50 nts of length added by the mitochondrial polyA polymerase (mtPAP) [123]. As in the cytosol, translation in mitochondria is a complex, multi-step process that requires several different factors for initiation, elongation, termination and recycling (reviewed in [115]). For this purpose mitochondria possess their own 55S-ribosomes, called mitoribosomes, which are multi-member complexes [124], [125]. They consist of a large subunit (LSU, 39S) and a small subunit (SSU, 28S) composed of nuclear encoded ribosomal proteins, and the mitochondrial encoded 16S and 12S rRNAs. Besides, an (mt)tRNA ((mt)tRNA^{Val} or (mt)tRNA^{Phe}) is needed to form the structural scaffold for the central protuberance, analogous to the 5S-rRNA in cytoplasmic ribosomes [126] (see Figure 1.17). Interestingly, mitoribosomes are anchored in the IMM, which is believed to facilitate the insertion of newly synthesized proteins into the compartment of need. As most of the (mt)tRNAs do not provide a 5’-UTR and lack a 5’-cap, it is unclear how (mt)mRNAs are recognized and transported to the mitoribosome. Lastly, it should be mentioned in the course of translation that the decoding of (mt)mRNAs slightly differs from that of cytosolic mRNAs. This means that some codon triplets are translated differently into amino acids [127].

1.2.3 Functions

Mitochondria are classically known for their essential role in the production of energy in form of ATP. This primary cellular energy carrier is generated by aerobic respiration in a process, termed the oxidative phosphorylation (OXPHOS). The chain of reactions required for this process is carried out by 5 enzyme complexes and two mobile electron carriers that work closely together in the mitochondrial respiratory chain (see Figure 1.8). These five complexes are referred to as complex I-V (Cpx I-V) and are located in the IMM. They utilize a series of electron transfer reactions derived from reducing equivalents to establish a proton gradient across the IMM. This electrochemical gradient build up by Cpx I-IV results in the proton-motive force that drives the production of ATP by Cpx V [128].

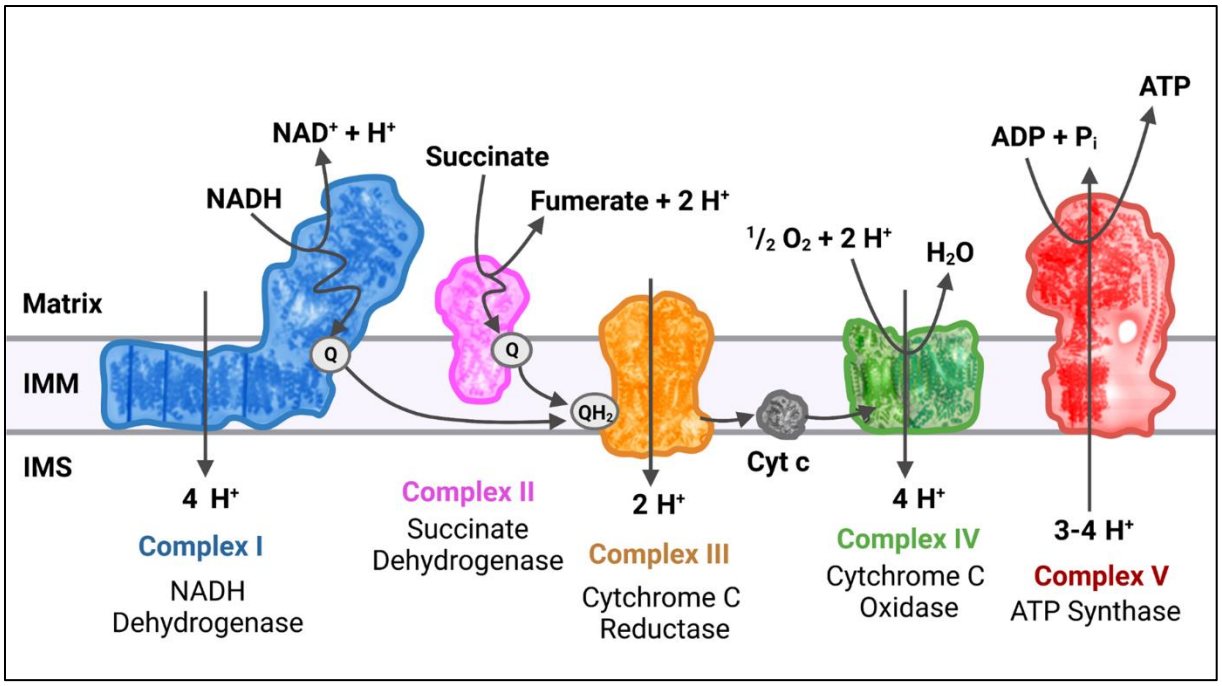

Figure 1.8: Schematic representation of the respiratory chain in mitochondria. Complex I oxidizes NADH to NAD^+ to reduce Ubiquinone (Q) to Ubiquinol (QH_2). This electron transfer is coupled to the transport of four protons from the mitochondrial matrix into the inner membrane space (IMS). Complex II oxidized succinate to fumarate and reduces Q without the translocation of protons. In the next step, eletrons are transferred from QH_2 to Cytochrome c (Cyt c) via complex III accompanied by the translocation of 2 protons. Finally, four molecules of Cyt c are used to reduce oxygen (O_2) to water. This process is catalyzed by complex IV and 4 protons are simultaneously transferred. The proton gradient thus created is the driving force for complex V to generate ATP. Electron and proton transfer processes are depicted with grey arrows. IMM= Inner mitochondrial membrane. Figure adapted from [109] and [129].

The aforementioned process begins with Nicotinamide adenine dinucleotide (NADH), which is generated during glycolysis in the cytoplasm and during the citric acid cycle in the mitochondrial matrix. The oxidation of NADH and the simultaneous reduction of Ubiquinone is performed by Cpx I alias NADH dehydrogenase. This redox reaction is coupled with the translocation of 4 protons from the matrix to the intermembrane space (IMS) [130]. In parallel,

Cpx II alias Succinate dehydrogenase oxidizes succinate to fumarate, whereby no protons are transported. Similar to Cpx I, the thereby released electrons are transferred to Ubiquinone, which is reduced to Ubiquinol. Since Ubiquinol is able to diffuse along the IMM, it encounters Cpx III alias Cytochrome c oxidase. Here, it is oxidized and the resulting electrons are transferred to Cytochrome c (Cyt c), with additional two protons being displaced across the membrane. Interestingly, the resulting Ubiquinone remains in the membrane and can be recycled by Cpx I and II [131]. In the last step of the electron transport chain (ETC), a term that comprises Cpx I-IV, Cpx IV alias Cytochrome c oxidase catalyzes the transfer of electrons from the reduced Cyt c to molecular oxygen. Its reduction to two water molecules requires four electrons transfered from Cyt c together with four protons, which are taken from the matrix. This reaction generates both a proton and charge gradient across the IMM, because matrix protons are consumed from the matrix and electrons originate from the IMM [130]. So as consequence of the ETC, a total of ten protons are pumped from the matrix into the IMS, where they accumulate and thereby generate an electrochemical proton gradient termed the mitochondrial membrane potential (MMP or $\Delta\Psi$). $\Delta\Psi$ together with the high proton concentration in the IMS results in the protonmotive force, which is couples the ETC to the activity of Cpx V alias ATP Synthase. Cpx V comprises two domains, the extramembranous (called F_1) and transmembrane (called F_O), and functions in a rotational motor mechanism [132]. Hereby, protons from the IMS re-enter the matrix harnessing the protonmotive force. The movement of protons through the F_O is coupled to the rotation that results in the addition of a phosphate to adenosine diphosphate (ADP) to synthesize adenosine triphosphate (ATP) in the F_1 domain [132].

Mitochondria are best known for producing ATP via OXPHOS, however, they are also of key relevance in various physiological and pathophysiological pathways. For example, mitochondria mediate a variety of events during apoptosis, e.g. the release of Cyt c (which activates caspases) and the loss of the $\Delta\Psi$ [133]–[135]. Besides, multiple lines of evidence indicate that mitochondria-derived reactive oxygen species (ROS) also influence homeostatic signaling pathways to control cell proliferation and differentiation and contribute to stress signaling pathways [136]–[138]. In addition, mitochondria are the main cellular source of NADH, which is produced, among others, during the conversion of long-chain fatty acids to Acetyl-CoA (β-oxidation) and in the citric acid cycle (series of chemical reactions to release energy stored in Acetyl-CoA). Biosynthesis of other important molecules such as hormones, neurotransmitters, lipids and Fe-S proteins also takes place in the mitochondria [137], [139]. Furthermore, mitochondria are also involved in inflammatory processes and regulate the Ca^{2+} homeostasis by modulating the spatiotemporal distribution of this second messenger [140], [141]. Especially in neurons, this ability is essential for controlling neurotransmitter release, neurogenesis and neuronal plasticity [137], [142].

1.2.4 Complex I

In context of this thesis, Cpx I alias NADH dehydrogenase is of particular importance. Therefore, the following section will discuss the structure and function of this enzyme more in detail. As Cpx I is the major entry point for electrons to the respiratory chain, it is assumed to be the rate-limiting step in overall respiration and hence plays a central role in the generation of ATP. Besides, it is the largest and most elaborate protein of the ETC, with the entire holoenzyme reaching a molecular weight of ~1 MDa [143]–[145]. Therefore, its biogenesis requires a large number of assembly factors [146].

In humans, Cpx I consists of 45 subunits, 7 of which are encoded in the mtDNA (ND1-6 and ND4L), while the remainder are encoded in the nuclear DNA (subunits with the initial letters NDUF) [143]. The 7 mitochondrial subunits, along with 7 of the nuclear-encoded subunits, are the so-called core subunits that are essential for a functional enzyme. These 14 subunits are highly conserved across species and homologous to the 14 subunits of the bacterial Cpx I (see structure of *T. thermophilus* in Figure 1.9). During the course of evolution, Cpx I has acquired 31 supernumerary subunits, however, as the core subunits are thought to be sufficient for Cpx I function, the role of the supernumerary subunits is not entirely clear. They are likely to assist in the assembly, regulation and stability of the complex and might as well play a nonspecific role in protecting the core subunits against oxidative damage [147], [148]. Of note, Cpx I also requires the noncovalent binding of coenzymes, namely Flavin mononucleotide (FMN) and 9 iron-sulfur clusters which are incorporated in the structure of the core subunits [144], [149].

In all species, Cpx I exhibits a characteristic L-shaped structure with two distinguishable arms (see Figure 1.9). The lipophilic membrane arm, which contains all the mtDNA-encoded subunits, is embedded in the inner mitochondrial membrane. The hydrophilic peripheral arm protrudes into the matrix [150]. Here, NADH derived from the matrix is oxidized to NAD^+ and H^+, and electrons are transferred to the primary electron acceptor FMN. The 95 Å long electron transfer pathways through the enzyme proceeds from FMN through seven conserved Fe-S clusters (N3→N1b→N4→N5→N6a→N6b→N2) [144] (see Figure 1.9). Interestingly, only seven of the 9 Fe-S clusters are involved in the normal electron transfer pathway. The remainder are thought to be essential for the stability of Cpx I and cluster N1a was additionally proposed to play a role in the prevention of oxidative damage [151]–[153]. Subsequently, electrons are transferred to Q at an unusual elongated binding site, located at the interface between the hydrophilic and the lipophilic membrane arm. The latter contains three antiporter-like subunits (ND5, ND2 and ND4), each of which is able to transport one proton per Q molecule from the matrix into the IMS. Two other subunits in the membrane arm (ND4L and ND6) also allow one proton to pass, so that a total of 4 protons are translocated per Q molecule. In general, Cpx I can be considered as a sophisticated microscale pump, as it couples the

redox energy of electron transfer to the proton translocation by adopting two different conformational states [154]. In the transition between these two states, ND5, the most distal core subunit of the membrane arm, plays a crucial role. ND5 in humans (homolog of NuoL in *E. coli* and Nqo12 in *T. thermophilus*) provides next to the antiporter-like structure a 110 Å long amphipathic α-helix, spanning almost the entire length of the membrane arm (see Figure 1.9). It was proposed that the conformational changes after the reduction of Q at the interface of the two enzyme arms may drive the long amphiphatic α-helix of ND5 in a piston-like motion, thereby tilting transmembrane helices of ND4, ND2, ND4L and ND6 resulting in the translocation of protons [144], [155]. Although it is not entirely clarified to date whether ND5 alone is capable of implementing the conformational shift, it is undisputable that ND5 plays an essential role for the function of Cpx I [156], [157].

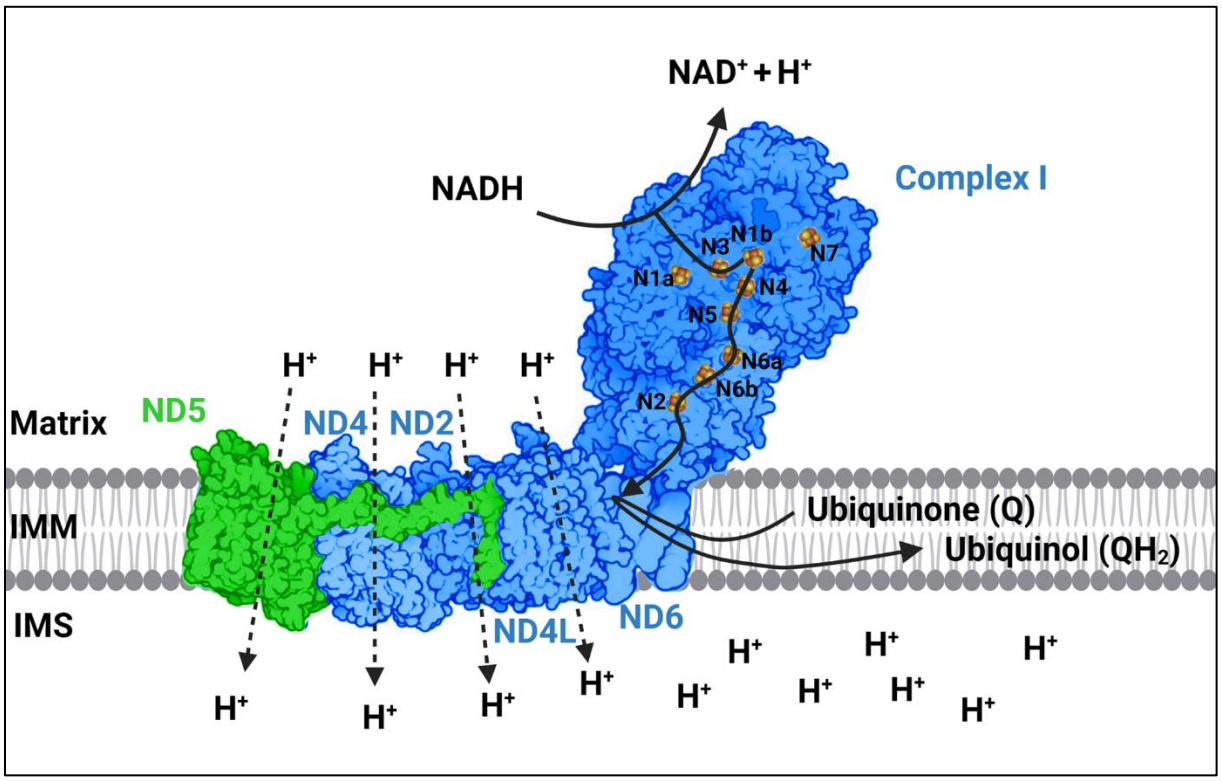

Figure 1.9: Ilustration of the structure of Cpx I from *T. thermophilus*. Core subunits of Cpx I are shown in blue. In the membrane domain, there are four antiporter-like subunits, each of which transports one proton per Ubiquinone molecule into the IMS. The bacterial subunit Nqo12 (in humans termed ND5) is highlighted in green. It provides a long amphiphatic helix extending from the most distal part of the membrane domain into the region where Ubiquinone is reduced to Ubiquinol. Nqo12/ND5 is thought to act like a piston in the catalytic reaction of Cpx I by moving all antiporter-like subunits after the reduction of Ubiquinol thereby causing the translocation of 4 protons. In consequence protons accumulate in the IMS. Nqo13, Nqo14, Nqo11 and Nqo10 correspond to subunits ND4, ND2, ND4L and ND6 in humans. For simplicity, only the latter names are labeled in the figure. Figure adapted from [158].

As mentioned above the core subunit ND5 is essential for the function of Cpx I. In addition, mutations in the genetic sequence of this highly conserved core subunit are known to cause several types of mitochondriopathies, for example, the Leigh Syndrome (LS) [159]. LS is a neurodegenerative disorder that usually begins before 1 year of age and leads to death

within months or years. Usually these patients display normal development during the first months of life (≤ 7 months), followed by the loss of the acquired skills, hypotonia due to cardiomyopathy, eye symptoms (e.g. nystagmus) and global developmental delay [159], [160]. Also dysmorphic features, spasticity, muscle weakness and even paralysis may occur [160]. In general, the term “mitochondriopathies” comprises diseases that are caused by either sporadic or inherited mutations in nuclear or mitochondrial encoded genes, that induce defects in mitochondrial function resulting in the deterioration of cellular energy supply and the entire metabolism of cells [161]. The respective disease symptoms are primarily noticeable in tissues that have a high energy consumption, including the nervous system, heart and skeletal muscles, and the optic nerve. Hence, mutations in *MT-ND5* can also lead to development of Leber’s hereditary optic neuropathy (LHON) [162]. LHON is the most common maternally inherited eye disease caused by the selective degeneration of retinal ganglion cells and their axons, resulting in the loss of the central vision and potentially blindness [163]. This disorder affects predominantly young adult males and can also be caused by other mtDNA mutations [163]. The third disease pattern attributable to mutations in *MT-ND5* is a syndrome consisting of mitochondrial encephalomyopathy, lactic acidosis, and strokelike episodes, abbreviated as MELAS [159]. The MELAS syndrome was first reported in children and is characterized by recurrent focal neurological deficits, lactic acidoses, epilepsy and a comparably short posture [164]. The striking clinical feature, the “strokelike episodes” are typically associated with a good clinical recovery, but neurological deficits accumulate over time and may progress to dementia [165]. Of note, as all mitochondriopathies, MELAS can occur in different ages with many different clinical phenotypes, ranging from hearing loss to diabetes mellitus [166]. 80% of patients suffering from MELAS carry the A3243G mutation in the mitochondrial encoded $tRNA^{Leu(UUR)}$ gene, however, in some cases it could also be traced back to mutations in *MT-ND5* [159]. At this point it should be mentioned that symptoms of LHON, MELAS and LS may also occur in overlapping syndromes and frequently so-called ragged-red fibres (RRFs) are histopathologically identified in muscle cells, representing the accumulation of morphologically and biochemically abnormal mitochondria [159], [167]–[169]. Similarly, a mutation in *MT-ND5* (G13042A) was found in a patient with an overlap syndrome of MELAS and the myoclonus epilepsy with RRFs (MERRF) [170]. Besides, it is of great importance, that mutations in *MT-ND5* have often been shown to result in a decreased activity of Cpx I [159], [169]. In general, it has been noticed that at least 40% of all mitochondrial disorders are associated with mutations in subunits of Cpx I [171].

Moreover, Cpx I is considered to be the major source of ROS production in mitochondria (along with Cpx III). ROS are important molecules in various signaling pathways, e.g. in apoptosis, but they can also exert several cell-damaging effects. Even during regular Cpx I function, the transfer of electrons to molecular oxygen via electron leaks causes the mild

production of superoxide anion radicals, the proximal mitochondrial ROS [172]. There is evidence that these superoxide anions are generated at two distinct sites of Cpx I. First, the reduced FMN in the active site of NADH oxidation has been identified in studies of isolated enzyme complexes and second, studies of intact mitochondria or submitochondrial particles have suggested a mechanism involving the Q-binding site [173]. Most likely, both sites contribute to the generation of superoxide anions and also the iron-sulfur clusters N1a and N2 are discussed to be involved [171]. In general, ROS are thought to play a role as signaling molecules to activate various cellular pathways including protein kinase C, mitogen-activated protein kinase (MAPK), PI3K, Akt, and p38 MAPK, as well as Ca^{2+} signaling [143]. Importantly, several mutations in genes encoding Cpx I subunits (amongst others in *MT-ND5*) have been linked with elevated ROS levels [174]–[176].

Several lines of evidence indicate that mitochondrial ROS generation is the major source of oxidative stress in the cell [177]. Indeed, the production of superoxide anion radicals can also lead to the formation of hydrogen peroxide (H_2O_2) and peroxynitrite ($ONOO^-$) [172]. It is assumed that lower concentrations of ROS are essential for normal cellular signaling pathways (e.g. in immune response, inflammation, synaptic plasticity), whereas higher concentrations and long-time exposure of ROS cause damage to cellular macromolecules such as DNA, lipids and proteins, ultimately resulting in necrosis and apoptotic cell death [28], [178]. Interestingly, ROS can also affect Cpx I to generate more free radials, and Cpx I-derived ROS have been shown to enhace the activity of BACE1 promoting APP cleavage through the amyloidogenic pathway [143], [179], [180] (more information in section 1.1.4). In general, ROS have been suggested to contribute to a large number of diseases associated with mitochondrial dysfunction, amongst others neurodegenerative diseases [137]. For example in AD, growing evidence links the ROS-mediated damages with molecular targets including mitochondrial function, the protein quality control system and autophagic pathways affecting the proteostasis balance [181]. In this scenario, oxidative stress should be considered as not only a major feature in the pathophysiology of AD, but also a potential target to combat the progression of the disease [181]. Likewise, Cpx I dysfunction was frequently associated with mitochondrial diseases, aging and neurodegenerative diseases, e.g. Parkison's disease (PD) [147]. So in summary, Cpx I appears to play an important role in the development and therapy of AD, which has been shown in recent publications [102], [143], [182]–[186].

1.2.5 Role of Mitochondria in Alzheimer's disease

As mentioned in section 1.1.5 the "amyloid cascade hypothesis", which was postulated by Hardy and Higgins in 1992 leaves many unanswered questions. Since Aβ peptides are natural products of the APP metabolism, this hypothesis does not explain, why the balance of

Aβ production and clearance is lost during the progression of AD. Besides, the exact mechanism by which amyloidogenic APP processing is triggered in humans is still not known. Moreover, the hypothesis disregards the fact that aging is the most important risk factor to develop LOAD. That means, the exact mechanism linking aging and AD is not known so far. Looking at mitochondria opens up avenues that could answer these unresolved questions.

Mitochondrial dysfunction in AD

Mitochondrial dysfunction is a common feature of age-related neurodegenerative diseases and mounting evidence suggests that it is an early and potentially causative event in AD [102], [187]–[190]. To date, a large body of research has demonstrated mitochondrial abnormalities in brains of AD patients. Next to glucose hypometabolism, several activity changes in mitochondrial enzymes including thiamine diphosphate (TDP), a critical coenzyme of pyruvate dehydrogenase and α-ketoglutarate dehydrogenase have been described [190]–[192]. Besides, a reduced metabolic rate of oxygen was measured in the frontal, parietal and temporal cortex of AD patients, which provides direct evidence for a reduced mitochondrial function through the ETC [188], [193], [194]. Interestingly, the cerebral metabolic rate of oxygen showed a significant correlation with the severity of dementia [194]. In line with the decreased oxygen consumption, enzyme activities in mitochondria isolated from autopsied AD brains demonstrated a generalized depression of all ETC complexes [195]. The most dramatic reduction was found for Cpx IV (alias cytochrome c oxidase), which was confirmed numerous times in the literature [191], [195]–[197]. In case of Cpx IV, the impairment is known to be caused by the direct binding of the Aβ peptide to the subunit COX1 [198], [199]. However, several groups also observed a reduced acitivity of Cpx I in AD models and brains of AD patients, among them a recent meta-analysis that evaluated 125 studies [182], [183], [200]–[202]. Likewise, proteomic and differential gene expression studies showed a downregulation of Cpx I subunits in AD brain specimen [203]–[208]. It must be mentioned, that the results vary between different studies, and apparently the findings from mitochondrial and nuclear-encoded genes need to be considered separately. Importantly, the trigger for the downregulation of Cpx I subunits and the exact mechanism for the impairment of Cpx I in AD is not fully understood. On the one hand, there is evidence that tau reduces Cpx I activity by down-regulating Cpx I subunits [202], [209]. On the other hand, Cpx I dysfunction has also been measured numerous times as a consequence of the Aβ peptide and in Aβ-based models [202], [210]–[214]. Importantly, the exact mechanism of Aβ causing Cpx I impairment is currently unclear. Merely one study investigated the interactions of $A\beta_{1\text{-}42}$ and a human brain cDNA library expressed on M13 phages and suggests that this inhibitory effect might be caused by the direct binding of Aβ to the ND3 subunit of Cpx I [215]. Of note, further studies to investigate Cpx I dysfunction in Aβ-based AD models failed to materialize.

In addition, a large number of mitochondrial parameters were found to be reduced in both AD patients and AD model systems [188], [189]. For example a reduction of the MMP, ATP levels and the respiratory control ratio (RCR) was measured in HEK cells overexpressing wild-type APP and APP carrying the Swedish mutation (KM670/671NL) [179], [216]. This was accompanied by an increase of ROS levels (determined as superoxide anion radials) and altered mitochondrial morphology [179]. Interestingly, mitochondrial dysfunction was even observed in blood cells obtained from AD patients. For example AD lymphocytes exhibited a reduced endogenous basal respiration rate and a diminished respiratory control ratio (coupled OXPHOS capacity divided by leak flux), whereas mitochondrial mass was unchanged [217]. Besides, the MMP was significantly decreased in CD4+ lymphocytes of AD patients and already in individuals with MCI [217]. Likewise, the susceptibility of Cpx I to Rotenone was enhanced and the basal level of apoptosis was reduced in these two groups in comparison to healthy controls [217], [218]. These findings are in line with numerous further studies that reported elevated ROS levels, measured as DNA damage, and elevated apoptosis in lymphocytes from AD patients and mice transgenic for human mutant APP (reviewed in [217], [219]). For this reason, mitochondrial parameters in lymphocytes are discussed as potential peripheral biomarkers for the detection of AD [102], [218].

Along with the observations mentioned so far, deficits in so-called mitochondrial dynamics were frequently reported in AD. Mitochondria are highly dynamic organelles undergoing continuous fusion and fission in the cytoplasm. This processes are essential for maintaining a healthy pool of mitochondria with proper distribution [188]. Altered size and number of mitochondria, shifted to a rather fragmented mitochondrial network have been reported in AD brains and models [179], [210], [220], [221]. Excessively fragmented mitochondria result in mitochondrial bioenergetics deficits through negative impact to the proper complex assembly that is critical for the ETC function [188]. Besides increased levels of Aβ and phosphorylated tau can induce ROS production, which causes not only fragmentation mitochondria but also promotes defective mitophagy. Mitophagy is a cellular process whereby damaged mitochondria are selectively removed and this process was also found to be impaired in AD (recently reviewed in [222], [223]). Likewise, mitochondrial axonal trafficking deficits were reported in pyramidal neurons of AD patients resulting in an abnormal distribution of mitochondria [221]. Disruption of both anterograde and retrograde transport caused by Aβ, either due to faulty mitochondria or impaired mitochondrial transport system, leads to a decreased proportion of healthy mitochondria or an increased portion of damaged mitochondria at synapses, where an extensive energy supply is needed [224]. Therefore abnormal changes in mitochondrial transport in AD are under intensive studies. Of note, overexpression and/or phosphorylation of tau is another negative regulator for mitochondrial movement and elevated calcium levels may also modulate mitochondrial transport [188].

In addition to the mitochondrial defecits mentioned above, the biogenesis of nuclear encoded mitochondrial proteins was found to be impaired in AD. For example, Qin *et al.* demonstrated the reduced expression of the peroxisome proliferator-activated receptor γ coactivator 1α (PGC-1α) in AD patients and model mice [225]. PGC-1α is considered the master regulator of mitochondrial protein expression and regulates mitochondrial respiration through interactions with transcription factors NRF1 & 2, which in turn promote the expression of TFAM [226]. Additionally, the import of nuclear encoded proteins is disturbed by oxidative stress and APP. APP forms a stable complex with mitochondrial outer and inner translocases in AD brains, which likely blocks the mitochondrial import machinery and decreases the ETC capacity [227]. Similarly, Aβ is translocated to mitochondria through interaction with TOM and accumulates at the mitochondrial christae [228]. In general, if the import of nuclear proteins is successful, the mitochondrial presequence protease (PreP) cleaves off the presequence of mitochondrial matrix proteins. This maturation process was found to be decreased in the temporal lobe of AD patients and in transgenic AD mice likely mediated to oxidative stress [229]. Interstingly, PreP is also capable of degrading $A\beta_{40}$ and $A\beta_{42}$, revealing that Aβ degradation might be impaired by the reduced PreP activity [229], [230]. Despite of the impairment of this mitochondrial protease and further evidence demonstrating accumulation of mitochondrial proteins in AD, more studies about alterations in mitochondrial proteastasis in AD are needed.

Furthermore, reduced mtDNA copy numbers were significantly reduced in microdissected pyramidal neurons from AD hippocampi compared to healthy controls [231]. Whether mtDNA variability is involved in the development of AD remains inconclusive. On the one hand, no primary mtDNA mutations were directly associated with AD, on the other hand some studies suggest that single nucleotide polymorphisms (SNPs) and germline variants (e.g. haplogroups) likely play a role in AD [188]. Besides, levels of oxidized nucleic acids in mtDNA were found to be significantly elevated in preclinical AD (PCAD) and MCI patients, which likely represents a consequence of increased mitochondrial ROS levels and points to an early involvement of oxidative stress in the pathogenesis of AD [232]. In particular levels of 8-oxoguanine and the corresponding repair enzyme 8-oxoguanine glycosylase 1 (OGG1) were increased [232]. Other modifications in mtDNA may also affect its transcription and function. For example, elevated 5-methylcytosine levels were detected in the D-loop region of mtDNA in brain samles with AD-related pathology [233]. In contrast, peripheral blood analysis of mtDNA from human AD patients revealed a decrease methylation of the D-Loop in LOAD patients [234]. Therefore, the implication of these findings to the pathogenesis of AD still remains to be explored.

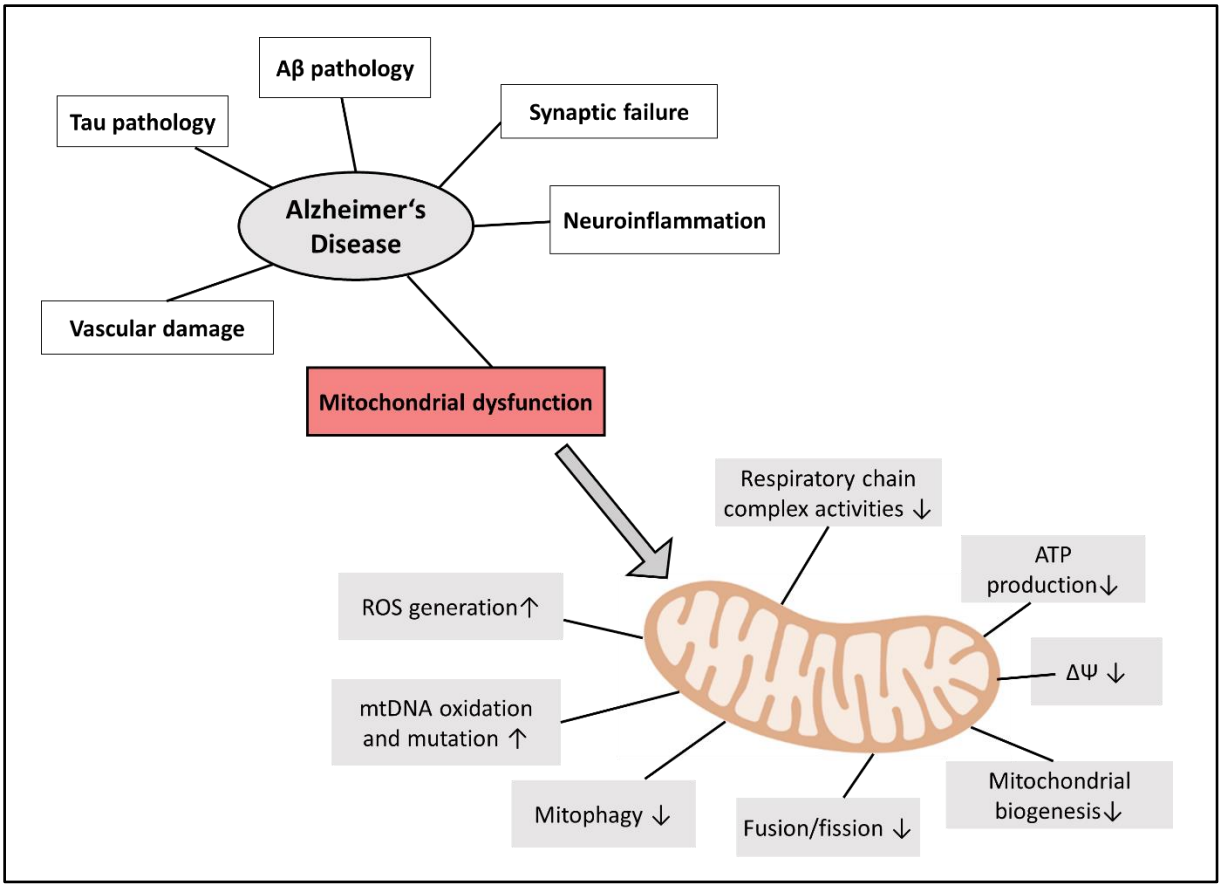

Figure 1.10: The hallmarks that characterize AD as a multifactorial disease are summarized in the top left of the figure. The lower right side focuses on mitochondria-related functions that are severely impaired in AD. Since growing evidence suggests mitochondrial dysfunction to be an early and possibly causative event in AD, this research area is of particular interest for the development of new therapeutic drugs. Figure adapted from [235].

In summary, mitochondrial dysfunction indisputably plays a pivotal role in the pathogenesis of AD. In conjunction with the much-publicized amyloid and tau pathology, mitochondrial dysfunction significantly contributes to the development of the disease and may even serve a causative function. By now, most scientists agree that AD is a multifactorial disease in which vascular damage, neuroinflammation and synaptic failure (amongst others) are additionally involved [4], [44], [235], [236]. These factors are not further discussed in this thesis, because they are not related to the investigated hypothesis. However, a comprehensive summary of the features of mitochondrial dysfunction is presented in Figure 1.10. Mitochondrial dysfunction is particularly relevant because it has been established as an early and prominent event in the neuropathology of AD. Mitochondrial defecits were frequently found before the extracellular accumulation of Aβ plaques and therefore this feature is of tremendous interest to cure or prevent pathological changes [219], [235], [237]–[239]. Besides numerous evidence indicates that restoration of mitochondrial function by therapeutic approaches or antioxidant dient offers a potential target to delay the onset or slow the progession of AD [189].

Mitochondrial dysfunction in brain aging

Mitochondrial function is known to be an important determinant of the aging process [240]. At the same time aging is the most prominent risk factor for a variety of neurodegenerative diseases including AD. This is evident from the fact that the prevalence of AD increases tremendously with age [5]. Likewise, the incidence rate increases exponentially after 60 years of age [30]. The complex mechanisms underlying brain aging are to date only partly understood, however, several hypotheses have been proposed to explain this intricate phenomenon. One salient and well-characterized alteration is that the mitochondrial efficiency is impaired in aged individuals. In a general manner, a decrease in mitochondrial OXPHOS activity, affecting the protein level and activity of ETC complexes was observed, especially for Cpx I, IV and V [28], [241]. Of note, mitochondrial efficiency and Cpx activities were also decreased in different AD models and AD patients [28], [102]. Besides, aging is marked by a gradual increase in brain oxidative stress and consequent damages e.g. oxidized proteins, lipids and nucleic acids which directly impair the cellular function [178]. This led to the “free-radicals theory of aging” which was stated in 1956 by Harman and postulates that aging is a consequence of free radicals attacking cells and tissue [242]. In general, it can be stated that ROS production and ROS degradation become imbalanced during the aging process, whereby it must be mentioned that mitochondria represent the main site of ROS formation [243]. In particular the human brain is very susceptible to oxidative stress due to thee reasons. First, it has a high oxygen demand (~20% of body basal oxygen, although it represents only 2% of the body weight) [243]. Second, polyunsaturated fatty acids are more abundant, and third, the antioxidant defense is rather low in comparison to other organs [244]. As mentioned above mitochondria are the major source of oxidative stress. ROS levels generated by OXPHOS proteins induce oxidative modifications in the mtDNA (due to their close proximity), which in turn lead to a reduced OXPHOS function and decreased ATP levels. Since neurons have high requirements of ATP, this interdependence is thought to contribute to the pathogenesis of AD [28]. Importantly, the activity of Cpx I from the ETC was frequently reported to be decreased in the aging brain and Cpx I-derived ROS appear to be a major player in the brain aging scenario [179], [245], [246]. Vice versa, the mitochondrial Cpx I is specifically susceptible to oxidative stress as it is spatially located in the inner mitochondrial membrane. Especially the iron-sulfur clusters can be a site of direct ROS attack. These oxidative modifications might in turn increase the ROS production of Cpx I. Besides 7 of the 14 essential core subunits of Cpx I are encoded in the mtDNA, which is the reason why oxidative mtDNA modification strongly affect Cpx I. In line with this, several groups reported reduced protein levels and a decreased activity of Cpx I in aged individuals and aged NMRI-mice [247], [248]. As mentioned above, an impairment of Cpx I, increased ROS levels, and mitochondrial dysfunction were also found in

AD models and patients. Since mitochondrial dysfunction increases with age, it has been proposed that this feature represents the missing link between aging and LOAD [28].

Mitochondrial cascade hypothesis

The mitochondrial cascade hypothesis was first stated in 2004 by Swerdlow and Kahn [249]. In contrast to the amyloid cascade hypothesis, Swerdlow and Kahn first placed mitochondria at the beginning of the pathological cascade that ultimately leads to neuronal death in AD. According to them, genetic variations in both nuclear and mitochondrial genes encoding ETC proteins and a resulting reduced ETC activity are the main culprit for the development of LOAD. Defects in the respiratory chain are accompanied by an individually enlevated ROS production rate. The increase of oxidative stress attacks mtDNA, which further exacerbates mitochondrial dysfunction. In addition, ROS stimulate the formation of Aβ from APP, which in turn causes multiple mitochondrial deficits. These mutual damages of the mtDNA, ETC complexes and other mitochondrial components culminate in mitochondrial dysfunction leading to a reduced cellular energy supply, impaired neuroplasticity and finally cell death as one major pathomechanism underlying the continuum from brain aging over mild cognitive impairment to initial and advanced LOAD. As described above elevated ROS levels are a major characteristic of aging, so the mitochondrial cascade hypothesis offers an attractive explanation for why advancing age is the main risk factor for AD. Of note, the mitochondrial cascade hypothesis does not reject the amyloid cascade hypothesis, but rather states that the amyloid cascade is triggered by mitochondrial dysfunction. The literature often refers to the chicken-and-egg controversy because it cannot be clearly proven whether mitochondrial dysfunction causes Aβ overproduction or vice versa. However, there are many findings supporting the role of mitochondrial dysfunction as the main culprit in LOAD. For example, Aβ does not harm cells that were artificially depleted of mtDNA (ρ^o) and therefore lack a functional ETC [214]. This potently argues that a direct Aβ-mitochondria interaction is highly relevant in AD. Besides, epidemiologic studies found that among affected parents of AD subjects, females were overrepresented [250]–[252]. This may be a hint that maternally inherited genetic factors contribute to the AD risk, pointing to mtDNA gene mutations as a potential trigger. Likewise, mitochondrial DNA haplogroup variations and SNPs also seem to affect an individual's risk of developing AD [253]–[256]. However, the results across different mtDNA association studies have not been consistent, which has led to some concerns about the reliability of individual reports [241]. Furthermore, cytoplasmic hybrid (="cybrid") studies of persons with LOAD showed that the mtDNA at least partly determines the mitochondrial ETC efficiency, OXPHOS capacity and ROS production [257], [258]. AD cybrid lines also exhibited an altered calcium homeostasis, a lower MMP, an abnormal mitochondrial morphology, an activation of the molecular stress response pathway, higher levels of apoptosis proteins and an excessive Aβ

aggregation (reviewed in [241]). In addition, it is known that the mtDNA acquires mutations during the course of an individual's life, especially the brain, as it represents the tissue with the greatest rate of oxidative metabolism and a concomitant high ROS production [259], [260]. According to the mitochondrial cascade hypothesis, mtDNA mutational burden within individual cells reaches a threshold at which resultant mitochondrial dysfunction becomes critical. So by exceeding an individually different threshold, the accumulation of damages and the lack of ATP initiates a collapse in cellular bioenergetics leading to cellular dysfunction, and ultimately neuronal death and dementia. As mentioned above, mitochondrial ETC function was consistently reduced in brains of aged individuals. It was also evidenced that a decreased ETC activity shifts the non-amyloidogenic α-secretase mediated processing of APP towards the β-secretase mediated processing pathway. This was shown by inhibition of Cpx I with Rotenone and the inhibition of Cpx IV with sodium azide [179], [261], [262]. These findings argue that amyloidogenesis follows mitochondrial dysfunction. Likewise, mitochondrial dysfunction is more anatomically widespread in AD than Aβ deposits, which suggests that mitochondrial dysfunction cannot entirely be attributed to Aβ [263]. There are even hints, that tau phosphorylation might be promoted by mitochondrial dysfunction, as AD fibroblasts exposed to an ETC uncoupler displayed elevated Tau levels [264] and inhibition of Cpx IV increased tau phosphorylation in rats [265]. So in summary, the mitochondrial cascade hypothesis posits that mitochondrial dysfunction represents the primary pathology in LOAD that drives both Aβ plaques and tau tangle formation.

Within the framework of the mitochondrial cascade hypothesis, Cpx I of the respiratory chain occupies a specific role. Since Cpx I dysfunction has been consistently reported in aged animals and humans, this may provide the link between aging and the development of AD. As Leuner *et al*. postulated in 2012, Cpx I dysfunction might be the starting point and driving force of the above mentioned amyloid cascade hypothesis, as Cpx I-derived ROS enhance amyloidogenic APP processing. This was impressively demonstrated in four steps (see Figure 1.11). First, they demonstrated that inhibition of Cpx I by the potent Cpx I inhibitor Rotenone leads to an increase of superoxide anion radicals and cellular ROS in HEK cells. Second, they detected a significant increase of the BACE1 activity in HEK APPwt and APPsw cells (both transfected with an plasmid coding for wild-type APP or APP including the Swedish mutation), which were shown to displayed markly elevated basal ROS levels. In the third step, increased $A\beta_{1\text{-}40}$ levels were measured in HEK cells after incubation with Rotenone (24 h, 25 µM). This was impressively restored by Vitamin C (1000 µM). This indicates on the one hand, that ROS enhance the amyloidogenic processing of APP to Aβ and on the other hand, that this shift can

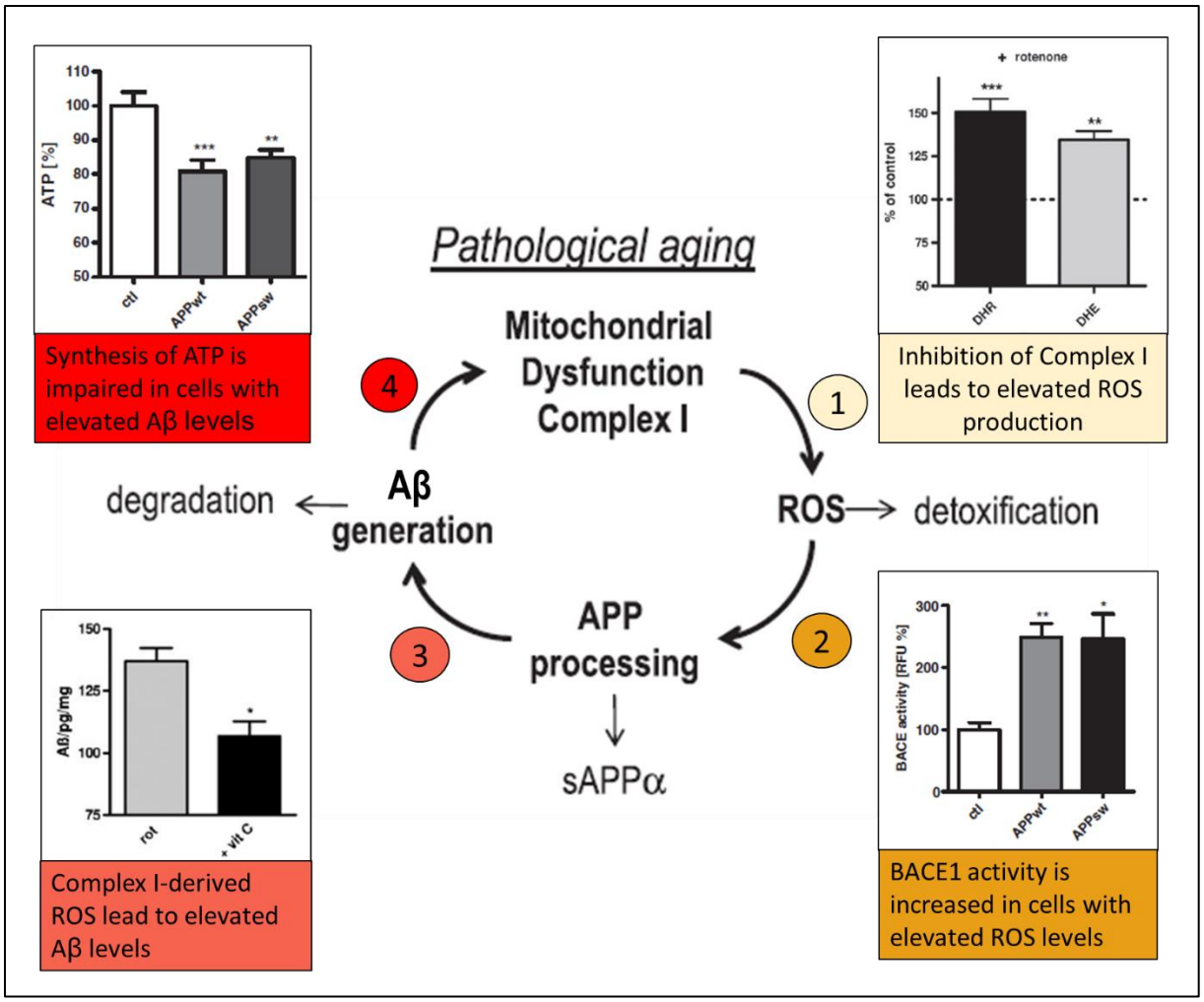

Figure 1.11: Schematic illustration of mitochondrial dysfunction in pathological brain aging ultimately leading to AD. In the normal aging process of the brain, there is a balance between mitochondrion-derived ROS, APP processing and Aβ generation on the one side, and ROS detoxification and Aβ degradation on the other side. During the development of AD, this equilibrium is disrubted as Cpx I-derived ROS enhance the activity of BACE1 and more Aβ is generated. Aβ further impairs mitochondrional function, thereby creating a vicious circle. (1) Superoxide anion radicals measured by dihydroethidium (DHE) and cytosolic ROS measured by dihydrorhodamin (DHR) in HEK cells after 2 h of treatment with Rotenone (25 µM). (2) BACE1 acitivity in untransfected HEK control cells (ctl) and HEK cells transfected with a plasmid coding for wildtype APP (APPwt) or for APP including the swedish mutation (APPsw). Both transfected cell lines showed higher ROS levels in previous experiments (data provided in [179]). RFU= relative fluorescence units. (3) $A\beta_{1\text{-}40}$ levels in HEK cells after 24 h treatment with Rotenone (rot) (25 µM) and after ROS scavenging by vitamin C (vit C) (1000 µM). (4) ATP levels were significantly decreased in HEK APPwt and APPsw cells in comparison to untransfected controls (ctl). Both cell lines showed elevated ROS levels and $A\beta_{1\text{-}40}$ in previous experiments (data provided in [179]). Figure and graphs adapted from [179], where more information about the experimental details can be found.

be mediated by Cpx I-derived ROS. In a fourth step, elevated Aβ levels were in turn shown to attenuate mitochondrial function, as demonstrated by lower ATP levels in HEK APPwt and APPsw cells. This results in a vicious circle between mitochondrial dysfunction, elevated ROS levels and amyloidogenic APP processing, which is initiated by Cpx I dysfunction. This is of particular importance, because Cpx I dysfunction and elevated ROS levels are common characteristics of aging. It can therefore be assumed that these events intiate a viscious cycle,

which is further accelerated by genetic and environmental factors and the gradual increase of Aβ levels over years and decades [28], [102]. Besides several groups showed that hyperphosphorylated tau also induces Cpx I dysfunction which further fuels this viscious cycle [202], [209], [266], [267]. When an individual threshold is reached and compensatory mechanisms fail to cope, the resulting reduced ATP generation leads to cellular and synaptic dysfunction, which ultimately causes to neurodegeneration and dementia. So together with other AD-associated risk factors such as the APOE4 status, low physical and cognitive activity, genetic mutations or other diseases, mitochondrial dysfunction might be the crucial factor of the initiation of the AD pathology. Of note, recent data suggest that the combined effect of oxidative stress due to aging and slightly elevated Aβ levels initiate AD long before the clinical onset [268]. Likewise, in a Cpx I deficient mouse model (due to inactivation of the subunit Ndufs4), Aβ levels were increased and this alteration was observed even before the occurance of notable pathology or behavioral effects [179].

The fact that an increase of ROS leads to an elevated Aβ production via up-regulation of BACE1 has also been demonstrated by many other groups [180], [261], [269]. Whether this is caused by an impairment of Cpx I directly by Aβ or by Aβ aggregation in an alternative way is unclear. Besides the exact mechanism of ROS generation in AD is not entirely clarified. Nevertheless, many indications suggest that mitochondria are the driving force of the amyloid pathology ultimately leading to LOAD. One impressive example is the case of a 53 year old woman who developed AD-like Aβ plaques due to mitochondrial dysfunction alone (MELAS patient with a point mutation in the (mt)tRNA$^{Leu(UUR)}$ gene) [270]. The significant role of mitochondrial dysfunction also implies that mitochondria represent an attractive target for the future treatment of LOAD.

1.3 *N*^{1}-Methyladenosine (m^{1}A)

1.3.1 RNA modifications

DNA and RNA contain, next to the four canonical nucleobases (Adenine (A), Cytosine (C), Guanine (G) and Thymine (T) in DNA or Uracil (U) in RNA), a number of modified nucleosides that extend their chemical information content [271]. RNA is particularly rich in modifications, which is obviously an adaptation to its highly complex and variable functions [271]. To date, more than 170 RNA modifications have been characterized, and recent publications announcing new modifications indicate that this list is most likely not yet complete [272]–[274]. This phlethora of modifed nucleosides is introduced post-transcriptionally and ranges from methylations over hydroxylations to more complex structures, e.g. in the case of Wybutosine (yW) or Queuosine (Q). The latter two representatives exhibit extensions of the

heterocyclic structure, which is why they are so-called hypermodified bases. The most commonly occurring modifications are methylations at different positions of the nucleobase, such as 5-methylcytidine (m^5C) or 6-methyladenosine (m^6A) or methylations at the 2'-O of the ribose, such as 2'-O-methyladenosine (Am). The nomenclature of modifications is thereby primarily oriented by the basic structure of the nucleobase and the indexed number represents the modified position. For instance, "m^1A" is an adenosine with a methylation at position 1 of the purine nucleobase (see Figure 1.12A). If the ribose is modified, the nucleobase (and a potential modification within the nucleobase) is mentioned first followed by the ribose modification. An example would be "Am", which represents a 2'-O-methylated adenosine. A further type of nucleotide modification involves atomic substitution, as in the case of 4-thiouridine (s^4U), which is formed from Uridine through oxygen-sulfur substitution [275]. In general, the vast majority of hitherto identified RNA modifications occurs in tRNA, which is also the most widely studied RNA species in this regard [276]. mRNA and rRNA are modified to a lesser exent, but are also of great importance due to their implication in the protein biosynthesis. Furthermore, RNA modifications have been reported in long noncoding RNA (lncRNA), microRNA (miRNA), circular RNAs (circRNAs) and small nuclear RNAs (snRNAs) [276]–[278].

RNA modifications have been identified across all three kingdoms of life. Some of those modifications are highly conserved in different life domains, whereas others are specific for a particular branch or even group of species [277]. Examples of modifications that have been identified in bacteria as well as in archaea and eukarya include 7-methylguanosine (m^7G), m^1A and Am [277]. Dependent on organism and RNA type, modifications vary in abundance and composition, and their functions range from being crucial for the functionality of highly abundant and extensively modified tRNA [279] to being major players in the mRNA-associated regulation of gene expression [280]. Human rRNAs are highly modified with 228 sites detected in the human 80S ribosome [281]. Interestingly, only 14 different types of modification were found in this case, comprising mainly 2'-O methylated nucleotides (Nms) and pseudouridine (Ψ) and a few base modifications [281]. In contrast, tRNAs are also highly modified, but display a high variety of RNA modifications. Just as with rRNAs, the quantity and composition of modified sites in tRNA greatly differs between different species. For example, tRNAs from gram-negative and gram-positive bacterial species (e.g. *E. coli*) exhibit methylations at seven different positions, while the thermophilic bacterium *T. thermophilus* shows some extra tRNA methylation sites [277]. tRNA modification profiles in eukaryotes are comparatively well conserved from yeast to humans, with only a few additional sites discovered in higher eukaryotic tRNAs. In contrast, eukaryotic mitochondrial tRNAs are sparsely modified, with only few methylations found at positions 26, 37 and 54 in *S. cerevisiae* and at position 9, 10, 32, 34*, 48*/49*/50*, 54 and 58* in mammals (*asterisk signifies transiently formed modifications)

[277]. Similarly, mRNAs exhibit relatively low stochiometries of modifications that differ greatly in their composition compared to tRNA and rRNA. A recent study from 2021 even showed that the modification patterns are sufficient to distinguish different RNA species (tRNA, mRNA, 28S-rRNA and 18S-rRNA) from each other [282]. This fact is obviously related to the different functions of the mentioned RNA species in the cellular organization. As mentioned earlier, RNA modifications can exert a variety of cellular functions, inculding the stabilization of secondary structures (in tRNA), facilitating an efficient and accurate protein synthesis through the ribosome (in rRNA), modulation of the protein biosynthesis (in mRNA) and many more [280], [283]–[286]. Besides, they are increasingly recognized as modulators of pathophysiology in the context of mRNAs [287]–[292]. The multitude of modifications and their myriad interactions, newly coined and extended the term "epitranscriptome".

RNA modifications are dynamic and reversible, involving catalysis of various effector proteins capable of depositing and removing them. Collectively, these proteins are known as RNA-modifying proteins (RMPs), which fall into three groups: So-called “writers” are enzymes that deposit RNA chemical marks, “eraser” are enzymes that remove them, and “readers” selectively recognize and bind to specific RNA modifications. Due to the many different roles of RNA modifications and their involvement in various diseases it follows that mutations and dysregulations of RMPs are also associated with human diseases including cancer, genetic birth defects and neurological diseases [287], [293], [294].

1.3.2 m^1A structure and characteristics

The RNA modification m^1A (=m^1rA) was discovered for the first time by D.B. Dunn in 1961 and shortly thereafter, he was able to isolate the modified mononucleotide from RNA [295], [296]. m^1A denotes an adenosine base with a direct cyclic methylation at the N^1 of the purin nucleobase (see Figure 1.12A). Therefore m^1A carries a positive charge under physiological conditions, similar to N^3-methylcytidine (m^3C) and N^7-methylguanosine (m^7G), dramatically changing its electro-chemical interactions [297]. As a consequence, the pK_a value at N^6 of m^1A was found to be 8.25 at 25°C [298]. Of note, the protonated m^1A form can rearrange to m^6A, which is favored by alkaline conditions (so-called “Dimroth rearrangement”) [298]. Both the positive charge and the steric hindrance by the N^1-methylgroup in m^1A perturb the canonical Watson-Crick (WC) base pairing of A:T or A:U (see Figure 1.12B). Therefore, m^1A leads to alterations of the secondary structure and RNA-protein interactions on the one hand, and to misincorporations and truncations during reverse transcription (RT) reactions on the other hand. Misincorporations in the complementary cDNA strand are a result of an unstable mismatch with other nucleosides by forming Hoogsteen (HG) base pairs enabled by rotation of the purine base ~180° around the glycosidic bond [299]. In DNA, N^1-

methyldeoxyadenosine (m^1dA) is considered as a form of alkylation damage, which also leads to false base pairing and genomic mutations and thus needs to be repaired [300]. Interestingly, m^1A forms HG base pairs in B-DNA but not in A-RNA. This is likely due to the higher flexibility of the deoxyribose ring lacking the 2'-OH group, which leads to an accommodation of m^1dA-dT HG base pairs in DNA. In contrast, the five-membered sugar in A-RNA is more rigid, thermodynamically disfavoring HG base pairs and disrupting m^1rA-rU duplex structures. Of note, stably formed m^1rA-dT HG base pairs have been observed in [299], explaining the high propensity of m^1A to cause mismatch in cDNA. Moreover, m^1A displays a high rate of strand elongation stall in RT reactions, which is why it is a so-called "hard-stop modification", as are m^3C and *N*^{1}-methylguanosine (m^1G) [301]. Both misincorporations and truncations, together with nucleotide skipping events provide a specific RT signature, which can be used to detect and quantify m^1A methylation levels depending on the used reverse transcriptase [302]. Whenever m^1A is mentioned in the following thesis, it refers to RNA modification (m^1rA), not DNA modification (m^1dA).

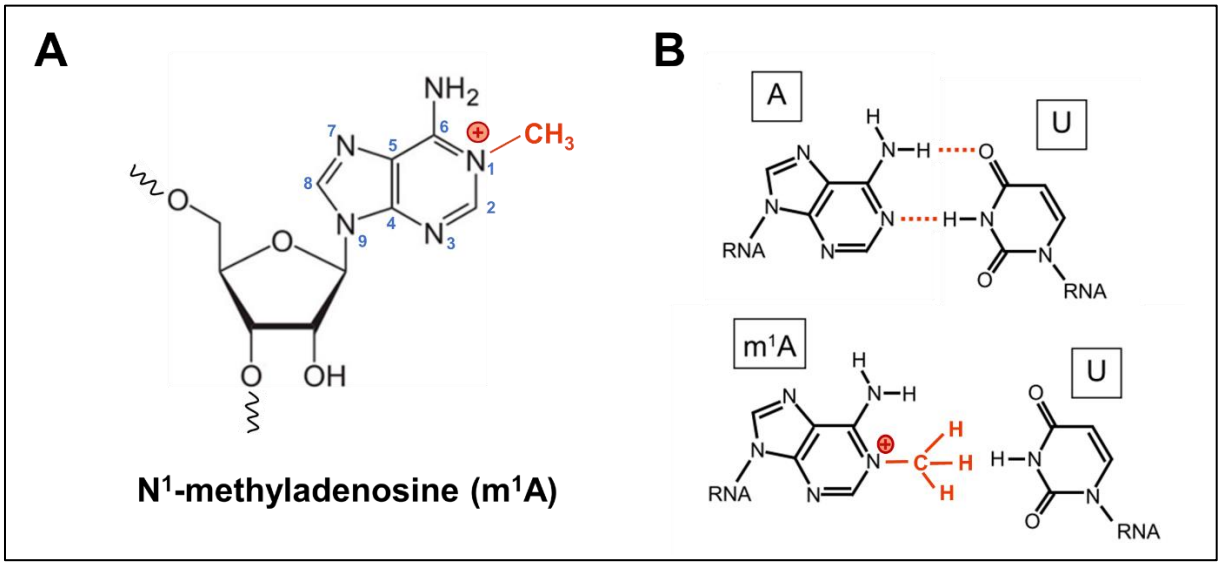

Figure 1.12: N1-methylation of adenosine confers a positive charge on the nucleobase. A) Chemical structure of m^1A. The features highlighted in red (methylgroup and positive charge at N^1) distinguish m^1A from the unmodified counterpart adenosine (A). Standard numbering convention of purin nucleotides is indicated in blue. **B)** The *N*^{1}-methylation in adenosine disturbs Watson-Crick base pairing with Uridine (U). Figure adapted from [303] and [304].

m^1A is among the top 25 most-studied RNA modifications [305]. It is a prevalent and reversible post-transcriptional modification that decorates different RNA species with high abundances in tRNAs and rRNAs and low levels found in mRNAs [306]. In tRNAs of bacteria, archaea and eukaryotes it occurs at position 9, 14, 16, 22, 57 and 58 [305]. Whereas m^1A^9 and m^1A^{58} in mammalian tRNAs are the most explored and most frequent spots, m^1A^{14} has only been identified in cyt(tRNA)^{Phe} from mammals, m^1A^{22} has only been detected in bacterial tRNA, and m^1A^{57} has been identified only transiently in archaea [303], [306]. m^1A^{16} is unique to human

(mt)tRNA^{Arg} and its frequency is approximately 20% [307]. Besides, in mitochondria, the m^{1}A^9 modification is quite abundant and has been found in 11 (mt)tRNA species, while m^{1}A^{58} is a minor modification with a 17% frequency found in 4 (mt)tRNA species [307]. For rRNAs, an m^{1}A site located in the peptidyl transfer center of the ribosome is conserved in yeast (m^{1}A^{645} in 25S-rRNA) and humans (m^{1}A^{1322} in 28S-rRNA) [284], [305], [308]. Likewise, m^{1}A^{947} is conserved between vertebrates in the 16S-rRNA of mitochondrial ribosomes [309]. In contrast, the abundance of m^{1}A in mRNA has long been a subject of controversy. Using a commercial antibody directed against the m^{1}A nucleobase, m^{1}A residues were first estimated in 2016 to range from thousands to tens of thousands, with high frequencies found in the 5'-untranslated regions (5'-UTRs) of cytosolic mRNAs [310], [311]. Almost at the same time, in 2017, diverging data suggested a much lower number of m^{1}A in mRNAs in the low double-digit range, comprising 9 sites in cytosolic mRNAs, 5 sites in (mt)mRNAs, and one site in the lncRNA *MALAT1* [312]. Interestingly, m^{1}A^{1374} in the mitochondrial encoded ND5 mRNA was among the few consensual sites and was even confirmed by a third independent research group [313]. Since a limited specifity for the above mentioned commercial antibodies was reported by two different groups in 2019, most scientists by now agree that only a small number of m^{1}A sites are present in mRNAs [305], [313], [314].

The functions of m^{1}A vary depending on RNA species and modified position. For instance, the well-studied m^{1}A^9 and m^{1}A^{58} modifications found in both cytosolic and (mt)tRNAs have been linked to structural stability and correct folding of tRNAs. This has been investigated in detail for the human (mt)tRNA^{Lys}, where m^{1}A^9 prevents the A^9-U^{64} WC base pairing thereby shifting the equilibrium between an extended hairpin structure and the functional "L-shape" structure in favor of the latter one [279], [283], [315]. In case of m^{1}A^{58}, a higher structural thermostability was observed in modified tRNAs from *Thermus thermophilus* [316]. In addition, the m^{1}A^{58} methylation of cytosolic tRNAs was shown to enhance protein translation efficiency [317]. Besides, there is evidence that m^{1}A levels in tRNA increase dynamically in response to oxidative stress, as exemplified with H_2O_2 in yeast [318]. In both mitochondrial and cytosolic rRNA, m^{1}A stabilizes tertiary rRNA interactions and seems to be involved in proper ribosome function [308], [309]. Besides, recent studies based on technical advances in analytical chemistry and high-throughput sequencing methods have revealed crucial roles of m^{1}A mRNA modification in gene expression regulation and biological processes [306]. The numerous effects of m^{1}A in mRNA are described in detail in section 1.3.4.

1.3.3 Writers, readers and erasers of m^{1}A

As a dynamic and reversible post-transcriptional RNA modification, m^{1}A can be installed by methyltransferases (writers), removed by demethylases (erasers) and recognized by m^{1}A-

dependent RNA-binding proteins (RBPs) (readers). Depending on organism, RNA species and position, different enzymes take over these functions, while one enzyme can also be responsible for several sites. The methyltransferase complex for m^1A^{58} in cytosolic tRNA was first identified in *Saccharomyces cerevisiae* comprising the non-catalytic subunit Trm6 (=tRNA methyltransferase 6) and the catalytic subunit Trm61 [319]. While Trm6 is responsible for tRNA binding, Trm61 is crucial for binding the ubiquitous cofactor S-adenosyl-L-methionine (SAM) and the catalytic function [320]. The conserved homolog of this complex in humans consists of TRMT61A and TRMT6 [321] (an overview of m^1A-modifying proteins in humans is given in Figure 1.13). The demethylases for nuclear-encoded tRNAs all belong to the AlkB family of Fe(II)/α-ketoglutarate-dependent dioxygenases, including α-ketoglutarate-dependent dioxygenases AlkB homolog 1 (ALKBH1), ALKBH3 and α-ketoglutarate-dependent dioxygenases FTO (FTO) [306], [322], [317]. For the two m^1A sites in yeast 25S-rRNA the two adenine-N(1)-methyltransferases Rrp8 and Bmt2 were reported for m^1A^{645} and m^1A^{2142} respectively [323]. The human homolog of Rrp8 is nucleomethylin (NML), which catalyzes the only m^1A site at position 1322 in the 28S-rRNA [308]. NML possesses a Rossmann-fold methyltransferase-like domain that binds to SAM, which also acts as a methyl donor in this case [324]. The m^1A reader protein YTH domain-containing family protein 3 (YTHDF3) was identified in HEK293T cells, because it showed a high ability to bind to a human 28S-rRNA-derived m^1A sample, which was detected via RNA immunoprecipitation analysis [325]. As indicated above, tRNA methylating proteins can also be responsible for the methylation of other RNA species. For example, the TRMT6/TRMT61A complex was shown to mediate m^1A modificiation in cytosolic mRNAs [312]. This complex requires a consensus GUUCRA motif and a tRNA T-loop-like structure for substrate recognition in mRNAs, which is similar to tRNA recognition [312]. Moreover, it was proposed that m^1A in mRNA can be demethylated by ALKBH3 [310], [311], [326], and that YTHDF1-3 and YTH domain containing protein 1 (YTHDC1) act as m^1A readers [327], [328].

In mitochondria, tRNAs are methylated at position 9 by a bipartite complex consisting of the tRNA methyltransferase 10 homolog C (TRMT10C) and the short chain dehydrogenase/ reductase family 5C member 1 (SDR5C1) (see Figure 1.13). In this complex, TRMT10C acts as catalytic core and is needed for tRNA binding, while SDR5C1 forms a tetramer, which is thought to fulfill a scaffolding function (more information in section 1.4). The TRMT10C-SDR5C1 complex displays dual specifity as it is also able to catalyze m^1G^9 modification in mt-tRNAs [329]. Interestingly, there are hints that this complex as well methylates m^1A^{1374} in the mitochondrial ND5 mRNA, as m^1A-induced mismatches dramatically increased after overexpression of TRMT10C in HEK293T cells and decreased after treatment with siRNA [312]. Of note, it is currently unclear whether SDR5C1 is also mandatory for m^1A methylation

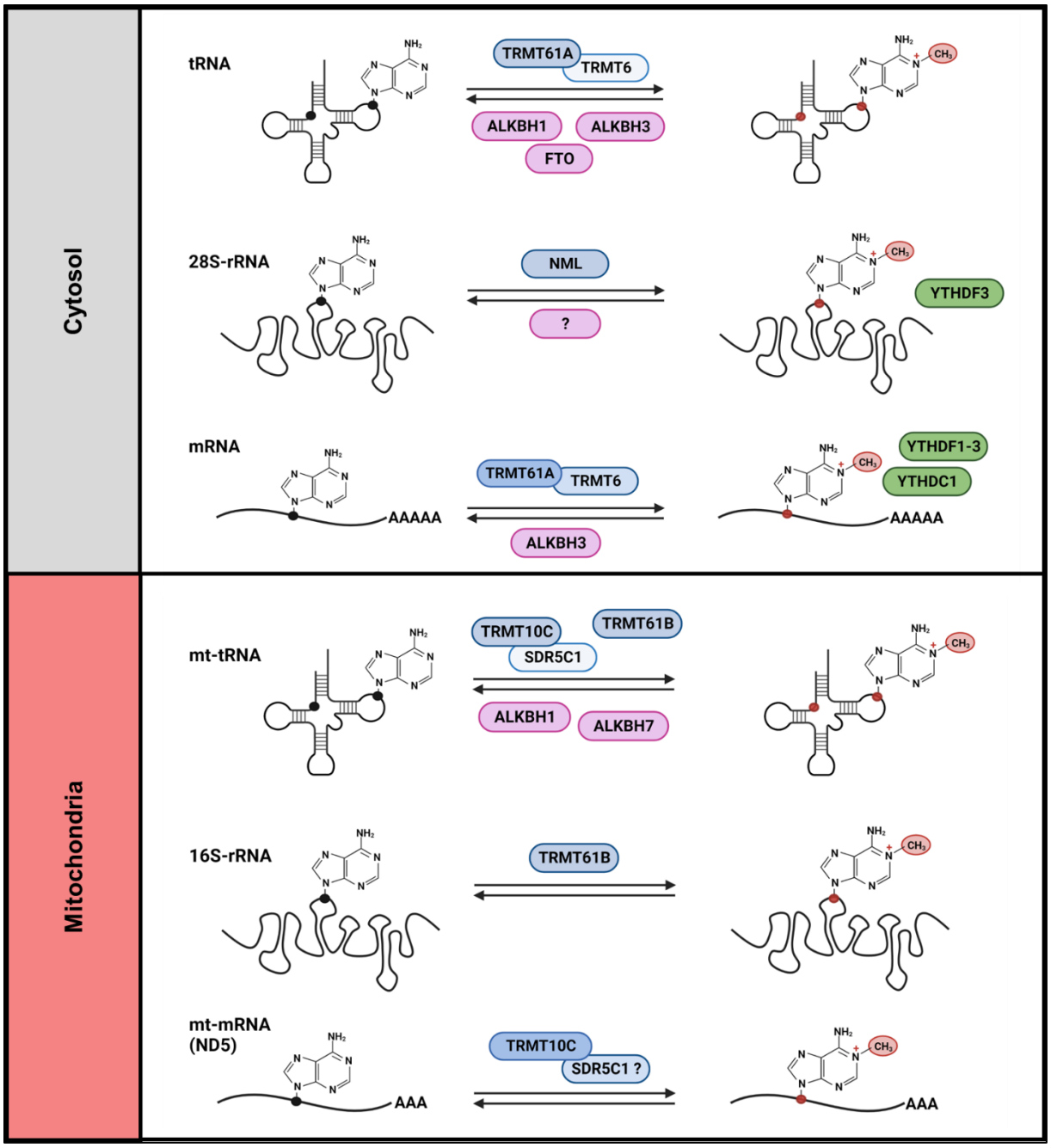

Figure 1.13: Overview of the most important m^{1}A-modifying proteins for different types of RNA in humans. The nuclear (top panel) and mitochondrial (bottom panel) encoded RNAs are reversibly methylated by m^{1}A writers (shown in blue, with dark blue indicating the catalytic core subunit of the methylase complex), demethylated by m^{1}A erasers (pink), and bound by m^{1}A-dependet RBPs/ m^{1}A readers (green). TRMT= tRNA methyltransferase, ALKBH= α-ketoglutarate-dependent dioxygenase alkB homolog, FTO= α-ketoglutarate-dependent dioxygenase alkB homolog FTO, NML= nucleomethylin, YTHDF= YTH domain-containing family protein, YTHDC1= YTH domain-containing protein 1, SDR5C1= short chain dehydrogenase/reductase family 5C member 1. Figure adapted from [306].

in this case. The methyltransferase TRMT61B is also responsible for several m^{1}A sites, namely m^{1}A^{58} in several mt-tRNAs and m^{1}A^{947} in the mitochondrial 16S-rRNA [309], [330]. The assumed eraser enzymes in mt-tRNA are ALKBH1 and ALKBH7, as knockout of ALKBH1

increased the level of m^1A^{58} in mt-$tRNA^{Lys}$ and knockout of ALKBH7 led to higher methylation levels in pre-tRNAs [331], [332].

1.3.4 Implications of m^1A in mRNA

According to [333], m^1A in mRNA accounts for ~0.01% of all adenosines in mammalian cell lines. So unlike m^6A, wich is the most abundant internal mRNA modification (~0.5% m^6A/A), m^1A quantities are relatively low [282], [333], [334]. However, the effects of m^1A on the structure and function of RNA are stronger in comparison to m^6A, due to the presence of the additional positive charge in the modified nitrogen [335]. Several current studies suggest that the m^1A methylation does affect the fate of mRNAs via interactions with reader proteins on the one hand, and direct effects on the ribosome on the other hand. For instance, one publication suggests that the binding of YTHDF2 to m^1A sites in cytosolic mRNAs leads to destabilization and decay of the modified transcripts, in a similar manner as m^6A [328]. Similarly, a recent study from 2022 reported that m^1A in the ATP5D (nuclear encoded subunit of mitochondrial complex V) mRNA negatively regulates its translation, probably due to increased binding to YTHDF1 [336]. Besides, another study claims that the binding of YTHDF3 to m^1A decreases the abundance and promotes degradation of the insulin like growth factor 1 receptor (IGF1R) mRNA [325]. However, this study should be taken with caution because an antibody-preenrichment has been used to detect m^1A in this case, and the presence of m^1A in the IGF1R mRNA has not been verified by other groups. In studies using *in vitro* systems, m^1A at position 2 of a codon triplet in mRNA has been shown to severly inhibit peptide bond formation by the ribosome, reducing the rate of peptide bond formation by three orders of magnitude [337]. Likewise, Hoernes *et al.* reported an inhibitory effect of m^1A on translation in HEK293T cells, transfected with synthetic modified transcripts [338]. In this case, the impediment of m^1A was even indepent of the position within the codon triplet. In line with this, coupling polysomal fractionation with the detection of m^1A-induced mismatch revealed lower mismatch rates in the heavy polysomal fractions [312]. This indicates the inefficient translation of m^1A-containing transcripts and was observed for both cytosolic (e.g. PRUNE and BRD2) and mitochondrial encoded mRNAs (ND5). Similarly, the enhanced decay of Aurora A mRNA (a master suppressor of ciliogenesis) and the inhibition of its translation was reported after depletion of ALKBH3 [339]. As ALKBH3 is assumed to be the eraser of m^1A in the Aurora A mRNA, this data supports the idea that m^1A leads to translation repression and enhances mRNA decay. Conversely, overexpression of ALKBH3 enhanced mRNA stability and protein level of CSF-1, a cytokine which leads to poor prognosis in ovarian and breast cancers [340]. Likewise, the targeted m^1A demethylation with a CRISPR-Cas13d-based tool (called “REMOVER”) increased the stability of PRUNE1 mRNA and the lncRNA MALAT1 [326]. Only

Li *et al.* [341] and Dominissini *et al.* [311] reported an increased translation efficiency of cytosolic m^1A-modified transcripts, however, it was shown that these studies exhibited considerable methodological deficits [314], [342]. In summary, there is much evidence to suggest that m^1A in mRNA inhibits the translation process, either by interacting with reader proteins or by directly affecting the ribosome.

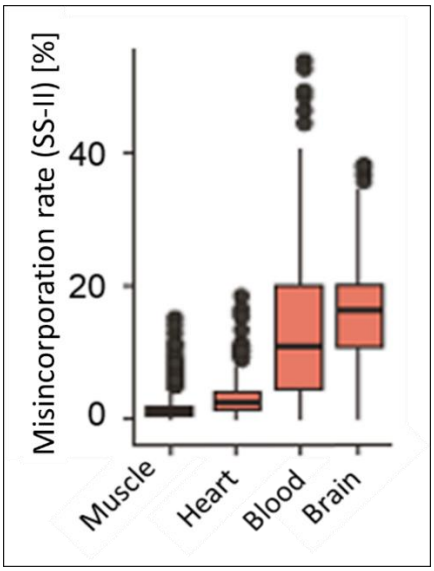

Figure 1.14: m^1A methylation levels in ND5 mRNA are highly tissue-specific. Misincorporation rates at position 1374 in ND5 mRNA after RT with SuperScript II (SS-II). Reanalysis of publicly available RNA-seq data obtained from the GTEx collection. Data and graph adopted from [312], for clarity reasons the graph has been abridged.

Another interesting hypothesis is that m^1A-methylated transcripts are protected from degradation e.g. in stress granuli in the event of acute stress. Firstly, Alriquet *et al.* detected higher m^1A levels in stress granuli than in the cytosolic mRNA pool, and observed higher protein levels derived from an m^1A-modified synthetic mRNA after heat shock than derived from an equivalent unmodified transcript [343]. Secondly, Safra *et al.* postulated that m^1A would mark particularly stable transcripts in the development of oocytes [312]. This assumption arose because they observed extremely high m^1A levels (~75% mismatch) at position 1374 of the mitochondrial ND5 mRNA in oocytes and comparably low levels in blastocytes, where the zygotic mitochondrial transcription already started. The hypothesis was further confirmed by the incubation of HEK293T cells with Actinomycin D, which induces transcriptional arrest. The longer the incubation with Actinomycin D was, the higher the m^1A-induced mismatch rates in ND5 were detected, further supporting the link between m^1A methylation and mRNA stability [312]. Interestingly, this publication also demonstrated a highly tissue-specific distribution of m^1A^{1374} in ND5 by analyzing > 9000 RNA-seq datasets obtained from the GTEx collection. Thereby, low m^1A methylation levels were observed in muscle and heart tissue, whereas comparably high levels were observed in blood and brain tissue. Considering the stabilizing

function of m^1A in ND5 proposed by Safra *et al.*, this might enable the long transit of mRNAs through the axon (from the nucleus of a neuron to the synapses).

1.3.5 RNA modifications in AD

RNA modifications have been associated with a large variety of diseases, most notably cancer and neurological disorders [287]. In the case of AD, many links have been drawn to m^6A and m^6A-associated writer, reader and eraser proteins. For instance, several studies reported the reduced expression of methyltransferase-like protein 3 (METTL3), a writer and reader of m^6A, in AD model mice and human AD brains (reviewed in [344]). The treatment of rat primary neurons with Aβ significantly reduced protein levels of METTL3, and vice versa, overexpression of METTL3 rescued Aβ-induced synaptic loss and cognitive impairment in mice [345]. In addition, the m^6A eraser FTO was overexpressed in cells and mice treated with $Aβ_{1-40}$, again suggesting lower m^6A methylation levels in AD [346]. Interestingly, m^6A methylation also interferes with the expression of Aβ-related proteins, such as APP and BACE1, e.g. m^6A readers affected the translation of APP mRNA and the splicing of BACE1 [347]. Moreover, there is much evidence that m^6A is involved not only in the metabolism of Aβ but also in that of tau. For example, METTL3 accumulation positively correlated with levels of insoluble neurofibrillary tangles in postem AD brains [348]. In brains of a 3xTg AD mouse model, the upregulation of FTO was observed to activate the phosphorylation of tau and accelerate the pathological hallmarks of AD [349]. In addition, the absence of m^6A writers and erasers (METTL3, METTL14 and YTHDF) enhanced tau toxicity in a *Drosophila* AD model [350]. Even in mitochondrial dysfunction, which plays a significant role very early in the pathogenesis of AD, m^6A seems to be involved. For instance, inhibition of FTO ameliorated mitochondrial dysfunction in astrocytes of a strepotozotocin-induced AD cell model, indicating that m^6A RNA methylation is required for a proper mitochondrial function [351]. Likewise, m^6A is engaged in the regulation of oxidative stress, another important factor in the development of AD. Arsenit-induced oxidative stress altered m^6A methylation levels and the m^6A readers YTHDF1 and 3 were found to promote stress granuli formation [352], [353]. Besides, METTL3 seems to attenuate oxidative stress and in consequence its knock-down led to synaptic loss and neuronal death *in vivo* [345]. Even in the function of microglia and the regulation of anti-inflammatory and proinflammatory responses, m^6A has been implicated [347]. As growing evidence suggests that the overactivation of microglia contributes to the pathogenesis of AD, this is of particular interest. In general, numerous publications have shown that m^6A and its readers and erasers play an essential role in the human brain, in both brain development and synaptic plasticity, the basis of all learning and memory processes [354]. So in summery, m^6A

and m^6A-related proteins are crucial for the human brain's function and they have been associated with numerous AD-related pathologies.

Apart from m^6A, a recent study has linked the RNA modification m^1A to AD for the first time [355]. This group detected lower methylation levels in 5xFAD mice at position 9 of 4 mitochondrial tRNAs and at position 58 of 15 cytosolic tRNAs. Interestingly, the hypomethylation correlated with a reduced tRNA expression only in mitochondrial but not in cytosolic transcripts. Besides, they observed significantly decreased protein and mRNA levels of the m^1A writer TRMT10C and its enzymatic partner SDR5C1 in cortices of 5xFAD mice. In a tau-based *Drosophila* AD model they further demonstrated that the knock-down of TRMT10C (=roswell in flies) and SDR5C1 (=scully in flies) aggravates tau toxicity. Although this study suffers from shortcomings, e.g. no information about age and sex of the mice is given, it provides evidence that m^1A RNA methylation is implicated in the pathogenesis of AD. In line with that, a RNA-Seq study performed with laser capture microdissected astrocytes from AD subjects and healthy elderly controls, detected significantly lower mRNA levels of TRMT61B, the writer enzyme of m^1A^{58} in (mt)tRNAs [356].

In comparison, a rather unspecific analysis of RNA fragments revealed that the modification pattern of certain RNA fragments differs between AD patients and healthy controls [357]. For instance, in the 15-20 nucleotide (nt) fraction of prefrontal cortex RNA a significant increase of Cm, m^7G, Gm and m^3C, and a significant reduction of $m^{2,2,7}G$ and $m^{2,2}G$ was detected. These alterations were partly specific for vascular or non-vascular AD. A similar but slightly different pattern was observed for the 30-40 nt RNA fraction of these samples, and beyond that, the percentage of tRNA-derived fragments (tsRNA) was increased in AD patients. As RNA sequencing of these samples yielded reductions of certain tsRNA and rRNA-derived fragments (rsRNA), this study clearly indicates that the composition and modification pattern of small RNAs is altered in AD.

Lastly, it is worth noting that defecits in adenosine to inosine (A-to-I) RNA editing have been reported in AD. A-to-I editing is an epigenetic mechanism that alters the coding part of mRNAs, which may lead to recoding and amino acid substitution in the resulting protein, potentially modifying its biochemical properties. Editing levels were diminished mainly in the hippocampus and to a lesser extend in the temporal and frontal lobe of AD patients [358]. As A-to-I editing is performed by the ADAR (adenosine deaminase acting on RNA) enzyme family, these proteins were also investigated and an altered mRNA expression of ADAR1 and ADARB1 has been observed. These results, together with the above mentioned findings, indicate that RNA modifications and their corresponding enzymes are clearly involved in the pathogenesis of AD, and further investigation might open up new avenues for the development of therapeutic strategies against AD.

1.4 TRMT10C

1.4.1 TRMT10C: Structure, functions and family members

TRMT10C is a multifunctional protein that plays a pivotal role in the maturation of mitochondrial RNAs and is thus critical for the mitochondrial function. In humans, it fulfills three different tasks. First, it constitutes part of the mtRNase P complex, which cleaves pre-(mt)tRNAs at their 5'-ends, thereby liberating all RNA species from the primary mitochondrial transcript [359] (more information in section 1.4.2). Second, it catalyzes the N^1-methylation of adenosine and guanosine residues at position 9 (m^1R^9) in (mt)tRNAs [329]. And third, it was shown to install the m^1A site at position 1374 in the mitochondrial encoded mRNA of ND5 [312]. From this multitude of functions it follows that several synonyms for TRMT10C (=tRNA methyltransferase 10 homolog C) exist, e.g. MRPP1 (=mitochondrial RNase P protein 1) or RG9MTD1 (RNA Guanine-9 methyltransferase domain containing 1). Besides, the homolog in *Drosophila melanogaster* is called "roswell", while in mice and rat TRMT10C is used as well.

The gene *TRMT10C* is encoded in the nucleus in chromosome 3 (location: 3q12.3)[10]. The full protein comprises 403 amino acids with a molecular mass of ~47 kDa, but a splice variant of 292 amino acids also exists[11]. The basal isoelectric point is 9.4 and several post-translational modifications, such as phosphorylation and acetylation have been detected[12]. Like almost all mitochondrial proteins, TRMT10C is transcribed in the nucleus, translated in the cytosol, and then imported into mitochondria. Therefore it contains a mitochondrial target sequence (MTS) with a length of 39 amino acids [360]. In general, MTS are about 15-70 amino acids long and bear positively charged residues, that direct the transport of proteins into mitchondria [361]. These canonical sequences are located at the N-terminal of a given protein and consist of an alternating pattern of hydrophobic and positively charged residues. In the case of TRMT10C, the MTS is also ahead of the N-terminal domain (NTD) (see Figure 1.18). The NTD is involved in pre-(mt)tRNA binding and enables dimerization of a TRMT10C homodimer [362]. In addition, TRMT10C features a dual-specificity C-terminal methytransferase domain (MTD) linked to the NTD by a short adapter sequence [360]. Both the NTD and the methyltransferase domain are required for the methylation of (mt)tRNAs at position 9 [362]. The corresponding methyl group donor in this case is the typical cofactor SAM. Of note, though TRMT10C harbors the catalytically active methyltransferase domain, it additionally requires the presence of SDR5C1 to fulfill its function of m^1R^9 methylation [329], [362]. Moreover, using recombinant proteins it was observed that TRMT10C alone is able to

[10] https://www.genecards.org/cgi-bin/carddisp.pl?gene=TRMT10C
[11] http://www.ensembl.org/Danio_rerio/Gene/Splice?db=core;g=ENSDARG00000041575;r=1:508885-513786
[12] https://www.phosphosite.org/proteinAction.action?id=23682&showAllSites=true

bind to (mt)tRNAs (probably via the C-terminal region), but the binding is enhanced by SDR5C1 [329]. As both proteins are needed for m^1R^9 methylation, it was assumed that SDR5C1 may either assist in a direct interaction with pre-(mt)tRNAs or stabilize a catalytically important structural element in TRMT10C. For the sake of completeness, it must be said that not all (mt)tRNAs carry a purine at position 9. For instance, the (mt)$tRNA^{Met}$ contains a C at position 9 and is therefore not methylated by TRMT10C and SDR5C1 [307]. Regarding the m^1A methylation at position 1374 in the mitochondrial ND5 mRNA, it can be assumed that TRMT10C as well requires assistance of SDR5C1, because (except for the surrounding sequence) adenosines in mRNA and tRNA are structural analogous. However, this has never been experimentally proven so far. As further explained in section 1.4.2, TRMT10C and a tetramer of SDR5C1 are also part of the mtRNase P complex, together with the protein only RNase P catalytic subunit (PRORP). For this reason SDR5C1 is also referred to as MRPP2 (=mitochondrial RNase P protein 2). Interestingly, the TRMT10C-SDR5C1 subcomplex also enhances the efficiency of 3'-end processing catalyzed by the mitochondrial RNase Z (mtRNase Z) [363]. This protein encoded in the *ELAC2* gene cleaves mitochondrial pre-tRNAs at their 3'-end and is therefore necessary, just like mtRNase P, to release (mt)tRNAs from the primary mitochondrial transcript [364]. Intriguingly, the processing of the mitochondrial precursor transcript occurs in a precisely defined sequence. First, the TRMT10C-SDR5C1 subcomplex binds to pre-(mt)tRNAs and methylates the A or G at position 9, then PRORP affiliates the subcomplex and cleaves pre-(mt)tRNAs at their 5'-end. Thereafter, TRMT10C and SDR5C1 retain the (mt)tRNA product and promote the 3'-end processing by mtRNase Z [120], [363]. Of note, mtRNase P and mtRNase Z are responsible for cleavage of both the heavy and the light mitochondrial precursor transcript. Besides, it can be stated that the TRMT10C-SDR5C1 complex represents a tRNA maturation platform, because it also presents the nascent tRNA to the mitochondrial CCA-adding enzyme and enhances its activity [363]. This enzyme catalyzes the 3'-terminal addition of a CCA triplet, completing the three core processing steps that are required for nearly all (mt)tRNAs.

TRMT10C belongs to the large superfamily of SPOUT RNA methyltransferases, which harbor a characteristic SpoU-TrmD (SPOUT) fold. SpoU (previous name of TrmH) and TrmD were originally considered to be unrelated, however, about two decades ago a bioinformatic study suggested that they share a common evolutionary origin [365]. Hence a single superfamily was formed and named the SPOUT superfamily. These proteins act as tRNA modifying enzymes in archaea, prokaryotes and eukaryotes, and catalyze the SAM-dependent N^1-methylation of specific purine residues, pseudouridine or the 2'-O-methylation of ribose moieties [366]. Next to tRNA, also rRNA and mRNA can be modified by SPOUT proteins [277], [312], [367]. Historically, SPOUT enzymes have been the 4th unrelated type of SAM-dependent MTase structures determined bei X-ray crystallography, hence named "class IV". By

comparison, “Class I” of RNA methyltransferases (MTases) are Rossmann-fold MTases, representing the largest superfamily of SAM-dependent MTases, as they comprise RNA and DNA MTases [303]. Examples of Rossmann-fold MTases are TRMT61A and TRMT61B mentioned in section 1.3.3.. SPOUT MTases are the second largest superfamily [303]. Interestingly, all MTases responsible for m^1A modification belong to either the Rossmann-fold or the SPOUT superfamily of MTases. Since both groups utilize SAM as methyl donor, m^1A methylation is linked to the occurrence of ATP and methionine, the precursors of SAM catabolism [303]. A number of crystal structures solved by the structural genomics initiative revealed a common fold of SPOUT MTases, the so-called “α/β knot” fold. This unusual “α/β knot” fold describes a conserved topology of the common core in SPOUT proteins and can therefore be called “SPOUT fold”. This SPOUT fold is the catalytically active domain and binds the SAM cofactor [368]. The typical architecture of this active site comprises a parallel β-sheets of 5-7 strands, sandwiched between two layers of 5-8 α-helices [367]. This α/β knot fold comes in two subtypes, which differ in the number of flanking α-helices, with TRMT10C belonging to subtype 2 [303]. Many SPOUT MTases contain next to the SPOUT fold additional nucleic binding domains, indicating their primary function as MTases towards nucleic acids. As mentioned above, TRMT10C belongs to the superfamily of SPOUT MTases, however, these MTases are further divided into subfamilies named either “Trm” or “Trmt” followed by a numer (e.g. Trm10) or a letter (e.g. TrmD), depending on the kingdom of origin for the enzyme. TRMT10C belongs to the Trm10 subfamily [366]. These enzymes all catalyze the SAM-dependent methylation at position 9 in tRNAs, but display different specificities. For instance, yeast Trm10 and the human TRMT10A enzyme, which catalyze cytosolic tRNA methylation are specific for m^1G^9 [303]. In contrast, Trm10 of the archaeon *S. acidocaldarius* exhibits m^1A^9 specificity [303]. Thus, the dual specificity for m^1G^9 and m^1A^9 of the human TRMT10C in mitochondria represents an unusual ability. In general, many SPOUT enzymes form a dimer structure to exert their catalytic function. However, it was reported that yeast Trm10 and the archaeal Trm10 (aTrm10) are monomeric enzymes, meaning that catalytic pockets are formed in one subunit [369], [370]. Notably, some scientists argue for a separation of Trm10 and aTrm10 families to be distinguished as independent enzyme families, because a recent crystal structure study revealed that the catalytic amino acid residues in aTrm10 are different from those in Trm10 [369]. Besides is it worth to mention, that the m^1G^9 modification in tRNA seems to be regulated by the relative amounts of substrate tRNA and the Trm10 enzyme, because overexpression of Trm10 in yeast lead to m^1G^9 modification in tRNAs that are normally unmodified [371].

Higher eukaryotes encode up to 3 Trm10 paralogs (TRMT10A, B and C) and all three are encoded in the human genome. Remarkably, the methylation activity and substrate specificities of these enzymes are distinct. TRMT10A is most similar to Trm10 in *S. cerevisiae*

and methylates a subset of nuclear-encoded tRNAs in the cytosol. Interestingly, it is specific for m^1G9, whilst TRMT10B is the first m^1A^9-specific tRNA MTase found in eukaryotes [372]. In consequence, the old name for TRMT10B RG9MTD3 (=RNA guanosine-9 methyltransferase domain containing 3) is by now inappropriate. Of note, neither all cytosolic tRNAs that have G9 are methylated by TRMT10A *in vivo*, nor all tRNAs containing A9 are methylated by TRMT10B. A recent study even suggests that TRMT10B is responsible for only one nuclear-encoded tRNA [372]. Yet, it is unclear how the respective enzymes identify their corresponding target tRNA. Interestingly, TRMT10A and B do not require an additional partner protein for the methylation process [372]. So the fact that TRMT10C requires SDR5C1 for catalysis is unusual and contrasts with all functionally characterized Trm10 enzymes. Besides, TRMT10C has the ability to catalyze both m^1G^9 and m^1A^9 methylation and is a strictly mitochondrial MTase [329], [373]. So TRMT10C virtually takes over the function of TRMT10A and TRMT10B in mitochondria. This dual specificity is surprising considering that N^1 of guanosine is protonated at physiological pH, while the N^1 of adenosine is not [372]. Furthermore, it is interesting to note that neither Trm10 nor TRMT10A and B are essential for the growth of yeast or human cell lines, respectively [372], [374]. Nonetheless, loss-of-function mutations in TRMT10A are associated with a severe neurodevelopmental disorders and early-onset diabetes [294], [375]–[378]. The reason why mutations in TRMT10A only affect particular tissues (brain and pancreas), although this enzyme should in theory be important in all tissues, is unclear.

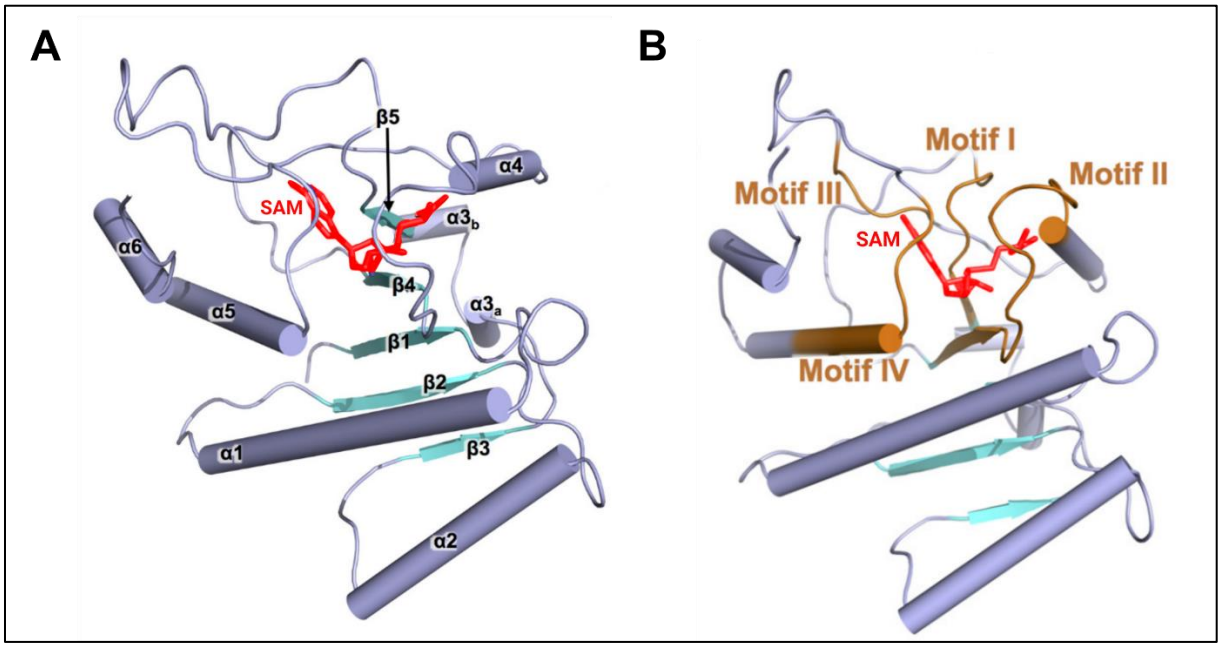

Figure 1.15: Crystal structure of the typical α/β knot fold in TRMT10C. A) Cartoon representation of TRMT10C methyltransferase domain (MTD). SAM ligand is shown in red sticks, helices α1-6 are labeled in purple, strands β1-5 are labeled in cyan. **B)** Slightly rotated structure from A), the four conserved motifs of the Trm10 familiy are labeled in brown. Figures adapted from [362].

The exact mechanism of how TRMT10C performs the N^1 methylation of A^{1374} in the mitochondrial mRNA ND5 is so far unknown. However, in 2017, a crystal structure of TRMT10C MTD was published illustrating the catalytically active site and the binding of the cofactor SAM (see Figure 1.15A) [362]. This publication revealed the MTD secondary structure consisting of 5 β-sheet strands flanked by 6 α-helices, representing the canonical α/β knot fold of SPOUT enzymes. SAM is embedded between β4 and β5, and surrounded by the four typical motifs I-IV that are highly conserved within the Trm10 family (see Figure 1.15B). SAM is hold at place by hydrogen bonds between its adenine, ribose and methyl moiety and several polar amino acids, among them lysine and glutamine residues, and the canonical aspartate 314, which is suggested to act as the general base to enable the m^1R^9 methylation process [329]. However, the exact mechanism of m^1A methylation is not resolved so far. There are only hints for the N^1 methylation of G^9 in (mt)tRNAs, since a cryo-EM structure of TRMT10C-SDR5C1-PRORP and the pre-$tRNA^{Tyr}$ was resolved in 2021 [360]. This structure revealed that the MTD of TRMT10C is located next to the pre-tRNA substrate and contacts its acceptor-, D- and anticodon arm (see Figure 1.16A). The pre-tRNA is positioned and held in place through interactions with the NTD of TRMT10C and SDR5C1, explaining why both are required for the methylation process (more illustrations in [360]). The MTD of TRMT10C is positioned directly adjacent to the region surrounding G^9, which is flipped out of the tRNA fold and buried into the active site. Within the binding pocket several amino acids are thought to keep the guanosine at place, mainly glutamine and asparagine residues via hydrogen bonds [360]. These polar amino acids potentially ensure the selectivity for purines over pyrimidines. The SAM cofactor is also embedded in the active site and is completely surrounded by TRMT10C. In this process, motif 2 of TRMT10C occupies a special role, because its asparagin 314 (D314) is directed to the N^1 of guanosine, where it withdraws electron density and thus facilitates the uptake of the methyl group from SAM. For this reason, the asparagine at this site is highly conserved and corresponds, for example, to D210 in human TRMT10A and D235 in human TRMT10B [372]. Interestingly, in archaeal homologs, a second asparate residue was proposed to be specifically required for adenosine methylation [369]. However, according to sequence alignment, this second aspartate is not conserved in human TRMT10B or TRMT10C. The exact mechanism of purine methylation has been studied most extensively for guanosine (m^1G), e.g. in studies on the m^1G^{37} specific SPOUT family member from *H. influenzae* showed that first the N^1 atom is deprotonated by an aspartate or glutamate residue (general base) and then, the resulting negative charge the adjacent O atom is stabilized by an arginine residue (intermediate charge stabilzer) [379]. Subsequently, the activated N^1 atom starts a nucleophilic attack on the reactive methyl group of SAM, generating m^1G and S-adenosyl homocysteine (SAH) as reaction products [380]. As mentioned above, the mechanism for formation of m^1A is not fully elucidated

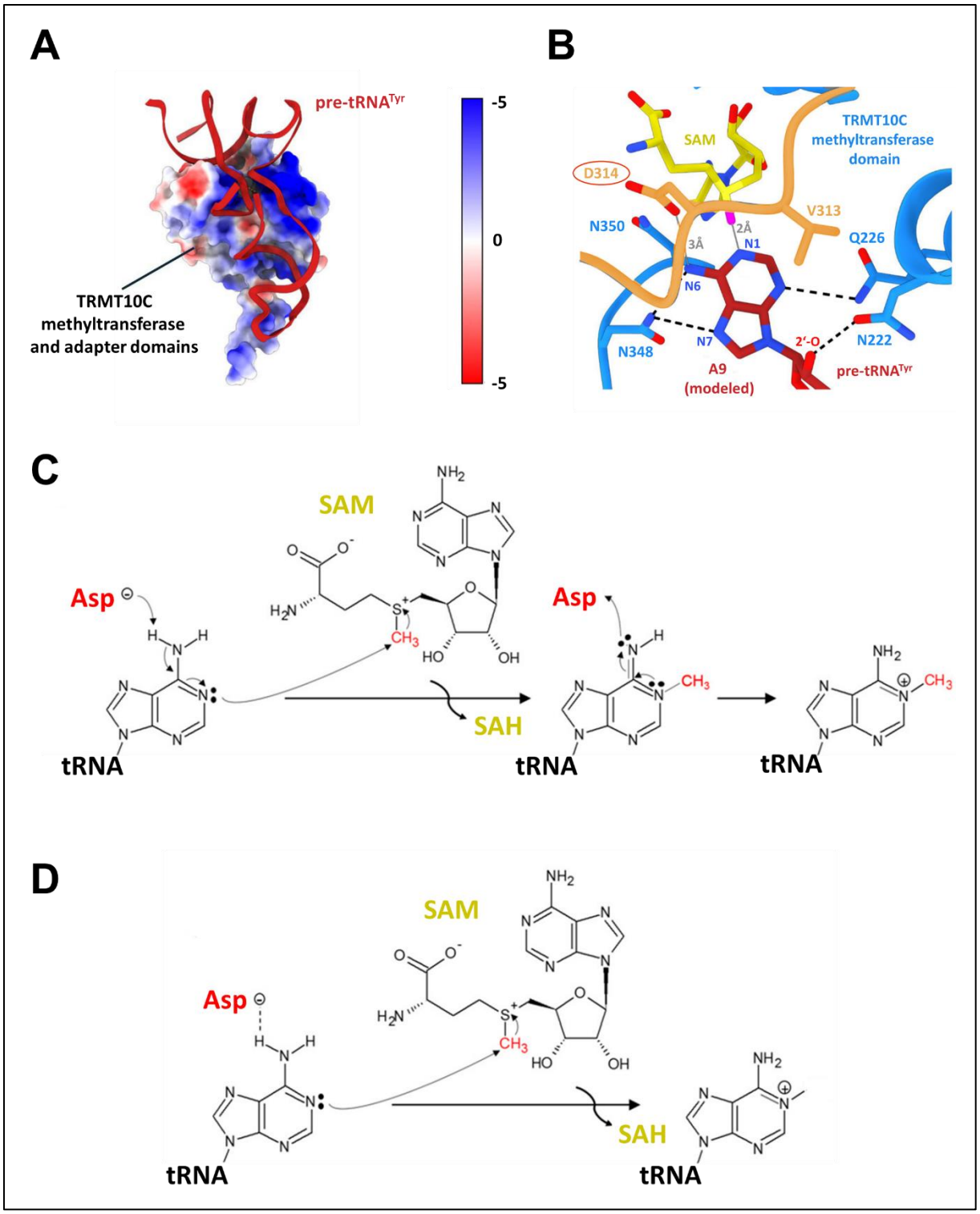

Figure 1.16: Mechanism of N^1 methylation on adenine bases by TRMT10C. A) Electrostatic surface potential for TRMT10C methyltransferase and adapter domains. The tRNA backbone (red) interacts with positively charged regions on the TRMT10C surface. **B)** Close-up view of the active methyltransferase site in TRMT10C including SAM and A^9 from pre-$tRNA^{Tyr}$ in the pre-catalytical mode. Adenine was modeled in the active site by computational replacement of guanine by adenine in the SAM-bound crystal structure. The aspartate residue (D314), which is suggested to initiate the catalytical mechanism is encirceled in red. Motif II residues of TRMT10C are shown in brown, hydrogen bonds are labeled as dashed black lines, nitrogen atoms are show in blue, oxygen atoms in bright red, the transferable methyl group in pink. Distances between A9-N1 and D314-N6 are shown as solid grey lines. **C)** Suggested mechanism for m^1A methylation in SPOUT enzymes, based on studies with TrmI and m^1A^{58}. In this version aspartate is the catalytic base. **D)** Alternative suggested mechanism for m^1A methylation…

…based on studies with TrmI and m^1A^{58}. In this version aspartate serves merely to position the cofactor and methylation site for the reaction. Figure A)+B) adapted from [360], figure C)+D) adapted from [303].

yet. Nevertheless, two mechanisms have been proposed [303]. In the first, mechanism, a deprotonation by asparatat takes place as the initial step (see Figure 1.16C). Since the N^1 atom of guanosine is protonated under physiological conditions, whereas the N^1 of adenosine is not, this step is thought to occur at the exocyclic N^6 atom, resulting in the formation of an imino tautomer. In consequence, the lone pair of the N^1 atom for nucleophilic attack is activated and attacks the reactive methyl group of SAM. The second mechanism is similar, with the difference that aspartate does not deprotonate the N^6 atom, but rather serves to position the target adenosine for the methylation reaction with SAM (see Figure 1.16D). A computational model in which guanine in the above-mentioned crystal structure of TRMT10C was substituted for adenine, confirms this assumption (see Figure 1.16B) [360].

1.4.2 mtRNase P

As mentioned above, TRMT10C forms part of the mtRNase P complex, which is responsible for processing of mitochondrial RNAs and thus constitutes a key event in the mitochondrial gene expression. In humans, the mtDNA is transcribed by POLRMT (with the help of several transcription factors), which generates polycistronic primary transcripts that comprise (mt)rRNAs and (mt)mRNAs, flanked by (mt)tRNAs (more information in section 1.2.2.). Therefore the endonucleolytic cleavage of (mt)tRNA sequences at their 5’ and 3’ borders liberates all (mt)RNA species (with some few exceptions). These processing steps are performed at the 5’-end by mtRNase P and at the 3’-end by mtRNase Z in transcripts of both the heavy and the light mtDNA strand. Whereas mtRNase Z alias ELAC2 is a single-subunit enzyme, mtRNase P is a tripartite complex consisting of TRMT10C, SDR5C1 and PRORP (see Figure 1.17) [359], [364]. The TRMT10C-SDR5C1 subcomplex is also responsible for the m^1R9 methylation of (mt)tRNAs, a step which is thought to precede the cleavage process [329]. In order to produce functional mitochondrial RNAs, all transcripts undergo further maturation steps. For example, (mt)mRNAs are differentially polyadenylated by mtPAP (more information in section 1.2.2). In the case of (mt)tRNAs, several chemical modifications are installed, a CCA-triplet is added and the corresponding amino acid is attached via aminoacylation. The 16S and 12S (mt)rRNAs are also chemically modified and folded, and subsequently form the mitoribosome together with an $(mt)tRNA^{Val}$ and several proteinaceous subunits [381]. Finally, the assembled mitoribosome, (mt)mRNAs and (mt)tRNAs come together in the translation apparatus enabling the protein biosynthesis of all mitochondrial encoded proteins.

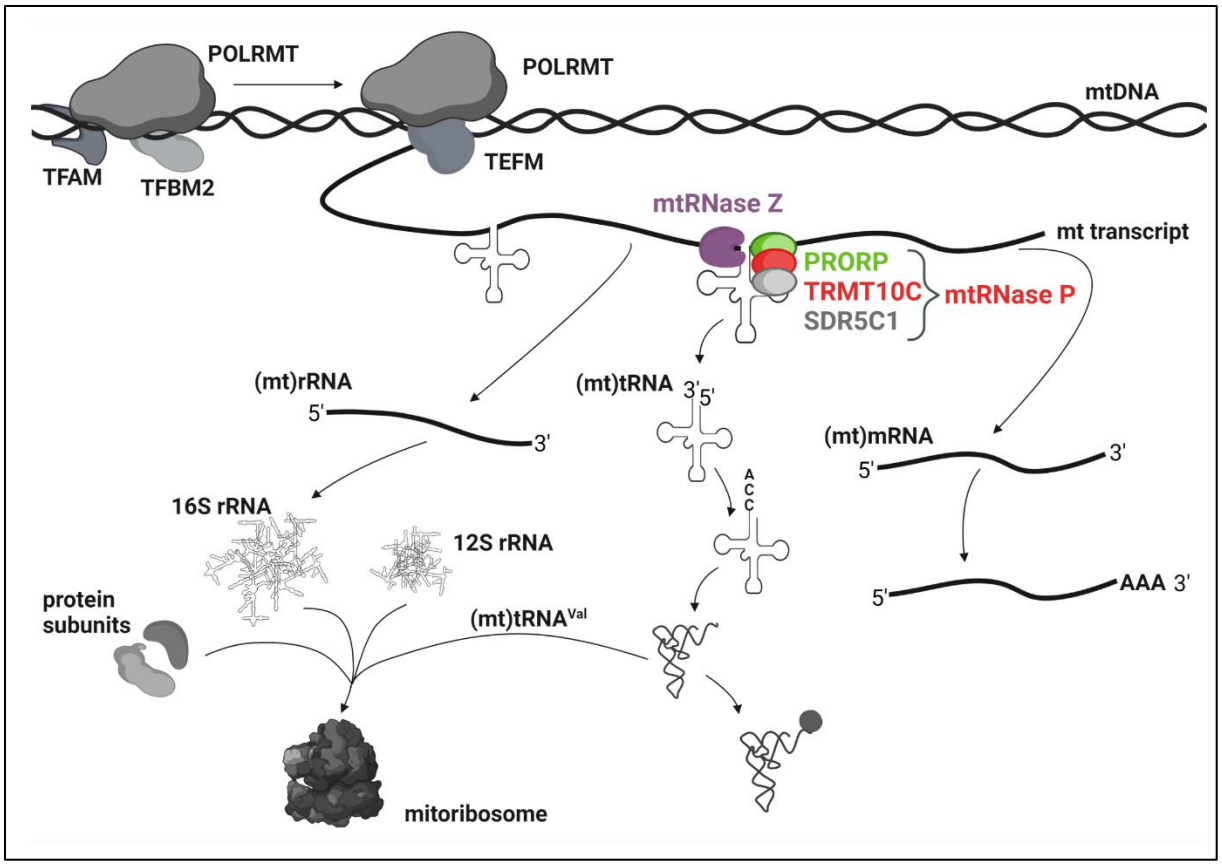

Figure 1.17: Overview of transcription and RNA processing in human mitochondria. The initiation of transcription requires the association of the mitochondrial RNA polymerase (POLRMT) with two transcription factors (TFAM and TFB2M). During the elongation process POLRMT is accompanied by the mitochondrial transcription elongation factor TEFM. The processing of (mt)tRNAs from the polycistronic mitochondrial primary transcript (mt transcript) is performed by mtRNase Z and mtRNase P at the 3'- and at the 5'-end respectively and likely occur cotranscriptionally. The mtRNase P consists of 3 subunits: PRORP, TRMT10C and SDR5C1 (simplified representation). The liberated (mt)rRNAs are processed, chemically modified, and form together with (mt)tRNA^{Val} and proteinaceous subunits the mitochondrial ribosome (mitoribosome). (mt)tRNAs are extended with a CCA triplet, chemically modified, and the corresponding amino acid is added via aminoacylation. (mt)mRNAs are differentially extended with a polyA tail. Figure adapted from [381].

In general, RNase P enzymes are responsible for processing the 5' border of pre-tRNAs in all three kingdoms of life. In most bacteria, archaea and many eukaryotes, they are ribozymes composed of a catalytic RNA and a varying number of accessory protein factors [360]. However, some eukaryotic organisms additionally or alternatively contain single-subunit protein-only RNase P enzymes (PRORPs) that act in nuclear and organellar RNA processing [382]. The three components of the human mtRNase P were identified for the first time in 2008 [359]. Using a combinatorial purification/proteomics approach, it was observed that TRMT10C, SDR5C1 and PRORP form together the human mtRNase P complex, which performs 5'-end processing of pre-(mt)tRNAs. Since all until then known mtRNase P enzymes were ribozymes, composed of an RNA plus one or more proteins, it was unusual that the human mtRNase P did not require a *trans*-acting RNA component for catalysis. In addition to 5'-end maturation, the TRMT10C-SDR5C1 subcomplex also executes m^1R^9 methylation of (mt)tRNAs by using

the cofactor SAM [329]. It can be assumed that TRMT10C and SDR5C1 first bind to the pre-(mt)tRNA and PRORP is recruited in a subsequent step, yet the presence of PRORP was shown to enhance the methylation activity of TRMT10C and SDR5C1 [383], [384]. Besides, it is known that TRMT10C and SDR5C1 form a strong complex, whereas PRORP binds the complex weakly [359]. And it was proposed that TRMT10C might be like a limiting building block of mtRNase P *in vivo*, as its overexpression alone was sufficient to increase its activity [359]. Although PRORP habors the catalytically active site for tRNA processing, the presence of TRMT10C and SDR5C1 is needed to switch PRORP into a fully productive active state [384]. This fact is surprising as other homologs of PRORP, e.g. plant and trypanosomal RNase P enzymes, are active as single proteins [384]. However, as (mt)tRNAs do not provide structurally conserved elements, as bacterial, plant and cytosolic tRNAs do, TRMT10C and SDR5C1 appear to compensate for this absence and take over the recognition process. Regarding the composition of mtRNase P, a stoichiometry of two TRMT10C, four SDR5C1 and one PRORP monomer was suggested in 2018, in combination with one pre-(mt)tRNA molecule [362]. In line with this, a recent cyro-EM structure revealed that TRMT10C is embedded between PRORP and a SDR5C1 homotetramer (see Figure 1.18) [360]. However, whether one or two TRMT10C subunits are required is still unclear. The authors of [360] presume that two TRMT10C monomers could be present in either parallel or anti-parallel orientation potentially binding two pre-(mt)tRNAs at the same time. As the MTS of all mitochondrial proteins is cropped after entering the mitochondrion, PRORP contains a C-terminal metallonuclease domain and a pentatricopeptide repeat (PPR) domain linked by the central domain harboring one zinc ion. Whereas the metallocunclease domain harbors the catalytically active site for 5’ processing, the PPR provides a positively charged binding groove involved in (mt)tRNA binding. The exact mechanism for tRNA cleavage by mtRNase P is not known so far, yet PRORP metallonucleases are thought to employ a two-metal-dependent mechanism during which one metal activates the nucleophile while the other stabilizes the transition state [360]. These divalent metal ions are preferably Mg^{2+} ions, which are also required in all RNA-based RNase P enzymes [385]. The methyltransferase domain and the NTD of TRMT10C encase the pre-tRNA and the intervening adapter helix links TRMT10C to the SDR5C1 homotetramer (more information in section 1.4.1). Between the adapter helix and the NTD TRMT10C forms an “adapter loop”, which is stabilized by hydrophobic interactions with SDR5C1. Concerning the localization, it can be assumed that RNA processing by mtRNase P occurs cotranscriptionally in small speckles named mitochondrial RNA granules (MRGs) [115]. As a recent publication has shown, bi-allelic variants in *PRORP* lead to multisystem diseases with variable phenotypes ranging from sensorineural hearing loss and primary ovarian insufficiency to developmental delay and brain white matter changes [386]. Besides, knock-down of all mtRNase P homologs in *Drosophila melanogaster* larvae resulted

in significantly reduced ATP levels, highlighting the importance of mtRNase P for the mitochondrial function [387].

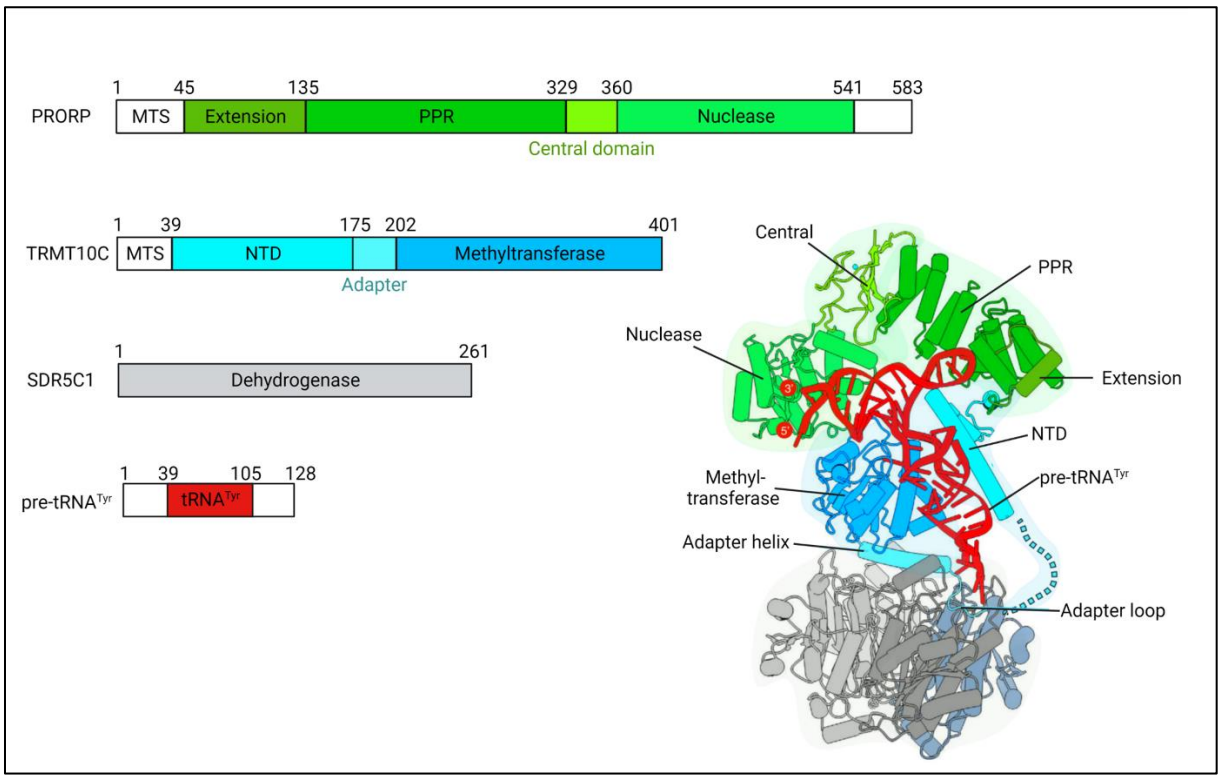

Figure 1.18: Cartoon representation of the human mtRNase P complex based cryo-EM and crystal structures. Domain representation of mtRNase P subunits and the substrate pre-tRNA^{Tyr} are shown on the upper left. PRORP domains are represented in shades of green, TRMT10C domains in shades of blue, SDR5C1 domains in shades of grey and the pre-tRNA is labeled in red. Numbers correspond to amino acid length for PRORP, TRMT10C and SDR5C1, or for the nucleotide number in the tRNA^{Tyr} sequence (according to canonical tRNA numbering). Mitochondrial target sequences (MTS), leader and trailer sequences are shown in white, and are not visible in the cartoon representation of the mtRNase P. On the bottom left side a cryo-EM structure of mtRNase P fitted with crystal structures of TRMT10C, SDR5C1 and PRORP is depicted. PPR= pentatricopeptide repeat domain, NTD= N-terminal domain. Figure adapted from [360].

In addition to MRPP2, several synonyms exist for SDR5C1, e.g. hydroxysteroid-17β-dehydrogenase 10 (HSD17B10), amyloid β-binding dehydrogenase (ABAD) or endoplasmic reticulum-associated amyloid β-peptide binding protein (ERAB). This well-known enzyme is encoded by the X chromosome in gene *HSD17B10* and as the number of synonyms suggest, it is a multifunctional protein that fulfills several metabolic roles. On the one hand, SDR5C1 oxidizes alcohols on a variety of substrates with the cofactor NAD^+ and on the other hand, it is able to reduce aldehydes and ketones by using NADH [388]. For instance, it is involved in the β-oxidation cycle by oxidizing short-chain and brached-chain fatty acids in mitochondria. Likewise, SDR5C1 is required for the catabolism of isoleucine, in which it catalyzes the conversion of a hydroxyl to a ketone group [389]. It also plays a significant role in neurosteroid and sex steroid metabolism as it oxidizes the neuroactive steroid allopregnanolone and converts 17β-estradiol to estrone, thereby maintaining the balance of estradiol/estrone in

neurons [390], [391]. Lastly, it forms part of the human mtRNase P complex as mentioned above. Here, it forms a homotetramer in which each monomer adopts a Rossmann-fold and harbors a dehydrogenase active site [360]. Of note, every SDR5C1 monomer in mtRNase P complex carries a NADH cofactor bound in its dehydrogenase active site [360]. With regard to AD, it should be mentioned that SDR5C1 is able to bind amyloid β [392]. Biochemical studies of this amyloid β-SDR5C1 interaction showed that binding already occurs at nanomolar concentrations, however, concentrations of two orders of magnitude higher were required to inhibit the dehydrogenase activity of SDR5C1 towards different alcohols [187], [393]. This data suggests that Aβ is probably required in its oligomeric form to occupy the binding site and to cause the observed conformation change. This amyloid β-SDR5C1 interaction disrupts the balance of estradiol and estrone, shifting to a reduction of estradiol [391]. As estradiol has remarkable effects in neuron protection this decrease was found to boost the generation of ROS (via lower levels of antioxidants, higher levels of cytosolic Ca^{2+} and defects in the respiratory chain), to induce apoptosis (via lower expression of antiapoptotic proteins, higher expression of proapoptotic proteins, a reduced ability to sequester Ca^{2+} in mitochondria and the enhanced release of Cyt c) and to elevate the generation of pathological hallmarks (such as amyloid β petides and plaques and phosphorylated tau) [391]. In line with this, the inhibition of SDR5C1 restored the amyloid β-mediated deregulation of estradiol and as a consequence, several SDR5C1 inhibitors were designed and tested to treat AD [394]–[397]. The tremendous importance of SDR5C1 for the mitochondrial function and the human body in general becomes clear considering that mutations in the *HSD17B10* gene cause the rare, but severe HSD10 disease. This unusual neurodegenerative childhood disorder is characterized by progressive neurodegeneration, cardiomyopathy or both, due to mitochondrial dysfunction [398]. Though there is significant heterogeneity in the clinical manifestations, many patients with *HSD17B10* gene mutations show cognitive and/or physical delay already in infancy, and most of them die very young [388], [389], [398]–[401]. Even though SDR5C1 takes over multiple cellular functions, the symptoms of HSD10 disease are thought to originate from the disruption of the mtRNase P [398], [401].

1.4.3 Involvement of TRMT10C in human diseases

Considering the vital role of TRMT10C in (mt)RNA processing and methylation, it is plausible that mutations in the *TRMT10C* gene cause severe mitochondrial deficits. As a matter of fact, this has been observed in two unrelated individuals carrying recessive mutations in *TRMT10C* (p.Arg181Leu and/or p.Thr272Ala). These two patients presented already at birth lactic acidosis, hypotonia, feeding difficulties, defects in brain development and deafness, and died at 5 month of age after respiratory failure [293]. A closer biochemical analysis showed

that those mutations lead to decreased TRMT10C protein levels and increased amounts of pre-(mt)RNAs, pointing to an impairment of mitochondrial RNA processing [293]. Besides, the investigation of skeletal muscle samples revealed deficiencies in Cpx I and IV of the respiratory chain, indicating that the mitochondrial protein synthesis was hampered as well. This assumption was confirmed by means of Western blot (WB) and Blue-native PAGE analysis, which showed that both Cpx I and IV subunits and the amount of assembled Cpx I and IV was reduced in subject fibroblasts. In line with this, the lentiviral transduction of wild-type TRMT10C rescued the defects in both (mt)RNA processing and mitochondrial protein synthesis [293]. Interestingly, no altered m^1R^9 methylation was measured in (mt)tRNAs of those fibroblasts, suggesting that the described defects were due to defective RNA processing rather than defective RNA methylation. Similar symptoms (hypotonia, cognitive decline, deafness and high lactate levels) were reported from an third unrelated two-month-old girl, carrying the homozygous p.Arg181Leu mutation [402].

Apart from mutations, an altered mRNA expression of TRMT10C has been associated with various types of cancer. For instance, TRMT10C mRNA was found to be elevated in gastric, gynecological, liver and non-small cell lung cancer [403]–[406]. Besides the survival rate of patients with gynecological, hepatocellular or oral squamous cell carcinoma was significantly decreased in patients displaying high TRMT10C mRNA levels [405], [407], [408]. Consistent with this, knock-down of TRMT10C in different cell lines resulted in significantly lower cell migration rates, suggesting an enhancement of the malignant behaviour of cancer cells by TRMT10C [405]. Likewise, TRMT10C mRNA was found to correlate with ABCC3, a protein that is thought to exacerbate glioma proliferation [409]. However, the data is ambiguous. That means while high TRMT10C mRNA levels correlated with poorer survial in lung cancer, the increased TRMT10C mRNA expression correlated with better survival in renal cancer[13]. Besides, the comparison of RNA-Seq data from 17 different tissues out of the human cancer gene atlas (TCGA) revealed a low cancer tissue specificity of TRMT10C mRNA[12]. Moreover, it should be mentioned, that TRMT10C is not the only RNA modification regulator (term includes writer, reader and eraser) that has been implicated in cancer diseases. As recent publication has shown, the crosstalk of different RNA modification regulators seems to define tumor microenvironment, cancer hallmarks and the prognosis of lung adenocarcinoma [410]. Remarkably, TRMT10C has been linked not only to cancer but also to AD. A recent publication examined the mRNA and protein expression of TRMT10C in 5xFAD mice and observed significantly reduced protein and mRNA levels [355]. In addition, knock-down of the TRMT10C homolog Rosswell aggravated the eye phenotype in a tau-based Drosophila AD

[13] https://www.proteinatlas.org/ENSG00000174173-TRMT10C/pathology

model [355]. Lastly, loss of function alleles of Roswell were shown to cause lethality in flies, pointing to the essential role of TRMT10C in all living organisms [411].

2 Motivation and Objectives

Alzheimer's disease (AD) is the most common progressive neurodegenerative disease. Today, it affects millions of people worldwide and the number of cases will further increase due to the elevated life expectancy. Even though the U.S. Food and Drug Administration (FDA) this year approved a new antibody that may moderately decelerate cognitive decline, there is still no treatment that can halt or even reverse the symptoms of AD. Besides, the initial mechanism that triggers AD is not conclusively clarified. However, the amyloid precursor protein (APP) and its cleavage product Aβ are known to play a crucial role in the pathogenesis, as mutations in genes encoding APP or an APP cleavage enzyme (PSEN1 and 2) result in a rare familial form of AD (FAD) [64]. APP is encoded on chromosome 21, therefore people with trisomy 21 have a greatly increased risk of developing AD [65]. The APP cleavage product Aβ can form neurotoxic oligomers, protofibrils and fibrils, which are the main component of extracellular amyloid plaques, the most important hallmark of the disease, alongside intracellular tau tangles [412], [413]. Because Aβ is regarded as the main culprit in the late-onset AD (LOAD), maximum therapeutic efforts are centered towards this peptide. However, most anti-Aβ antibodies developed to date failed to demonstrate clinical efficacy in humans (reviewed in [414]). Some antibodies have been shown to mediate the removal of amyloid plaques, but the extent of the clinical benefit from these drugs is under intense debate [415], [416]. Interestingly, recent findings demonstrate an important role of mitochondrial dysfunction early in the pathophysiology of LOAD. Several mitochondrial parameters were found to be impaired, such as the mitochondrial membrane potential, mitochondrial dynamics and ATP synthesis via the respiratory chain Cpx I-V [102], [196], [417]. Especially the function of Cpx IV is diminished, but several studies, among them a recent meta-analysis, also highlight the decreased activity of Cpx I [182], [183], [202]. Whereas the impairment of Cpx IV can be explained by a direct binding of Aβ to one of its subunits [198], the exact mechanism how Cpx I is aggrieved in AD is still not fully understood. Cpx I is the starting point of the electron transport chain generating ATP, the energy source for almost all cellular processes. As ATP synthesis was found to be reduced in AD patients and neurons have a very high energy demand, the investigation of Cpx I is of particular interest.

In 2017, the RNA modification N^1-Methyladenosine (m^1A) was found for the first time in mitochondrial mRNAs ((mt)mRNAs) [312], [341]. The one m^1A site manifesting the highest methylation levels was detected in the mRNA of ND5 (=NADH dehydrogenase subunit 5), a subunit of Cpx I. ND5 is one of the core subunits of Cpx I and considered to be essential for the couping of the redox reaction and the translocation of protons into the intermembrane space [155]. These translocated protons are the engine for the ATP synthase (Cpx V) to

generate ATP. The absence of ND5 was shown to almost eliminate the activity of Cpx I [156] and mutations in ND5 are known to cause severe mitochondriopathies (e.g. LHON [163] and MELAS [418]). Though some m^1A sites on mRNA are highly discussed, the m^1A site at position 1374 of ND5 is unanimously reported by several independent groups [313], [341], [419]. In addition, TRMT10C was proposed to be the corresponding writer enzyme installing m^1A at this specific site. Since the methylation of adenosine adds a positive charge to the base, it can be assumed that m^1A^{1374} disrupts the mitochondrial translation process. This scenario has also been suggested by several groups [312], [338], [341]. Thus, high m^1A^{1374} methylation levels can be expected to lower the synthesis of ND5. In consequence, Cpx I function would be reduced implicating mitochondrial respiration defecits and mitochondrial dysfunction.

Therefore, the present thesis aims to investigate whether elevated levels of m^1A^{1374} in the mRNA of ND5, installed by TRMT10C, might cause Cpx I impairment and mitochondrial dysfunction in AD. For this purpose, four experimentally verifiable hypotheses were postulated:

(i) Protein expression of the writer enzyme TRMT10C might be altered in AD cell and animal models as well as in AD patients.

(ii) m^1A^{1374} methylation levels of ND5 mRNA might change in dependence of TRMT10C protein expression.

(iii) ND5 protein levels might be altered as a consequence of m^1A mRNA methylation. Therefore, increased m^1A^{1374} modification would result in a decreased ND5 protein content and vice versa.

(iv) Reduced ND5 protein expression might lower the activity of Cpx I and consecutively impair mitochondrial function.

To scrutinize these hypotheses a wide range of methods was utilized ranging from WB analysis and mitochondrial respiration assays to the implementation of a site-specific m^1A analysis method. This self-designed method to estimate m^1A^{1374} methylation levels is based on misincoporations introduced by m^1A into the complementary cDNA strand during reverse transcription. After subsequent polymerase chain reaction (PCR) and Illumina sequencing, a bioinformatic analysis yields misincorporation rates at the desired position indicating m^1A methylation levels in die original sample. This method was employed for AD model cells and the bioinformatic analysis was applied to RNA-Seq data from human AD patients. Besides, TRMT10C and ND5 protein levels were examined in AD model cells and mice, and frontal cortex tissue of AD patients. To investigate whether the hypotheses (i)-(iv) are linked in a chain of ensuing effects, the above mentioned parameters were also investigated in HEK cells overexpressing TRMT10C.

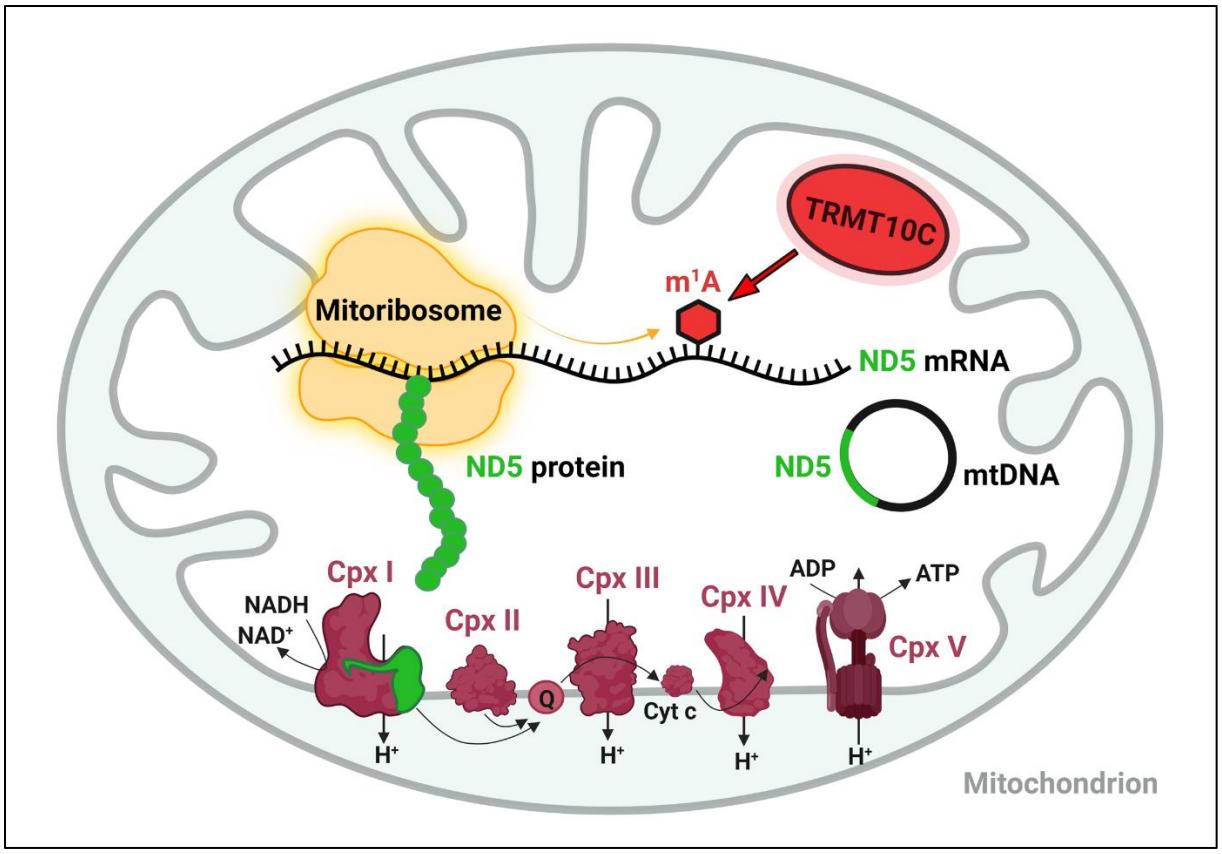

Figure 2.1: Illustration of the hypotheses (i)-(iv) investigated in this dissertation. ND5 (green) is a mitochondrial encoded protein and a subunit of complex I (Cpx I) from the respiratory chain. At position 1374 of the ND5 mRNA adenosine can be methylated (m^1A) by the writer enzyme TRMT10C (red). As m^1A disrupts Watson-Crick base pairing it is thought to impede the synthesis of ND5 by the mitoribosome. The absence of ND5 or an inefficienct translation is hypothesized to result in Cpx I impairment and a decrease of the mitochondrial respiration. TRMT10C= tRNA methyltransferase 10C, ND5= NADH-dehydrogenase subunit 5, m^1A= N1-methyladenosine, Cpx I-V= complex I-V, Q= Ubiquinone, Cyt c= cytochrome c, think black arrows represent the flow of electrons (e^-) oder protons (H^+) or the catalysis of NADH to NAD^+ and ADP to ATP. Due to space limitations, the chemical reactions have not been stoichiometrically adjusted.

Investigation of the presented hypotheses aimes to unravel the mechanisms underlying mitochondrial dysfunction in AD, because understanding the molecular processes involved in AD is the first step to develop future therapeutic strategies. Since all of the drugs studied in the last decades have failed to demonstrate satisfatory effects, the discovery of new drug targets is essential to improve the current therapy of AD.

3 Materials and Methods

3.1 Materials

3.1.1 Instruments and Consumables

Table 3.1: List of all instruments used in this thesis.

Instrument	Manufacturer
CO_2 incubator HERAcell	Heraeus Instruments, Hanau, DE
Transmitted light microscope AE20	Motic Deutschland GmbH, Wetzlar, DE
Centrifuge Labofuge 400 Function line	Heraeus Instruments, Hanau, DE
Centrifuge Universal 320R	Hettich GmbH, Tuttlingen, DE
Hettich rotor 1689-A	Hettich GmbH, Tuttlingen, DE
Hettich rotor E3258	Hettich GmbH, Tuttlingen, DE
Optima™ LE-80K Preparative Ultracentrifuge	Beckman Coulter, Fullerton, US
Beckman Type 60 Ti rotor	Beckman Coulter, Fullerton, US
Coulter Particle Counter Z Series	Beckman Coulter, Fullerton, US
Cell counting chamber Neubauer improved	Paul Marienfeld, Lauda Königshofen, DE
Liquid nitrogen freezing container LS3000	Taylor-Wharton, Mildstedt, DE
Freezing container Nalgene®	Thermo Fisher Scientific, Waltham, US
Repeating pipetter Multipette® M4	Eppendorf, Hamburg, DE
Millipore Direct-Q® 3 UV	Merck Millipore, Darmstadt, DE
Pipette controller accu-jet® pro	Brand GmbH, Wertheim, DE
Safety cabinet Lamin Air HB2448, HB2478	Heraeus Instruments, Hanau, DE
Microcentrifuge MiniStar silverline	VWR International, Radnor, US
Drying chamber Hotmaker 2000	Heraeus Instruments, Hanau, DE
Ultra-low freezer FORMA 900 Series	Thermo Fisher Scientific, Waltham, US
Vortex-Mixer Genie® 2	Scientific Industries, Bohemia, US
Orbit™ LS Laboratory shaker	Labnet, Edison, US
Water bath WNB 22	Memmert GmbH, Schwabach, DE
Water bath type 3044	Koettermann GmbH, Uetze, DE
Liebherr MEDLine Refrigerator	Liebherr, Bieberach an der Riß, DE
Liebherr Glass line Öko super	Liebherr, Bieberach an der Riß, DE
Autoclave FOM/B50	Fedegari Autoclavi SPA, Albuzzano, IT
Balance PB3002 DeltaRange	Mettler Toledo, Ohio, US
Analytical balance AG245	Mettler Toledo, Ohio, US
NanoDrop™ OneC UV-Vis Spectrophotometer	Thermo Fisher Scientific, Waltham, US
NanoDrop™ 2000 Spectrophotometer	Thermo Fisher Scientific, Waltham, US
4200 TapeStation System	Agilent Technologies, Santa Clara, US
Heating block	A. Hartenstein, Würzburg, DE
Block thermostat	A. Hartenstein, Würzburg, DE
Glashomogenizer Potter S	B. Braun Biotech, Melsungen, DE

pHenomenal® pH 1100L	VWR International, Radnor, US
Magnetic stirrer IKAMAG™ RET	IKA-Werke GmbH, Staufen, DE
Fusion Pulse TS	Vilber, Collégien, FR
QuantStudio 5	Thermo Fisher Scientific, Waltham, US
Thermocycler Biometra® T-gradient	Watman, Maidstone, GB
Thermocycler peqSTAR	VWR International, Radnor, US
Gel chamber Large format LSG-400-20	C.B.S. Scientific, San Diego, US
Wheaton™ Dounce Tissue Grinder	VWR International, Radnor, US
Hamilton™ 1000 Series syringe	Thermo Fisher Scientific, Waltham, US
LLG-Volumetric flask	Lab Logistics Group, Meckenheim, DE
Single-channel pipettes PIPETMAN Classic (P1000, P200, P20, P10)	Gilson, Middleton, US
Single-channel pipettes (P1000, P200, P20, P10)	Eppendorf, Hamburg, DE
Makro pipettes Pipetman (10 mL, 5 mL)	Gilson Incorporated, Middleton, US
Duran Bottles (2 L, 1L, 500 mL, 100 mL)	Schott AG, Mainz, DE
Mini-PROTEAN® Tetra Cell Vertical Electrophoresis Set, including handcast gels	Bio-Rad Laboratories, California, US
Mini Cell Buffer Dams	Bio-Rad Laboratories, California, US
Roller for use with blotting apparatus	Bio-Rad Laboratories, California, US
Gel releaser	Bio-Rad Laboratories, California, US
PowerPac™ Basic Power Supply	Bio-Rad Laboratories, California, US
Instrument tray white	Burkle Inc, New York, US
Mini-PROTEAN® Tetra cooling unit	Bio-Rad Laboratories, California, US
Typhoon TRIO+ Variable Mode Imager	GE Healthcare, Chicago, US
Seahorse XFe 96 Extracellular Flux analyzer	Seahorse Bioscience, Massachusetts, USA
OROBOROS Oxygraph-2k High-resolution Respirometer	Oroboros Instruments GmbH, Innsbruck, AT
Opera Phenix™ High-Content Screening System	Perkin Elmer, Waltham, USA
Digital dual timer C5080	TFA-Dostmann, Wertheim, DE
Miele Professional PG 8583	Miele, Gütersloh, DE
Large ice maker	Manitowoc, Milwaukee, US

Abbreviations according to ISO 3166-1: DE= Germany, US= United States of America, GB= Great Britain, IT= Italy, CH= Switzerland, FR= France, CA=Canada, AT= Austria

Table 3.2: List of all Consumables used in this thesis.

Consumables	**Manufacturer**
EasYFlask™ Nunc™ cell culture flasks (175 cm², 75 cm², 25 cm²)	Thermo Fisher Scientific, Waltham, US
Greiner CELLSTAR® dish (143 cm², 58 cm², 21 cm²)	Merck KGaA, Darmstadt, DE
Pipette tips (1000 µL, 200 µL, 20 µL)	Sarstedt, Nümbrecht, DE
Makro pipette tips Typ Gilson (5 mL, 10 mL)	Starlab International GmbH, Hamburg, DE
TipOne® filter tips	Starlab International GmbH, Hamburg, DE
Combitips advanced™	Eppendorf, Hamburg, DE

Reaction tubes (2 mL, 1.5 mL, 0.5 mL)	Sarstedt, Nümbrecht, DE
Nuclease-free reaction tubes SafeSeal (2 mL, 1.5 mL, 0.5 mL)	Sarstedt, Nümbrecht, DE
Light protection reaction tubes	Grainer bio-one
PCR Tubes	Sarstedt, Nümbrecht, DE
Polypropylene tube (50 mL, 15 mL)	Greiner Bio-one, Frickenhausen, DE
Cryovial 2 mL	Thermo Fisher Scientific, Waltham, US
Serological pipettes (25 mL, 10 mL, 5 mL, 2 mL)	Sarstedt, Nümbrecht, DE
Sartorius Sterile filter pore size 0.2 µm	Thermo Fisher Scientific, Waltham, US
Sample vessel for Coulter Counter	Carl Roth GmbH, Karlsruhe, DE
Applied Biosystems™ MicroAMP™ Optical 96-well Reaction plates	Thermo Fisher Scientific, Waltham, US
Applied Biosystems™ MicroAMP™ Optical adhesive film	Thermo Fisher Scientific, Waltham, US
Cell scraper 28 cm	Greiner Bio-one, Frickenhausen, DE
KIMTECH Science tissue	Thermo Fisher Scientific, Waltham, US
Seahorse XFe-96 Cell Culture Microplates	Agilent Technologies, Santa Clara, US
Disposal plastic bags	Sarstedt, Nümbrecht, DE
VIS Cuvettes for NanoDrop™	Eppendorf, Hamburg, DE
RNase Zap™	Thermo Fisher Scientific, Waltham, US
Feather™ Single-use scalpels	Thermo Fisher Scientific, Waltham, US
Ultracentruge tubes for Ti60 rotor	Beckman Coulter, Fullerton, US
TapeStation D1000 Screen Tapes	Agilent Technologies, Santa Clara, US
Gloves (latex and nitrile)	VWR International, Radnor, US
Polyvinylidene fluoride (PVDF) membrane	Thermo Fisher Scientific, Waltham, US
Whatman® gel blotting paper, Grade GB003	Merck KGaA, Darmstadt, DE
Weighing pan	A. Hartenstein, Würzburg, DE
Magnetic stirring bars	VWR International, Radnor, US
Pasteur pipettes, short form, Kimble®	DWK Life Sciences GmbH, Mainz, DE
Fisherbrand™ latex dispensing bulb	Thermo Fisher Scientific, Waltham, US
Hamilton™ Needle with blunt tip (17G)	Thermo Fisher Scientific, Waltham, US
Aluminum foil	neoLab, Heidelberg, DE
Nanosep® MF Centrifugal devices with Bio-Inert® membrane 0.45 µm	Pall Corporation, New York, US
Disposable plastic syringe Soft-ject®	A. Hartenstein, Würzburg, DE
Cannula for plastic syringe Neo-ject® 21G	A. Hartenstein, Würzburg, DE
Autoclave sterilization tape	A. Hartenstein, Würzburg, DE

3.1.2 Chemicals and Kits

Table 3.3: List of all Chemicals used in this thesis.

Chemicals	Manufacturer
Ambion® Nuclease-free water	Thermo Fisher Scientific, Waltham, US
Bovine Serum Albumin (BSA) Fraction V	Carl Roth GmbH, Karlsruhe, DE
Penicillin/Streptomycin (10.000 U/mL)	Thermo Fisher Scientific, Waltham, US
Blasticidin S HCl	Thermo Fisher Scientific, Waltham, US

Geneticin™ (G418 Sulfate) solution	Roche, Basel, CH
Gibco Fetal calf serum (FCS)	Thermo Fisher Scientific, Waltham, US
Hyromycin B (50 mg/mL)	Thermo Fisher Scientific, Waltham, US
Dulbecco's Modified Eagle Medium (DMEM) (high glucose + glutamine 2 mM) REF: 41965-039	Thermo Fisher Scientific, Waltham, US
Tetracycline hydrochlorid powder T7660	Merck KGaA, Darmstadt, DE
Polysorbat (Tween® 20)	Carl Roth GmbH, Karlsruhe, DE
Dimethyl Sulfoxide (DMSO) ≥ 99.5%	Carl Roth GmbH, Karlsruhe, DE
Trypan blue solution 0.4%	Thermo Fisher Scientific, Waltham, US
cOmplete™ mini protease inhibitor cocktail	Roche, Basel, CH
Ammonium persulfate (APS)	Thermo Fisher Scientific, Waltham, US
Rotiphorese® Gel 30% Acrylamid mix	Carl Roth GmbH, Karlsruhe, DE
Tetramethylethylendiamin (TEMED)	Carl Roth GmbH, Karlsruhe, DE
ROTI®Load	Carl Roth GmbH, Karlsruhe, DE
PageRuler™ Prestained protein ladder	Thermo Fisher Scientific, Waltham, US
GE Healthcare Amersham™ ECL Prime Western blot detection reagent	Thermo Fisher Scientific, Waltham, US
Protein Assay Dye Reagent Concentrate	Bio-Rad Laboratories, California, US
Percoll® P1644	Merck KGaA, Darmstadt, DE
Saccharose	Merck Millipore, Darmstadt, DE
Ethylene glycol-bis(2-aminoethylether)-N,N,N′,N′-tetraacetic acid (EGTA)	Merck KGaA, Darmstadt, DE
Trizma® base	Merck KGaA, Darmstadt, DE
Coulter Isoton II Diluent	Beckman Coulter, Fullerton, US
Rotiphorese® Sequencing gel concentrate (#3043.1)	Carl Roth GmbH, Karlsruhe, DE
Rotiphorese® Sequencing gel diluent (#3047.1)	Carl Roth GmbH, Karlsruhe, DE
Rotiphorese® Sequencing gel buffer concentrate (#3050.1)	Carl Roth GmbH, Karlsruhe, DE
Rotiphorese® 10x TBE buffer (#3061.2)	Carl Roth GmbH, Karlsruhe, DE
Manganese (II) chloride solution	Merck KGaA, Darmstadt, DE
TapeStation DNA Reagents (D1000 Ladder and Sample buffer)	Agilent Technologies, Santa Clara, US
Rotenone	Thermo Fisher Scientific, Waltham, US
dNTP mix (10 mM each)	Thermo Fisher Scientific, Waltham, US
Glycogen, RNA grade	Thermo Fisher Scientific, Waltham, US
GelRed® Nucleic Acid Gel Stain	Biotium Inc., Fremont, US
TRI Reagent®	Thermo Fisher Scientific, Waltham, US
Chloroform ≥ 99.5%	Merck KGaA, Darmstadt, DE
2-Propanol, HPLC quality	Carl Roth GmbH, Karlsruhe, DE
Ethanol 99.5% Ph. Eur. ultra pure	Carl Roth GmbH, Karlsruhe, DE
Ammonium acetate (NH_4Ac)	Merck KGaA, Darmstadt, DE
Methanol ≥ 99.5%	Thermo Fisher Scientific, Waltham, US
GeneRuler Low Range DNA Ladder	Thermo Fisher Scientific, Waltham, US

6x DNA Loading Dye	Thermo Fisher Scientific, Waltham, US
Rotiphorese® 10x TBE buffer	Carl Roth GmbH, Karlsruhe, DE
Formamide 47671	Merck KGaA, Darmstadt, DE
Poly-L-lysine solution	Merck KGaA, Darmstadt, DE
Taqman™ fast advanced master mix	Thermo Fisher Scientific, Waltham, US
Ethylendiamin tetraacetic acid (EDTA) disodium salt dihydrate	Carl Roth GmbH, Karlsruhe, DE
Phenylmethylsulfonyl fluoride (PMSF)	Carl Roth GmbH, Karlsruhe, DE
Polyethyleneglycol alkylphenylether (Triton-X100)	Carl Roth GmbH, Karlsruhe, DE
Sodium Deoxycholate	Merck KGaA, Darmstadt, DE
Tris(hydroxymethyl)-aminomethan (Tris)	Carl Roth GmbH, Karlsruhe, DE
Glycine ≥ 99%	Carl Roth GmbH, Karlsruhe, DE
2-Mercaptoethanol	Merck KGaA, Darmstadt, DE
Hydrochloric acid (HCl) 37%	Merck KGaA, Darmstadt, DE
Sodium Hydroxide (NaOH) pellets	Carl Roth GmbH, Karlsruhe, DE
Sodium Chloride (NaCl)	Carl Roth GmbH, Karlsruhe, DE
Sodium dihydrogen phosphate monohydrate ≥ 98%	Carl Roth GmbH, Karlsruhe, DE
Potassium chloride ≥ 99.5%	Carl Roth GmbH, Karlsruhe, DE
Potassium dihydrogen phosphate	Merck KGaA, Darmstadt, DE
Sodium Dodecyl Sulfate (SDS)	Thermo Fisher Scientific, Waltham, US

Table 3.4: List of all Kits used in this thesis.

Kits	**Manufacturer**
High-Capacity cDNA Reverse Transcription Kit (including MultiScribe™)	Thermo Fisher Scientific, Waltham, US
DNase I digestion Set E1010	Zymo Research, Irvine, US
MvaI (BstNI) (restriction enzyme and buffer)	Thermo Fisher Scientific, Waltham, US
SuperScript™ IV Reverse Transcriptase (enzyme, buffer and dithiothreitol (DTT))	Thermo Fisher Scientific, Waltham, US
EpiScript™ RNase H Reverse Trascription Kit (enzyme, buffer and DTT)	Lucigen LGC Biosearch Technologies, Hoddesdon, GB
Platinum™ SuperFi™ DNA Polymerase (enzyme, buffer and GC enhancer)	Thermo Fisher Scientific, Waltham, US
NEBNext® Multiplex Small RNA Library Prep set for Ilumina (Set 1-4)	New England Biolabs Inc, Ipswich, US
Seahorse XF Cell Mito Stress Kit 103015-100	Agilent Technologies, Santa Clara, US

3.1.3 Primers, Antibodies and TaqMan® Assays

Table 3.5: List of all Primers used in this thesis.

Primer	Sequence	Manufacturer
P5 PCR primer (human)	AAT GAT ACG GCG ACC ACC GAG ATC TAC ACA CAC TCT TTC CCT ACA CGA CGC TCT TCC GAT CTA CCC CAC CCT ACT AAA CCC	Custom-designed, ordered at Integrated DNA Technologies (IDT)
ND5 RT primer (human)	AGA CGT GTG CTC TTC CGA TCT NNN NNN NGT AAT GAG AAA TCC TGC G	Custom-designed, ordered at IDT, NNN NNN N is a unique molecular identifier (UMI), which has not been used in the final analysis
P5 PCR primer (mouse)	AAT GAT ACG GCG ACC ACC GAG ATC TAC ACA CAC TCT TTC CCT ACA CGA CGC TCT TCC GAT CTG ACC CAG ACC TCA TAA ACC CA	Custom-designed, ordered at IDT
ND5 RT primer (mouse)	AGA CGT GTG CTC TTC CGA TCT NNN NNN NGA GAT GAC AAA TCC TGC A	Custom-designed, ordered at IDT, NNN NNN N is a UMI, which has not been used in the final analysis

Table 3.6: List of all Antibodies used in this thesis.

Antibody	Manufacturer	Catalog number	Dilution
Anti-APP (Y188)	Abcam, Cambridge, GB	ab32136	1:1 000
Anti-TRMT10C (human samples)	Aviva Systems Biology, San Diego, US	Arp40877_p050	1:1 000
Anti-TRMT10C (murine samples)	Merck KGaA, Darmstadt, DE	SAB2105440	1:250
Anti-GAPDH	Abcam, Cambridge, GB	ab181602	1:10 000
Anti-β-Actin	Merck KGaA, Darmstadt, DE	A1978	1:2 000
Anti-ND5	Abcam, Cambridge, GB	ab92624	1:1 000
Anti-SDR5C1 (human samples)	Abcam, Cambridge, GB	ab10260	1:500
Anti-SDR5C1 (murine samples)	Abcam, Cambridge, GB	ab137455	1:500
Anti-PRORP (human samples)	Abcam, Cambridge, GB	ab185941	1:1 000
Anti-PRORP (murine samples)	Santa Cruz, California, US	Sc-390380	1:1 000
Anti-mouse IgG secondary antibody	Thermo Fisher Scientific, Waltham, US	31430	1: 5 000
Anti-rabbit IgG secondary antibody	Merck KGaA, Darmstadt, DE	A0545	1:10 000

Table 3.7: List of all TaqMan® Assays used in this thesis.

TaqMan® Assay	Manufacturer	TaqMan® ID
Applied Biosystems™ TaqMan® Assay ND5	Thermo Fisher Scientific, Waltham, US	Hs02596878-g1
Applied Biosystems™ TaqMan® Assay GAPDH	Thermo Fisher Scientific, Waltham, US	Hs99999905_m1

3.1.4 Buffers, Solutions and Media

20% SDS Solution:
20 g SDS
Ad 100 mL purified H_2O
adjust pH to 7.2 with 37% HCl

10% APS Solution:
100 mg APS
Ad 1 mL purified H_2O
store aliquotes at -20°C in the dark

1.5M Tris-HCl pH=6.8:
121.1 g Tris
800 mL purified H_2O
adjust pH to 6.8 with 37% HCl

1.5M Tris-HCl pH=8.8:
121.1 g Tris
800 mL purified H_2O
adjust pH to 8.8 with 37% HCl

1M Tris-HCl pH=7.4:
80.7 g Tris
800 mL purified H_2O
adjust pH to 7.4 with 37% HCl

10x Tris Buffered Saline (TBS) buffer:
24.2 g Tris 200 mM
87.8 g NaCl 1500 mM
ad 1000 mL purified H_2O
adjust pH to 7.5 with 37% HCl and autoclave

0.5% TBST buffer:
100 mL 10x TBS buffer
5 mL Tween® 20
Ad 1000 mL purified H_2O

0.1% TBST buffer:
100 mL 10x TBS buffer
1 mL Tween® 20
Ad 1000 mL purified H_2O

5% BSA Blocking solution:
10 g BSA
Ad 200 mL 0.1% TBST buffer

1% BSA solution:
1 g BSA
Ad 200 mL 0.1% TBST buffer

10x Running buffer:
30.2 g Tris
144 g Glycine
50 mL 20% SDS solution
Ad 1000 mL purified H_2O

10x Transfer buffer (without SDS):
30.2 g Tris
144 g Glycin
Ad 1000 mL purified H_2O
autoclave

1x Running buffer:
100 mL 10x Running buffer
Ad 1000 mL purified H_2O

1x Transfer buffer (without SDS):
100 mL 10x Transfer buffer
200 mL Methanol
Ad 1000 mL purified H_2O

1M NaCl Solution:
0.585 g NaCl

0.5 EDTA Solution pH=8:
23.26 g EDTA x 2 H_2O

Ad 10 mL	purified H_2O

Ad 100 mL	purified H_2O
adjust pH to 8 with NaOH	

Radioimmnoprecipitation assay (RIPA) buffer for protein isolation:

1.25 mL	1M Tris-HCl pH=7.4
3.75 mL	1M NaCl Solution
250 µL	Triton-X100
0.125 g	Natirum Deoxycholate
0.125 mL	20% SDS
0.25 mL	0.5M EDTA pH=8
Ad 25 mL	purified H_2O
store at 4-8°C in the dark	

Phosphate Buffered Saline, Ca^{2+} and Mg^{2+} free (PBS CMF):

8 g	NaCl
0.2 g	KCl
0.2 g	KH_2PO_4
1.5 g	Na_2HPO_4
Ad 1000 mL	purified H_2O
autoclave	

PMSF stock solution 100 mM:

175 mg	PMSF
10 mL	2-Propanol
store aliquots at -20°C	

Stripping solution:

10 mL	SDS 20%
12,5 mL	Tris-HCl pH=6.8
77.5 mL	purified H_2O
0.8 mL	2-Mercaptoethanol

Isolation buffer (IB):

54.7 g	Saccharose 320 mM
380 mg	EGTA 2mM
605 mg	Trizma® Base 10 mM
Ad 500 mL	purified H_2O
adjust pH to 7.4 at 4°C	

100%-Percoll® solution:

5.47 g	Saccharose 320 mM
38 mg	EGTA 2mM
60.5 mg	Trizma® Base 10 mM
Ad 50 mL	Percoll®
adjust pH to 7.4 at 4°C	

12%-Percoll® solution:

9 mL	100%-Percoll® solution
66 mL	IB

26%-Percoll® solution:

12 mL	100%-Percoll® solution
34 mL	IB

40%-Percoll® solution:

12 mL	100%-Percoll® solution
18 mL	IB

Loading buffer for DNA separation:

45 mL	Rotiphorese® 1x TBE
5 mL	Formamide

Ammonium Acetate 0.5 mM:

1.927 g	NH_4Ac
ad 50 mL	purified H_2O, Nuclease-free

5x RT Buffer without Mg^{2+}:

250 mM	Tris-HCl, pH=8.3
250 mM	KCl
Ad 1000 µL	purified H_2O
add $MnCl_2$ just before the RT with a final concentration of 5 mM in each tube	

Medium HEK293 untransfected (Ctl):

500 mL	DMEM
50 mL	FCS (heat-inactivated)
50 U/mL	Pen/Strep

Medium for cell freezing:

95%	Medium of corresp. cell line
5%	DMSO

Medium HEK293 APPwt:	
500 mL	DMEM
50 mL	FCS (heat-inactivated)
50 U/mL	Pen/Strep
400 µg/mL	G418

Medium HEK293 APPsw:	
500 mL	DMEM
50 mL	FCS (heat-inactivated)
50 U/mL	Pen/Strep
400 µg/mL	G418

Medium HEK293 T-Rex-cells (Ctl):	
500 mL	DMEM
50 mL	FCS (heat-inactivated)
50 U/mL	Pen/Strep
5 µg/mL	Blasticidin S

Medium HEK293 T-Rex pTRMT10C:	
500 mL	DMEM
50 mL	FCS (heat-inactivated)
50 U/mL	Pen/Strep
5 µg/mL	Blasticidin S
100 µg/mL	Hygromycin B

3.1.5 Cell lines

Human Embryonic Kidney 293 (HEK293) cells are a specific immortalized cell line derived from embryonic kidney cells of a female human fetus exposed to sheared fragments of adenovirus typ 5 DNA. The first publication of this cell line was provided by Graham *et al.* in 1977 [420]. Due to the transfection process a 4.3 kbp fragment of viral DNA was integrated into chromosome 19, coding for the viral proteins E1A and E1B, which interfere with cell cycle control pathways and counteract apoptosis [421]. The HEK293 cell line grows as an adherent monolayer on surfaces and is among the most commonly used cell lines in research. The exact origin of the kidney tissue is unknown, but it is believed to originate from an aborted or miscarried fetus. The number 293 is traced back to the sample number in Graham's experiment.

HEK293 ut, APPwt and APPsw

HEK293 cells were transfected with a DNA construct (pCMV695) harboring the human wild-type *APP695*-gene (APPwt), inserted downstream of a cytomegalovirus promotor by means of the FuGENE 6™ transfection reagent (Roche Diagnostics) [216], [422]. These cells stably express the human APPwt protein, hence displaying elevated APP protein levels and a ~7x enhanced $A\beta_{40}$ secretion [216]. HEK293 APPsw cells were generated in the same way, but in this case the *APP* gene contains the Swedish KM670/671NL mutation. This double mutation is located immediately adjacent to the β-secretase cleavage site in APP and has been reported in two large swedish families. This mutation has been shown to increase total $A\beta_{1\text{-}XX}$ peptide levels by facilitating APP cleavage by BACE1 and thereby disfavors the generation of amyloidolytic $A\beta_{11\text{-}XX}$ peptides. While other familial AD mutations in APP and the presenilin gene skew Aβ production to larger, more aggregation-prone forms, the Swedish mutation increases overall production of $A\beta_{11\text{-}XX}$ with multiple reports showing increased production and

secretion of $A\beta_{40}$ and $A\beta_{42}$[14]. In the case of HEK293 APPsw, these cell display not only higher APP levels than APPwt, but also ~10x higher $A\beta_{40}$ secretion than APPwt [216]. While APPwt cells represent a model for early/intermediate LOAD, APPsw represent a model for the late stage of LOAD. Untransfected HEK293 cells model healthy control individuals and were therefore referred to as Ctl in all experiments with APPwt and APPsw. HEK293 Ctl, APPwt and APPsw cells were kindly provided by the research group of Prof. Dr. _____ (Goethe University, Frankfurt, Germany).

HEK293 T-Rex Ctl and pTRMT10C cells

For the Tetracycline-induced overexpression of TRMT10C the complete coding sequence including its native initiation codon context in frame with a C-terminal FLAG-tag was introduced in a pcDNA™5/TO© plasmid and cloned by PCR [359]. Afterwards, HEK293 T-Rex™ cells (Invitrogen, R71007) were transfected with this pcDNA™5/TO-TRMT10C-FLAG

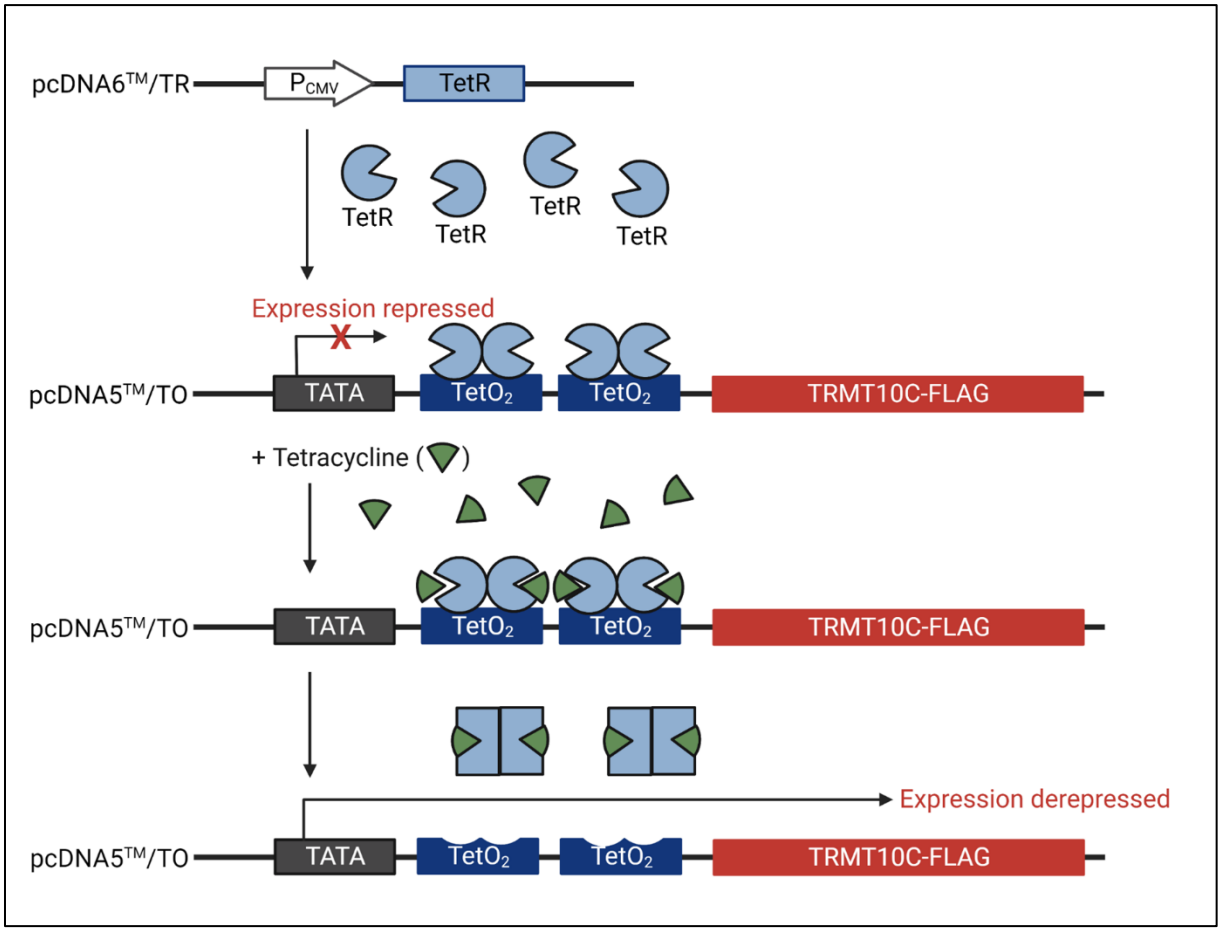

Figure 3.1: Mechanism of Tetracycline-regulated expression of TRMT10C-FLAG in the HEK293 T-Rex™ System. The TetR protein is expressed in all cultured cells transfected with the pcDNA6™/TR plasmid (Ctl and pTRMT10C cells). A TetR homodimer binds to the Tet operator 2 ($TetO_2$) sequence in the inducible expression vector pcDNA5™/TO (only present in pTRMT10C cells) and represses the initiation of the transcription. Upon addition, Tetracycline binds to the TetR homodimers and the…

[14] https://www.alzforum.org/mutations/app-k670m671delinsnl-swedish

…following conformational change releases TetR from the $TetO_2$ sequence. In consequence the transcription is initiated and TRMT10C-FLAG expression is derepressed.

plasmid and stable cell lines were selected (in the following termed pTRMT10C cells). The HEK293 T-Rex™ System is by default transfected with a pcDNA™6/TR© plasmid encoding the Tet repressor protein (TetR). In the absence of Tetracycline, the TetR forms a homodimer that binds with extremely high affinity to two Tet Operator ($TetO_2$) binding sequences. Two $TetO_2$ sites are located in the promoter of the inducible expression pcDNA™5/TO vector serving as binding sites for 4 TetR molecules (or 2 homodimers). Binding of the TetR homodimers to the $TetO_2$ sequences represses transcription of TRMT10C in pTRMT10C cells (see Figure 3.1). Upon addition, Tetracycline binds with high affinity to each TetR homodimer in a 1:1 stoichiometry and causes a conformational change in the repressor that renders it unable to bind the $TetO_2$ sequence. The TetR-Tetracycline complex then dissociated from the $TetO_2$ and allows induction of transcription from the TRMT10C gene. pTRMT10C and HEK293 T-Rex™ Ctl cells were kindly provided by Prof. Dr. Walter Rossmanith (University of Vienna, Austria).

3.1.6 Animals

5xFAD mice express human APP and PSEN1 transgenes, carrying in sum five different FAD-linked mutations, downstream of the neuron-specific mouse Thy1 promoter. Three of the five mutations are located in the *APP* gene, the Swedish (KM670/671NL), the Florida (I716V) and the London (V717I) mutation, and two of them, the M146L and L286V mutation in the *PSEN1* gene[15]. 5xFAD mice almost exclusively generate $A\beta_{42}$ and as these five mutations additively increase $A\beta_{42}$ production, intraneuronal aggregated $A\beta_{42}$ already accumulates at 1.5 months of age [76]. Amyloid plaques first occur at an age of 2 months in the hippocampus and cortex and spread with advancing age throughout the whole hippocampus, larger parts of the cortex, the thalamus, brainstem and the olfactory bulb, but seem to be absent in the cerebellum [76]. These pathologic alteration result in neuronal loss at about 6 month of age and cognitive deficits at about 5 months of age [76]. All of the used 5xFAD and Wild-type (Wt) mice were kindly provided by the research group of Prof. Dr. _____ (University Medical Center, Mainz, Germany) and originally bought from Jackson Laboratory with a C57BL6/J background. Therefore 5xFAD mice were stably cross-bred with wild-type C57BL6/J mice. The age of 5xFAD mice and wild-type littermates at the day of dissection was 42-55 weeks, which is equivalent to 10-12 months. Female and male mice were used in balanced proportions. All experimental procedures were carried out in accordance with the European Communities Council Directive regarding care and use of animals for experimental procedures (for housing conditions and genotyping see [423]). All mice were euthanized using cervical dislocation or

[15] https://www.alzforum.org/research-models/5xfad-c57bl6

inhalation of narcotic isoflurane. After euthanization, the relevant brain regions (hippocampus, cortex and cerebellum) were dissected and shock-frozen in liquid nitrogen.

3.1.7 Human samples

Human brain material was collected by the rapid autopsy program of the Netherlands Brain Bank (NBB), which provides post-mortem specimens from clinically well documented and neuropathologically confirmed cases. In order to receive the samples, a detailed application was submitted to the NBB located in Amsterdam. This application was approved with the project number 1341. In total 32 human cerebral cortex samples were received, sectioned from the superior frontal gyrus (gfs) part 3 and 4 (see Figure 3.2). All of these samples were used for WB analysis, however, as some of these samples originated from the same individuum, only one tissue sample per individuum was included in the final analysis. For simplicity the resulting individuals were labeled with AD1-13 or Ctl 1-12 for control samples. So in total 13 AD (5 male + 8 female) and 12 controls (6 male and 5 female) were studied with

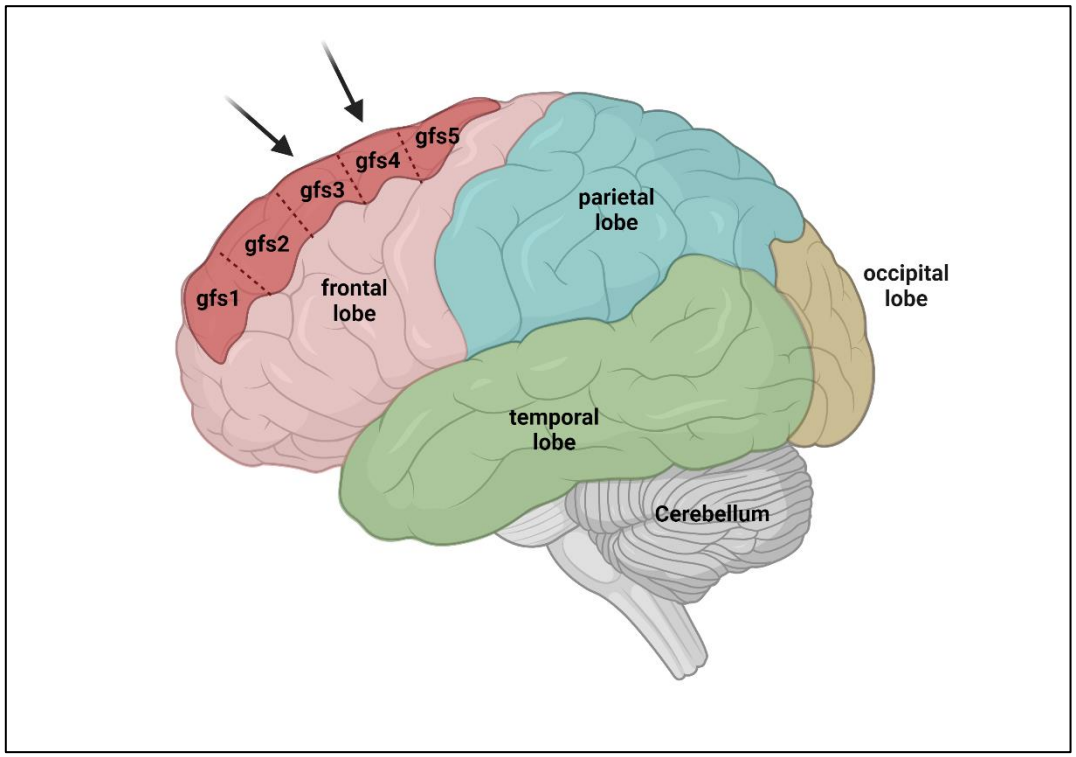

Figure 3.2: Location of the gyrus frontalis superior (gfs) part 1-5 in the human brain according to the NBB. Frontal, parietal, temporal and occipital lobe are indicated in pale colors, the cerebellum is shown in dark grey. For the experiments in this thesis gfs part 3 and 4 was used from both AD patients and healthy controls.

a mean age of 83.9 ± 8.1 years (AD) and 85.1 ± 9.0 years (Ctl) (numbers given as Mean ± SD). The mean Braak stage was 4.7 ± 0.6 in AD patients and 2.5 ± 1.0 in healthy controls. Detailed information about age, sex and Braak stage of all individuals is shown in Table 3.8.

All research involving the NBB samples was conducted according to the ethical declaration of the NBB. All cases were neuropathologically confirmed, using conventional biochemical techniques, and diagnosis performed using the Consortium to Establish a Registry for Alzheimer's Disease (CERAD) criteria. Non-disease controls had no history or symptoms of neurologic or psychiatric disorders and were clinically not demented. Gfs 3+4 was selected for both AD patients and healthy controls.

Table 3.8: Patient details of frontal cortex samples from the NBB presented for each individual.

Individual	Diagnosis	Sex	Age [years]	Braak stage
AD1	Alzheimer's disease	f	88	5
AD2	Alzheimer's disease	f	86	5
AD3	Alzheimer's disease	f	81	6
AD4	Alzheimer's disease	f	88	4
AD5	Alzheimer's disease	f	72	5
AD6	Alzheimer's disease	f	98	5
AD7	Alzheimer's disease	f	87	4
AD8	Alzheimer's disease	f	76	4
AD9	Alzheimer's disease	m	80	4
AD10	Alzheimer's disease	m	78	5
AD11	Alzheimer's disease	m	86	4
AD12	Alzheimer's disease	m	97	5
AD13	Alzheimer's disease	m	74	5
Ctl1	Non-demented control	f	83	2
Ctl2	Non-demented control	f	90	3
Ctl3	Non-demented control	f	76	2
Ctl4	Non-demented control	f	71	2
Ctl5	Non-demented control	f	85	3
Ctl6	Non-demented control	f	84	3
Ctl7	Non-demented control	m	92	4
Ctl8	Non-demented control	m	102	3
Ctl9	Non-demented control	m	93	0
Ctl10	Non-demented control	m	72	2
Ctl11	Non-demented control	m	86	3

Ctl12	Non-demented control	m	87	3

3.1.8 Human datasets

In this thesis, three publicly available RNA-Seq data sets were analyzed, one of which contained single-cell RNA-Seq (scRNA-Seq) data. While two of them only published gene expression results, one of them provided sequencing raw data allowing the quantification of mismatch at position 1374 in the mRNA of ND5.

The “Aging, Dementia and Traumatic Brain Injury (TBI) Study” data set

The “Aging, Dementia and TBI Study” data set was generated from the Adult Changes in Thought (ACT) Study [424] and contains transcriptomic data of the hippocampus (Hipp.), the temporal cortex (TCx), the prefrontal cortex (PCx) and the white matter of the prefrontal cortex (PCx(WM)) from 107 aged donors (including control and AD patients, with and without TBI). Importantly, these brain tissue pieces were dissected and processed as bulk preparation and the diagnosis was given by NINCDS-ARDA criteria (for more information see [425]). The data of the “Aging, Dementia and TBI Study” data set was retrieved from http://aging.brain-map.org/download/index (RRID:SCR_014554, Allen Institute for Brain Science, University of Washington Medicine, and Kaiser Permanente Washington Health Research Institute, US) on the 20th of January 2020. In the final analysis male patients with a confirmed AD diagnosis and without TBI incident were selected from the data set and normalized FPKM (fragments per kilobase per million mapped fragments) values were compared to controls (also without TBI incident). This led to n=13-15 control (Ctl) and n=5-8 AD cases (number varies between the four brain regions) with an average age of 92.7 ± 6.2 for Ctl and 86.5 ± 3.8 for AD, and an average Braak stage of 1.1 ± 1.1 in Ctl and 3.6 ± 2.1 in AD patients (numbers given as Mean ± SD).

scRNA-Seq data from Mathys *et al.*

As mentioned above one data set contained scRNA-Seq data. In this case, RNA-Seq data was generated from prefrontal cortex tissue (Brodmann area 10) as usual and subsequently divided into 6 different cell type groups, namely excitatory neurons, inhibitory neurons, astrocytes, oligodendrocytes, precursor-oligodendrocytes and microglia by specific cell type marker genes. The corresponding study performed by Mathys *et al.* [426] analyzed 80,660 single-nucleus transcriptomes from 48 individuals (24 AD + 24 Ctl) and provided fold change (FC) and adjusted p-values (padj) (adjusted by a two-sided Wilcoxon-rank-sum test) of all significantly altered genes, among them TRMT10C and SDR5C1. PRORP and ND5 were not listed. In both Ctl and AD patients, 12 male and 12 female individuals were included. The

24 AD patients were further divided into an early-stage (n=15, 7 males + 8 females) and a late-stage group (n=9, 5 males and 4 females). Early-stage AD subjects showed amyloid burden, but modest neurofibrillary tangles and cognitive impairment. The average Braak stage of early-stage AD patients was 4.3 ± 0.8, of late-stage AD it was 5.3 ± 0.5, of all AD patients it was 4.7 ± 0.9, and of Ctl it was 2.5 ± 0.9 (all numbers are given as Mean ± SD). The average age of those groups was not stated, however, the authors claimed that they matched the age between Ctl and AD patients. The diagnosis was determined by means of CERAD and NIA-Reagan Scores (for more information see [426]).

Data set from the National Center for Biotechnology Information (NCBI) Sequence Read Archive (SRA), Project PRJNA720779

As mentioned above only one group provided raw data reads of their RNA-Seq study and could therefore be used to determine mismatch rates at position 1374 in ND5. In this study performed by Guennewig *et al.* [427] two brain regions were analyzed obtained from post-mortem brains of 5 AD subjects and 5 healthy controls. These two brain regions, the moderately affected precuneus and the mildly affected primary visual cortex, were selected to model the changes between an early- and a late-stage of the pathological AD cascade. The groups of Ctl and AD were matched for age (Ctl: ⌀78, AD: ⌀ 76), post mortem interval (PMI) (Ctl: ⌀ 18h, AD: ⌀ 11h) and RIN values (Ctl: ⌀ 6.9, AD: ⌀ 6.9). All AD patients were at Braak stage 4. No information was given about the sex of AD patients and Ctl, however, the authors mentioned that genders were matched between these two groups (more information in [427]). Raw data from Guennewig et al. [427] retrieved through the NCBI SRA homepage (project number PRJNA720779).

3.1.9 Software and Statistics

Table 3.9: List of all Softwares and Programs used in this thesis.

Name	Manufacturer	Description
QuantStudio Design & Analysis v. 1.4.3	Thermo Fisher Scientific, Waltham, US	Analyzing qPCR results
Microsoft Excel v. 16.57	Microsoft, Washington, US	All kinds of calculations
Microsoft PowerPoint v. 16.57	Microsoft, Washington, US	Designing figures and tables
MicrosoftWord v. 16.57	Microsoft, Washington, US	Thesis structure, texts and tables
GraphPad PRISM v. 9.2.0	GraphPad Software Inc., San Diego, US	Graphs and Statistics

ImageLab v. 6.1	Bio-Rad Laboratories, California, US	Analyzing Western blot images
FastQC v. 0.11.9	S. Andrews, Braham Institute	Quality control for Illumina sequencing reads
Trimmomatic v. 0.39	Bolger A. M., Lohse M., Usadel B. [428]	Read trimming tool for Illumina NGS data
Bowtie2 v. 2.4.1	B. Langmead and S. L. Salzberg [429]	Read alignment to reference
SAMtools v. 1.10	H. Li *et al.* [430]	Merging forward and reverse reads
IGV v. 2.8.0	J. T. Robinson *et al.* [431]	Visualization of alignment
BioRender Premium	Sciences Suite Inc., Toronto, CA	Drawing figures

Statistics

All data was analyzed with standard statistical methods performed in GraphPad PRISM v. 9.2.0. In most cases an unpaired t-tests was applied, otherwise it is stated in the legend of the corresponding figure. Before using t-tests, raw data was checked for Gaussian distribution. Data are mainly presented as Mean ± SEM and the result of at least three independent experiments. Data points that were regarded as an extreme statistical outliner were excluded. Concerning human data, some individuals carrying the G13708A SNP were excluded from the final analysis. If this was the case, it was stated in the figure legend and the corresponding data points were marked in red.

3.2 Methods

3.2.1 Cell culture

HEK293 APPwt and APPsw cells were cultured in DMEM supplemented with 10% heat-inactivated FCS, 50 U/mL penicillin, 50 µg/mL streptomycin and 400 µg/mL G418 at 37°C in a huminidified incubator containing 5% CO_2. Untransfected HEK293 Ctl cells were cultured in the same medium excluding G418. In the medium of APPwt and APPsw cells G418 is required to culture only cells carrying the pCMV695 plasmid.

HEK293 T-Rex™ Ctl and pTRMT10C cells were cultured in DMEM supplemented with 10% heat-inactivated FCS, 50 U/mL penicillin and 50 µg/mL streptomycin. In order to select for the pcDNA™6/TR© vector 5 µg/mL Blasticidin S was added in the medium of both cell lines. Selection of transfected pTRMT10C cells was achieved by a hygromycin resistance in the pcDNA™5/TO© plasmid and 100 µg/mL hygromycin in the corresponding cell culture medium. HEK293 T-Rex™ Ctl and pTRMT10C cells were kept at 37°C in a humidified

incubator containing 5% CO_2. 24 hours before the experimental procedure pTRMT10C as well as 293 T-Rex™ Ctl cells were incubated with 0 µg/mL and 1 µg/mL Tetracycline.

All cells were split every 3-5 days in a 1:10 ratio (cell suspension : new medium). Cells were seeded 2-3 days before an experimental procedure (isolation of proteins, RNA or mitochondria) and simultaneously synchronized by washing with ice-cold PBS CMF. Only passage numbers 3-9 were used for experiments which was counted from the time point of defreezing. To freeze cells in liquid nitrogen, 5% DMSO was added into the appropriate cell culture medium, then 2 million cells were filled in Cyrovials and stored in the Nalgene® freezing container at -80°C. To thaw cells, the Cryovial was thawn in hands and then transferred into full medium. After centrifugation (1,000 x g, 5 min, 21°C), the cell pellet was resuspended in prewarmed full medium (37°C) and then seeded in a small cell culture flask. The next day, the old medium was replaced by fresh medium in order to remove dead cells.

3.2.2 Isolation of proteins

Cells were synchronized with ice-cold PBS CMF and then seeded into Greiner CELLSTAR® dishes (58 cm^2) three days in advance of the experimental procedure (shorter growing periods are stated in the figure legend of the corresponding experiment graph). 24 hours (h) prior to use, the medium was exchanged with fresh medium or medium containing 1 µg/mL Tetracycline. On the day of the protein isolation cells were washed twice with PBS CMF and lysed on ice in 200 µL RIPA-PMSF mixture (100:1). Regarding 5xFAD and Wt mice, the animals were sacrificed by decapitation under isoflurane anesthesia. Their brains were quickly removed and the three regions of interest (hippocampus, cerebral cortex and cerebellum) were dissected manually and then shock-frozen in liquid nitrogen. Tissue samples were stored at -80°C until protein isolation with RIPA-PMSF was performed. For one hippocampus 400 µL RIPA-PMSF was added, for cortex and cerebellum of one hemisphere 800 µL RIPA-PMSF was used. Before RIPA-PMSF addition, the latter two were cut into pieces with a scalpel in order to accelerate cell degradation. Dissolution of the tissue in the buffer was further enhanced with the Potter S homogenizer. The human tissue obtained from the NBB was treated the same way with a proportion of 800 µL RIPA for 50-100 mg of tissue.

After incubation of cell samples with RIPA-PMSF buffer on ice for 15 minutes (min), cells were collected with a cell scraper and transferred into reaction tubes. These tubes were then incubated again for 30 min on ice, whereas mice and brain tissue was incubated in total 45 min in tubes on ice. In the next step, all tubes were centrifuged (10,000 x g, 4°C, 10 min) leaving cell debris in the pellet and isolated proteins in the supernatant. From this supernatant 2x 20 µL were utilized for the protein determination assay and the remainder was mixed with proteinase

inhibitor solution (one cOmplete™ mini protease inhibitor cocktail tablet solved in 1 mL purified H_2O) in a 10:1.1 ratio. These isolated protein solutions were stored as aliquots at -80°C. Total protein content was determined by means of the Protein Assay Dye Reagent Concentrate (Bio-Rad #5000001). This colorimetric assay based on the Bradford method uses the absorbance shift of the dye when it is bound to amino acids of proteins. Therefore unkown protein concentrations can be determined by comparison with a BSA calibration curve. So in a first step, the absorbance of a BSA calibration curve of (1000 µg/mL, 20 µg/mL, 10 µg/mL, 5 µg/mL, 2.5 µg/mL and 1.25 µg/mL BSA in purified H_2O) was determined and in the second step two 1:100 and two 1:1000 dilutions of the samples were measured. For both calibration curve and samples 800 µL protein solution and 200 µL Protein Assay Dye Reagent Concentrate were mixed and incubated 5 min in the dark. Likewise, one blank (1000 µL H_2O) and one zero reference (800 µL H_2O + 200 µL Protein Assay Dye Reagent Concentrate) were prepared. In the end, all solutions were transferred into cuvettes and photometrically measured in the NanoDrop™ OneC UV-Vis Spectrophotometer. The program of this instrument automatically calculates protein concentrations of the original samples.

3.2.3 Western blot

SDS-PAGE

Whole protein extracts of cells and mice were separated via SDS polyacrylamide gel electrophoresis (SDS-PAGE). 1-3 days before use, gels were poured in the Mini-PROTEAN® handcast gel set. First of all, glass plates were cleaned with ethanol and paper tissue to remove disturbing gel residues. Then, the running gel was prepared by mixing purified H_2O, 30% Acrylamid mix, 1.5M Tris-HCl pH=8.8, SDS and APS (composition of both stacking and running gel are shown in Table 3.10). The catalyst TEMED was added last, just before pouring the gel. To obtain an even surface 100 µL isoropanol was carefully applied onto the running gel. After 45 min of polymerization, isoropanol was discarded and the stacking gel was poured on top. Ingredients of the stacking gel are similar to the running gel, except for 1.5M Tris-HCl with pH=6.8. When the stacking gel was poured a comb with 10 or 15 pockets was inserted carefully. Until the day of use, the gels including glass plates were wrapped in a damp paper tissue and stored at 4°C in the refrigerator. At the day of the WB, the gel was installed in the electrode of the Mini-PROTEAN® Tetra Cell electrophoresis Set and the chamber was filled with 1x chamber buffer. Then 20-40 µg protein per lane and water were mixed with ROTI®Load in a 3:1 ratio, and loaded on the 10% gel. 6 µL PageRuler™ prestained protein ladder was applied to the outer pockets. The SDS-PAGE was run for at 80 V for 30 min and then at 120 V for about 1 h.

Table 3.10: Recipe for one SDS polyacrylamide gel.

Running gel (10%)		**Stacking gel**	
1.925 mL	Purified H_2O	1.37 mL	Purified H2O
1.7 mL	30% Acrylamid mix	0.34 mL	30% Acrylamid mix
1.3 mL	1.5M Tris-HCl pH=8.8	0.26 mL	1.5M Tris-HCl pH=6.8
25 µL	20% SDS solution	10 µL	20% SDS solution
50 µL	10% APS solution	20 µL	10% APS solution
2 µL	TEMED	2 µL	TEMED

Western blotting

Prior to the transfer, fibre pads of the Mini-PROTEAN® Tetra Cell Set and Whatman® gel blotting paper (cut to the size of the gel) were precooled in ice-cold 1x transfer buffer and stored in the fridge for 15 min. Then samples were transferred from the gel onto a PVDF membrane in the Mini-PROTEAN® Tetra Cell Set with a transfer time of 1 h (100V) at 4°C. In order to guarantee a low temperature during the whole process, the chamber was placed in the cold room and a cooling unit was added into the chamber. After the transfer, the membrane was blocked with 5% BSA solution (1 h, 21°C) on the Orbit™ LS Laboratory shaker. At this point, the membrane was cut between the reference protein and the protein of interest in most of the cases. If the reference protein and the protein of interest were too close, the membrane was stripped after imaging as described in the section below. The membranes were washed three times with 0.5% TBST buffer (15 min, 10 min and 5 min) and incubated with the appropriate primary antibody overnight at 4°C (antibody was diluted in 1% BSA solution according to Table 3.6). The next day, membranes were again washed with 0.5% TBST buffer (15 min, 10 min and 5 min) and incubated with the secondary antibody (1 h, 21°C) on the Orbit™ LS Laboratory shaker. For APP, PRORP, TRMT10C, ND5 and GAPDH the anti-rabbit IgG antibody was used, and for ERAB and β-Actin the anti-mouse IgG antibody was used. Both secondary antibodies are conjugated with horseradish peroxidase (HRP). HRP is an enzyme that catalyzes the conversion of chemiluminescent substrates enabling the detection of targets such as proteins in photometric assays. In the last step, membranes were again washed three times with 0.5% TBST (15 min, 10 min and 5 min).

Detection and analysis

In order to determine levels of the desired proteins the membranes were incubated with Amersham™ ECL Prime Western blot detection reagent according to manufacturer's instructions. Afterwards the membrane was analyzed in the Fusion Pulse TS with the chemiluminescence setting. Reference protein and protein of interest were identified by comparison to the protein ladder (TRMT10C: 47 kDa, SDR5C1: 27 kDa, APP: 87 kDa, ND5: 67 kDa, β-Actin: 42 kDa, GAPDH: 36 kDa). As for PRORP, Isoform 4 (57 kDa) was quantified

in each Blot. The generated image was loaded into ImageLab v. 6.1. and the signal for each sample was determined. Then the ratio between the protein of interest and the reference protein was calculated in Microsoft Excel v. 16.57 and the percentage of each sample was given in relation to the mean of the corresponding control (Mean Ctl = 100%).

Membrane stripping

If the reference protein and the protein of interest were too close to each other, the membrane could not be cut and was therefore stripped after the first image. In this case, the membrane was incubated with the pre-warmed stripping solution at 60 °C. After two washing steps with 5% TBST (2x 10 min at 21°C), the membrane was again blocked with 5% BSA solution (1 h, 21 °C), washed again three times with 5% TBST (15 min, 10 min and 5 min) and then incubated with the appropriate primary antibody. In all cases, the protein of interest was determined in the first run and the reference protein was assessed after stripping. As the antibodies for β-Actin and GAPDH possess a high affinity, it was sufficient to incubate the membrane for 1 h at room temperature (21°C). In the next step, the membrane was washed three times with 5% TBST (15 min, 10 min, 5 min) and then incubated with the corresponding secondary antibody (diluted in 1% BSA solution). After a last washing step with 5% TBST (15 min, 10 min and 5 min), the membrane was analyzed as described in the previous section.

3.2.4 Isolation of total RNA

Two to three days in advance of the RNA isolation, cells were washed with ice-cold PBS CMF for synchronization and seeded into small Greiner CELLSTAR® dishes (21 cm²). At a confluency of 70-80% cells were harvested in 1 mL TRI Reagent® by pipetting up and down to dilute colonies in the liquid. Cell suspension was transferred into a reaction tube and dissolution of the cells was supported by vortexing and incubation at 21°C for 5 min. In the next step, 200 µL chloroform was added and mixed thoroughly in the Vortex-Mixer Genie® 2. After a second incubation step of 10 min (at 21°C), the cell suspension was centrifuged (16,000 x g, 4°C, 15 min). The upper aqueous phase was taken and mixed in a 1:1 ratio with 2-Propanol. Besides 1 µL Glyogen was added and the mix was incubated for 5 min (at 21°C) and again centrifuged (16,000 x g, 4°C, 10 min). As the obtained pellet contains the RNA, the supernatant was removed and discarded. Then, the RNA pellet was washed twice with an ice-cold ethanol solution (75% in purified H_2O) combined with a centrifugation step (16,000 x g, 4°C, 5 min). Afterwards, the whole supernatant was carefully and entirely removed, and the pellet was air-dried for about 5 min. In the end, RNA was reconstituted in 10-20 µL nuclease-free water and RNA concentrations were determined in the NanoDrop™ OneC UV-Vis Spectrophotometer.

Before using the RNA, puritiy values were checked and only samples with an A260/280 ratio >2.0 and an A260/230 ratio >1.5 were used for qPCR and the m^1A^{1374} analysis method. If this was not the case, a purification was performed with 5M NH_4Ac solution. For this, the RNA sample was replenished with nuclease-free water to 44 µL and both 1 µL Glycogen and 5 µL 5M NH_4Ac solution were added (end concentration 0.5M NH_4Ac). The following RNA precipitation was performed by adding 150 µL ethanol (-80°C), vortexing and incubation for 1 h at -80°C. After this, all samples were centrifuged (15,379 x g, -5°C, 45 min) and the obtained supernatant was removed. The RNA pellet was washed twice with 100-250 µL of a 75% ethanol solution and a combined centrifugation step (15,379 x g, -5°C, 10 min). In the last step, the supernatant was entirely removed and the pelletwas air-dried for about 5 min. Then, the pellet was diluted in 10 µL nuclease-free water and the new concentration was determined in the NanoDrop™ OneC UV-Vis Spectrophotometer.

3.2.5 Generation of mitochondrial extracts

In order to enrich the desired mitochondrial mRNA mitochondria were isolated from HEK Ctl, APPwt and APPsw cells. Therefor cells were washed with ice-cold PBS CMF and seeded into large Greiner CELLSTAR® dishes (143 cm²) (8 plates for each cell line). After two days of growing, the medium was exchanged and on the third day the isolation of mitochondria was performed based on Sims *et al.* [432]. In brief, cells were collected in 10 mL ice-cold IB (pH= 7.4 at 4°C), the combined suspensions were centrifuged (1,000 x g, 4°C, 5 min) and the pellets were resuspended in 7 mL of a 12%-Percoll® solution. The obtained cell suspension was homogenized using a Wheaton™ Dounce Tissue Grinder (V_{max}= 7 mL) with ten loose and ten tight strokes. Then, the homogenates were carefully applied onto previously prepared discontinuous percoll gradients consisting of 7 mL 26%-Percoll® layered above 4 mL 40%-Percoll® (see Figure 3.3). For a better differentiation of the two gradient layers, a few drops of Trypan blue solution can optionally be added to the 40%-Percoll® solution. The homogenates of one cell line were split on two gradients. Before the ultracentrifugation, all tubes were weighed and, if necessary, topped up with 12%-Percoll® until all tubes weighed the same. A first ultracentrifugation step was performed in a fixed angle rotor (Beckman Type 60 Ti) in the Optima™ LE-80K Preparative Ultracentrifuge (30 700 x g, 14 min, 4°C). Afterwards the lower intermediate layer was collected with a disposable Soft-ject® plastic syringe and 17G Hamilton™ needles with blunt tips (see again Figure 3.3). Here, care was taken to ensure that as little material as possible was absorbed into the syringe from the overlying layers. The obtained mitochondrial extracts were united in a new ultracentrifugation tube and filled with IB up to 20 mL. Here, attention was again paid to a uniform weight of all tubes. After the second ultracentrifugation (16,700 x g, 4°C, 12 min) mitochondria were accumulated in a fluffy pellet.

This pellet was transferred with 500 µL IB into a new reaction tube and after a last centrifugation step (7,300 x g, 4°C, 5 min) the resulting pellet was dissolved in 800 µL TRI Reagent® to immediately start isolation of mitochondrial RNA. Further steps were performed as described in section 3.2.4.

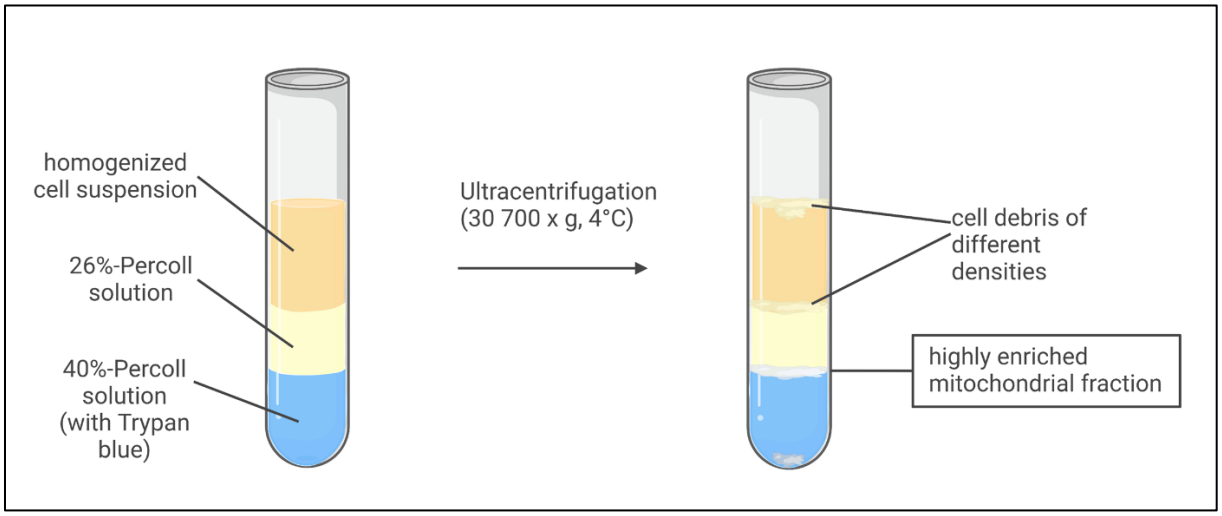

Figure 3.3: Typical appearance of a centrifuge tube at the beginning and at the end of the density gradient ultracentrifugration step. On the left hand side a discontinuous percoll gradient is shown consisting of a 26%-Percoll above a 40%-Percoll solution. The previously homogenized cell suspension (diluted in 12%-Percoll) is layered on top. After ultracentrifugation with 30,700 x g at 4°C mitochondria are enriched in the lower intermediate layer as indicated in this illustration.

3.2.6 Site-specific m^1A^{1374} analysis method

DNA digestion with DNase I

First of all, total RNA and RNA from mitochondrial extracts were incubated with DNase I (1 U/10 µL) and 10x DNase digestion buffer according to the manufacturer's instructions (21°C, 15 min) in order to eliminate any existing DNA contamination. Afterwards, an additional phenol-chloroform extraction was performed as described in section 3.2.4. to remove the residual DNase I. In brief, 1 mL TRI Reagent® and 200 µL chloroform was added, then samples were vortexed and centrifuged (16,000 x g, 4°C, 15 min). Afterwards, the upper aqueous phase was taken and mixed in a 1:1 ratio with 2-Propanol. Besides 1 µL Glyogen was added and the mix was incubated for 5 min (at 21°C) and again centrifuged (16,000 x g, 4°C, 10 min). In the next step, the supernatant was removed and the RNA pellet was washed twice with ice-cold 75% ethanol combined with a centrifugation step (16,000 x g, 4°C, 5 min). In the end, the RNA pellet was air-dried for about 5 min and then reconstituted in 10-20 µL nuclease-free water. RNA concentrations were determined in the NanoDrop™ OneC UV-Vis Spectrophotometer.

Library Preparation

For the reverse transcription X µL DNase treated RNA (X= volume of 2 µg RNA), 1 µL dNTP mix, 12.5-X µL nuclease-free water and 0.5 µL of a target-specific RT primer (stock solution= 100 µM) (primer sequence in Table 3.5) were mixed and incubated for 5 min at 75°C. In the following incubation step on ice (4°C, 5 min) the RT primer anneals to the corresponding RNA sequence. Next 1 µL SuperScript™ IV (SS-IV) (end concentraion= 10 U/µL), 1 µL DTT (end concentration= 5 mM) and 4 µL 5x RT buffer were added, mixed and incubated for 2 hours at 50°C for primer elongation. Afterwards, the RT enzyme was inactivated at 80°C for 15 min. As illustrated in Figure 3.4, the RT primer contains a target-specific sequence complementary to the mRNA of ND5 and part 1 of the p7 sequencing primer, which is complementary to the NEBNext® Multiplex Small RNA Library Prep Set for Illumina® p7 primers that enable indexing in the following PCR. The PCR was conducted with 10 µL RT product, 0.5 µL Platinum SuperFi (end concentration= 0.04 U/µL), 5 µL 5x SuperFi buffer, 0.5 µL dNTP mix, 5 µL 5x GC Enhancer, 1.25 µL of a custom-designed p5 forward primer (sequence in Table 3.5) (end concentration= 0.5 µM) and 0.5 µM of an individual reverse p7 primer from the NEBNext® Multiplex Small RNA Library Prep Set for Illumina®. The custom PCR p5 primer contains the flow cell binding sequence 1, the p5 sequencing primer site and a target-specific sequence complementary to the cDNA of ND5 (see Figure 3.4). The commercial p7 index kit primers introduce individual barcodes for each sample and additionally contain the p7 sequencing primer site (part 2) as well as the second flow cell binding sequence. The PCR was then started in Thermocycler peqSTAR with a specific protocol comprising an initial denaturation step at 98°C (2 min), 30 cycles at 98°C (15 min), 63°C (1 min) and 72°C (2 min), and a final extension step at 72°C (5 min).

To verify synthesis of the desired PCR amplicon, a digestion with MvaI (BstNI) can optionally be performed. This enzyme cleaves within a sequence (5'…CC↓WGG…3') close to m^1A^{1374} which allows to check whether the desired amplicon or a wrong product (e.g. primer dimers) have been amplified. So for this quality control step 10 µL PCR product, 1 µL MvaI, 2 µL 10x buffer R and 12 µL nuclease-free water were mixed and incubated according to the manufacturers instructions (1 h, 37°C). If this optional digestion step is to be conducted, it is recommended to put one sample as duplicate into the PCR so that one product can be digested and the other product can be used to generate sequencing results.

In the next step, PCR and digestion products were separated on a 10% denaturing PAGE and the desired amplicon was purified via size selection. To pour the gel, 100 mL of a 10% Acrylamidemix gel solution with Urea were mixed with 400 µL of a 10% APS solution and 50 µL TEMED. The Acrylamide gel solution was mixed before in a 50:40:10 ratio of Rotiphorese® Sequencing gel concentrate, Rotiphorese® Sequencing gel diluent and

Rotiphorese® Sequencing gel buffer concentrate. The dimensions of the gel were 35 cm x 20 cm x 0.1 cm (height x width x depth) and a comb with 15 pockets was used. After 15 min of gel polymerization, the comb was removed and the gel was installed into a large format gel chamber LSG-400-20 covered with 1x TBE in the upper chamber. 1x TBE buffer was produced by diluting Rotiphorese® 10x TBE buffer in nuclease-free water in a 1:10 ratio. 1x TBE was

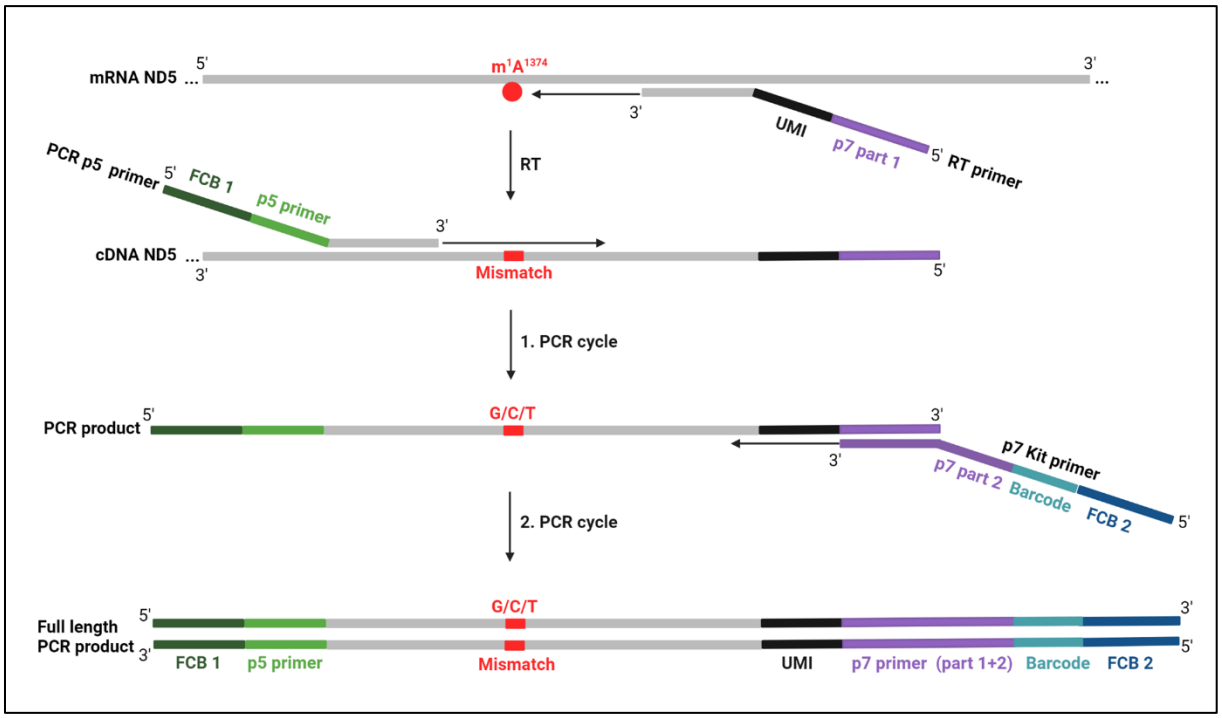

Figure 3.4: Schmatic overview of primer design and primer binding during library preparation for the m^{1}A^{1374} analysis method. The custom-designed RT primer binds to the mRNA of ND5 downstream of m^{1}A^{1374} (red) due to a target-specific complementary sequence. Besides the RT primer contains a unique molecular identifier (UMI, black) and part I of the p7 primer sequence (purple). After RT with SS-IV m^{1}A-induced mismatch (red) is incorporated in the cDNA of ND5. In the following PCR the custom-designed PCR p5 primer binds upstream of position 1374 with a sequence complementary to the cDNA of ND5. The PCR p5 primer additionally contains the p5 read seq primer (light green) and the flow cell binding sequence 1 (FCB1, dark green). In the second PCR cycle the p7 Kit primer is able to bind to the PCR product of the first cycle due to the complementary p7 sequence introduced by the RT primer. This part includes both p7 read seq primer and the p7 index seq primer, which are both used in the subsequent sequencing run. Moreover, the p7 Kit primer contains a sample-specific Barcode sequence (turquoise) in order to trace back all reads to the sample of origin, and the flow cell binding sequence 2 (FCB 2, dark blue). So in the end, the full length PCR product provides all sequences needed for Illumina sequencing (PE 75 mode).

also poured into the chamber on the bottom of the apparatus. The gel was pre-heated for about 10 min with 15 Watt (W). The whole PCR product solution (25 µL) was mixed with the same volume of DNA loading buffer and carefully injected into the gel pockets. Besides, 1 µL GeneRuler Low Range DNA Ladder, 4 µL 6x DNA Loading Dye, 5 µL nuclease-free water and 10 µL DNA loading buffer were combined and applied into the outer pockets. Then, the apparatus was covered with the corresponding lid, connected to the PowerSupply and run for about 2 h (15 W). When the electrophoresis was completed, the gel was detached from the apparatus and stained via incubation in a GelRed® solution (1:2 mixture of GelRed® Nucleic

Acid Gel Stain and 1x TBE) for 15 min. Afterwards, the gel was wrapped in a transparent plastic foil and scanned in the Typhoon TRIO+ Variable Mode Imager (Mode: Fuorescence, 200 micron, 450 PTM). On the basis of the obtained image, the MvaI digestion was visually verified and the expected full-length PCR product was excised at the height of 200 bp and above. The corresponding gel bands were transferred into reaction tubes and covered with 250 µL 0.5M NH_4Ac solution. In order to elute the DNA from the gel fragments, this solution was incubated overnight in a shaker (at 25°C and 750 rounds per minute (rpm)). The next day, the liquid phase was transferred into Nanosep® MF Centrifugal devices and centrifuged (10,000 x g, 5 min, 21°C) to remove any remaining gel fragments. The obtained filtrate was then mixed with 1 µL Glycogen and 700 µL 100% ethanol (temperature -80°C), vortexed and incubated for 1 h at -80°C. The following centrifugation (15,379 x g, 45 min, -5°C) conveys the precipitated DNA into a pellet and thus the supernatant was removed. The pellet was washed with 70% ethanol (100 µL) in combination with a centriguation step (15,379 x g, 10 min, -5°C). After the washing step, the ethanol was entirely removed and the pellet was air-dried for about 5 min. In the end, the pellet was resuspended in 5-10 µL nuclease free water and the concentration of the obtained DNA amplicon was determined in the NanoDrop™ 2000. Prior to sequencing, the prepared libraries were screened on D1000 ScreenTapes in the 4200 TapeStation System to check for adapter dimer contamination (quality control). Samples were then analyzed on an Illumina MiSeq platform in 2 x 75 bp paired-end mode, demultiplexed and the resulting FASTQ files used for further analysis.

Bioinformatic analysis

All fastq.gz-files were quality-controlled in FastQC v. 0.11.9 to assess presence of adapter sequences and Q-scores [433]. Then reads were trimmed with Trimmomatic v. 0.39, removing any remaining Illumina-related adapter sequences. Next, the trimmed reads were aligned to the reference sequence (human MT-ND5 cDNA Sequence Transcript-ID: ENST00000361567.2 or mouse MT-ND5 cDNA sequence Transcript-ID: ENSMUST00000082418.1, both from ensemble.org) using Bowtie2 v. 2.4.1 [429]. The alignment output was stored in BAM format. The two BAM files, one for the forward and one for the reverse reads correspondingly, were merged using SAMtools v. 1.10 [430]. Visualization of read coverage and mismatches was done by IGV v. 2.8.0 [431]. Mismatch rates were calculated in Microsoft Excel v. 16.57 by dividing the sum of all reads containing G, T or C at position 1374 by the number of total read counts. The jump rate was calculated by dividing the number of reads with deletions at position 1374 by the number of total read counts. Trimming and alignment parameters are listed in Table 3.11.

Table 3.11: Commands including trimming and alignment parameters.

java -jar /path/to/Trimmomatic-0.39/trimmomatic-0.39.jar PE -phred33 <input 1> <input 2> <paired output 1> <unpaired output 1> <paired output 2> <unpaired output 2> ILLUMINACLIP:/path/to/Trimmomatic-0.39/adapters/TruSeq3-PE-2.fa:2:20:7 LEADING:30 TRAILING:30 SLIDINGWINDOW:4:20 MINLEN:8 AVGQUAL:30
bowtie2 --no-1mm-upfront -D 15 -R 2 -N 0 -L 10 -i S,1,1.15 -p <number of processor cores - 2> -x '/path/to/Bowtie2_indexed_ND5_reference' -1 <mate 1> -2 <mate 2> -S <output.sam>

3.2.7 Quantitative PCR

In the first step, total RNA with high purity values (A260/280 > 2.0 and A260/230 > 1.5) was used to synthesize single-stranded cDNA by means of the High-Capacity cDNA Reverse Transcription Kit. According to the manufacturer's instrucctions, a 2x RT Master mix including 2 µL 10x RT buffer, 0.8 µL 25x dNTP mix, 2 µL 10x RT random primer, 1 µL MultiScribe™ and 4.2 µL nuclease-free water (volumes are given for one reaction and need to be scaled up to the corresponding number of samples) was prepared and briefly vortexed. Then, 10 µL RT Master mix were transferred into PCR tubes and mixed with the same volume of different total RNA samples. For this purpose, each sample was in advance diluted with nuclease-free water to obtain a concentration of 1 µg RNA/ 10 µL (results in 1 µg/ 20 µL during the reverse transcription process). Tubes were then sealed and briefly centrifuged in the Microcentrifuge MiniStar silverline to spin down contents and to elimate any air bubbles. Afterwards, tubes were then placed in the Thermocycler Biometra® T-gradient and a protocol comprising three steps (10 min at 25°C, 120 min at 37°C, 5 min at 85°C) was started. Once finished, cDNA samples were either used directly or stored at -20°C.

Before starting the qPCR, the Taqman™ fast advanced master mix and the Applied Biosystems™ TaqMan® Assay for ND5 and GAPDH were thawn on ice. Then, a qPCR master mix comprising 10 µL Taqman™ fast advanced master mix, 1 µL TaqMan® Assay and 7 µL nuclease-free water (each volume is given per one reaction) was prepared for both ND5 and GAPDH. Then, cDNA samples (concentration after RT = 1 µg/ 20 µL) were diluted in a 1:10 ratio with nuclease-free water to obtain a concentration of 5 ng/µL. In the next step, 2 µL of each sample (resulting in 10 ng/well) were placed into the Applied Biosystems™ MicroAMP™ Optical 96-well Reaction plate as two triplicates (3 wells for the detection of the target gene ND5 and 3 well for detection of the reference gene GAPDH). To avoid liquid artifacts and to ensure precise pipetting, a new pipette tip was used for each sample well. Additionally, one triplicate was filled with 2 µL nuclease-free water as no template controls. Then, 18 µL of the qPCR Master mix were added into each well with one triplicate filled with the ND5 and one triplicate filled with the GAPDH master mix for each sample. Afterwards, the plate was sealed with Applied Biosystems™ MicroAMP™ Optical adhesive film, centrifuged (1,000 x g, 4°C,

2 min) and then placed in the QuantStudio5 qPCR apperatus. The common protocol for all TaqMan® Assays starts with an incubation at 50°C for 2 min, continues with 95°C for 2 min to activate the polymerase and ends with 40 cycles including a DNA denaturation phase (95°C, 1 second) and a primer annealing/extenstion phase (60°C, 20 seconds). In the end, quality control and analysis of the resulting data was performed using the QuantStudio Design & Analysis software (v. 1.4.3) according to the manufaturer's instructions.

3.2.8 Analysis of human databases

Data of the "Aging, Dementia and TBI Study" data set was retrieved from http://aging.brain-map.org/download/index (RRID:SCR_014554, Allen Institute for Brain Science, University of Washington Medicine, and Kaiser Permanente Washington Health Research Institute, US) on the 20th of January 2020. Normalized FPKM values of the genes SDR5C1, TRMT10C, MT-ND5 and PRORP were extracted from the data set and saved in an Excel sheet together with the associated donor information using a custom R script (R Core Team 2018, v.3.6.0). The processing of the raw data was kindly accomplished by _____ _____ (Institute of Molecular Biology, Mainz). For the final analysis male patients with a confirmed AD diagnosis and without TBI incident were selected and normalized FPKM values were compared to controls (also without TBI incident) using Microsoft Excel v. 16.57 and GraphPad PRISM v. 9.2.0.

The scRNA-Seq study performed by Mathys *et al.* [426] provided fold change (FC) and adjusted p-values (padj) of all significantly altered genes in the supplementary material, among them TRMT10C and SDR5C1. PRORP and ND5 were not listed. For the comparison of AD vs. Ctl, early-stage AD vs. Ctl and late- vs. early-stage AD, the $\log_2$ FC and padj.-values of TRMT10C and SDR5C1 were visualized in heatmaps using the python package seaborn [434]. This visualization step was kindly performed by _____ (working group of Prof. Dr. _____, Johannes Gutenberg University of Mainz).

For the analysis of m^1A-induced mismatch at position 1374 in the mRNA of ND5, raw data reads of the precuneus and the primary visual cortex generated by Guennewig *et al.* [427] were downloaded from the NCBI SRA (project PRJNA720779). In the next step, the scripts written for the m^1A^{1374} analysis method were adapted and employed as described in section 3.2.6. This bioinformatic step was kindly conduced by _____ (working group of Prof. Dr. _____, Johannes Gutenberg University of Mainz).

3.2.9 Quantification of mitochondrial and cytosolic tRNAs

Relative content of mitochondrial tRNAs compared to the cytosolic tRNA pool was quantified in HEK293 T-Rex™ Ctl and pTRMT10C cells both untreated and treated with Tetracycline (24 h, 1 µg/mL). Therefore, fluorescently labeled hybridization oligos comprising a 40 nt long DNA stretch complementary to the 3'-end of each mitochondrial and cytosolic tRNA isoacceptor were custom-designed (purchased at biomers.net). The exact sequences of these oligos are not listed in this thesis, as they are part of an unpublished manuscript. Probes targeting the mitochondrial fraction were labeled with Cyanine-5 (Cy5), whereas probes targeting cytosolic tRNAs were labeled with 6-carboxyfluorescein (6-FAM). The mixture of 22 mitochondrial and 44 cytosolic oligos was hybridized with total RNA from all samples generated as described in section 3.2.4. Afterwards, the mix was applied on a native polyacrylamide gel to physically separate oligo-tRNA hybrids from excess oligo. Finally, fluorescence intensities of hybrid bands were measured in the Typhoon TRIO+ Variable Mode Imager and the ratio of Cy5 ((mt)tRNAs) to 6-FAM (cytosolic tRNAs) was compared across cell lines and four biological replicates. Experimental procedure and bioinformatics analysis were kindly conducted by _____ (working group of Prof. Dr. _____, Johannes Gutenberg University of Mainz).

3.2.10 Oxygen consumption and MMP measurements

Respiration assay in the Seahorse XFe 96 Extracellular Flux analyzer

Mitochondrial respiration was assessed in HEK293 T-Rex™ Ctl and pTRMT10C cells using the Seahorse XF Cell Mito Stress Kit according to the manufacturer's instructions. The Oxygen consumption rate (OCR) was measured in a Seahorse XFe 96 Extracellular Flux analyzer. Therefore, both Ctl and pTRMT10C were seeded two days prior to the experiment on Seahorse XFe 96 Cell Culture Microplates (80,000 cells per well) previously coated with Poly-L-lysine. 24 h later, the regular growth medium was replaced with DMEM containing 1 µg/mL Tetracycline. On the day of the assay, cells were washed once with PBS and the growth medium was replaced for XF Base Medium supplemented with 1 mM Pyruvate, 2.5 mM Glucose and 2 mM L-glutamine, and subsequently incubated for 1 h in a non-CO_2 incubator at 37°C. Measurements of the Basal respiration were recorded three times for ~12 min in advance of the first injection. 1 µM of Oligomycin (ATP synthase inhibitor), 1 µM of Carbonyl cyanide-p-trifluoromethoxyphenylhydrazone (FCCP) (mitochondrial uncoupler), and a mixture of 1 µM of Rotenone and Antimycin (inhibitors of the Cpx I and III, respectively) were injected sequentially (see Figure 3.5). The three measurements were taken in 20 min each. During the last injection, cells were labeled with 1.7 µM Hoechst to quantify the number of nuclei per well

for data normalization. The experiment was performed and analyzed by _____ at the University Medical Center, Mainz, Germany. Unfortunatelly, she did not provide detailed information on the used chemicals, which is why these products were not included in the “Material” section (section 3.1).

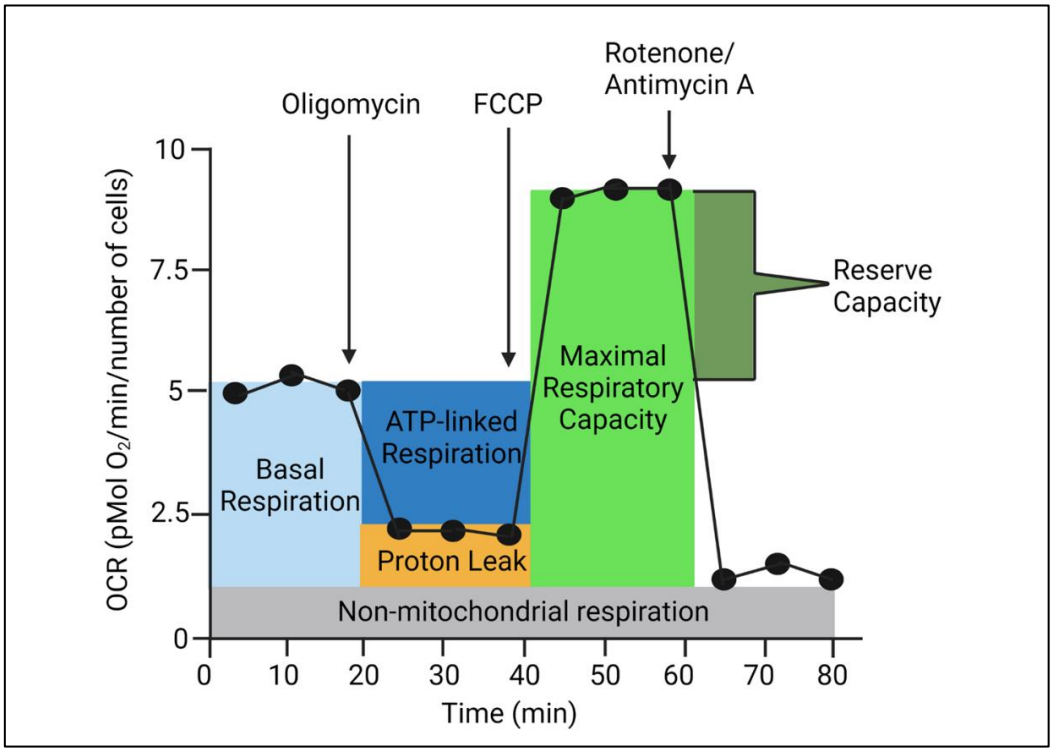

Figure 3.5: Representative oxygen consumption curve of HEK293 T-Rex™ Ctl cells from measurements in the Seahorse XFe 95 Extracellular Flux analyzer including resultant respiration parameters. Initially, the Basal respiration was measured in advance of the first injection. After addition of 1 µM Oligomycin (ATP Synthase inhibitor), the oxygen consumption drops and the resultant difference indicates the respiration linked to ATP (=ATP Turnover). Next, 1 µM FCCP (mitochondrial uncoupler) was added inducing pore formation in the IMM enabling protons to pass from the IMS into the matrix. As a compensatory mechanism the oxygen consumption rises until the Maximal respiratory capacity (=ETS Capacity) is reached. At the end of the protocol, a 1 µM mixture of Rotenone and Antimycin A (Cpx I and III inhibitors) is injected which decreases oxgen consumption to a minimum revealing the Non-mitochondrial respiration. The difference between the ATP-linked respiration and the Non-monitochondrial respiration results from protons that leak through the IMM. For this reason, this intermediate volume is reffered to as Proton leak. The difference between Maximal respiration and ATP-linked respiration is called Reserve capacity.

Respiration assay in the OROBOROS Oxygraph-2k

Mitochondrial respiration was additionally measured in the OROBOROS Oxygraph-2k High-resolution Respirometer. In brief, 2,000,000 cells were seeded two days prior to the experiment in 10 cm^2 dishes. 24 h later, the regular growth medium was replaced with DMEM containing 1 µg/mL Tetracycline. The next day, cells were detached with Trypsin, counted, and 2,000,000 cells were filled into the OROBOROS Oxygraph-2k High-resolution Respirometer. The Basal cellular respiration state (=Basal respiration) was measured first. Then, the mitochondrial coupling state (=Proton leak), non-coupled respiratory capacity (=Maximal

respiratory capacity) and the residual oxygen consumption (=Non-mitochondrial respiration) were tested using 2 µM Oligomycin, 1 µM FCCP and 1 µM Rotenone/Antimycin (similar to measurements in the Seahorse XFe 95 Extracellular Flux analyzer). The experiment was performed and analyzed by _____ at the University Medical Center, Mainz, Germany. Unfortunatelly, she did not provide detailed information on the used chemicals, which is why these products were not included in the “Material” section (section 3.1).

Mitochondrial membrane potential (MMP)

The MMP was analyzed in HEK293 T-Rex™ Ctl and pTRMT10C cells incubated with and without 1 µg/mL Tetracycline for 24 h. Therfore, 10,000 cells were seeded in a Greiner black 96-well plate with transparent bottom. On the day of the experiment, the medium was changed and replaced with Tyrode´s buffer containing 25 nM tetramethylrhodamine, methyl ester (TMRM) for 15 min at 37°C to evaluate the MMP. Cell nuclei were stained with 1 µg/mL Hoechst solution. Live cell imaging was performed with the dyes present during image acquisition at 37°C and 5% CO_2 with a 40x magnification in an automated confocal spinning disk Opera Phenix™ High-Content Screening System. Z-stacks with 6 planes (0.5-1 µm) and 24 images per well were acquired. 2 µM FCCP was added after imaging to quench the TMRM signal. Quantitative image analysis was done with the PhenoLOGICTM machine learning plugin. Afterwards, the ratio of treated and untreated cells was calculated in Microsoft Excel v. 16.57 and visualized in GraphPad PRISM v. 9.2.0. The experiment was performed and analyzed by _____ at the University Medical Center, Mainz, Germany. Unfortunatelly, she did not provide detailed information on the used chemicals and softwares, which is why these products were not included in the “Material” section (section 3.1).

4 Results

As a first step to investigate the hypotheses (i)-(iv) postulated in section 2, the levels of TRMT10C, m^1A^{1374} and ND5 were examined in HEK293 AD model cells (section 4.1). Then, a cell system that enables the selective overexpression of TRMT10C was studied to scrutinize the causative connection between TRMT10C, m^1A^{1374} methylation, ND5 protein levels and mitochondrial dysfunction (section 4.2). Subsequently, 5xFAD mice were employed in order to investigate the hypotheses in a whole AD model organism (section 4.3) and finally, the obtained results were verified in cortex tissue and RNA-Seq data from AD patients (section 4.4) to assess their relevance in human LOAD cases.

4.1 Investigation of HEK293 AD model cells

As a first step TRMT10C, m^1A and ND5 levels were examined in HEK293 AD model cells. To consider different types of AD, two distinct model cell lines (APPwt and APPsw) were used. HEK293 APPwt cells are stabily transfected with a DNA construct harboring the human wild-type APP-695 gene, inserted downstream of a cytomegalovirus promoter [216]. In humans, the APP gene is encoded on chromosome 21, therefore APPwt cells simulate the situation of APP overabundance similar to the situation in trisomy 21 patients. Since people with Down syndrome are at enormous risk (~97%) of developing AD [65], APPwt cells can be regarded as a model for LOAD. Due to the overproduction of APP, the generation of APP cleavage products is enhanced in this cell line as well. For instance, it was shown that APPwt cells show seven times higher $A\beta_{1\text{-}40}$ levels than the untransfected control cell line [216].

APPsw cells are stabily transfected with the same vector as APPwt, but bearing the Swedish double mutation in the APP-695 gene (K670M/N671L). These cells display even higher levels of APP than APPwt cells, and as a result of the mutation more APP cleavage products are generated through the amyloidogenic pathway. For example, $A\beta_{1\text{-}40}$ levels in APPsw cells are another 10x higher than in APPwt cells [216]. Therefore they simulate the case of FAD or a very late stage of LOAD. For both cell lines untransfected HEK293 served as control (Ctl).

4.1.1 TRMT10C protein expression in HEK293 cells

As a first indicator of m^1A^{1374} methylation, the expression of the writer enzyme TRMT10C was examined in the aforementioned AD cell models, following hypothesis (i). Via Western blot

the expression of TRMT10C was investigated in all three cell lines (Ctl, APPwt, APPsw). Besides, β-Actin was quantified to normalize for aberrant protein loading. In addition, APP protein levels were analyzed to double-ceck the stable transfection. As it was shown in Selkoe *et al.* [435] APP occurs as a heterogeneous group of differently spliced isoforms in a range of 110 to 135 kDa in neuronal and nonneuronal tissue. Therefore the entire band in this area was assessed.

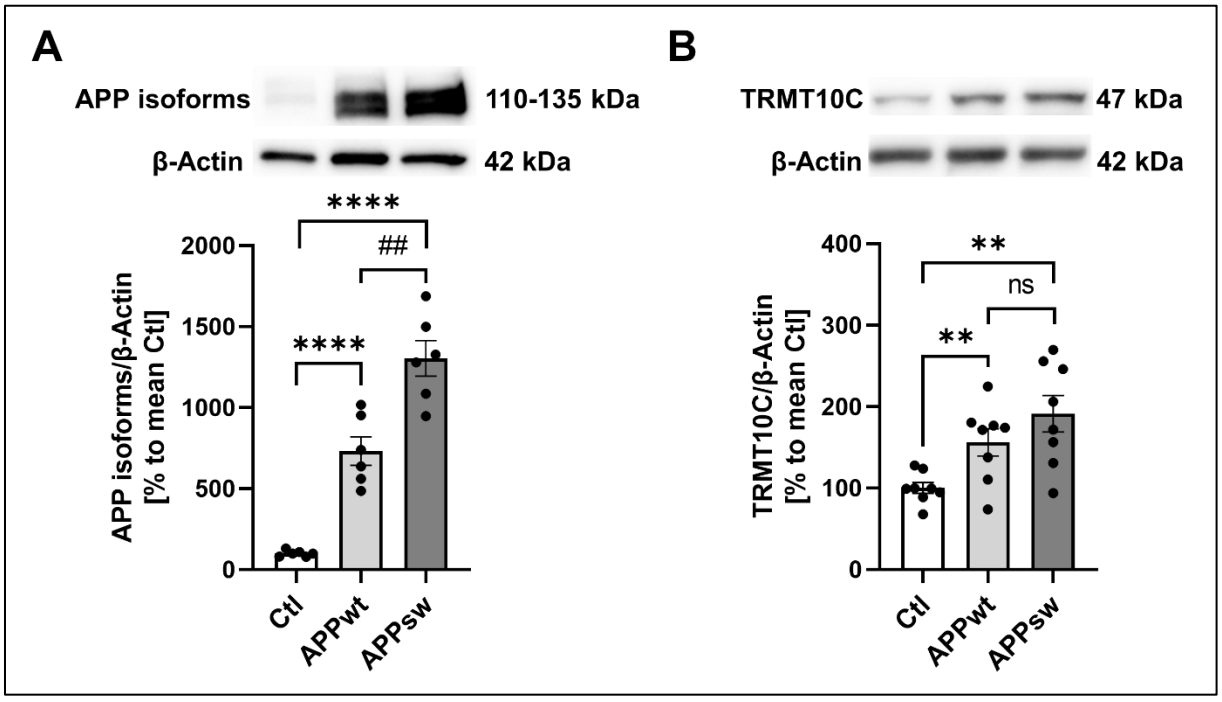

Figure 4.1: Overexpression of wild-type and mutant APP in HEK293 cells is associated with an upregulation of TRMT10C. A) Western blot results of APP in Ctl, APPwt and APPsw cells. A representative membrane is displayed in the upper panel. The results confirm that APP expression is dramatically increased in APPwt and even higher in APPsw cells. Mean ± SEM, n= 6 biological replicates, unpaired t-test. **B)** Western blot of TRMT10C reveals significantly increased TRMT10C protein levels in APPwt and APPsw cells in comparison to Ctl. A representative membrane is shown in the upper panel. Mean ± SEM, n= 8 biological replicates, unpaired t-test. **A)-B)** **p<0.01, ****p<0.0001.

APPwt cells show a strong overexpression of APP compared to Ctl (Figure 4.1A). The mean value of APPwt is 732%, reflecting more than seven times higher APP levels in APPwt cells than in Ctl. Likewise, APPsw cells present a strong APP overexpression, which is even higher than in APPwt (Figure 4.1A). On average, APPsw cells display a value of 1305% indicating 13 times higher levels of APP than in Ctl. The differences between both AD model cell lines and Ctl, as well as the difference between APPwt and APPsw, are highly significant.

Interestingly, TRMT10C protein levels are also significantly elevated in APPwt and APPsw cells compared to Ctl (Figure 4.1B). Similar to APP, the overexpression is more pronounced in APPsw cells than in APPwt. The augmentation in APPwt reaches 156%, whereas TRMT10C protein levels almost double in APPsw (196%) in comparison to Ctl. In this

case, the difference between APPwt and APPsw is not significant. These results suggest that TRMT10C expression is increased as a direct or indirect consequence of APP overexpression.

4.1.2 SDR5C1 and PRORP expression in HEK293 cells

It is known that TRMT10C strictly requires the presence of SDR5C1 to methylate adenosine and guanosine at position 9 in (mt)tRNAs [329]. For processing of the mitochondrial primary transcript, a third protein subunit, called PRORP, is additionally recruited [359]. To be precise, PRORP, TRMT10C and a SDR5C1 tetramer form together the tripartite mtRNase P complex, which cleaves the mitochondrial primary transcript by processing (mt)tRNAs at their 5' ends [360]. As of today, it is unclear whether SDR5C1 and PRORP are also required for the methylation of adenosine in (mt)mRNA or whether TRMT10C may function as a stand alone enzyme in this case. Therefore it was studied, if the overexpression of TRMT10C in APPwt and APPsw is accompanied by alterations in SDR5C1 and PRORP protein levels. Using Western blot the expression of both proteins was examined in Ctl, APPwt and APPsw.

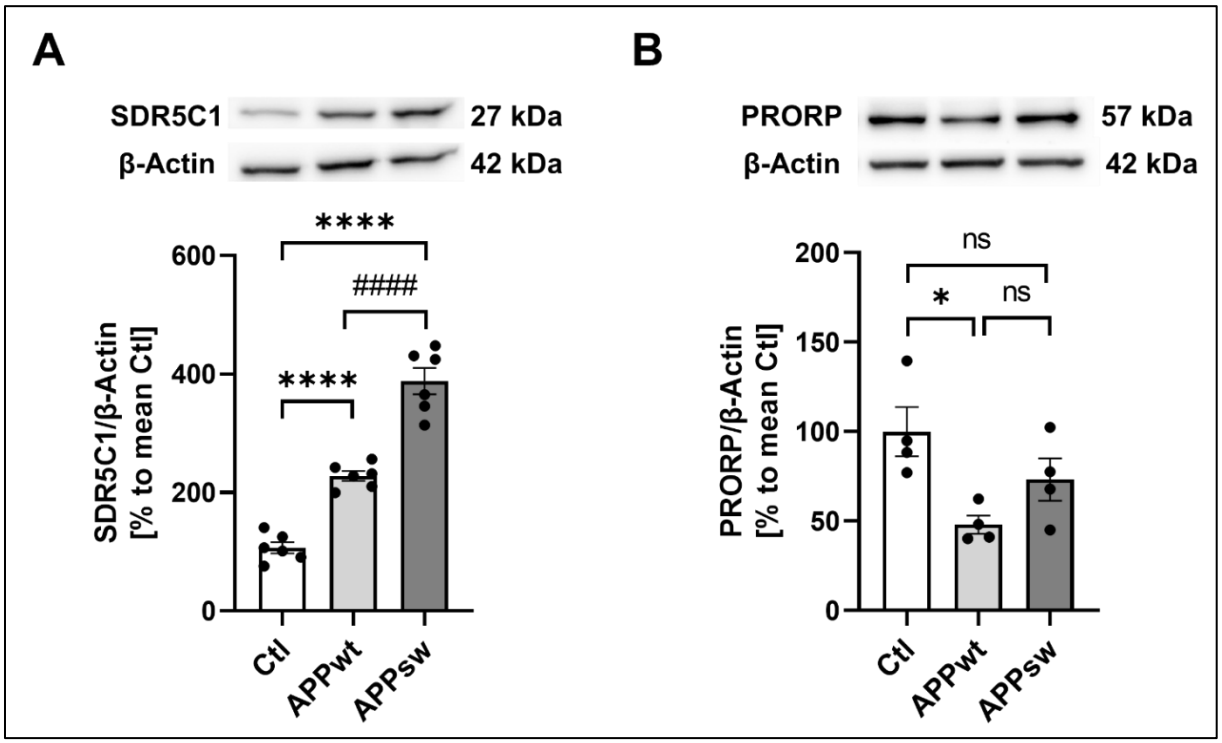

Figure 4.2: SDR5C1 protein levels are dramatically increased in HEK293 APPwt and APPsw cells. PRORP protein levels are decreased excusively in APPwt cells. A) Western blot results of SDR5C1 in Ctl, APPwt and APPsw cells. A representative membrane is shown in the upper panel. SDR5C1 levels are highly elevated in APPwt cells and even higher levels are reached in HEK APPsw. Mean ± SEM, n= 6 biological replicates, unpaired t-tests. **B)** Western blot results of PRORP in Ctl, APPwt and APPsw cells. A representative membrane is shown in the upper panel. PRORP levels are significantly decreased in APPwt cells in comparison to Ctl. PRORP expression in APPsw is not significantly altered in comparison to Ctl and APPwt. Mean ± SEM, n= 4 biological replicates, unpaired t-tests. **A)-B)** ns= not significant, *p<0.05, ****p<0.0001, ####p<0.0001.

In APPwt cells a strong upregulation of SDR5C1 is observed in comparison to Ctl. Likewise, APPsw cells show dramatically increased SDR5C1 protein levels. Both findings are highly significant. The intensity of the SDR5C1 band in APPsw (388%) is a lot higher than in APPwt (228%) and this difference is again highly significant. Interestingly, PRORP manifests a different behaviour. In APPwt cells, PRORP protein levels are significantly decreased. No significant change is detected in APPsw in comparison to both APPwt and Ctl. In summary, the behavior of SDR5C1 is similar to that of TRMT10C (Figure 4.1), whereas PRORP exhibits a different behavior.

4.1.3 m^1A^{1374} methylation levels in HEK293 cells

Since the expression of writer enzyme TRMT10C and the scaffolding protein SDR5C1 were elevated in APPwt and APPsw cells, the question arose whether methylation of m^1A^{1374} in ND5 mRNA was also altered in these cells (hypothesis (ii)). To this end, a site-specific analysis method was established, which is based on RT-PCR and Illumina sequencing. As m^1A impedes Watson-Crick base pairing it induces misincorporations at the opposite site in the newly synthesized cDNA strand during the RT. In the next step, the m^1A-surrounding sequence is amplified by use of PCR with individual sample barcodes and a high-fidelity PCR enzyme (Platinum SuperFi). After Illumina sequencing and a bioinformatics analysis including trimming and quality control, reads can be aligned to the human MT-ND5 reference sequence. At the end of the process, total read counts and the base composition at each individual position in the amplicon are displayed in IGV (v. 2.8.0.). The misincorporation rate can be calculated for a specific position by dividing the sum of misincorporated bases (T, G and C) in all sequenced cDNAs by the total number of read counts. As it has been shown several times in the literature, it can be assumed that the proportion of mismatch at a given position is correlated with the amount of m^1A in the original sample [341], [436].

Next to nucleotide misincorporations, this method offers a second possibility to estimate stochiometries of m^1A within a specific target sequence. Because, if a polymerase encounters m^1A during RT, there is a certain probability that the proximate base in the newly synthesized cDNA strand will be overleaped. These nucleotide skipping events, termed jumps, are detectable as deletion in the sequencing data and represent a second independent parameter to assess m^1A methylation levels [437]. It is important to mention that m^1A can also induce synthesis abortion during the RT process. These truncated cDNAs cannot be amplified in the following PCR, because they lack one of the two PCR primer binding sites. For this reason, only strands containing misincorporations and jumps can be assessed in the final analysis of sequencing data, while truncated reads cannot be evaluated in this experiment setup.

The frequency and proportion of misincorporation, jumps and abortions, merged from all sequenced cDNAs, yield the so-called RT signature. It is dependent on multiple factors, comprising the kind of base preceding the modified site, the type of RNA modification, the polymerase used and applied reaction conditions [438], [439]. For example, replacing Mg^{2+} with Mn^{2+} in the reaction buffer was shown to enhance the read-through capability of the RT, thus leading to an increase of nucleotide skipping events and to a drop of arrest rates. This was exemplified by m^1A-containing positions in tRNAs [437].

Determining optimal reaction conditions for the m^1A^{1374} analysis method in HEK293 Ctl cells

To verify whether the substitution of Mg^{2+} by Mn^{2+} is also beneficial in the case of m^1A^{1374} in ND5 mRNA, both conditions were tested with total RNA from HEK293 Ctl cells in an initial experiment. Thereby, the RT was performed once with the commercially available RT buffer containing 5 mM $MgCl_2$, and once with a custom-made RT buffer including 5 mM $MnCl_2$. All other buffer components and reaction conditions remained unchanged. Furthermore, two different polymerases were tested, namely SS-IV and EpiScript, to identify the most appropriate RT conditions for this m^1A site.

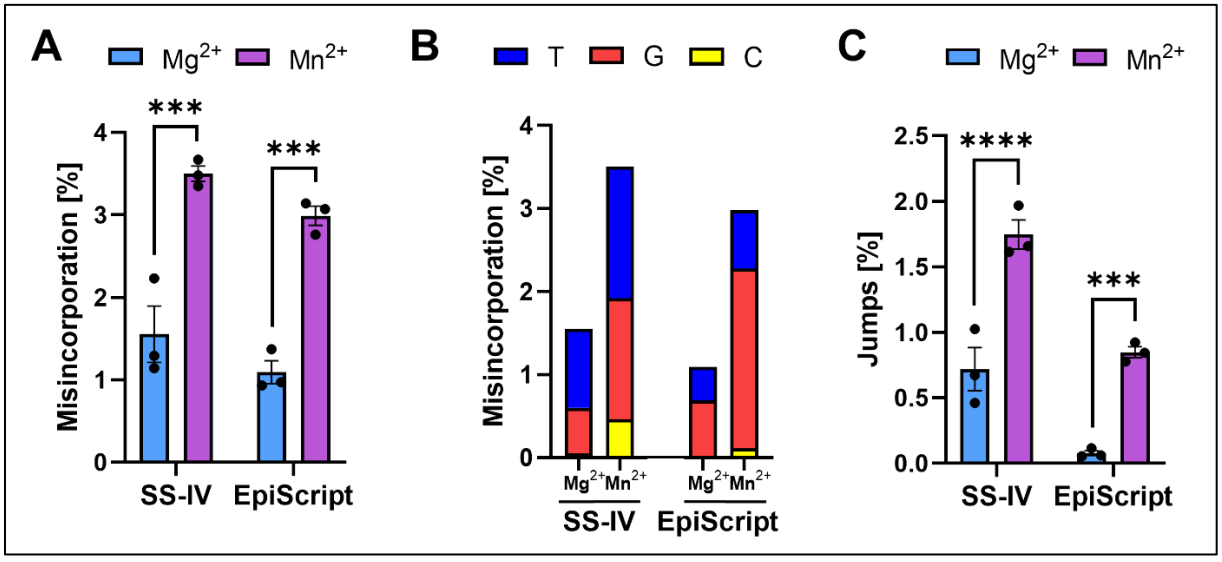

Figure 4.3: Manganese ions in the RT buffer boost m^1A-induced misincorporations and jumps. A) Total RNA from HEK293 Ctl cells was subjected to RT with SS-IV and EpiScript both with RT primers targeting ND5. For each reverse transcriptase the RT was performed with the commercially available buffer, containing 5 mM $MgCl_2$ and with a self-made RT buffer, where $MgCl_2$ was substituted by 5 mM $MnCl_2$. After PCR and Illumina sequencing mismatch rates at position 1374 in ND5 mRNA were evaluated. Mn^{2+} significantly raises misincorporation levels. This applies for SS-IV and EpiScript. Mean ± SEM, n= 3 biological replicates, unpaired t-tests. **B)** Data from A) subdivided according to the averaged composition of misincorporated bases. Mn^{2+} does not alter mismatch composition. T=Thymidine, G= Guanosine, C= Cytidine. **C)** Sequencing data from A) was analyzed for jumps at the equivalent position. Mn^{2+} significantly enhances the jump rate during RT with SS-IV and EpiScript. Mean ± SEM, n= 3 biological replicates, unpaired t-tests. **A)-C)** ***p<0.001, ****p<0.0001.

As can be seen in Figure 4.3A, a Mn^{2+}-containing RT buffer vastly increases m^1A-induced misincorpration rates. As for SS-IV, mismatch rates roughly double and the mean value rises from 1.55% to 3.50%. In the case of EpiScript, misincorporation rates nearly triple and the mean value increases from 1,09% to 2,99%. Both changes are highly significant.

Regarding Figure 4.3B, replacing Mg^{2+} by Mn^{2} does not seem to affect the mismatch composition. For both the Mg^{2+}- and the Mn^{2+}-containing buffer, mainly T and G is detected in the sequencing reads, indicating that m^1A preferentially induces incorporation of A and C during the RT process. However, Table 4.1 reveals that the ratio of misincorporated T, G and C is slightly changed, when comparing the relation of T, G or C to the total number of mismatches. Using Mn^{2+}, the proportion of T slightly decreases in case of both polymerases and proportionally more C and G appear. It cannot be ruled out that these changes occurred by chance.

Table 4.1: Amount of misincorporated T [%], G [%] and C [%] in relation to the total amount of mismatch [%] at position 1374 of ND5 mRNA. Data set from Figure 4.3.

Ratio $\frac{Base\ [\%]}{Mismatch\ [\%]}$	SS-IV, Mg^{2+}	SS-IV, Mn^{2+}	EpiScript, Mg^{2+}	EpiScript, Mn^{2+}
T	0.612	0.454	0.366	0.235
G	0.355	0.416	0.614	0.727
C	0.033	0.130	0.021	0.038

Not only the misincorporation, but also the jump rate is significantly elevated by replacing Mg^{2+} by Mn^{2} in the RT buffer (Figure 4.3C). For both SS-IV and EpiScript, jump rates more than double. And again, the augmentation is more pronounced for EpiScript. However, jump rates are generally at lower in reads generated with EpiScript than those generated with SS-IV. For example, the mean value of SS-IV with the Mg^{2+}-containing buffer is 0.72%, while for EpiScript it is only 0.08%. Also, with the Mn^{2+}-containing buffer, the mean value of SS-IV is higher (1.75%) than that of EpiScript (0.85%).

At this point, it must be mentioned that the use of Mn^{2+} in the RT buffer entails a substantial disadvantage. Because, even if the rate of misincorporations and jumps is elevated, the total amount of reads is dramatically reduced with Mn^{2+}. Thus, the number of total read counts in SS-IV drops by a power of ten from ~100 000 to about ~10 000. As for EpiScript, the number of total read counts falls by almost 3 orders of magnitude from ~1 000 000 to about 4 000. The massive reduction of total read counts due to Mn^{2+} not only reduces reliability of the results, but also massively complicates the handling during library preparation. While a clear amplicon band appears in the polyacrylamide gel after RT with Mg^{2+} and PCR, the amplicon band of samples from RT with Mn^{2+} and PCR is not visually recognizable (shown exemplarily in Figure 4.5). The theoretical length of the amplicon is 199 bp (more information in section 3 Materials and Methods), however, the band appears a

little higher in the denaturing gel and is therefore difficult to determine on basis of the marker. Since the Mg^{2+} sample shows only one clear band in the area around 199 bp (see Figure 4.5, red box, lane 2), this band can be cut out and purified easily. In the lane 1, were the Mn^{2+}

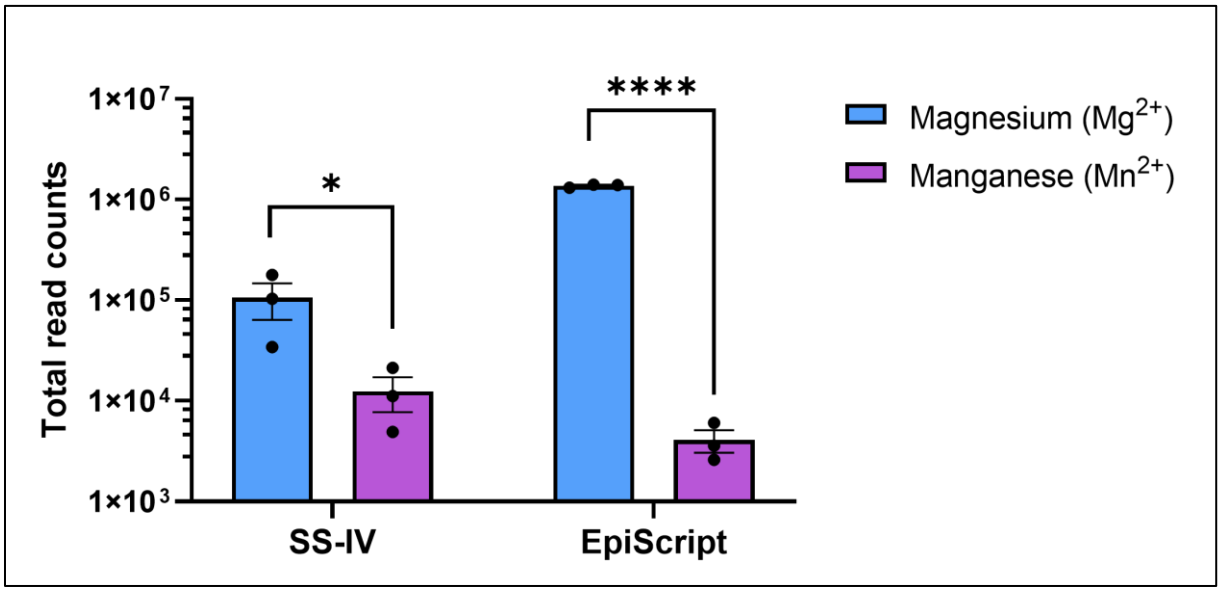

Figure 4.4: Total read counts of total RNA samples from HEK293 Ctl cells after RT-PCR with different RT conditions. Number of total read counts dramatically drops by using Mn^{2+} in the RT buffer. In the data set from Figure 4.3. the number of total read counts was determined with IGV (v. 2.8.0) for each sample and plotted in a logarithmic scale. Mn^{2+} decreases the obtained number of read counts in comparison to the Mg^{2+}-containing buffer. This applies for both of the investigated reverse transcriptases (SS-IV and EpiScript). Mean ± SEM, n= 3 biological replicates, unpaired t-tests. *p<0.05, ****p<0.0001.

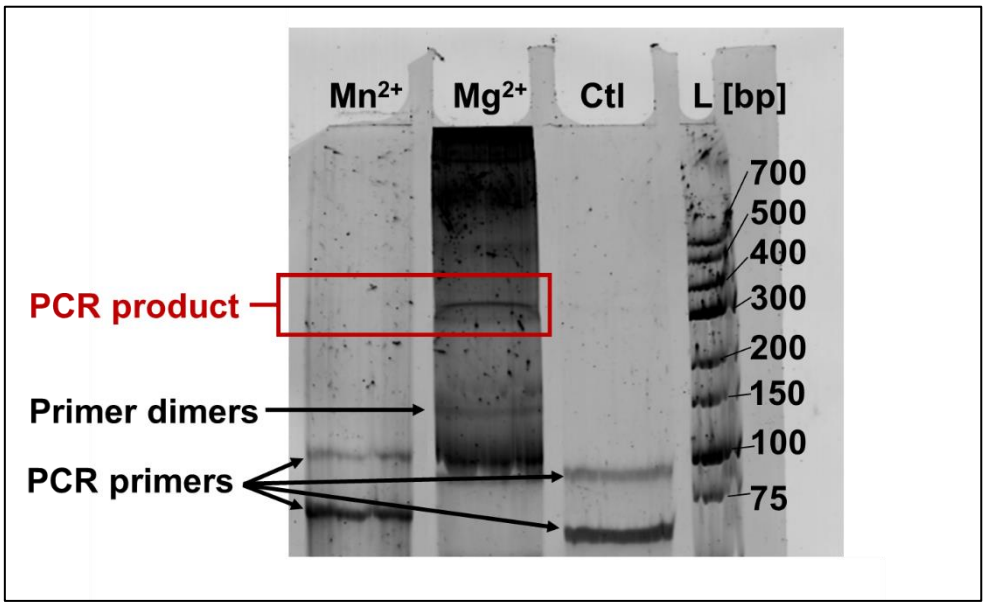

Figure 4.5: RT with Mn^{2+} causes massive handling problems because no clear amplicon band is visually recognizable after RT-PCR in the polyacrylamide gel. In this representative gel 2 µg of total RNA from HEK293 Ctl cells were subjected to RT with SS-IV. In one approach, RT was performed with 5 mM $MnCl_2$ (lane 1) in the RT buffer, and in the other approach, RT was performed with 5 mM $MgCl_2$ (lane 2). In the PCR control (lane 3), cDNA was replaced by water and PCR was conducted as usual. In lane 4, a low range ladder was applied. Ctl= PCR control, L= ladder, bp= base pairs. 10% denaturing polyacrylamide gel.

sample was loaded, the amplicon band is harder to make out. Hence, cutting out the band and the purification steps are more difficult. DNA yields are consequently lower and the whole sample might get lost during the isolation procedure. For this strong reason, a Mg^{2+}-containing RT buffer was chosen for the following analysis of m^1A^{1374} in HEK293 Ctl, APPwt and APPsw cells. Besides, the polymerase SS-IV was selected because, unlike EpiScript, it generates relatively high jump rates with a Mg^{2+} buffer, providing a second, indepedent parameter to assess m^1A methylation levels. In contrast, jump rates of EpiScript with Mg^{2+} were very low (~0.08%), which would make it very difficult to detect small differences.

Application of the m^1A^{1374} analysis method to total RNA from HEK293 cells

In the next experiment, total RNA was extracted from Ctl, APPwt, and APPsw cells and subjected to RT-PCR with SS-IV and Mg^{2+} to accurately determine m^1A^{1374} methylation levels. The reasons for choosing these parameters were explained in the previous section. After Illumina sequencing and bioinformatic analysis of the sequencing raw data, misincorporation and jump rates at position 1374 in ND5 were determined for each sample.

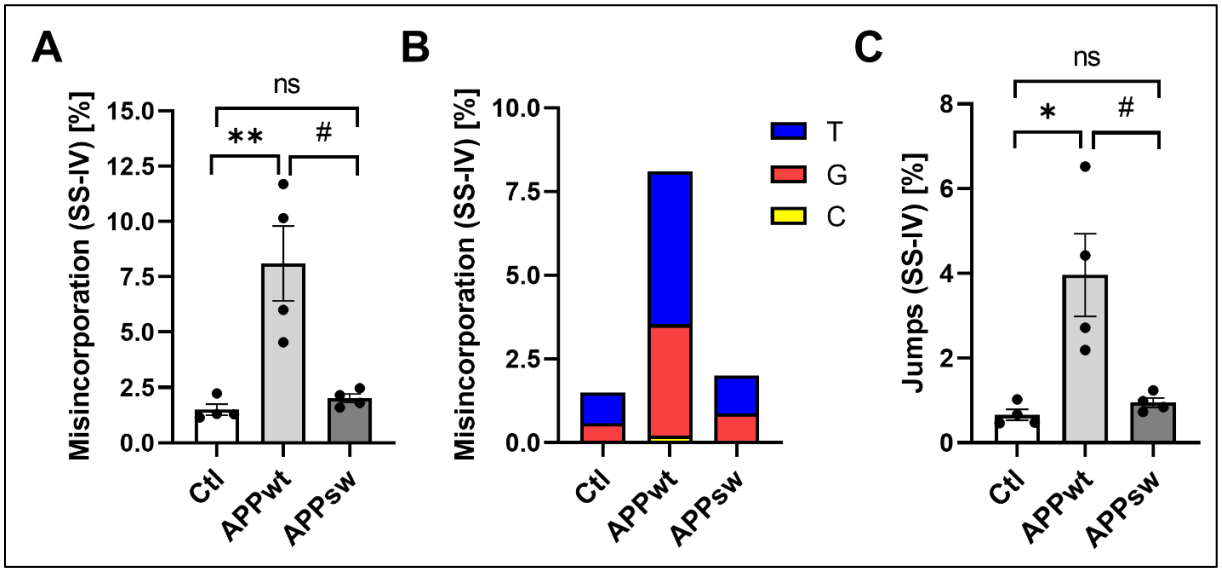

Figure 4.6: m^1A-induced misincorporations and jumps at position 1374 in ND5 are significantly elevated in total RNA samples from HEK293 APPwt cells. A) Misincorporation rate after RT with SS-IV, PCR and Illumina sequencing. Misincorporation levels are significantly increased in APPwt cells. Values of APPsw cells are not significantly altered in comparison to Ctl. Mean ± SEM, n= 4 biological replicates, unpaired t-tests. **B)** Data from A) subdivided according to the averaged composition of misincorporated bases. Mismatch consists maily of incorporated Thymidine and Guanosine in all three sample groups. T= Thymidine, G= Guanosine, C=Cytidine. **C)** Sequencing reads from A) were analyzed for jumps at the equivalent position. Jump rate was significantly increased in APPwt cells in comparison to Ctl. Jumps in APPsw were unchanged in comparison to Ctl. Mean ± SEM, n= 4 biological replicates, unpaired t-tests. **A)-C)** ns= not significant, *p<0.05, **p<0.01, #p<0.05.

m^1A-induced misincorporation levels at position 1374 of ND5 are significantly increased in APPwt cells in comparison to Ctl (Figure 4.6A). Ctl shows an average value of 1.5%, while the mean value of APPwt is 8.1%. In contrast, the mean value of APPsw is 2.0%, which is approximately in the range of Ctl. Thus, no significant change can be observed between APPsw and Ctl. However, the difference between APPwt and APPsw is significant. Since the samples were treated under the same RT conditions, no substantial changes are observed in the composition of mismatched bases (Figure 4.6.B and Table 4.2.). In all three cell lines, mainly T and G are found in the sequencing data, indicating that m^1A particularly leads to incorporation of A and C during the RT process.

Table 4.2: Amount of misincorporated T [%], G [%] and C [%] in relation to the total amount of mismatch [%] at position 1374 of ND5. Data set from Figure 4.6.

Ratio $\frac{Base\ [\%]}{Mismach\ [\%]}$	Ctl, total RNA	APPwt, total RNA	APPsw, total RNA
T	0.615	0.563	0.562
G	0.351	0.411	0.409
C	0.078	0.026	0.029

Of note, jump rates show the same pattern as misincorporation rates (Figure 4.6C). Hence, the jump rate of APPwt is significantly enhanced in comparison to Ctl and rises from 0.67% to 3.96%. Low jump rates are observed for APPsw cells (0.95% on average). The difference between APPwt and APPsw is significant, whereas no significant change is measured between APPsw and Ctl. The results from Figure 4.6A and Figure 4.6C clearly indicate enhanced m^1A^{1374} methylation of ND5 mRNA in APPwt compared to Ctl and APPsw.

Application of the m^1A^{1374} analysis method on mitochondrial extracts from HEK293 Ctl, APPwt and APPsw cells

The m^1A site examined in this section is located at position 1374 of the ND5 mRNA, which is mitochondrially encoded. Since mitochondrial RNAs account for less than 5% of the total RNA pool in healthy cells [440], it was verified wether an isolation of mitochondria prior to the m^1A analysis method could improve the accuracy of the method. Therefore, mitochondrial extracts from Ctl, APPwt, and APPsw cells were isolated by means of a discontinuous Percoll® gradient (more detailed description of the procedure in section 3 Materials and Methods) and subjected to RT-PCR with SS-IV and a Mg^{2+}-containing RT buffer. After Illumina sequencing and bioinformatics analysis, the following results were obtained.

Both misincorporation and jump rates are clearly elevated in mitochondrial extracts of APPwt cells in comparison to extracts of the other two cell lines (Figure 4.7A and Figure 4.7C). Whereas the misincorporation rate for Ctl and APPsw is around 5% (Ctl: ⌀ 5.7%, APPsw:

≙ 4.5%), the mean value for APPwt is 9.7%. The jump rate is also substantially higher in mitochondrial extracts from APPwt (3.5%) than in extracts from Ctl (1.8%) and APPsw (1.7%). However, only two biological replicates were sequenced, therefore no statement about statistical significance is possible. Once again, the composition of mismatch remains largely unchanged between the three cell lines (Figure 4.7B and Table 4.3).

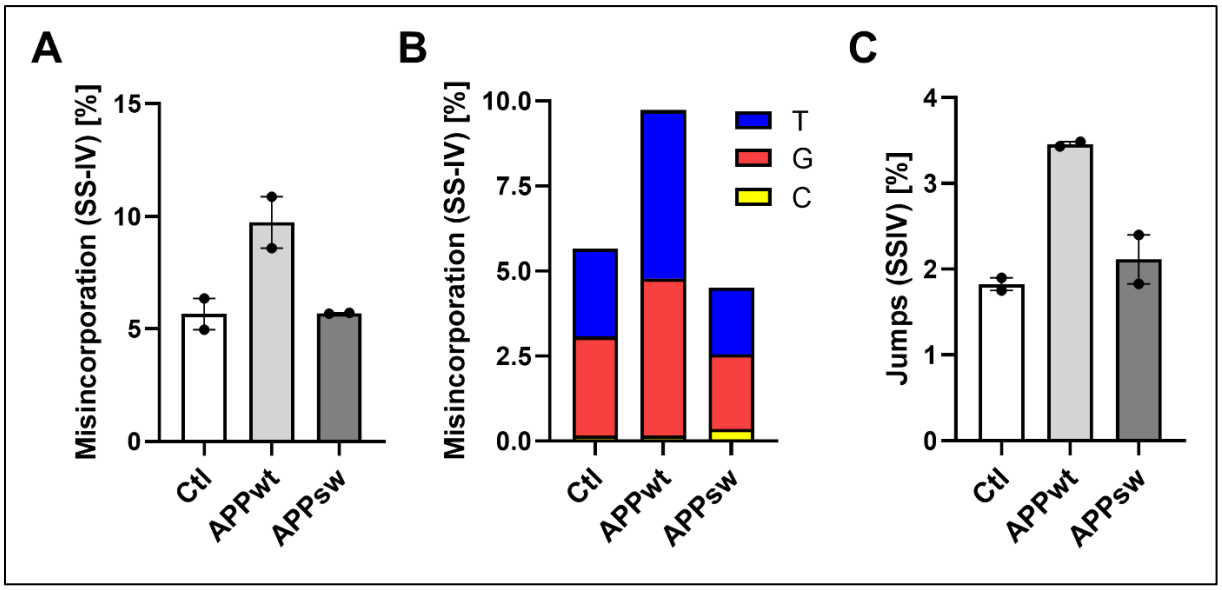

Figure 4.7: m^1A-induced misincorporations and jumps at position 1374 of the ND5 sequence. Mitochondrial extracts confirm elevated m^1A methylation levels in APPwt compared to Ctl and APPsw. A) Misincorporation rates in mitochondrial extracts obtained from Ctl, APPwt and APPsw reveal increased mismatch in APPwt, but not in APPsw. Mean ± SEM, n= 2 biological replicates. **B)** Data from A) subdivided according to the averaged composition of misincorporated bases. Mismatch consists maily of incorporated Thymidine and Guanosine in all three sample groups. T= Thymidine, G= Guanosine, C= Cytidine. **C)** Sequencing reads from A) were analyzed for jumps at the equivalent position. Jump rate was again increased in APPwt cells in comparison to Ctl. Jumps in APPsw were approximately on the same level as Ctl. Mean ± SEM, n= 2 biological replicates. **A)+C)** No statistics were performed due to the insufficient number of samples.

Table 4.3: Amount of misincorporated T [%], G [%] and C [%] in relation to the total amount of mismatch [%] at position 1374 of ND5. Data set from Figure 4.7.

Ratio $\frac{Base\ [\%]}{Mismatch\ [\%]}$	Ctl, mito. RNA	APPwt, mito. RNA	APPsw, mito. RNA
T	0.457	0.508	0.434
G	0.514	0.475	0.487
C	0.028	0.016	0.079

In the sequencing data mainly mismatches of T and G are observed (see Table 4.3), suggesting that m^1A preferentially induced incorporation of A and C during the RT process. The results of mitochondrial extracts again demonstrate, similar to the result obtained with total RNA, that m^1A^{1374} methylation levels are higher in APPwt cells in comparison to Ctl and APPsw.

4.1.4 ND5 protein and mRNA levels in HEK293 cells

The preceding experiments showed that the AD model cell line APPwt displays elevated levels of m^1A^{1374}. As it is known that m^1A hinders Watson-Crick base pairing, it was hypothesized that m^1A impedes the mitochondrial translation process and consequently decreases the protein synthesis of ND5 (hypothesis (iii)). To verify this presumption, the direct effect of increased m^1A^{1374} methylation on ND5 protein levels was examined in the next step. For this purpose, a Western blot of ND5 was performed with total protein extracts from HEK293 Ctl, APPwt and APPsw cells. Though polysome fractioning experiments suggested a repressive effect of m^1A on translation [312] and m^1A was shown to induce ribosome stalling [341], the direct effect of m^1A^{1374} on the ND5 protein level has never been studied before in the literature.

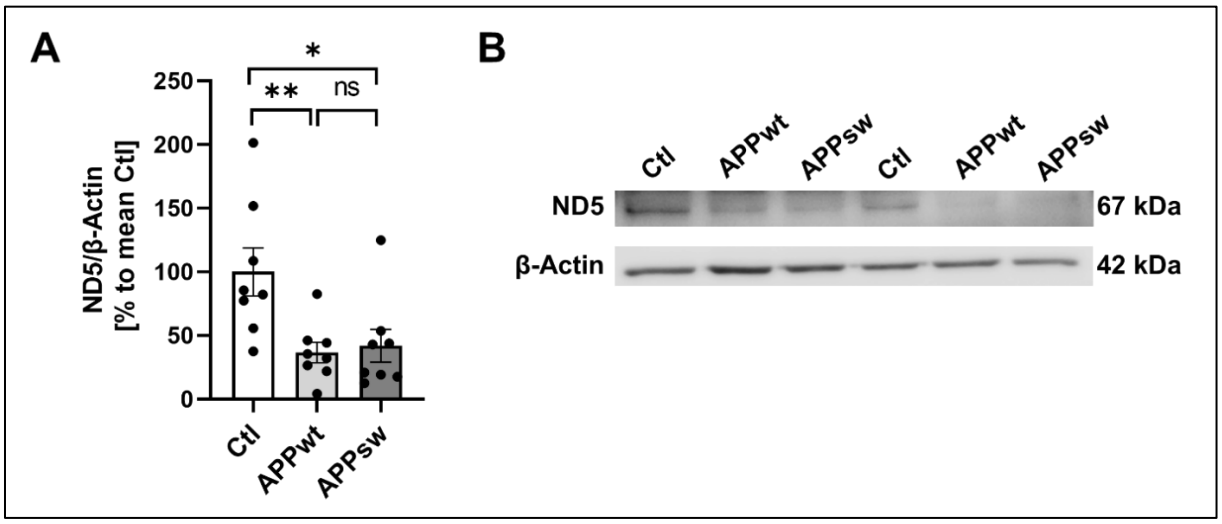

Figure 4.8: ND5 protein levels are reduced in HEK293 APPwt and APPsw cells. A) Western blot results of ND5 in Ctl, APPwt and APPsw cells reveala a significantly decreased ND5 protein content in APPwt and APPsw cells in comparison to Ctl. No significant difference is observed between APPwt and APPsw. Mean ± SEM, n= 8 biological replicates, unpaired t-tests. **B)** Representative Western blot membrane shows clear bands in Ctl and faint bands in APPwt and APPsw in protein extracts from two different days (n= 2 biological replicates). **A)** ns= not significant, *p<0.05, **p<0.01.

As demonstrated in Figure 4.8, the ND5 Western blot revealed significantly lower protein levels in HEK293 APPwt and APPsw cells compared to Ctl. APPwt reaches only 36% and APPsw 43% of the averaged ND5 amount of Ctl. Values of APPsw are approximately in the range of APPwt and the small difference between the mean values is not significant. The case of APPwt suggests that m^1A indeed disturbs the mitochondrial protein translation process, because this cell line displays elevated m^1A^{1374} methylation and at the same time decreased ND5 protein levels. In case of APPsw the matter is not that simple. Since this cell line did not show altered m^1A^{1374} methylation, the cause of the ND5 reduction is uncertain at this point.

To further assess the status of ND5 in these AD model cells and to complete the picture, the relative amount of ND5 mRNA was determined by qPCR. For this purpose, total RNA was

isolated from HEK293 Ctl, APPwt and APPsw cells using a TRIzol-based protocol. Subsequent cDNA synthesis was performed with the "High-Capacity cDNA Reverse Transcription Kit", comprising random primers and the reverse transcriptase MultiScribe™. Afterwards gene expression was measured in the QuantStudio™ 5 Real-Time-PCR System by means of specific TaqMan™ Assays for ND5 and GAPDH. Prior to the main experiment, only GAPDH levels were measured in HEK293 Ctl, APPwt and APPsw cells to investigate the suitability of this gene as a reference gene. Since absolute quantities of GAPDH were unaltered between all three cell lines in the preciding experiment, this gene was considered appropriate for normalization and selected as reference gene. Through the ΔΔCt method the amount of ND5 mRNA was calculated in the main experiment, normalized to GAPDH and expressed as a “fold change” relative to the ND5 mRNA level of Ctl.

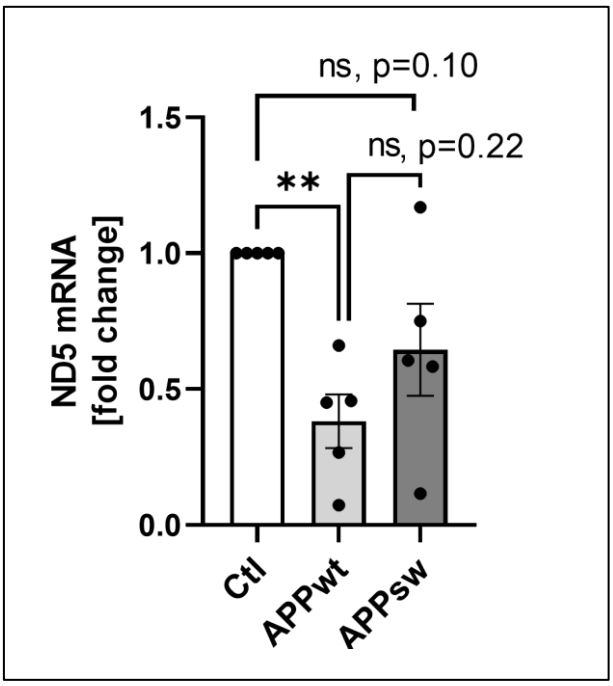

Figure 4.9: ND5 mRNA is significantly decreased in HEK293 APPwt cells in comparison to Ctl. After reverse transcription with the High-capacity cDNA Reverse Transcription Kit (including MultiScribe™), qPCR was performed using TaqMan® Assays for ND5 (target gene) and GAPDH (reference gene). mRNA was quantified via the ΔΔCt method. In APPwt significantly lower ND5 mRNA levels were measured in comparison to Ctl. In APPsw no significant change was detected in comparison to Ctl. Mean ± SEM, n= 5 biological replicates, One sample t-tests. ns= not significant, **p<0.01.

The qPCR measurement indicates that ND5 mRNA levels are significantly diminished in HEK293 APPwt cells in comparison to Ctl (Figure 4.9). This LOAD model shows an averaged fold change value of 0.38, which means that only 38% of mRNA is present compared to Ctl. In APPsw cells, the late-stage LOAD model, lower ND5 mRNA levels are observed in comparison to Ctl. The difference is not significant, but the p-value is 0.10, demonstrating a clear trend, which might become significant with a higher number of n. The mean value of APPsw is 0.64, which is higher than that of APPwt. However, this difference is not significant either (p= 0.22).

Comparing Figure 4.8 and Figure 4.9, it is noticeable that the patterns of ND5 protein and mRNA expression are slightly different. While protein levels are significantly decreased in both APPwt and APPsw compared to Ctl, mRNA levels appear to be lower in APPwt than in APPsw. Since ribosomes require mRNA for the biosynthesis of proteins, it is generally assumed that a lower mRNA content results in a reduced expression of the corresponding protein. So in the case of APPwt, the low mRNA and protein levels fit well together suggesting that the reduced protein levels are likely caused by the diminution of ND5 mRNA. However, as this cell line additionally showed increased m^1A^{1374} levels (see Figure 4.6 and Figure 4.7) and m^1A is thought to inhibit the protein biosynthesis of ND5, it can be assumed that both factors together are responsible for the strong reduction of the ND5 protein. In case of APPsw, the reason for the reduced protein expression is not that clear. Since these cells did not exhibit higher m^1A^{1374} methylation than Ctl, this modification cannot be the cause for the diminished ND5 protein expression. Likewise, the reduction of ND5 mRNA was not significant in APPsw cells in comparison to Ctl. However, the modest decrease (ns, p= 0.10) might already lower protein level of ND5. As mRNA is translated by several ribosomes simultaneously in a so-called polysome, even a slight decrease of the mRNA content might have large effects on levels of the corresponding protein. A second possibility would be that the enourmous Aβ load in APPsw and the ensuing detrimental effects on mitochondria accelerate degradation of ND5, thus leading to a lower protein content. However, a certain explanation cannot be given on basis of this data.

For the sake of completeness, it must be mentioned that m^1A^{1374} is known to hinder the reverse transcription process leading to truncated cDNA strands that might not be detected in the subsequent qPCR. This effect is particularly pronounced when an RT with low read-through efficiency, such as MultiScribe™, is used. According to the manufacturer MultiScribe™ is similar to the Moloney Murine Leukemia Virus RT M-MuLV. This polymerase is characterized by comparatively low mismatch and high truncation rates with respect to m^1A [302]. For example, arrest rates are more than twice as high as for SS-IV [302]. In the presented experiment setup comprising the High Capacity cDNA synthesis kit and TaqMan™ probes specific for the mRNA of ND5, it is plausible that some ND5 cDNA strands are truncated due to the high level of m^1A^{1374} in APPwt cells. However, these strands can still be amplified in the following qPCR, because in this case the TaqMan™ PCR primer sequences are located behind m^1A^{1374} (according to the manufacturer probes bind around position 1600). As the name implies, a reverse transcriptase always transcribes mRNA backwards, i.e. from the 3'- to the 5'-end. Hence, the cDNA strand which is later detected by the TaqMan™ probe is generated independent of truncations after m^1A^{1374}. That means that an erroneously reduced mRNA quantity in the final qPCR analysis as a consequence of m^1A-induced abortions during the RT process can be ruled out in this experiment setup.

Hypothesis (iv) was not investigated in these AD model cells because mitochondrial deficits have already been demonstrated in these cell lines in numerous previous studies [179], [216], [441], [442].

4.2 Effects of TRMT10C overexpression in pTRMT10C cells

In section 4.1, two AD model cell lines were investigated with regard to the hypotheses (i) - (iv) stated in section 2. In particular HEK293 APPwt cells, which represent a model for LOAD, confirmed all of the four assumptions. First, the writer enzyme TRMT10C was overexpressed. Second, m^1A^{1374} mRNA methylation of ND5 was enhanced. Third, ND5 protein levels were reduced, and fourth, it has been demonstrated in former studies, that these cells exhibit severe mitochondrial impairments, such as a reduction of ATP, a decrease of the MMP and deficiencies of respiratory chain complexes [179], [216]. However, the results so far did not allow to draw conclusions about a causal chain between these four findings, because all of the observations could be caused independent of each other by the numerous effects of APP overexpression and APP-derived fragments. For this reason, a system that enables the selective overexpression of TRMT10C was utilized for the next set of experiments. Thus, the direct effect of increased TRMT10C expression on m^1A^{1374} methylation, ND5 protein expression and the mitochondrial function could be examined without being affected by APP overexpression or downstream effects of APP-derived fragments.

4.2.1 Tetracycline-induced TRMT10C overexpression

One such system that offers the possibility to selectively overexpress TRMT10C is the commercially available T-Rex™ system (Invitrogen, Cat.No: V1033-20). These HEK293 cells are by default transfected with a plasmid encoding a Tetracyline-inducible repressor (TetR), which enables the Tetracycline-regulated expression of arbitrary proteins. For the following set of experiments HEK293 T-REx™ cells were used cotransfected with a second plasmid, providing the the full-length sequence of TRMT10C (including a FLAG-Tag) and its native initiation codon context [359]. In addition, this second plasmid contains the binding sequence of TetR downstream of a cytomegalovirus promoter. Thus it enables a selective expression of TRMT10C in the presence of Tetracycline (more information in section 3 Materials and Methods). This customized cell line will hereafter be referred to as pTRMT10C cells. Besides in all of the following experiments, the untransfected HEK293 T-Rex™ cells were additionally used as a control cell line and will hearafter be called Ctl.

First of all, the Tetracycline-dependent expression of TRMT10C in pTRMT10C cells was verified. Besides the optimal concentration of Tetracycline was explored. The manufacturer recommends the addition of 1 µg/mL Tetracycline into the usual cell culture medium and an incubation time of 24 h. However, since Tetracycline is known to affect mitochondrial function [443], [444], it was attempted to reduce the concentration of this substance as much as possible. For this reason, it was also tested whether the concentration of 0.1 µg/mL

Tetracycline is sufficient to ensure the expression of TRMT10C. Therefore, pTRMT10C cells were incubated with 0 µg/mL, 0.1 µg/mL and 1 µg/mL Tetracycline for 24 h. Afterwards, total protein extracts were isolated and a Western blot for TRMT10C (47 kDa) was performed. As the band of β-Actin (42 kDa) appears too close to that of TRMT10C and membrane stripping carries several disadvantages, GAPDH (36 kDa) was selected as reference enzyme. To better assess the expression of TRMT10C in absence of the inducer Tetracycline, extracts of Ctl treated with 0 µg/mL Tetracycline were also investigated. Furthermore, it was studied whether the functionality of the system is maintained at any stage of cell growth. Therefore, three similar experiments were performed. Once Tetracycline was added directly one day (24 h) after seeding. In the second approach, Tetracycline was added after two days (48 h) of growing, and in the third approach, Tetracycline incubation was started three days (72 h) after seeding.

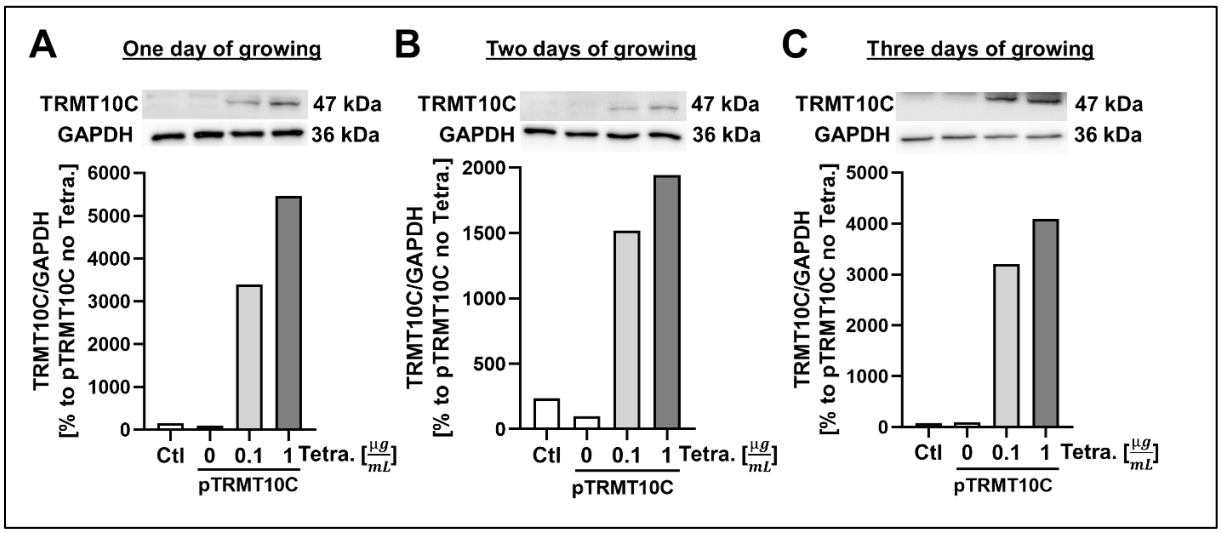

Figure 4.10: TRMT10C expression in pTRMT10C cells is dependent on the concentration of Tetracycline and independent of the duration between seeding and Tetracycline addition. A) One day after seeding 0.1 and 1 µg/mL Tetracycline was added to the medium of pTRMT10C cells and incubated 24 h until protein extraction. pTRMT10C cells in medium without Tetracycline (0 µg/mL) and Ctl without Tetracycline were cultivated as references. Western blot shows increasing TRMT10C protein levels in correlation with increasing Tetracycline concentrations. **B)** Experimental setup as in A), however, Tetracycline was added two days after cell seeding. TRMT10C expression is again elevated in pTRMT10Cs with increasing Tetracyline concentrations. **C)** Experimental setup as in A) + B), however, Tetracycline was added three days after cell seeding. TRMT10C expression is again enhanced after incubation with 0.1 µg/mL Tetracycline and even higher after incubation with 1 µg/mL Tetracycline. **A-C)** For each tested condition the Western blot membrane is shown in the upper panel and the corresponding analysis is presented the panel below. n= 1 biological replicate, Tetra.= Tetracycline. The experiment was performed by _____.

In Figure 4.10 it can be seen that the selective overexpression of TRMT10C in pTRMT10C cells works very well. At both 0.1 µg/mL and 1 µg/mL Tetracycline, a clear band is apparent in all images of the Western blot membrane in comparison to Ctl and pTRMT10C without Tetracycline. It can also be assumed that the expression of TRMT10C is proportional to the amount of Tetracycline added. At least a higher amount of TRMT10C was detected at 1 µg/mL than at 0.1 µg/mL Tetracycline in each of the 3 experiments. Furthermore, it was

demonstrated that the expression of TRMT10C is nearly abolished in absence of the inducer. Because at 0 µg/mL Tetracycline, the levels of TRMT10C in pTRMT10C cells are in the range of Ctl or even lower.

Comparing Figure 4.10A-C it is also evident that the expression system is independent of the cell growth status. Whether Tetracyline was added one day, two days or three days after seeding, the pTRMT10C cell system showed always the same pattern. That means regardless of the time between seeding and Tetraycline addition, the expression of TRMT10C was always successful. For this reason, cells were always seeded one day prior to Tetracycline addition in the following experiments, as it enables a fast and efficient experiment procedure. Furthermore, it should be mentioned that Ctl and pTRMT10C at 0 µg/mL Tetracycline show only very faint bands of TRMT10C in the Western blot image. One reason for this would be that TRMT10C protein levels in HEK cells are generally very low. On the other hand, a low antibody binding capacity could also result in weak protein bands. A third explanation would be that the strong bands of pTRMT10C at 0.1 and 1 µg/mL might be too intense at the exposure process, thereby making the bands of Ctl and pTRMT10C (at 0 µg/mL Tetracycline) appear less prominent.

4.2.2 m^1A^{1374} methylation levels in pTRMT10C cells

In section 4.2.1, it has been shown that pTRMT10C cells are well suited to specifically overexpress TRMT10C and to study downstream cellular processes. Therefore, the next step was to investigated whether overexpression of TRMT10C is directly correlated with increased m^1A^{1374} mRNA methylation, verifying hypothesis (ii). Although it was postulated in 2017 by Safra *et al.* [312] that TRMT10C is the writer enzyme of m^1A^{1374} in ND5 mRNA, this finding should be independently verified. Besides, it was explored whether the amount of TRMT10C and the stoichiometries of m^1A^{1374} methylation are directly correlated to each other. For this purpose, pTRMT10C cells were incubated with 0, 0.1 and 1 µg/mL of Tetracycline for 24 h. In order to assess the effect of Tetracycline per se, the Ctl cell line was treated in parallel with 0, 0.1 and 1 µg/mL Tetracycline for 24 h. In both cases, the incubation was started 24 h after seeding, as established in section 4.2.1. Then, whole cells were lysed and total RNA was extracted with a TRIzol-based protocol. Subsequently, the site-specific m^1A^{1374} analysis method (procedure described in section 3.2.6 and 4.1.3) was performed. In brief, a reverse transcription was conducted with SS-IV, dNTPs, a Mg^{2+}-containing buffer and a specific primer targeting ND5. After PCR with specific barcode primers, the sequence around m^1A^{1374} was amplified. Then the amplicon was purified via polyacrylamide gel electrophoresis and sequenced on an Illumina MiSeq platform in 2x 75 bp PE mode. The results of the final bioinformatics analysis are shown in Figure 4.11.

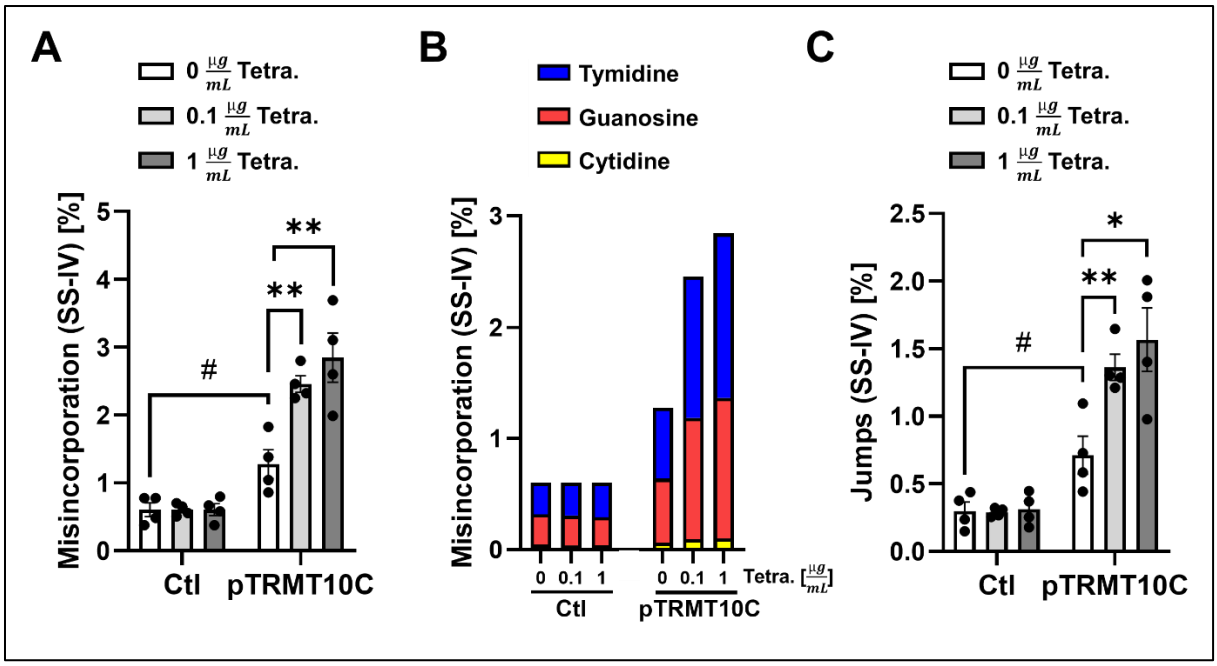

Figure 4.11: m^{1}A-induced misincorporations and jumps at position 1374 in the ND5 mRNA are significantly increased in pTRMT10C cells after Tetracycline-induced overexpression of TRMT10C. A) pTRMT10C and corresponding Ctl cells were seeded and the next day incubated with 0, 0.1 or 1 µg/mL Tetrcycline for 24 h. Afterwards total RNA was isolated and subjected to RT with SS-IV and a Mg^{2+}-containing buffer, PCR and Illumina sequencing. Misincorporation rates of m^{1}A^{1374} are significantly heightened in pTRMT10C cells treated with both 0.1 and 1 µg/mL Tetracycline. As for Ctl misincorporation rates remain unchanged upon Tetracycline addition, but are significantly lower without Tetracycline in comparison to pTRMT10C without Tetracycline. Mean ± SEM, n= 4 biological replicates, unpaired t-tests. **B)** Data from A) subdivided according to the averaged composition of misincorporated bases. Mismatch composition is not altered by Tetracycline. Thymidine (blue), Guanosine (red), Cytidine (yellow). **C)** Sequencing data from A) + B) was evaluated for jumps at position 1374 in ND5 mRNA. Jump rate is significantly elevated in pTRMT10C cells due to Tetracycline-induced TRMT10C overexpression. In Ctl cells no significant alterations upon Tetracyline addition is observed. In pTRMT10C cells at 0 µg/mL jump rates are significantly augmented in comparison to Ctl at 0 µg/mL Tetracycline. Mean ± SEM, n= 4 biological replicates, unpaired t-tests. **A)-C)** *p<0.05, **p<0.01, #p<0.05.

Strikingly, m^{1}A-induced misincorporations are significantly elevated in pTRMT10C cells after incubation with 0.1 and 1 µg/mL Tetracycline (Figure 4.11A). Importantly, misincorporation levels remain unchanged in Ctl after incubation with 0.1 and 1 µg/mL Tetracycline. This proves, that elevated TRMT10C protein levels in fact cause higher m^{1}A^{1374} methylation (either directly or indirectly). Moreover, it can be excluded that Tetracycline itself interferes with m^{1}A^{1374}, because mismatch rates in Ctl are on the same level with and without Tetracycline addition. Of note, the mean values of Ctl treated with 0, 0.1 and 1 µg/mL Tetracycline are all 0.60%, which impressively demonstrates the accuracy of this method. For pTRMT10C cells the mean value of 1.28% at 0 µg/mL Tetracycline rises to 2.46% at 0.1 µg/mL Tetracycline and 2.85% at 1 µg/mL Tetracycline. The difference between the latter two is not significant. Therefore, it is difficult to postulate a direct proportionality between TRMT10C protein and m^{1}A^{1374} methylation levels in this set up. Interestingly, the values of pTRMT10C in absence of Tetracycline are significantly higher than those of Ctl. This fact suggests that the pTRMT10C system yet shows a low expression of TRMT10C in absence of the inducer

Tetracycline and hence might be leaky. Apparently, this augmentation is miniscule and therefore no detectable in a Western blot (see Figure 4.10).

Obviously, the composition of mismatched bases at position 1374 is not altered between the investigated samples (see Figure 4.11B and Table 4.4). As in the preceding experiments mainly T and G appear in the sequenced reads, indicating that m^1A preferentially induced the incorporation of A and C into the newly synthesized cDNA strand during the RT with SS-IV.

Table 4.4: Amount of misincorporated T [%], G [%] and C [%] in relation to the total amount of mismatch [%] at position 1374 of ND5. Data set from Figure 4.11.

Ratio $\frac{Base\ [\%]}{Mismatch\ [\%]}$	Ctl, 0 $\frac{\mu g}{mL}$ Tetra.	Ctl, 0.1 $\frac{\mu g}{mL}$ Tetra.	Ctl, 1 $\frac{\mu g}{mL}$ Tetra.
T	0.475	0.489	0.516
G	0.447	0.445	0.416
C	0.078	0.065	0.068
Ratio $\frac{Base\ [\%]}{Mismatch\ [\%]}$	pTRMT10C, 0 $\frac{\mu g}{mL}$ Tetra.	pTRMT10C, 0.1 $\frac{\mu g}{mL}$ Tetra.	pTRMT10C, 1 $\frac{\mu g}{mL}$ Tetra.
T	0.500	0.518	0.520
G	0.452	0.444	0.444
C	0.048	0.038	0.036

In Figure 4.11C the frequency of nucleotide skipping events at position 1374 of ND5 in this data set is visualized. As in section 4.1.3, the jump rates display exactly the same pattern as misincorporation rates. Thus, jump rates of pTRMT10C are significantly enhanced at 0.1 and 1 µg/mL Tetracycline compared to pTRMT10C without Tetracycline treatment. The mean value of pTRMT10C in absence of the inducer is 0.71% and increases to 1.36% and 1.57% at 0.1 and 1 µg/mL Tetracycline, respectively. Of note, Ctl cells again exhibit significant lower jump rates than pTRMT10C without Tetracycline. This suggests once more that a small amount of TRMT10C is expressed in pTRMT10C cells even without the inducer. Mean values of Ctl with and without Tetracycline are again within a narrow range, between 0.29 and 0.31%, pointing to the high accuarcy of this method. Futhermore, it should be mentioned that the difference between pTRMT10C with 0.1 and 1 µg/mL Tetracycline is not significant. Therefore, it could not be statistically proven that m^1A^{1374} methylation proportionally increases with TRMT10C levels or the Tetracycline concentration. Therefore, only one of the two concentrations was used in the following experiments (1 µg/mL Tetracycline). This concentration allows markedly increased TRMT10C and m^1A^{1374} levels and therefore it represents a suitable system for studying the effects of TRMT10C and m^1A on ND5 protein synthesis and the mitochondrial function (see section 4.2.3 - 4.2.6).

4.2.3 ND5 protein expression in pTRMT10C cells

Although it was found in section 4.1.3 and 4.1.4 that HEK293 APPwt cells display enhanced TRMT10C and m^1A^{1374} levels, a causative relationship between these two events could yet not be proven. Likewise, the direct effect of m^1A^{1374} methylation on ND5 protein levels has not been studied so far in the literature. Although m^1A within an artificially generated mRNA was shown to block the cytosolic protein biosynthesis [338], the effect of m^1A must be evaluated sequence-dependent and might differ in mitochondria [341]. For this reason, it was examined in the next step how increased m^1A^{1374} methylation levels in the ND5 mRNA affect the synthesis of the corresponding ND5 protein.

As demonstrated in section 4.2.2, pTRMT10C cells exhibit significantly increased m^1A^{1374} modification levels after incubation with 1 µg/mL Tetracycline, thus enabling the selective overexpression of TRMT10C. For this reason, pTRMT10C cells were seeded in two different flasks. One day after seeding, the cell culture medium was replaced. In one flask the medium was exchanged by standard medium (0 µg/mL Tetracycline) and in the other flask by standard medium including 1 µg/mL Tetracycline. To evaluate the effect of Tetracycline per se on the ND5 protein expression, Ctl cells were also seeded and treated in the exact same way. After 24 hours of incubation, protein extracts were generated and a Western blot of ND5 was performed. As in section 4.2.1 GAPDH was selected as reference protein.

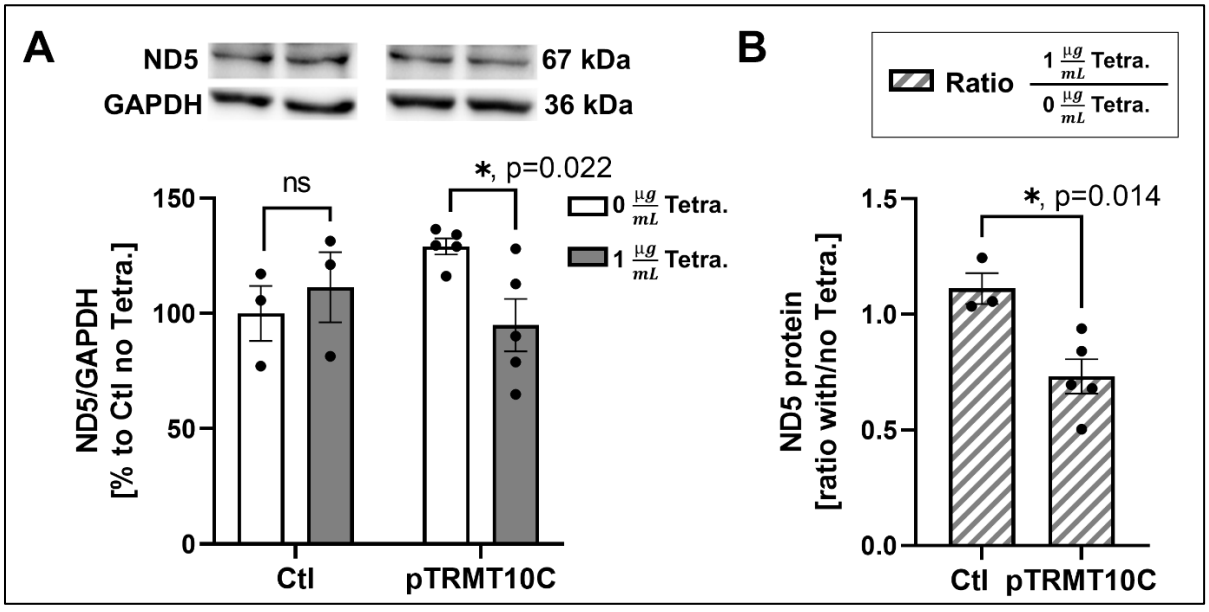

Figure 4.12: ND5 protein levels are significantly reduced after Tetracycline-induced TRMT10C overexpression. A) Western blot of ND5 in Ctl and pTRMT10C cells, both treated with 0 µg/mL and 1 µg/mL Tetracycline for 24 h. A representative membrane is shown in the upper panel. A significant diminution of the ND5 protein is observed in pTRMT10C cells after incubation with Tetracycline. No significant alteration is observed in Ctl at 1 µg/mL compared to 0 µg/mL Tetracycline. Mean ± SEM, n= 3 Ctl, n= 5 pTRMT10C, biological replicates, unpaired t-tests. **B)** Data from A) represented as ratio of ND5 intensities with (1 µg/mL) and without (0 µg/mL) Tetracycline treatment for each cell line. Ratio was calculated in order to compensate for the possible effect of Tetracycline per se on ND5 protein expression. The reduction of ND5 upon TRMT10C overexpression remains significant and reaches a

lower p-value. Mean ± SEM, n= 3 Ctl, n= 5 pTRMT10C, every n equals one biological replicate, unpaired t-test. **A)+B)** ns= not significant, *p<0.05. This experiment was performed by _____.

Strikingly, the Western blot of ND5 revealed significantly decreased ND5 protein levels in pTRMT10C cells after incubation with 1 µg/mL Tetracycline (p= 0.022) (Figure 4.12A). Looking at Ctl cells, no significant change in ND5 protein expression is observed due to Tetracycline. The levels of Ctl treated with 1 µg/mL Tetracycline appear a bit higher than those of Ctl without Tetacycline, however, this difference is far away from being significant. Nevertheless, this augmentation has an intresting effect, when comparing the ratios of treated to untreated cells (Figure 4.12B). The ratio of 1 µg/mL to 0 µg/mL was calculated for each cell line in order to couterbalance possible effects of Tetracycline per se. Due to the slight increase of ND5 in Ctl cells with Tetracycline treatment, the decrease of ND5 in pTRMT10C cells is actually greater than it seems in Figure 4.12A. But by calculating and comparing the ratios of pTRMT10C versus Ctl, the effect of Tetracycline is compensated and a lower p-value is reached (p= 0.14). Of note, the difference between the two cell lines becomes almost highly significant.

4.2.4 SDR5C1 and PRORP expression in pTRMT10C cells

As mentioned in section 4.1.2, TRMT10C is only capable of methylating adenosines and guanosines in mitochondrial tRNAs, when SDR5C1 is present [329]. However, it has not yet been shown that SDR5C1 is also mandatory for m^1A^{1374} mRNA methylation. Although the AD cell model of HEK293 APPwt cells displayed elevated TRMT10C levels accompanied by increased SDR5C1 and m^1A^{1374} levels in section 4.1, this did not prove the necessity of SDR5C1 in the methylation process. Moreover, it was not clear whether the augmentation of SDR5C1 is caused by the increase of TRMT10C or vice versa. A third possibility would be that both proteins regulated independent of each other. To address this question, it was examined whether overexpression of TRMT10C alone affects SDR5C1 protein levels. For this purpose, pTRMT10C cells were seeded in two flasks. The next day, the medium was exchanged once with and once without Tetracycline addition. As explained in section 4.2.2, a Tetracycline concentration of 1 µg/mL was selected. After an incubation period of 24 h, total protein extracts were prepared as described in section 3.2.2. Subsequently, a Western blot of SDR5C1 was performed. Again, the control cell line Ctl was treated in the same way to evaluate the effects of Tetracycline per se on SDR5C1. In this case, β-Actin (42 kDa) was chosen as reference protein because the GAPDH band (36 kDa) appears too close to the SDR5C1 band (27 kDa) making membrane cutting impossible. Although the membrane could be stripped, this potentially introduces errors that would affect protein normalization. Therefore, cutting the

membrane is preferable as it allows a simultaneous analysis of target and reference proteins. The results of this SDR5C1 Western blot are shown in Figure 4.13.

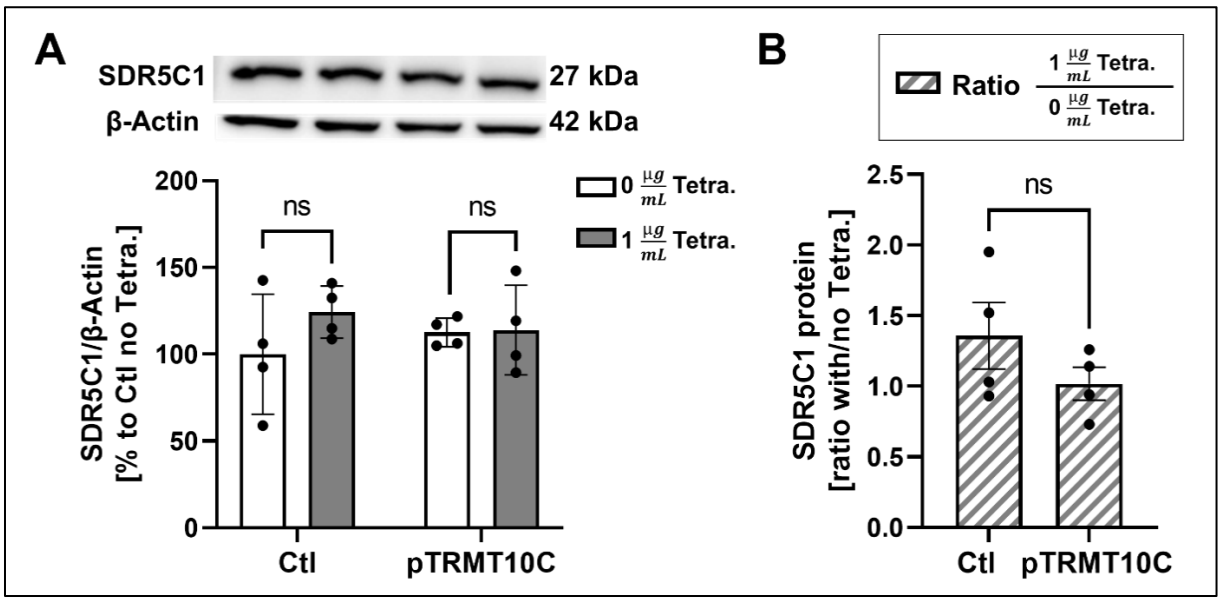

Figure 4.13: SDR5C1 protein levels do not change upon Teracycline-induced TRMT10C overexpression. A) Western blot results of SDR5C1 protein content in Ctl and pTRMT10C cells after incubation with 0 µg/mL and 1 µg/mL Tetracycline for 24 h. A representative Western blot membrane is shown in the upper panel. SDR5C1 is neither changed in Ctl nor in pTRMT10C after Tetracycline addition. Mean ± SEM, n= 4 biological replicates, unpaired t-tests. **B)** Data from A) represented as ratio of SDR5C1 intensities with (1 µg/mL) and without (0 µg/mL) Tetracycline treatment for each cell line. Ratio was calculated in order to compensate for the possible effect of Tetracycline per se on SDR5C1 protein expression. No significant alteration is observed between pTRMT10C and Ctl. Mean ± SEM, n= 4 biological replicates, unpaired t-test. **A)+B)** ns= not significant. This experiment was performed by _____.

The SDR5C1 Western blot in pTRMT10C and Ctl cells revealed no significant changes (Figure 4.13). For both pTRMT10C and Ctl, protein levels after Tetracycline treatment are more or less within the range of untreated cells (Figure 4.13A). The mean value of Ctl at 1 µg/mL Tetracycline is slightly higher than at 0 µg/mL, but the difference is not significant. To account for this slight increase due to Tetracycline, the ratios of 1 µg/mL to 0 µg/mL were calculated for both cell lines (Figure 4.13B). Thereafter the response of the two cell lines can be compared, however, the difference remained insignificant. These results suggest that the overexpression of TRMT10C alone does not affect SDR5C1 protein levels.

As it is known that TRMT10C forms the mtRNase P complex together with SDR5C1 and PRORP [359], the question arose whether TRMT10C levels might be correlated with those of PRORP. Though the AD model cell line HEK293 APPwt showed increased TRMT10C accompanied by decreased PRORP protein levels (see section 4.1.1 and 4.1.2), no causative relationship between the two findings could yet be proven. To scrutinize whether the reduction of PRORP might be directly caused by the augmentation of TRMT10C a PRORP Western blot was performed in pTRMT10C cells with and without Tetracycline. For this reason, the protein

extracts obtained in the upper part of this section were also analyzed for PRORP. In this case GAPDH could be utilized as reference protein, because the distance between the PRORP protein band (57 kDa) and the GAPDH protein band (36 kDa) was big enough to enable membrane cutting.

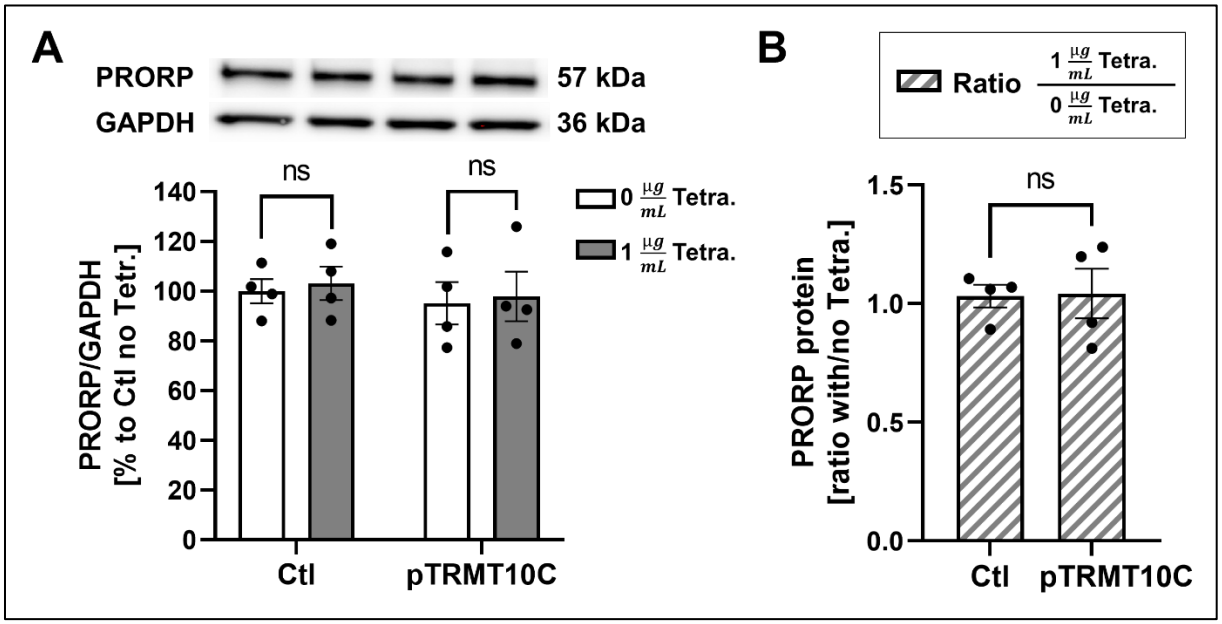

Figure 4.14: Tetacycline-induced overexpression of TRMT10C does not have an impact on PRORP protein levels. A) PRORP Western blot of Ctl and pTRMT10C cells treated with 0 µg/mL and 1 µg/mL Tetracycline for 24 h. A representative membrane is shown in the upper panel. PRORP expression is not altered by the addition of Tetracycline in Ctl and pTRMT10C. Mean ± SEM, n= 4 biological replicates, unpaired t-tests. **B)** Data from A) represented as ratio of PRORP intensities with (1 µg/mL) and without (0 µg/mL) Tetracycline treatment for each cell line. Ratio was calculated in order to compensate for the possible effect of Tetracycline per se on PRORP protein expression. There is no significant change between pTRMT10C and Ctl. Mean ± SEM, n= 4 biological replicates, unpaired t-test. **A)+B)** ns= not significant. The experiment was performed by _____.

In Western blots of PRORP no significant alterations were observed in both pTRMT10C and Ctl cells after incubation with 1 µg/mL Tetracycline for 24 h (Figure 4.14A). This indicates on the one hand, that the inducer Tetracycline does not affect PRORP protein expression and on the other hand, that the selective overexpression of TRMT10C does not have any impact on PRORP protein levels. Accordingly, no significant difference between the ratios of 1 µg/mL to 0 µg/mL was detected in pTRMT10C cells in comparison to Ctl (Figure 4.14B).

4.2.5 Mitochondrial respiration in pTRMT10C cells

In sections 4.2.1 - 4.2.3, the causative relationship between the hypotheses (i) – (iii) was clarified and confirmed. This means increased TRMT10C levels enhance m^1A^{1374} methylation and diminish ND5 protein levels. However, at this point, it was unclear whether the decrease of ND5 directly results in an impairment of Cpx I and consequently causes mitochondrial

dysfunction. Although a reduction of ND5 and numerous mitochondrial deficits were detected in the HEK293 APPwt AD cell model, a direct cause-and-effect relationship between these two events was not yet demonstrated. Therefore, the next experiment was set up to investigate how the decreased ND5 protein levels in pTRMT10C cells affect the function of the respiratory chain. For this purpose, the oxygen consumption rate (OCR) of pTRMT10C cells and Ctl was measured in a Seahorse XFe 96 analyzer.

Since Tetracycline is known to exert numerous effects on mitochondria [443], [444], pTRMT10C cells were treated with 1 µg/mL Tetracycline and compared with Ctl cells also treated with 1 µg/mL Tetracycline. Therefore, cells were seeded in Poly-L-Lysine-coated Seahorse XF-96 plates, and the medium was exchanged with a Tetracycline-containing medium 24 h before the experimental procedure. On the day of the assay, the growth medium was replaced by XF Base Medium and incubated for 1 h (37°C). At the beginng of the measurement, the basal respiration was recorded (= OCR in the first 3x 12 minutes). Then, 1 µM Oligomycin, an inhibitor of the ATP synthase, was added to determine proton leak and indirectly the ATP-linked respiration (ATP Turnover). In the next step, 1 µM FCCP was added to uncouple the oxidation from the phosphorylation process. Since FCCP evokes the transfer of protons from the intracellular space to the mitochondrial matrix bypassing the ATP synthase, the respiratory chain begins to compensate for this effect and operates at maximum capacity. At this point, the maximum capacity of the electron transport chain (ETS capacity) can be determined. In the further course, a 1 µM mixture of Rotenone, a Cpx I inhibitor, and Antimycin, a Cpx III inhibitor, was injected. These two agents entirely block the electron transport chain, revealing the non-mitochondrial oxygen consumption. A representative graph of the experimental procedure and OCR curves of pTRMT10C and Ctl are shown in Figure 4.15A. The experiment was conducted on three different days, which are for the sake of simplicity referred to as Day1, Day2 and Day3 in the following graph (Figure 4.15).

Remarkably, the basal respiration is significantly reduced in pTRMT10C cells compared to Ctl (Figure 4.15B). This suggests that the effectiveness of the respiratory chain is decreased in these cells due to the overexpression of TRMT10C and the associated reduction of ND5. On the other hand, the ETS capacity and the ATP Turnover shows no significant decline (Figure 4.15C+D). However, the ETS capacity indicates a tendency of reduced levels in pTRMT10C ($p= 0.22$) and the diminution of the ATP-linked respiration is almost significant ($p= 0.057$). The Proton-leak also appears to be tendentially decreased in pTRMT10C cells, but the difference is not significant ($p= 0.08$) (Figure 4.15E). Undoubtedly, the non-mitochondrial respiration is unchanged in the two cell lines, as all mean values are more or less at the same level (Figure 4.15F). This proves that the normalization to cell number was efficient and no systematic error was introduced during in the experimental procedure.

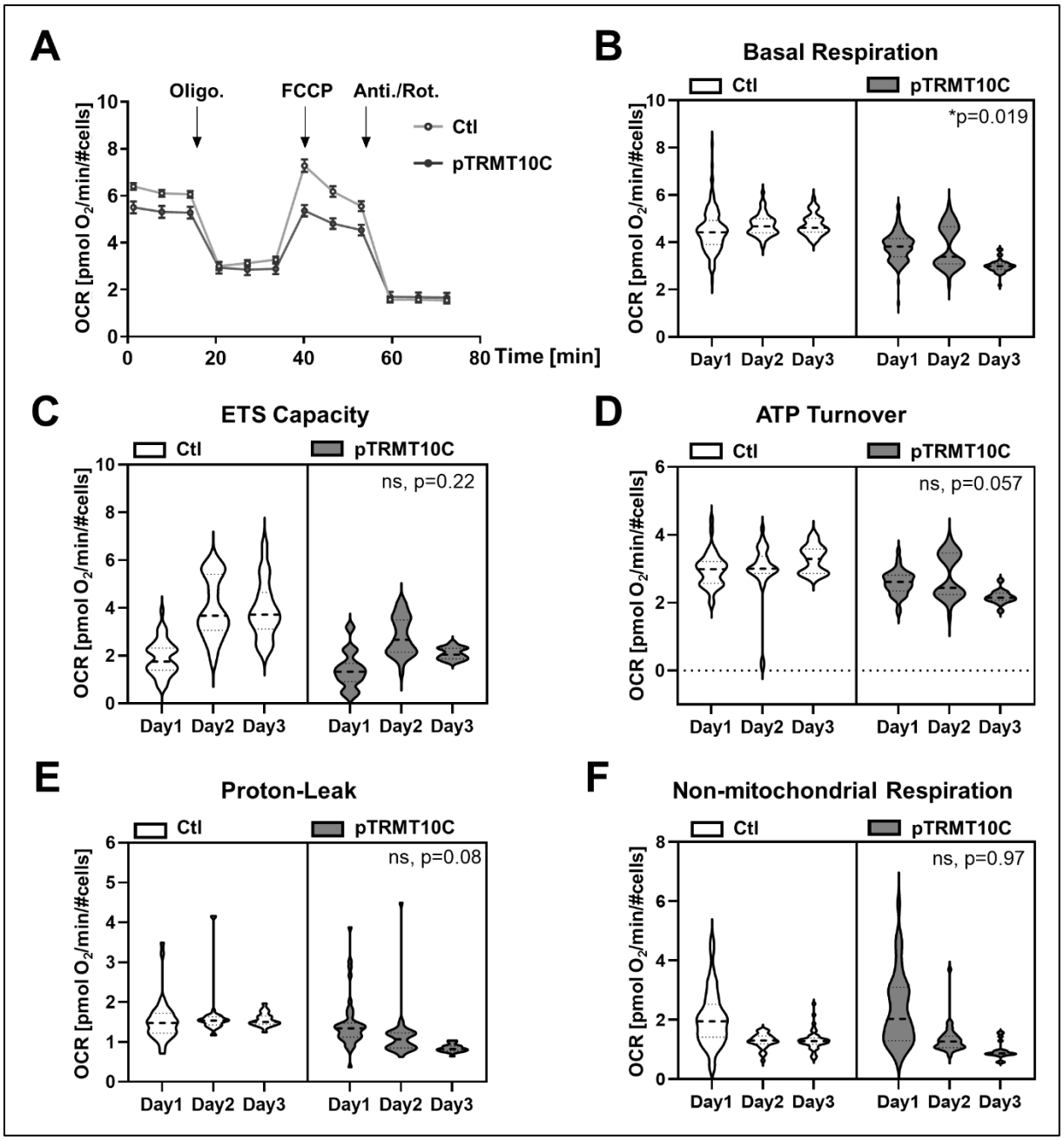

Figure 4.15: TRMT10C overexpression leads to a decrease of the basal mitochondrial respiration. **A)** Representative Oxygen consumption curve of Ctl and pTRMT10C cells. Measurement was performed in the Seahorse XFe 96 Extracellular Flux analyzer. During the experiment 1 µM of Oligomycin (Oligo.), 1 µM of FCCP and 1 µM of Antimycin and Rotenone (Anti./Rot.) was added in succession. Time points are marked by corresponding arrows. Mean ± 95%CI, n= 1 biological replicate. **B)** Violin plot for Basal Respiration reveals a significant reduction in pTRMT10C in comparison to Ctl. **C)** Violin plot for ETS Capacity shows no significant alteration in pTRMT10C versus Ctl. **D)** Violin plot for ATP Turnover indicates a decreased ATP synthesis rate (p= 0.057). **E)** Violin plot of Proton-Leak demonstrates no significant change between pTRMT10C and Ctl. **F)** Violin plot of Non-mitochondrial Respiration shows no difference between pTRMT10C and Ctl. **A)-F)** Ctl and pTRMT10C were incubated with 1 µg/mL Tetracycline 24 h prior to the measurement in the Seahorse XFe 96 Extracellular Flux analyzer. For all violin plots: Width of each plot differs by the amount of data at the given axis intercept, n= 3 individual experiments (indicated by Day1, Day2, Day3), nested analysis. OCR= Oxygen Consumption Rate. *p<0.05, ns= not significant. The experiment was performed by _____.

Measuring the oxygen consumption rate by means of the Seahorse XFe 96 analyzer is an appropriate method to evaluate the mitochondrial respiration. Unfortunately, however, the experiment could only be conducted three times (n= 3), because Seahorse XF 96 plastic plates were no langer available thereafter due to the global COVID-19 pandemic. For this reason, the experiment was repeated with another oxygen electrode, the OROBOROS Oxygraph-2k high-resolution respiromter and an n= 8 was achieved.

Two days before the measurement, Ctl and pTRMT10C cells were seeded in flasks and the next day incubated with 1 µg/mL Tetracycline for 24 h. Then, cells were trypsinized and 2 million cells of each cell line were placed into the chambers of the OROBOROS Oxygraph-2k. As in the Seahorse XFe 96 analyzer the Basal Respiration was measured in the beginning. Afterwards Oligomycin (2 µM) was added to determine the Proton-Leak. The subsequent injection of FCCP (1 µM) revealed the maximum capacity of th electron transport chain, termed ETS capacity. At the end, Rotenone (1 µM) and Antimycin (1 µM) were sequentially injected to assess the non-mitochondrial respiration.

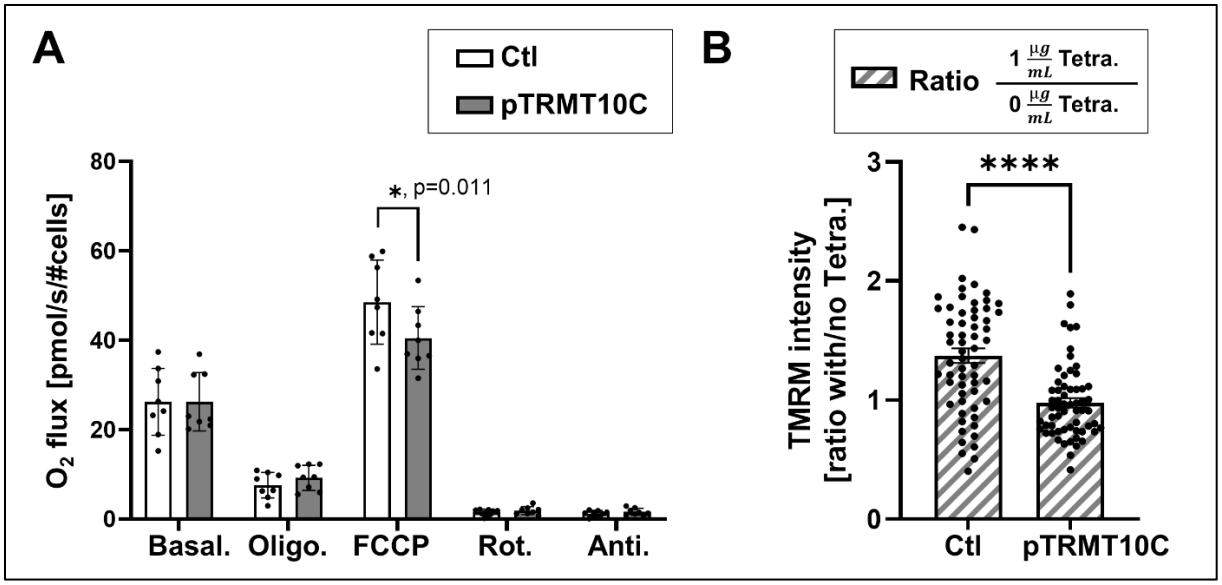

Figure 4.16: ETS capacity and the mitochondrial membrane potential are reduced in pTRMT10C cells. A) Oxygen consumption of Ctl and pTRMT10C cells in the OROBOROS Oxygraph-2k high resolution respirometer. Both cell lines were treated with 1 µg/mL Tetracycline for 24 h prior to the experimental procedure. 2 µM of Oligomycin (Oligo.), 1 µM FCCP and 1 µM of Rotenone (Rot.) and Antimycin (Anti.) were added successively. Basal respiration (Basal.) and coupled respiratory capacity induced by Oligomycin are not significantly altered in pTRMT10C versus Ctl. The non-coupled respiratory capacity (= ETS capacity) is significantly decreased in pTRMT10C cells in comparison to Ctl. Non-mitochondrial respiration after Rotenone and Antimycin addition shows no difference between Ctl and pTRMT10C. Mean ± SD, n= 8 biological replicates, two-way ANOVA. **B)** The mitochondrial membrane potential (MMP) was analyzed in Ctl and pTRMT10C cells treated and untreated with 1 µg/mL Tetra. for 24 h. 25 nM TMRM was added to stain for the MMP. Ratio of TMRM signals with (1 µg/mL) and without (0 µg/mL) Tetracycline reveals a highly significant reduction of the MMP in pTRMT10C cells versus Ctl. Mean ± SEM, each datapoint represents one individual well from n=4 different measurements, unpaired t-test. **A)+B)** *p>0.05, ****p>0.0001. Both experiments were performed by _____.

The result of the measurement in the OROBOROS Oxygraph-2k are shown in Figure 4.16A. Interestingly, the Basal respiration is not altered in pTRMT10C cells in comparison to Ctl in this instrument. Besides, the oxygen consumption after addition of Oligomycin (Proton-Leak) is not significantly altered between pTRMT10C and Ctl. However, in this case the ETS capacity mediated by FCCP is significantly decreased in pTRMT10C cells ($p= 0.011$). As in the Seahorse XFe 96 analyzer the non-mitochondrial respiration is unchanged between pTRMT10C and Ctl.

An additional parameter to assess mitochondrial function is the mitochondrial membrane potential (MMP). The MMP is generated by protons that are pumped into the intermembrane space by Cpx I, III and IV. The transmembrane potential of these protons is the engine for the synthesis of ATP through the ATP synthase (Cpx IV). That means, the higher the potential difference ($\Delta\Psi m$) across the mitochondrial membrane the more ATP is generated. And conversely, the lower $\Delta\Psi m$, the less effective is the eletron transport chain.

The MMP can be measured by staining cells with Tetramethylrhodamin-methylester (TMRM). To further examine the effect of m^1A^{1374} and decreased ND5 protein levels on mitochondrial function with a different approach, pTRMT10C and Ctl cells were subjected to TMRM staining. In contrast to the OROBOROS Oxygraph-2k, which features only two chambers, the TMRM staining enabled the investigation four different conditions: pTRMT10C treated and untreated with 1 µg/mL Tetracycline, and Ctl treated and untreated with 1 µg/mL Tetracycline. Therefore, both cell lines were seeded in 96-well plates with a transparent bottom. The next day, the medium was exchanged correspondingly and incubated for 24 h. On the day of the experiment, the medium was replaced by Tyrode's buffer containing 25 nM TMRM. In addition, samples were stained with 1 µg/mL Hoechst to normalize for the number of cells. Images were captured with a Live cell imaging setup and the quantitative analysis was performed by means of a machine leaning algorithm.

The results of the TMRM staining are shown in Figure 4.16B displayed as the ratio of treated (1 µg/mL Tetracycline) to untreated (0 µg/mL Tetracycline) cells. Obviously, incubation of Ctl cells with Tetracycline leads to an increase of the MMP, because the ratio for Ctl is on average clearly above 1 (mean value = 1.37). In pTRMT10C cells, the membrane potential does not appear to be altered by Tetracycline (mean value of the ratios = 0.98). However, because the ratios of Ctl are higher than those of pTRMT10C, a highly significant reduction in the MMP can be observed when comparing the ratios of both cell lines. In other words, the increase of the MMP that occurs by Tetracycline per se in Ctl cells is prevented in pTRMT10C cells by TRMT10C. In consequence, overexpression of TRMT10C and the subsequent reduction of ND5 via m^1A^{1374} can be assumed to induce a diminution of the MMP.

4.2.6 Mitochondrial and cytosolic tRNA quantification in pTRMT10C cells

TRMT10C not only methylates m^1A in (mt)tRNA and (mt)mRNA, but also functions as a subunit of mtRNase P together with PRORP and a SDR5C1 tetramer [360]. The mtRNase P is responsible for the endonucleolytic release of tRNA 5'-ends from mitochondrial primary transcripts [187]. In section 4.2.4, it was shown that protein levels of SDR5C1 and PRORP are not altered by overexpression of TRMT10C suggesting that the three subunits are regulated independent of each other. However, these findings do not rule out the possibility that elevated TRMT10C levels affect the activity of mtRNase P. It could be, for example that SDR5C1 and PRORP are present in excess and therefore the amount of TRMT10C alone determines mtRNase P activity. To address this question, cytosolic and mitochondrial tRNA levels were quantified in the following experiment.

To this end, total RNA was extracted from Ctl and pTRMT10C both treated and untreated with Tetracycline (1 µg/mL, 24 h). In the next step, tRNAs were hybridized with custom-designed oligonucleotides (oligos) complementary to the 3'-end of each mitochondrial and cytosolic tRNA isoacceptor. Of note, oligos targeting (mt)tRNAs were labeled with Cy5 and oligos targeting cytosolic tRNAs were labeled with 6-FAM. After a polyacrylamide gel electrophoresis, fluorescence intensities of hybrid bands could be measured and the ratio of Cy5 to 6-FAM was calculated indicating the relation of (mt)tRNA to cytosolic tRNAs.

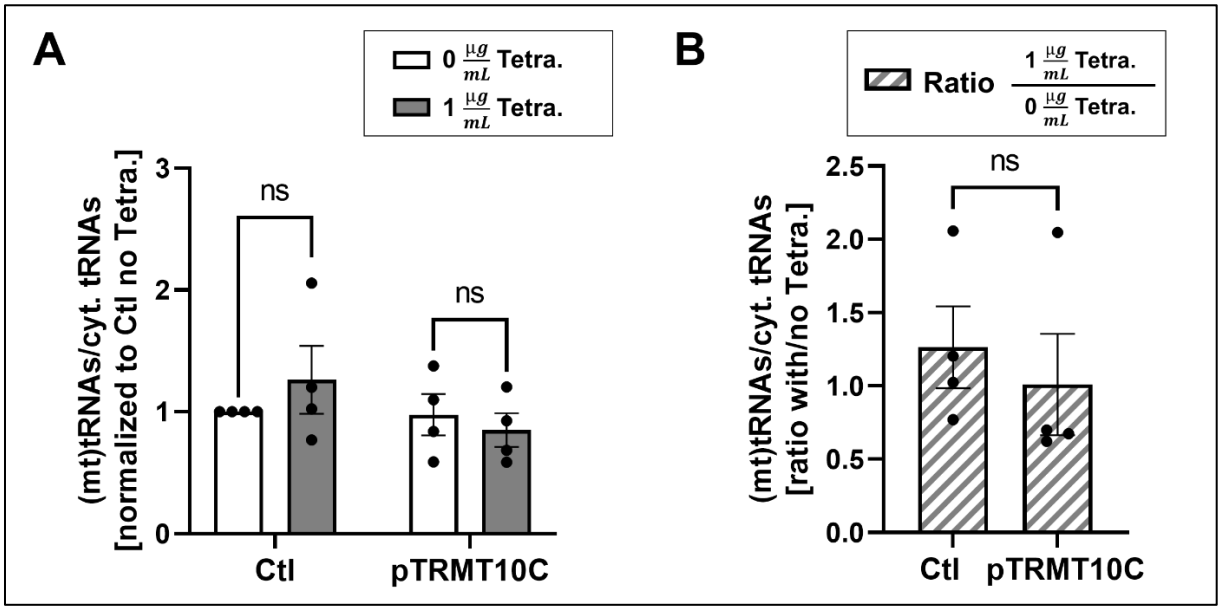

Figure 4.17: Levels of mitochondrial tRNAs are unaffected by TRMT10C overexpression. A) The amount of (mt)tRNAs relative to cytosolic (cyt.) tRNAs was assessed by tRNA specific primer hybridization. Oligos labeled with Cy5 targeting (mt)tRNAs and 6-FAM targeting cyt. tRNAs were hybridized with total RNA from Ctl and pTRMT10C cells, both treated and untreated with 1 µg/mL Tetracycline for 24 h. The ratio of (mt)tRNAs to cyt. tRNAs is not altered in Ctl and pTRMT10C cells after Tetracycline-induced overexpression. Mean ± SEM, n= 4 biological replicates, for every biological replicate the mean of 4 technical replicates was utilized, unpaired t-tests. **B)** Data from A) represented as ratio of values with (1 µg/mL) and without (0 µg/mL) Tetracycline treatment for each cell line. Ratio was calculated in order to compensate for the possible effect of Tetracycline per se on tRNA levels.

There is no significant change between pTRMT10C and Ctl. Mean ± SEM, n= 4 biological replicates, unpaired t-test. **A)+B)** ns= not significant. The experiment was performed by _____.

The quantification of tRNAs revealed no significant alteration in the ratio of mitochondrial to cytosolic tRNAs upon treatment with Tetracycline. This holds true for both pTRMT10C and Ctl cells (Figure 4.17A). Although Ctl cells treated with Tetracycline show a tendency of an increased ratio in comparison to Ctl untreated, this does not affect the evaluation of pTRMT10C cells. Because, after compensating for the effect of Tetracycline per se by calculating the ratios of 1 µg/mL to 0 µg/mL Tetracycline for both cell lines, the difference between pTRMT10C and Ctl remains insignificant (Figure 4.17B). Of note, this method cannot determine the activity of mtRNase P directly, however, it can be assumed that an impaired or enhanced activity of the mtRNas P would indirectly affect the ratio of (mt)tRNAs to cytosolic tRNAs. In consequence, this data indicates that the overexpression of TRMT10C alone has no effect on the activity of the mtRNase P.

4.3 Investigation of 5xFAD mice

In section 4.1 it was observed that the m^1A writer TRMT10C is upregulated in HEK293 APPwt and APPsw cells. Furthermore, altered protein levels of SDR5C1, PRORP and ND5 were detected in these AD model cell lines. The advantage of cell models in general is that the direct effect of one single manipulation (e.g. overexpression of APP) can be determined. However, the weakness of cellular models is the inability to reproduce the complex processes taking place in a whole organism. Moreover, the transferability of results obtained in HEK293 cells to neurons of human AD patients is limited, because the behaviour of neurons might differ from that of immortalized embryonic kidney cells. For this reason, the observations of section 4.1 should be reviewed in an AD model organism. To this end, 5xFAD mice were selected because they also represent a system based on increased APP expression and enhanced generation of Aβ, similar to HEK293 APPwt and APPsw.

5xFAD mice coexpress human APP and PSEN1 transgenes with a total of five AD-linked mutations: The Swedish (KM670/671NL), Florida (I716V), and London (V717I) mutation in APP, and two mutations (M146L and L286V) in PSEN1 [76]. This transgenic line was produced by pronuclear coinjection of mutated APP and PSEN1, both including the neuron-specifc mouse Thy1 promoter to drive overexpression in the brain [445]. 5xFAD mice are a widely used mouse model displaying many AD-related phenotypes and exhibiting a relatively early and severe disease progression [446]. Amyloid plaques are first detected in mice as young as two months of age, in the subiculum (part of the hippocampus) and layer V of the cortex. By six months plaques are found throughout the whole hippocampus and large parts of the cortex. In older mice, plaques are present in further regions, such as the thalamus, brainstem, and the olfactory bulb, but importantly they are absent in the cerebellum [76]. Neuronal loss occurs in multiple brain regions, beginning at about 6 months in those areas with the most pronounced amyloidosis, namely the subiculum and cortical layer V. Soluble $A\beta_{42}$ is detectable by 1.5 months in whole-brain homogenates and its levels increase consistently with age. $A\beta_{40}$ levels are substantially lower than those of $A\beta_{42}$, but also reach very high levels at the age of 6 and 9 months [76]. 5xFAD mice display a wide range of cognitive and motor deficits. Earliest cognitive impairments are observed at the age of 4-6 months [446]–[448]. Of note, this model is absent of tau tangles at any age.

In the following section it should be screened if 5xFAD mice display the same alterations as the HEK293 AD model cells. Furthermore, it was now possible to investigate in which brain regions the suspected changes occur. For this reason, female and male 5xFAD mice at the age of 42-55 weeks were sacrificed and three brain areas were dissected: The hippocampus, cortex and cerebellum. As mentioned above, the hippocampus is the earliest and most severely affected brain region in 5xFAD mice. Thus, changes in TRMT10C and ND5 protein

levels are assumed to be found here, if the hypotheses (i)-(iv) were also true in AD model organisms. The cortex is also heavily affected by AD pathology, whereas the cerebellum is devoid of amyloid in 5xFAD mice. Accordingly, the cerebellum is a kind of negative control. Meaning, if the hypotheses (i) – (iv) were specific to AD, no change would be observed in this brain region. Furthermore, it should be mentioned that male and female animals were deliberately used to study AD pathology in both sexes rather than unilaterally in one sex. Age-matched C57BL6/J wild-type (Wt) mice were used as corresponding control and a balanced mix of female and male Wt animals was selected as well.

4.3.1 TRMT10C protein expression in 5xFAD mice

First of all, it should be tested, if protein levels of TRMT10C are also altered in 5xFAD mice, following hypothesis (i). For this purpose, male and female 5xFAD mice at the age of 42-55 weeks were euthanized and hippocampus, cortex and cerebellum were manually dissected. After the isolation of proteins, a Western blot of TRMT10C was performed. All samples from the same brain region were applied to one gel for that they all could be compared on the same membrane during the imaging analysis. As reference enzyme GAPDH was chosen because it had already been shown to be suitable for these mice in other publications [446], [449]. In the final analysis, protein levels of 5xFAD mice for each brain region were expressed in relation to the respective mean value of Wt mice (see Figure 4.18B).

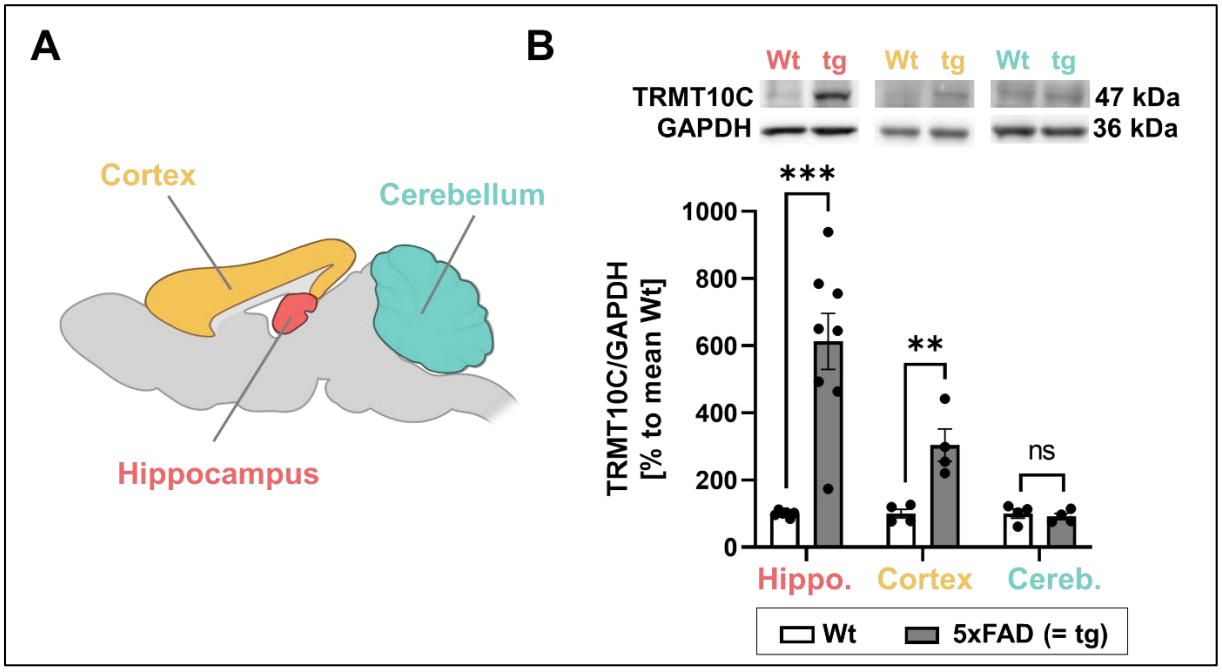

Figure 4.18: TRMT10C is overexpressed in hippocampi and cortices of 5xFAD mice. A) Sketch of localization of cortex, hippocampus and cerebellum in a mouse brain sagittal cut. Cerebral cortex is labeled in yellow, hippocampus in red and the cerebellum in turquoise. **B)** Western blot results of hippocampus (Hippo.), cortex and cerebellar (Cereb.) tissue from Wt and 5xFAD (= tg) mice. TRMT10C levels are significantly elevated in hippocampi and cortices of tg mice in comparison to Wt mice. Mean

± SEM, hippocampus: n= 6 wt n= 8 tg, cortex and cerebellum: n= 5 wt n= 5 tg, female + male mice, age= 42-55 weeks, unpaired t-tests. ***p<0.001, **p<0.01, ns= not significant.

The Western blot analysis revealed a dramatic upregulation of TRMT10C in hippocampi of 5xFAD mice (Figure 4.18B). Besides, TRMT10C levels in cortices of 5xFAD mice are significantly increased in comparison to Wt. However, in the cerebellum no difference was detected. Since male and female mice displayed the same phenotype, the results of both sexes were combined in the final analysis. Of note, TRMT10C is overexpressed in precisely those brain regions where high Aβ loads are reached and the AD pathology is particularly pronounced, and is absent in cerebellar extracts.

4.3.2 SDR5C1 and PRORP protein expression in 5xFAD mice

Since TRMT10C levels were vastly increased in the hippocampus and cortex of 5xFAD mice, the question arose whether protein expression of its enzymatic parter proteins are affected as well. For this purpose, the protein extracts obtained in section 4.3.1 were also analyzed for SDR5C1 and PRORP. The results of the corresponding Western blots are presented in Figure 4.19. Again, GAPDH was used as reference enzyme.

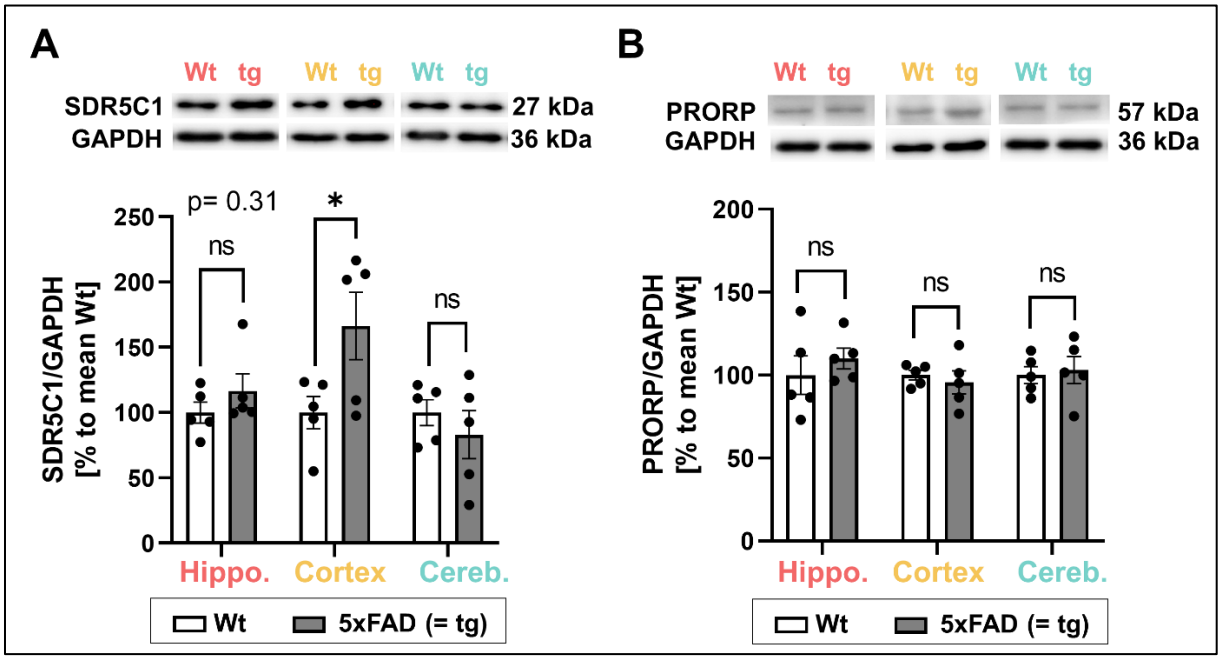

Figure 4.19: SDR5C1 protein levels are significantly increased in the cortex of 5xFAD mice, whereas PRORP protein expression is unchanged. A) Western blot results of SDR5C1 in three different brain regions of 5xFAD and Wt mice. A representative membrane is shown in the upper panel. SDR5C1 expression is significantly enhanced in cortex tissue of 5xFAD mice. In the hippocampus and cerebellum no significant changes are observed. **B)** Western blot results of PRORP in hippocampus, cortex and cerebellum of 5xFAD and Wt mice. In all three brain regions PRORP expression is not altered in 5xFAD mice in comparison to Wt. **A)+B)** Mean ± SEM, hippocampus (Hippo.), cortex (Cortex) and cerebellum (Cereb.): n= 5 wt and n= 5 tg, female + male mice, age= 42-55 weeks, unpaired t-tests, *p<0.05, ns= not significant.

The protein levels of SDR5C1 are not significantly altered in the hippocampus of 5xFAD mice compared to Wt (Figure 4.19A). However, a tendency towards increased levels can be observed (p= 0.31). Since in this case only an n of 5 was examined, the difference would possibly become significant with a larger number of animals. In the cortex, the overexpression is more pronounced and significant. Importantly, SDR5C1 expression is unchanged between 5xFAD and Wt in the cerebellum.

The protein expression of PRORP displays a different behaviour (Figure 4.19B). Here, no significant differences were detected between 5xFAD and Wt mice in all three brain regions. Not even a trend could be identified. This and the results of 4.3.1 suggest that, first, the mtRNase P subunits behave differently and, second, only the expression of SDR5C1 and TRMT10C is altered in AD.

4.3.3 Probing the m^1A^{1374} analysis method in 5xFAD mice

Regarding section 4.2.1 and 4.2.2, higher protein levels of the writer enzyme TRMT10C are expected to be associated with elevated m^1A^{1374} methylation. Accordingly, the highly significant overexpression of TRMT10C in the hippocampus of 5xFAD mice also suggests higher modification content in this brain tissue. However, the m^1A^{1374} modification site in the mRNA of ND5 has only been identified in human tissue and human cell lines so far, and has never been studied in mice brains or other murine tissue. Therefore, it was first necessary to determine whether an m^1A site at all exists in the ND5 mRNA from mice that is analogous to m^1A^{1374} in humans. Indeed, the alignment of the human and mouse ND5 sequence revealed an adenosine base at position 1374 that is in a homologous sequence context to human m^1A^{1374}. Moreover, this adenosine corresponds to the third base of a GCA codon triplet coding for alanine just like m^1A^{1374} in humans. In order to verify whether this adenosine base might be N^1-modified in mice, the m^1A^{1374} analysis method used in section 4.1.3 was adapted to the species mouse. For this purpose, both the RT primer and the p5 PCR primer were adjusted to the mouse ND5 sequence (primer sequence listed in 3.1.3). Except for these primer sequences, the experiment setup remained unchanged. This modified setup was applied to an exemplary mouse hippocampal sample to gain initial insights into m^1A^{1374} modification in mice.

As depicted in Figure 4.20, misincorporation rates at position 1374 were extremely low in this one investigated hippocampus sample. Although there were 626 reads (sum of 99, 262 and 265) containing mismatch at position 1374, this represents only 0.019% (sum of 0.003%, 0.008% and 0.008%) in relation to the total number of read counts (see Figure 4.20). When comparing these mismatch rates with the results of 1-11% in HEK293 cell samples (see section 4.1.3), this rate is extremely low suggesting a spontaneous mutation rather than m^1A-induced

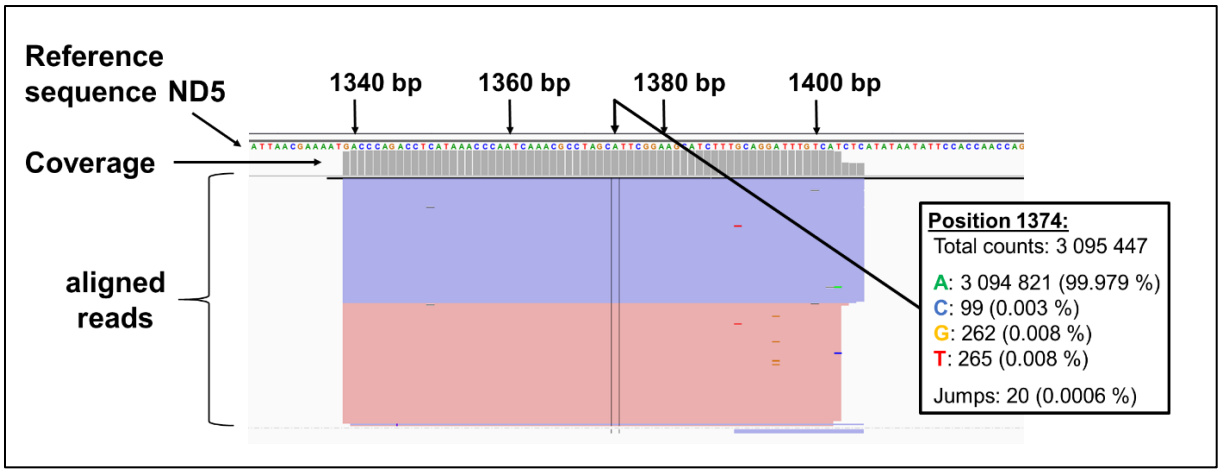

Figure 4.20: Visualization of mapped sequencing reads from an exemplar mouse hippocampus shows scarce misincorporation rates at position 1374 of ND5. The m^1A^{1374} analysis method was applied to murine tissue by means of adjusted RT and p5 PCR primers targeting the mouse ND5 mRNA sequence. Total RNA was isolated from one exemplar hippocampus of a Wt mouse (sex: male, age: 27 weeks) and used for RT-PCR (with SS-IV) ans subsequent Illumina sequencing. After trimming and alignment the above presented screenshot was taken in IGV (v. 2.8.0). Misincorporations rates of C, G, T and the number of jumps are extremely low, suggesting that little or no m^1A is present in mouse mRNA. Purple: forward reads, rose: reverse reads, colored horizontal bars (red, yellow, dark blue, green) represent misincorporated bases in individual reads.

mismatch. The jump rate at position 1374 is also vanishingly low with 0.0006% (equals 20 reads out of >3 million reads). In HEK293 cells, this value of jump rates were between 0.5% and 7%, which again indicates that these 0.0006% in 5xFAD mice are not m^1A-induced but might represent ordinary, spontaneous deletions. To evaluate the frequency of spontaneous mismatches and jumps in this experiment setup, the situation at the preceding and following position of the expected m^1A site were additionally considered (see Table 4.5). Since mismatch and jump rates at position 1373 and 1375 were more or less in the same range as those at position 1374, this result suggests that m^1A^{1374} is not methylated in mice. However, in order to proof the existence or absence of m^1A^{1374} in mice the experiment would have to be repeated with a different experimental set up including m^1A-immunoprecipitation or AlkB/ Dimroth treatment. For this reason, the experiment was not repeated with a higher number of samples.

Table 4.5: List of mismatch and jumps at position 1373 and 1375 in the mouse ND5 sequence. Data of one mouse hippocampus sample (depicted as well in Figure 4.20) is represented in a tabular list in order to estimate ordinary, spontaneous mismatches and jumps around the potential m^1A^{1374} site.

	Position C^{1373} [read counts]	Position C^{1373} Number in [%]	Position T^{1375} [read counts]	Position T^{1375} Number in [%]
Total read counts	3 095 404	100.000	3 095 383	100.000
A	103	0.003	122	0.004
C	3 094 854	99.982	540	0.017
G	53	0.002	116	0.004
T	394	0.013	3 094 605	99.975
Total mismatch	550	0.018	778	0.025
Jumps	46	0.001	82	0.003

4.3.4 ND5 protein expression in 5xFAD mice

In section 4.3.1 the hypothesis (i) was confirmed and an upregulation of TRMT10C was found in two brain regions of 5xFAD mice. As explained in the previous section a reliable assessment of m^1A^{1374} methylation levels in 5xFAD mice was not possible. For this reason, the hypothesis (iii) was investigated in the next step. To be precise, it was examined whether the upregulation of TRMT10C in the hippocampus and cortex of 5xFAD mice also coincides with decreased ND5 protein levels, as it was observed in HEK293 AD model cells and pTRMT10C cells. In section 4.2.2 and 4.2.3 it was shown that increased TRMT10C levels directly lead to elevated m^1A^{1374} and decreased ND5 protein levels. However, there is still the possibility that a mouse, as a whole organism, reacts different from a cell line. Therefore, a Western blot of ND5 was performed with 5xFAD and Wt mice. Again, the hippocampus, cortex and cerebellum was investigated and GAPDH was used as reference enzyme.

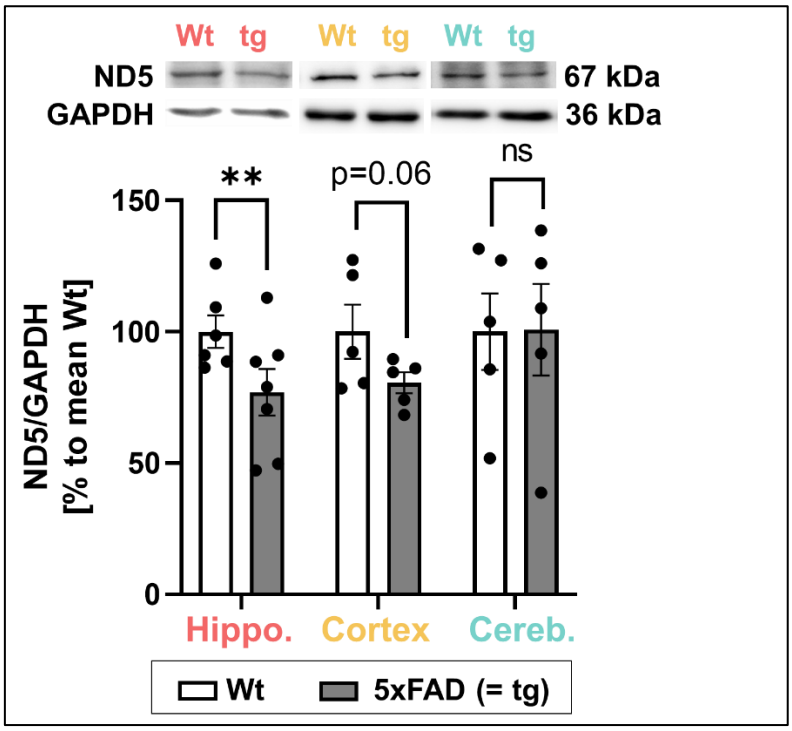

Figure 4.21: ND5 protein levels are significantly reduced in hippocampus tissue of 5xFAD mice. Western blot results of ND5 in hippocampus (Hippo.), cortex (Cortex) and cerebellar (Cereb.) tissue from 5xFAD and Wt mice. Representative membranes are displayed in the upper panel. ND5 protein levels are significantly diminished in hippocampi of 5xFAD mice. In cortices a trend towards decreased ND5 levels is visible (p= 0.06). In the cerebellum ND5 content of Wt and 5xFAD is unchanged. Mean ± SEM, hippocampus: n= 6 wt and n= 7 tg, cortex and cerebellum: n= 5 wt n= 5 tg, female and male mice, age= 42-55 weeks, unpaired t-tests, ns= not significant.

Strikingly, the Western blot showed a vast decrease of ND5 protein levels in hippocampi of 5xFAD mice compared to Wt (Figure 4.21). The values of the transgenic mice are on average 77% compared to the mean of Wt mice. Likewise, a reduction of ND5 is apparent in cortex samples, however, this decrease is just not significant (p= 0.06). At this point, it should

be noted that more hippocampus samples were provided than from the cortex and cerebellum. Therefore, there are seven 5xFAD data points given for the hippocampus and five data points given for the other brain regions. Thus, one can speculate that the decrease in ND5 in the cortex would fall below the significance threshold with a higher number of n. Of note, in the cerebellum no significant change was detected between transgene and Wt animals. Considering Figure 4.18, this data suggests that ND5 levels are decreased in exactly those brain regions of 5xFAD mice, where the TRMT10C expression was upregulated.

According to hypothesis (iv), the reduction of ND5 in the hippocampus and cortex of 5xFAD mice raised the question of whether Cpx I and the overall mitochondrial function are impaired as a consequence. Yet mitochondrial deficits have been found several times in 5xFAD mice [450]–[452]. Therefore, these experiments were skipped and the examination of hypotheses (i) - (iv) was pursued in human AD samples (see section 4.4).

4.4 Investigation of human brain tissue and RNA-Seq data from AD patients

In the final section of this chapter, the findings of the previous sections should be verified in human AD patients. Therefore, the hypotheses (i) – (iv) were tested sequentially on human brain tissue and publicly available RNA-Seq data sets.

Human brain tissue samples from AD patients and age-matched controls (Ctl) were provided by the Netherlands Brain Bank (NBB)[16]. This non-profit organization collects human brain tissue of donors with a variety of neurological and psychiatric disorders and also of non-diseased donors. Among them, Alzheimer patients are represented with a high number. Once a brain has been removed from its donor, it is macroscopically examined and dissected into several smaller pieces. Thereby a certain scheme is applied, yielding the hippocampus, amygdala, cortex and cerebellum, all subdivided into small tissue dices (see section 3.1.7). After a successful application process, a researcher can select from the frozen samples those anonymous individuals and brain sections that match best to his or her scientific question. Because hippocampal samples were limited in availability, cortex samples were selected for the following experiments. Here, frontal cortex samples (gyrus frontalis superior 3+4) were chosen because in this brain region pathophysiological changes are already evident in the early symptomatic AD stage [453]. When selecting the samples, care was taken to ensure that both AD and Ctl contained a balanced mixture of male and female individuals and the ages were matched between the two groups. Furthermore, it was aimed to select patients at the same Braak stage in order to exclude effects resulting from different AD stages. The Braak classification, introduced by Heiko Braak in 1991 [38], is based on the characteristic distribution of neurofibrillary tangles throughout the brain and enables a reliable differentiation of AD pathology between individuals by means of six stages. In stage 1 and 2 a mild to moderate burden is detectable in the transentorhinal cortex. In stage 3 and 4, an aggravated burden is observed in the transentorhinal and entorhinal cortex, two regions directly adjacent to the hippocampus. In stage 5 and 6, neurofibrillary tangles are found throughout the entire cortex. In this case, brain samples from individuals at Braak stage 5 and 6 were selected to ensure that the AD pathology has definitely reached the frontal cortex. Unfortunatelly, the NBB did not provide enough samples at these Braak stages to balance for sex and age, therefore also samples at stage 4 were included. The final tissue selection showed an average Braak stage of 4.7 ± 0.6 among AD patients, representing an intermediate AD stage [454] (for more information see Materials and Methods section 3.1.7).

[16] https://www.brainbank.nl/

The RNA-Seq data was retrieved from three different sources. To gain a general overview of the mRNA expression of the desired proteins (TRMT10C, SDR5C1, PRORP and ND5), the “Aging, Dementia and TBI Study” data set [425] was employed. This data set obtained from brains of AD patients and healthy controls is freely accessible through the “Allen Institute for Brain Science”[17] and represents a cohort from the Adult Changes in Thought (ACT) study [424]. In this Study, tissue samples were cut from the temporal cortex, hippocampus, parietal cortex and white matter of the parietal cortex. These bulk preparations were then subjected to RNA sequencing (RNA-Seq). Thereby, 377 samples were sequenced from a total of 107 brains and the results of this transcriptomic study were published as normalized fragments per kilobase per million mapped fragments (FPKM) including the associated donor information. Thus, FPKM values of TRMT10C, SDR5C1, PRORP and ND5 could be extracted and evaluated in all four brain regions in order to estimate the corresponding mRNA expression in AD patients. Of note, the study focused on the impact of TBI and therefore investigated a high number of TBI exposure cases. To assure that the consequences of TBI do not confound the possible results of AD pathology, all AD and control samples that had experienced TBI were excluded in the following analysis. Besides, only a part of the demented patients could be diagnosed with probable AD. Another part was diagnosed with vascular dementia or so-called possible AD. In consequence, only patients with a probable AD diagnose were included in the following analysis. Furthermore, this data set did not contain a balanced mixture of female (n=2-3) and male (n=8-13) AD patients. As two samples are not enough to perform separated statistics and a balanced mixture could not be reached, only male individuals were included in the following analysis. The results for TRMT10C, SDR5C1, PRORP and ND5 from the “Aging, Dementia and TBI Study” data set are shown in section 4.4.1 - 4.4.6.

The “Aging, Dementia and TBI Study” data set entails two major drawbacks. First, after excluding cases with TBI and uncertain diagnosis, only two female AD patients remained. As mentioned before, two samples are inappropriate to perform statistical tests, therefore only male samples could be assessed. Second, in the “Aging, Dementia and TBI Study” a bulk preparation was conducted. This poses the risk that cell-type specific effects might be “washed out” by the transcriptomes of surrounding cells. For this reasons, it was sought for a second data set in which single-cell RNA sequencing (scRNA-Seq) was conducted in AD patients. In consequence, a scRNA-Seq study performed by Mathys *et al.* [426] in 2019 was additionally analyzed. This data set was obtained from 48 individuals, among them 24 controls (Ctl) and 24 patients with varying degress of AD pathology. In both groups, the sexes were equally distributed (12+12) and the average age was almost the same. From these subjects, a part of the prefrontal cortex (Brodman area 10) was dissected and then the tissue was homogenized

[17] http://aging.brain-map.org/

and filtered with a cell strainer prior to the RNA-Seq analysis. In this way, 80 660 single-cell transcriptomes could be collected, which were subsequently divided into 6 different cell type groups based on specific marker genes. These six cell types were excitatory neurons, inhibitory neurons, astrocytes, oligodendrocytes, precursor-oligodendrocytes and microglia. The results of this scRNA-seq study were reported as fold change (FC) values, reflecting the ratio of mRNA in AD patients versus Ctl. Furthermore, an associated p-value was provided to assess the relevance of potential differences. In the following sections (4.4.1 & 4.4.3) FC and p-values of TRMT10C and SDR5C1 from this scRNA-Seq data set are visualized in heatmaps. In the case of PRORP, no FC and p-values were available because no significant differences were found in any of the six cell types. Likewise, no results were reported for ND5 as mitochondrial encoded genes were generally not included. Furthermore, it should be mentioned that the AD group was further divided into early and late-stage cases. Hence, AD versus Ctl, as well as early-stage versus Ctl, and late- versus early-stage AD could be compared.

In the two data sets mentioned above, the whole transcriptome was determined by means of RNA-Seq or scRNA-Seq. Thereby, mRNA expression levels were made available to the public as FPKM or FC values. However, for the analysis of m^1A^{1374} methylation leves in the ND5 mRNA, sequencing raw data files (.fastq-files) would be needed to assess m^1A-induced misincorporation rates. For this reason, a third data set providing freely accessbile sequencing raw data from AD patients and healthy controls was selected [427] and analyzed for m^1A^{1374}. A more detailed description of this data set can be found in section 4.4.5.

4.4.1 TRMT10C mRNA expression in AD patients

To evaluate the expression of TRMT10C in AD patients according to hypothesis (i), the first step was to analyze mRNA expression levels in the “Aging, Dementia and TBI Study” data set. Therefore, normalized FPKM values of AD patients were compared to Ctl in all four brain regions studied. Of note, only male patients with a confirmed AD diagnosis and without TBI incident were utilized, as explained in the previous section. Likewise, male patients without TBI were selected for the corresponding control group (Ctl).

Examination of the „Aging, Dementia & TBI Study“ data set showed a significant increase in TRMT10C mRNA expression in the white matter of the parietal cortex and a highly significant increase in the parietal cortex of AD patients (Figure 4.22). In the hippocampus and the temporal cortex no significant change could be detected. It should be noted, however, that both showed a trend towards elevated TRMT10C mRNA levels in comparison to Ctl. The

corresponding p-value was 0.21 in the hippocampus and 0.37 in the temporal cortex. Thus, TRMT10C mRNA expression seems to be clearly altered by AD.

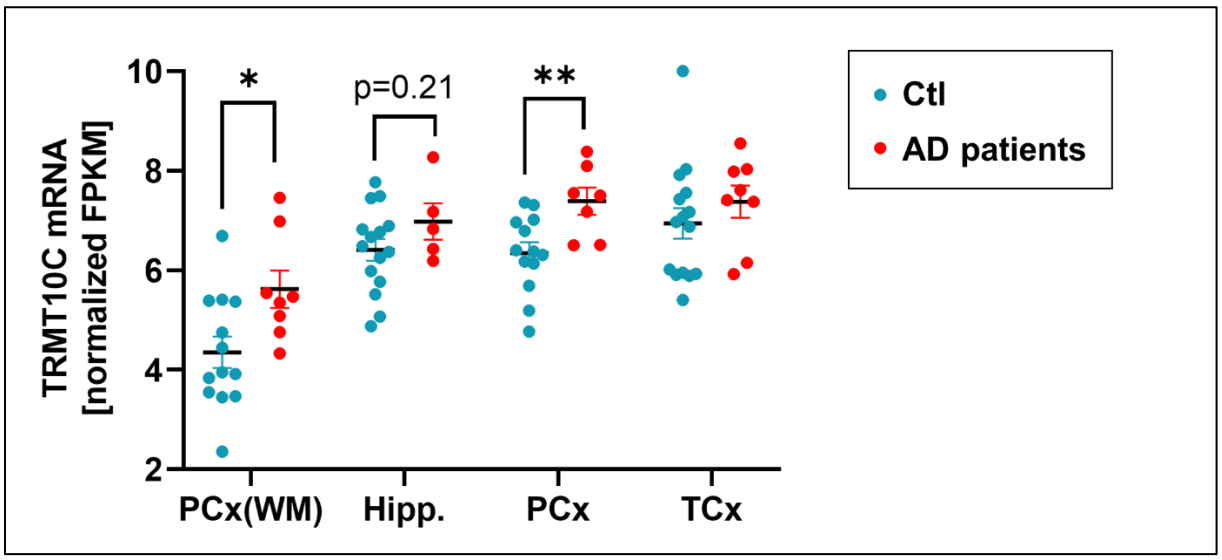

Figure 4.22: TRMT10C mRNA expression is significantly enhanced in the white matter of the parietal cortex and in parietal cortex samples from AD patients. Normalized FPKM values were extracted from the "Aging, Dementia & TBI Study" data set [425]. AD & Ctl: Male individuals without TBI. Mean ± SEM, n= 13-15 Ctl, n= 5-8 AD, multiple unpaired t-tests, *p<0.05, **p<0.01. PCx(WM)= white matter of the parietal cortex, Hipp.= hippocampus, PCx= parietal cortex, TCx= temporal cortex.

Going one step further, the mRNA expression of TRMT10C should be examined in scRNA-seq data from AD patients. Therefore, the publicly available data set of Mathys *et al.* [426] was consulted, in which six different cell types were analyzed in prefrontal cortex samples. This study provides $\log_2$ fold change (FC) and p-values resulting from the comparison of AD patients and healthy controls. Furthermore, AD patients were divided into early- and late-stage cases enabling a comparison between both disease stages (more information about this data set can be found at the beginning of section 4.4.)

The analysis of the scRNA-Seq data set revealed a highly significant overexpression of TRMT10C mRNA specifically in neurons of AD patients (Figure 4.23, first column). Comparing all AD cases with healthy controls showed a moderate, but highly significant increase in excitatory and inhibitory neurons of AD patients. The $\log_2$ FC value in excitatory neurons was +0.195, which $\log_2$-converted corresponds to a value of 1.14. This signifies that ~14% more TRMT10C mRNA fragments were found in AD patients than in Ctl. In inhibitory neurons, the $\log_2$ FC value is +0.238, corresponding to 18% higher TRMT10C mRNA content in AD. Of note, the alterations in astrocytes, oligodendrocytes, pre-oligodendrocytes and microgla were insignificant.

Regarding the early-stage AD group (second column), a similar picture emerges. Here, TRMT10C mRNA expression is also significantly enhanced in excitatory and inhibitory neurons, however, the augmentation is more pronounced in this group than in AD versus Ctl.

This becomes visible from the darker shades of red in the corresponding fields of the heat map (see Figure 4.23). In excitatory neurons, a log_2 FC value of +0.455 was measured, which means converted that mRNA levels are 37% higher in early-AD than in Ctl. In inhibitory neurons, the log_2 FC value was +0.497, representing 41% more TRMT10C mRNA in the early-stage AD group than in Ctl.

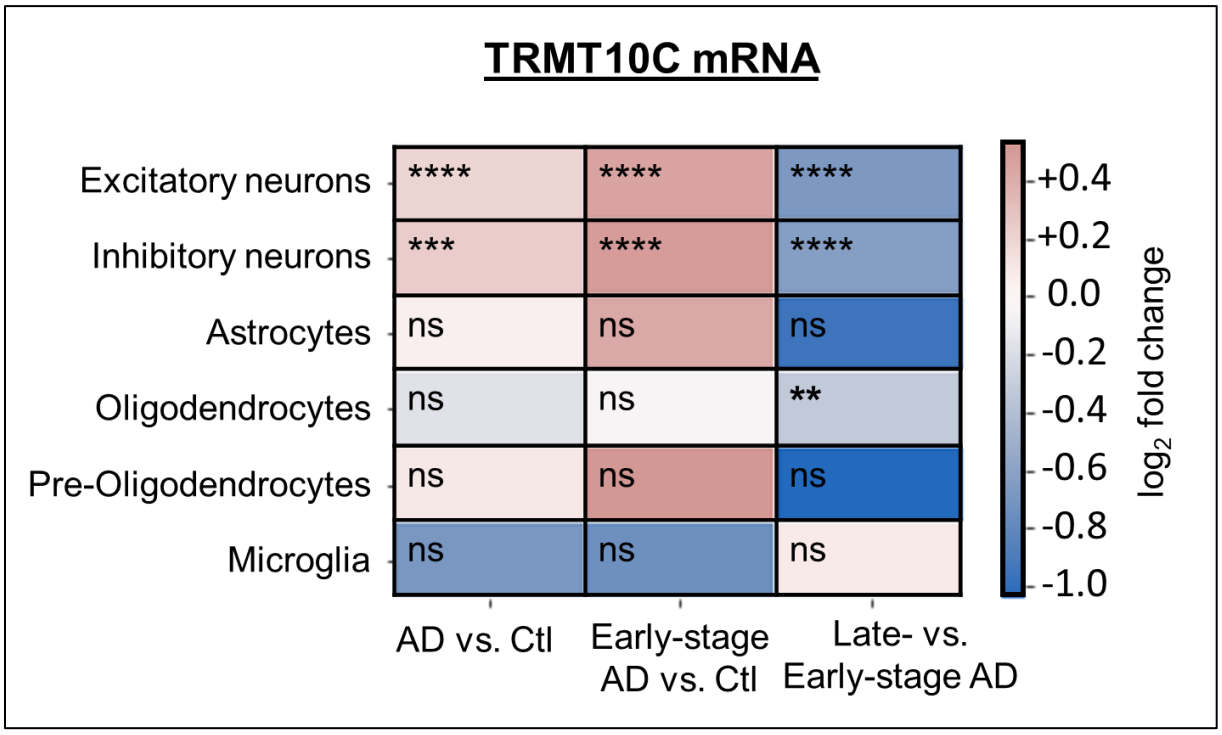

Figure 4.23: TRMT10C mRNA levels are altered exclusively in inhibitory and excitatory neurons of AD patients. Heatmap representing log_2 fold change (FC) values of TRMT10C mRNA expression in the scRNA-Seq data set from Mathys *et al.* [426]. The red or blue color of a box indicates the corresponding fold change value. Adjusted p-values (adj. p-vals) are entered as symbols in the corresponding box. TRMT10C mRNA is significantly upregulated in AD and early-stage AD in comparison to Ctl, but only in excitatory and inhibitory neurons. TRMT10C mRNA is downregulated in late-stage AD versus Ctl in neurons and oligodendrocytes. 80 660 transcriptomes were analyzed from prefrontal cortex tissue of 48 individuals. n= 24 Ctl, n= 24 AD (n= 15 early-stage AD, n=9 late-stage AD). ****adj. p-vals<0.0001, ***adj. p-vals<0.001, **adj. p-vals<0.01, ns= not significant.

The results of the late-stage AD group showed a rather different pattern (Figure 4.23, third column). Here, TRMT10C mRNA expression was also significantly altered in excitatory and inhibitore neurons, however, less mRNA was found in the late-stage than in the early-stage cases. Excitatory neurons displayed a log_2 FC value of -0.671, which means converted that mRNA levels were 37% lower in late-stage AD patients. In inhibitory neurons, the log_2 FC value was -0.628, indicating 35% less mRNA expression in late- compared to early-stage AD patients. Besides it is important to stress, that no significant changes were observed in astrocytes, pre-oligodendrocytes and microglia. Only in oligodendrocytes, a significant decrease of TRMT10C mRNA was detected. In this case, the log_2 FC value was -0.320, representing 20% lower mRNA levels in the late- versus the early-stage of AD.

4.4.2 TRMT10C protein expression in AD patients

Since TRMT10C mRNA levels were elevated in both RNA-Seq data sets, it was reasonable to assume that protein levels would also be elevated. However, it has been frequently shown in the literature that mRNA levels do not always correlate with the corresponding protein content [455]–[457]. Therefore, TRMT10C protein expression was examined the human frontal cortex tissue samples, obtained from the NBB. More information about the NBB and the selected samples is provided at the beginning of section 4.4 and in section 3.1.7. TRMT10C protein expression was determined by Western blot in AD patients and age-matched controls (Ctl). Prior to the first analysis, the suitability of GAPDH as reference enzyme was tested in these samples. Since the intensities of this protein did not vary more than 10% between all tested samples, it was considered to be appropriate for the following Western blot analysis.

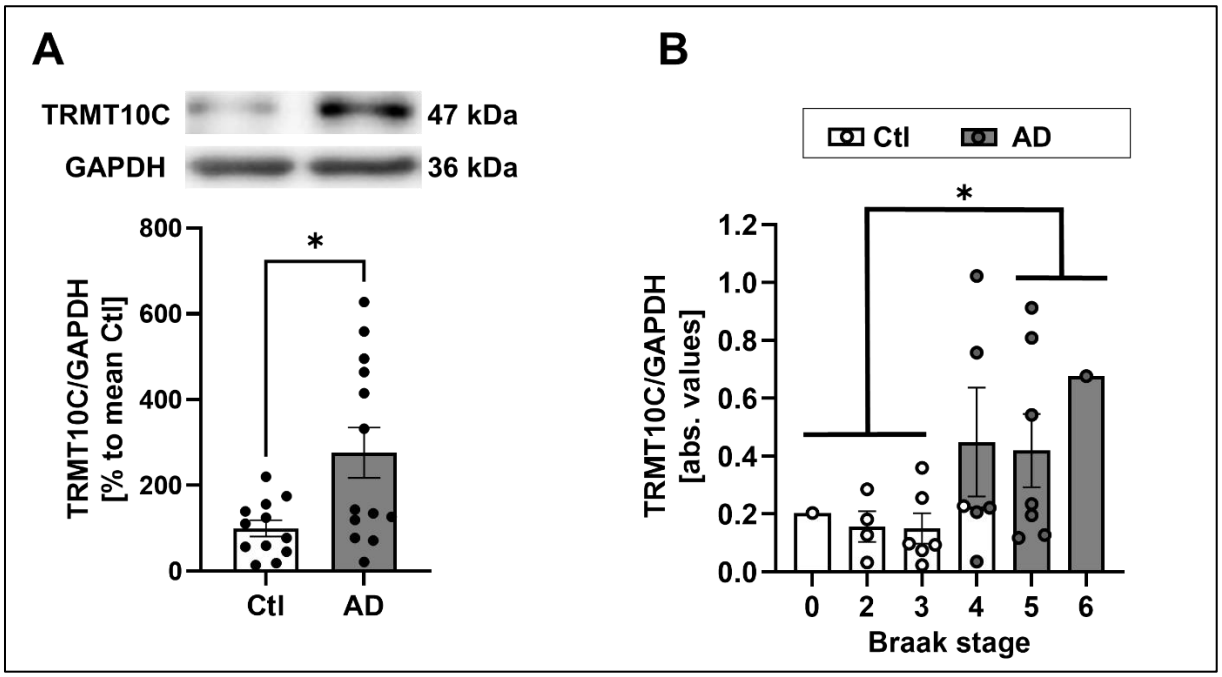

Figure 4.24: TRMT10C protein levels are significantly elevated in frontal cortex samples of human AD patients. A) Western blot results of TRMT10C in frontal cortex tissue from AD patients and age-matched controls, obtained from the NBB. A representative blot is shown in the upper panel. TRMT10C protein levels are significantly increased in AD patients. Mean ± SEM, n= 12 Ctl and n= 13 AD, female and male individuals, unpaired t-tests, *p<0.05. **B)** Data from A) subdivided by Braak stages of both AD patients and Ctl. A correlation of TRMT10C and Braak stage can be assumed because the difference between Ctl at Braak stage 1-3 and AD at Braak stage 5+6 is significant. Grey-filled points represent values of AD patients, white-filled points represent those of Ctl. Superimposed scatter plot, Mean ± SEM.

Strikingly, Western blot results of the human frontal cortex samples revealed a significant increase in TRMT10C protein levels in AD patients (Figure 4.24A). This matches well with the results of the previous section, where TRMT10C mRNA was found to be elevated in neurons generated from prefrontal cortex tissue of AD patients (Figure 4.23). However, it is not clear

from these results at which time point of the disease this alteration occurs. Therefore, Western blot data was split according to Braak stages of both AD and Ctl. The Braak stage offers a reliable classification of AD patients to determine and compare their stage of the disease based on the characteristic distribution of neurofibrillary tangles (more information about Braak stages at the beginning of section 4.4). As neurofibrillary tangles can also be found in healthy individuals, people from the Ctl group could also be divided by Braak stages. Plotting TRMT10C expression as a function of Braak stages indicates a possible correlation between these two parameters, because the augmentation between Ctl with Braak stage 0-3 and AD patients with Braak stage 5+6 was significant (Figure 4.24B). This data suggests that TRMT10C protein levels increase in the frontal cortex during the couse of AD.

4.4.3 SDR5C1 and PRORP mRNA expression in AD patients

In the previous sections, mRNA and protein levels of TRMT10C were found to be increased in brain tissue and RNA-Seq data of AD patients. As mentioned before, it known that TRMT0C requires enzymatic partner proteins to exert two out of three enzymatic functions. For the methylation of (mt)tRNAs at position 9 SDR5C1 is needed. To process and release (mt)tRNA at their 5'-ends from mitochondrial primary transcripts, PRORP is additionally required. Whether one or both of these enzymes are also necessary for the methylation of m^1A^{1374} is not known so far. Nontheless, overexpression of TRMT10C would be presumed to be accompanied by changes in the SDR5C1 and PRORP protein content in AD, as observed in the HEK AD model cell lines (section 4.1.2). However, it is unclear whether these changes would also be apparent at the mRNA level. For this reason, the mRNA expression of SDR5C1 and PRORP was studied in both of the RNA-Seq data sets utilized above. So below, the results of the "Aging, Dementia and TBI Study" data set and the scRNA-Seq from Mathys *et al.* [426] are presented.

The mRNA expression of SDR5C1 was not significantly altered in all of the four brain regions investigated in the "Aging, Dementia & TBI Study" data set (Figure 4.25). Although a downward trend can be observed in AD patients in the white matter of parietal cortex, the parietal cortex and the temporal cortex, these alterations are all not significant. As for TRMT10C, only male patients with a confirmed AD diagnosis and without TBI were used for the analysis. Likewise, only male individuals without TBI were considered in the control group (Ctl). Thus, the results are well comparable to the analysis of TRMT10C mRNA (Figure 4.22).

Given the limitations of RNA-Seq analysis in bulk preparations (explained at the beginning of section 4.4), SDR5C1 mRNA was also studied in the scRNA-Seq data set of Mathys *et al.* [426]. Interestingly, the expression of SDR5C1 mRNA was significantly increased

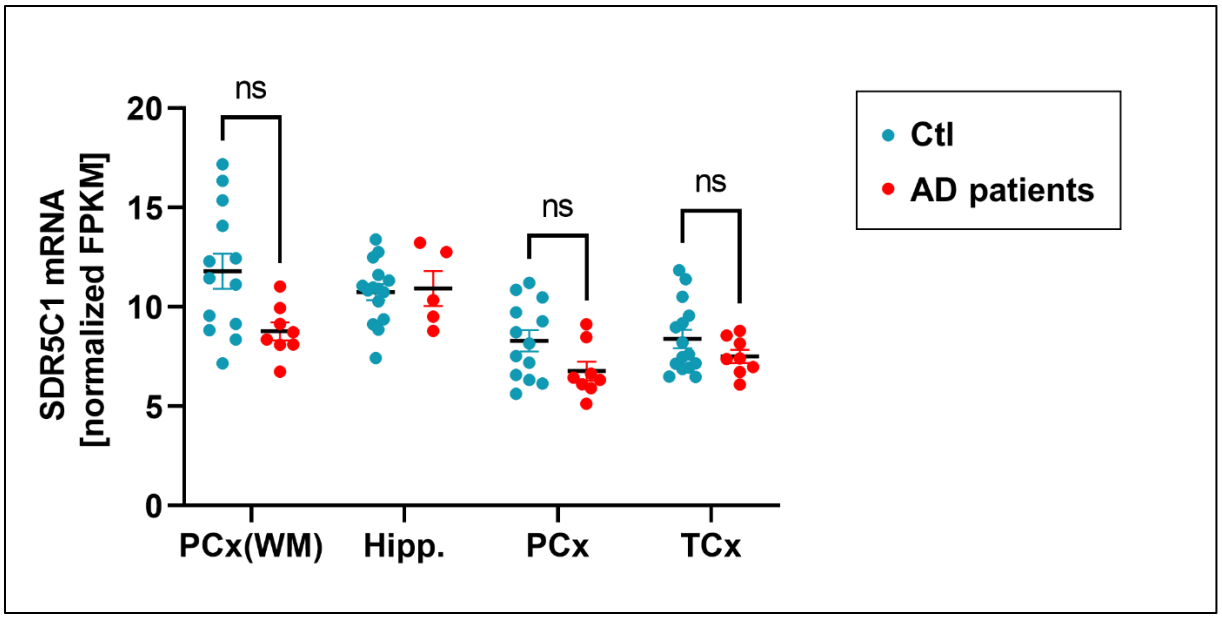

Figure 4.25: SDR5C1 mRNA expression is not altered in brain tissue of AD patients. Normalized FPKM values were extracted from the "Aging, Dementia & TBI Study" data set [425]. AD & Ctl: Male individuals without TBI. Mean ± SEM, n= 13-15 Ctl, n= 5-8 AD, multiple unpaired t-tests, ns= not significant. PCx(WM)= white matter of the parietal cortex, Hipp.= hippocampus, PCx= parietal cortex, TCx= temporal cortex.

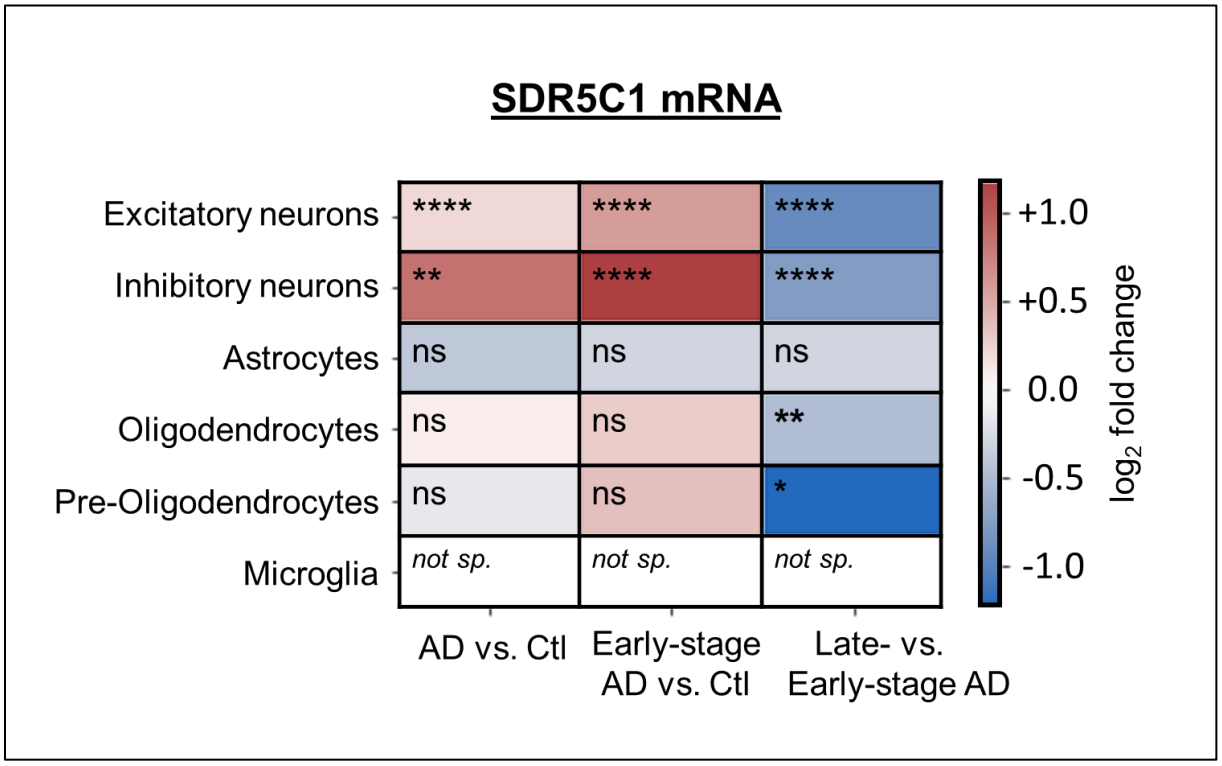

Figure 4.26: SDR5C1 mRNA levels are altered exclusively in inhibitory and excitatotry neurons of AD patients. Heatmap representing log_2 fold change values of SDR5C1 mRNA expression in the scRNA-Seq data set from Mathys *et al.* [426]. The color of a box indicates the corresponding fold change value, adj. p-vals. are entered as symbols in the corresponding box. SDR5C1 mRNA is significantly upregulated in AD and early-stage AD in comparison to Ctl, but only in excitatory and inhibitory neurons. SDR5C1 mRNA is downregulated in late-stage AD versus Ctl in neurons, oligodendrocytes and pre-oligodendrocytes. 80 660 transcriptomes were analyzed from prefrontal cortex tissue of 48 individuals. n= 24 Ctl, n= 24 AD (n= 15 early-stage AD, n=9 late-stage AD). ****adj. p-vals<0.0001, ***adj. p-vals<0.001, **adj. p-vals<0.01, ns= not significant, *not sp.*= not specified.

in neurons of AD patients versus Ctl (Figure 4.26, first column). In excitatory neurons, the log_2 fold change value is +0.214, which converted signifies an elevation of 16% compared to Ctl. As for inhibitory neurons, the rise of SDR5C1 mRNA was more pronounced, with a log_2 fold change value of +0.853, corresponding to 80% higher levels in AD. Of note, in astrocytes, oligodendrocytes and pre-oligodendrocytes no significant alterations were detected. In the case of microglia, no fold change values were stated in the data set, probably due to detection deficulties in a large fraction of the microglia population (explained in [426]).

Comparing early-stage AD versus Ctl (Figure 4.26, second column), a similar pattern is apparent. Again, SDR5C1 mRNA expression is significantly enhanced in neurons of early-stage AD patients, but unchanged in astrocytes, oligodendrocytes and pre-oligodendrocytes. However, the overexpression is much stronger than in AD versus Ctl. In excitatory neurons, the log_2 fold change value is +0.586, corresponding to 50% higher mRNA levels in early-AD patients. Remarkably, the log_2 fold change value in inhibitory neurons is +1.177 in early-AD compared to Ctl. After log_2 conversion this results in 126% higher mRNA levels, which signifies that mRNA quantity is more than doubled in the early-stage of AD.

Looking at the comparison of late- versus early- stage AD (Figure 4.26, third column), it is of notice that SDR5C1 mRNA levels are significantly decreased in neurons in the late-stage. In excitatory neurons the log_2 fold change value is -0.914, which means that mRNA expression is 47% lower in the late-stage compared to the early-stage. In inhibitory neurons, the log_2 fold change value is -0.765, corresponding to a 41% decreased mRNA expression in the late-stage. In astrocytes no significant changes were detected. However, in oligodendrocytes and pre-oligodendrocytes a significant downregulation was found in the late-stage of AD compared to early-stage AD. Unfortunately, the data set does not provide information about the comparison of late-stage versus Ctl.

As with SDR5C1, PRORP mRNA expression was analyzed in the same way in the “Aging, Dementia and TBI Study” data set [425]. And likewise, there were no significant differences observed in AD patients in all four investigated brain regions (Figure 4.27). In the white matter of the parietal cortex and the temporal cortex a tendency to decreased PRORP levels is visible, however, these alterations are not significant ($p= 0.12$ in PCx(WM) and $p= 0.20$ in TCx). Furthermore, it should be mentioned here that again only male AD patients with a confirmed AD diagnosis and without TBI were included in this evaluation. Similar to the analysis of SDR5C1 and TRMT10C, women were excluded because only two female AD samples were available. Furthermore, it should be emphasized that in the “Aging, Dementia and TBI Study” a bulk RNA-Seq analysis was conducted. This offers the disadvantage that minor changes in certain cell types, e.g. neurons, might be masked by the expression of the surrounding cell types. Due to these two limitations, the scRNA-Seq study from Mathys *et al.*

was additionally evaluated for TRMT10C and SDR5C1. In the case of PRORP, this single-cell data set does not provide FC and adj. p-vals, which implies that this enzyme did not show any significant alterations.

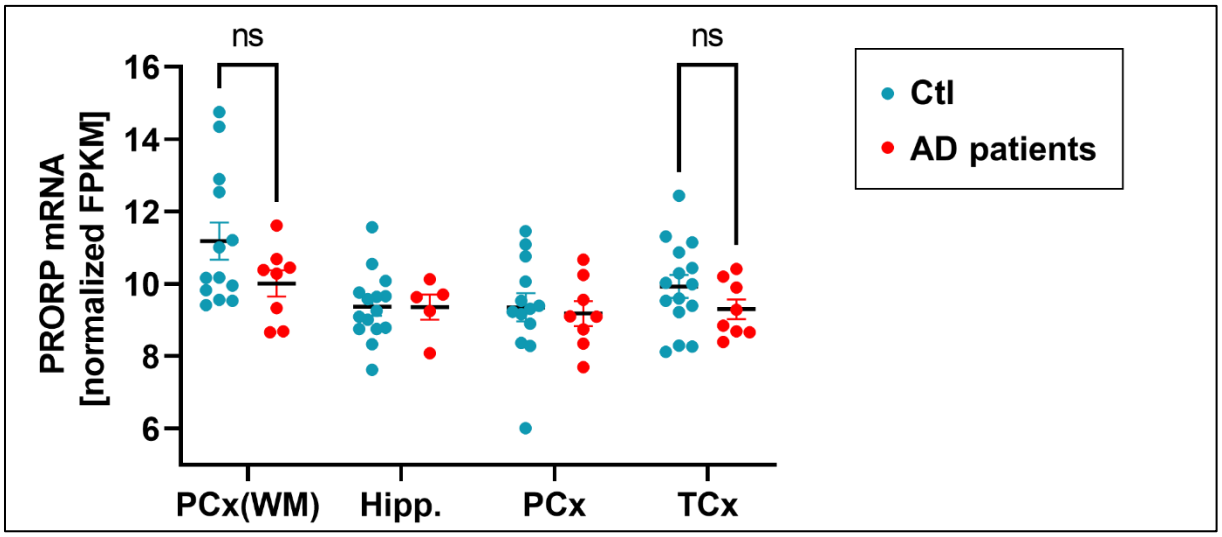

Figure 4.27: PRORP mRNA expression is not significantly altered in brain tissue from AD patients. Normalized FPKM values were extracted from the "Aging, Dementia & TBI Study" data set [425]. AD & Ctl: Male individuals without TBI. Mean ± SEM, n= 13-15 Ctl, n= 5-8 AD, multiple unpaired t-tests, ns= not significant. PCx(WM)= white matter of the parietal cortex, Hipp.= hippocampus, PCx= parietal cortex, TCx= temporal cortex.

4.4.4 SDR5C1 and PRORP protein expression in AD patients

Regarding mRNA expression no significant changes were detected for SDR5C1 and PRORP in the "Aging, Dementia and TBI Study" RNA-Seq data set using bulk preparations. In the scRNA-Seq study SDR5C1 showed significantly increased mRNA levels exclusively in neurons of AD patients, whereas PRORP mRNA was unchanged in all cell types. However, as mentioned above, mRNA levels do not always correlate with protein levels [455]–[457]. For this reason, the protein content of both proteins should be investigated in the human brain tissue of AD patients obtained from the NBB. Therfore, these frontal cortex samples were subjected to Western blot analysis for SDR5C1 and PRORP. As in section 4.4.2, GAPDH served as the reference enzyme.

In the Western blot of SDR5C1 no significant difference between the AD and Ctl group was detected (Figure 4.28A). Values of AD patients showed a relatively broad distribution ranging from 29.2% to 194.0% in relation to the mean of Ctl. The mean value of the AD group is 113%, so a slight upward trend can be estimated, but this elevation is far from being significant (p= 0.42). Furthermore, it was suggested that the broad deviation from the mean in the AD group might be caused by different SDR5C1 levels at different stages of the disease. Therefore, the data was subdivided by Braak stages for both AD and Ctl (Figure 4.28B). Here,

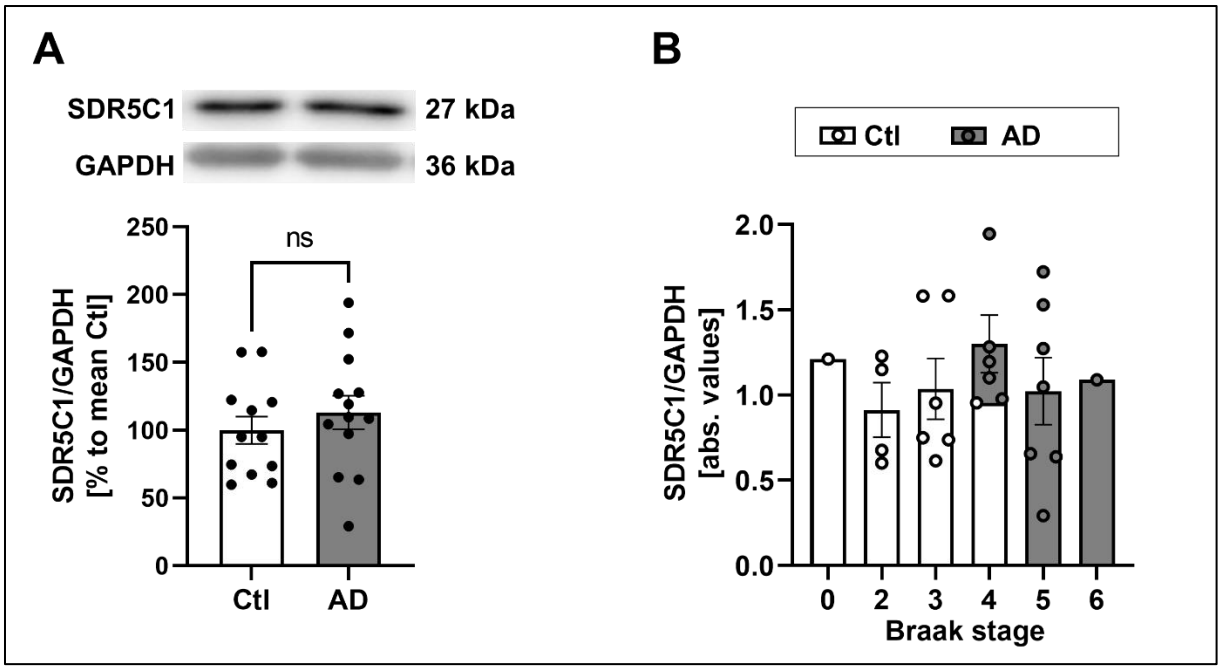

Figure 4.28: SDR5C1 expression is unchanged in frontal cortex tissue of human AD patients. A) Western blot results of SDR5C1 in frontal cortex tissue from AD patients and age-matched controls show no significant alterations between these two groups. A representative membrane is displayed in the upper panel. Mean ± SEM, n= 12 Ctl and n= 13 AD, female and male individuals, unpaired t-tests, ns= not significant. **B)** Data from A) subdivided by Braak stages of both AD patients and Ctl. No correlation between SDR5C1 and Braak stages is observed. Grey-filled points represent values of AD patients, white-filled points represent those of Ctl. Superimposed scatter plot, Mean ± SEM.

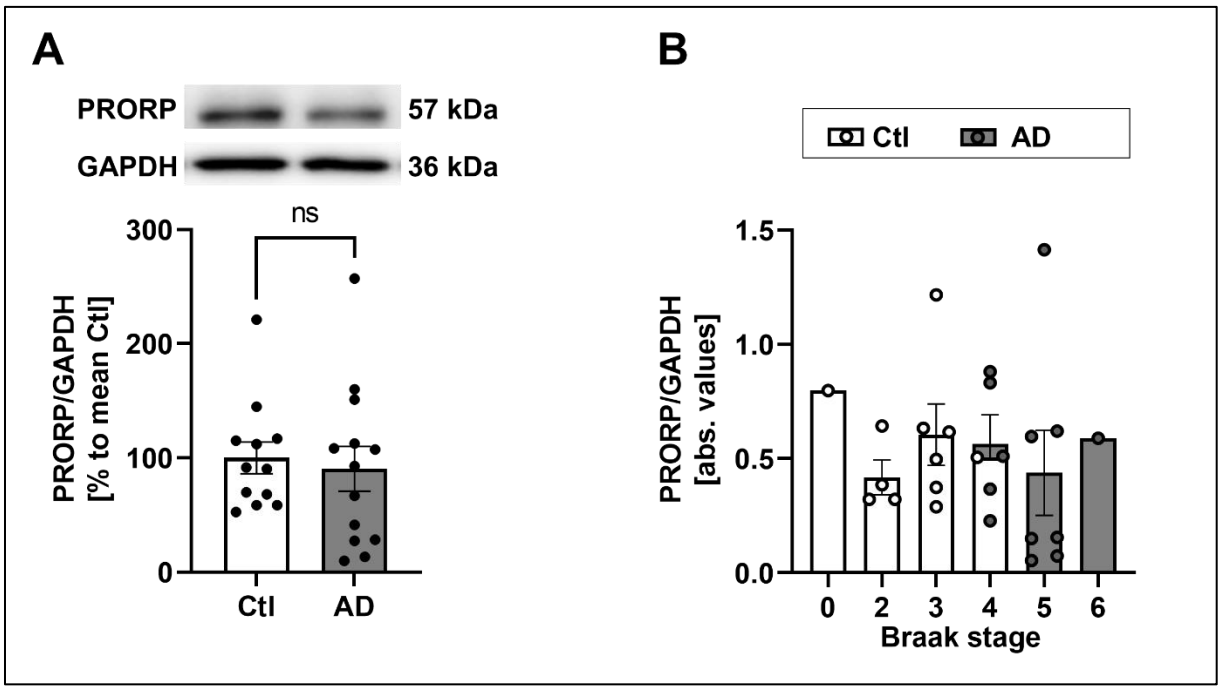

Figure 4.29: PRORP expression is not altered in frontal cortex tissue of AD patients. A) Western blot results of PRORP in frontal cortex tissue of AD patients does not show any alteration compared to Ctl. A representative membrane is displayed in the upper panel. Mean ± SEM, n= 12 Ctl and n= 13 AD, female and male individuals, unpaired t-tests, ns= not significant. **B)** Data from A) subdivided by Braak stages of both AD patients and Ctl. No correlation between PRORP and Braak stages is observed. Grey-filled points represent values of AD patients, white-filled points represent those of Ctl. Superimposed scatter plot, Mean ± SEM.

no correlation between Braak stage and SDR5C1 protein levels was observed, as all mean values varied around the same value.

In the same way, PRORP protein levels were examined in the frontal cortex tissue provided by the NBB. Again, the Western blot showed no significant changes between the AD and the Ctl group (Figure 4.29A). In this case, mean values of both groups were almost at the same level (AD: 91% related to the mean of Ctl) and again a broad distribution was observed in the AD group. To determine whether PRORP protein expression correlates with the disease stage, the data from Figure 4.29A was subdivided by Braak stages of all individuals. However, as for SDR5C1, no correlation was observed between these two parameters (Figure 4.29B). Mean values from each subgroup are more or less at the same level. Therefore, it cannot be concluded that the broad deviation is caused by different disease stages. Rather, it suggests that human brain samples simply display a high interindividual variability, which might be caused by different life styles (nutrition, genetics and more).

4.4.5 m^1A methylation levels in AD patients

Since increased TRMT10C levels were found in frontal cortex tissue of AD patients (section 4.4.1 & 4.4.2), the question arose whether m^1A^{1374} methylation is also elevated in AD patients. Following hypothesis (ii), m^1A-induced misincorportions in ND5 should be determined in AD patients. However, tissue samples from the NBB are provided after a long time of storage (up to 12 years in this set of samples). As freezing is known to damage RNA [282], no reliable m^1A^{1374} methlyation quantification could be conducted. Besides, none of the above databases provides sequencing raw data (.fastq files), which would be required to analyse m^1A-induced misincorporation and jump rates. For this reason, it was searched for a RNA-Seq study comprising publicly available raw data from AD patients. These data sets are scarce because RNA-Seq data contains very sensible information about the individuals. But fortunately, the NCBI Sequencing Read Archive (SRA) provides raw data of a RNA-Seq study conducted by Guennewig *et al.* [427] (PRJNA720779).

In this study, 10 post-mortem brains from AD patients and healthy age-matched controls were used for the RNA-Seq in order to explore differential gene expression in AD. In this bulk RNA-Seq appraoch, two brain regions were studied, the precuneus and the primary visual cortex. The precuneus is a trapezoidal structure that defines the posterior medial part of the parietal lobe in each brain hemisphere. This brain region is important for (self-) perception, visuo-spatial imagination and the storage of spatial information [458]. In doing so, it works closely together with the hippocampus [459]. The primary visual cortex is located in the occipital lobe and represents the principal telencephalic recipient of visual input in humans.

This brain region is essential for the conscious and initial processing of visual stimuli [460]. Of note, in the AD patients of this study the precuneus was moderately and the primary visual cortex was mildly affected by disease pathology. The editors claim that comparing these differently affected regions within the same AD brains enables modeling the course of the destructive processes leading to synaptic loss and neurodegeneration in AD [427]. This means that a mildly affected region represents an early time point and a moderately affected region represents an advanced time point within the pathologic cascade taking place in AD.

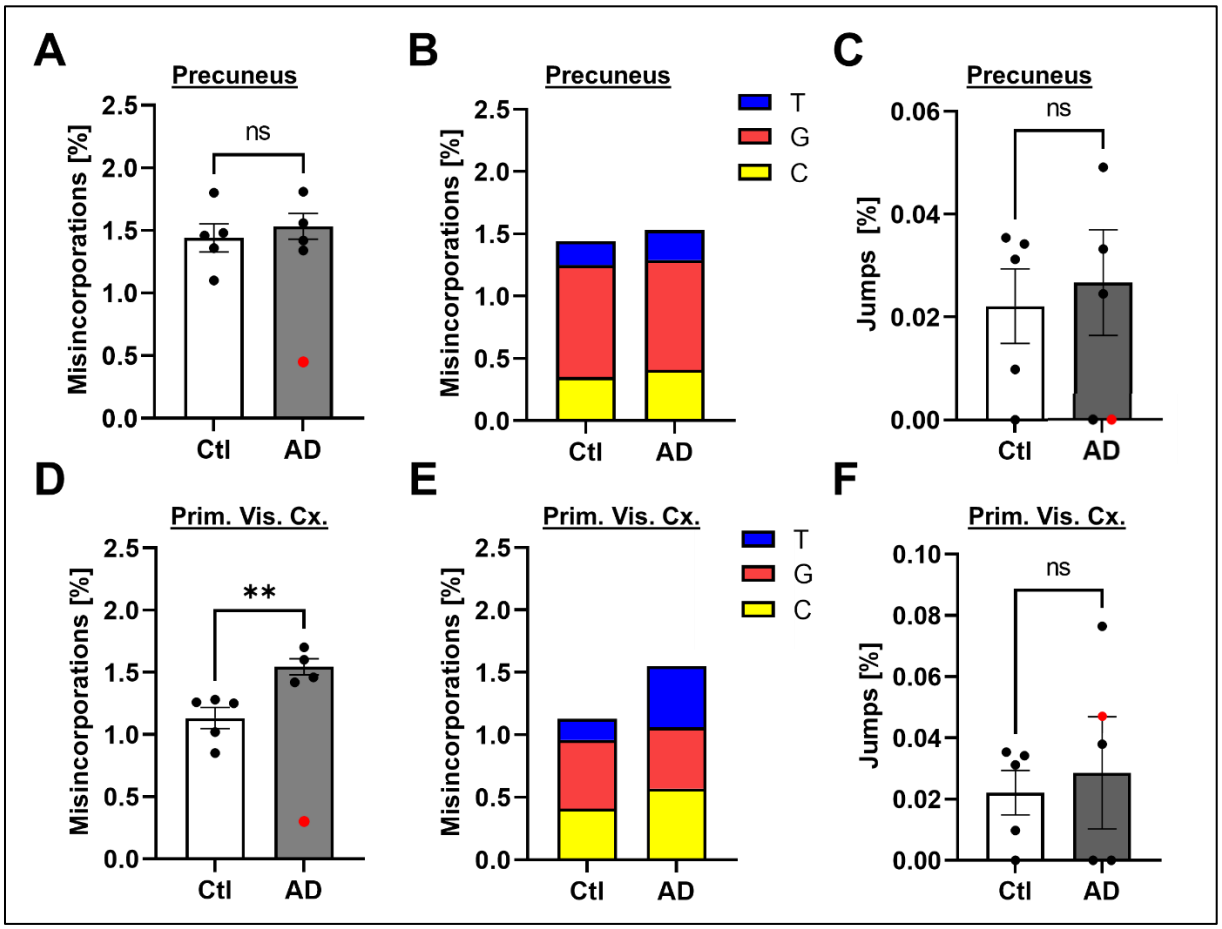

Figure 4.30: m^{1}A-induced miscorporations are significantly increased in the primary visual cortex of AD patients. A) Misincorporation rates at position 1374 of ND5 in the precuneus show no significant difference between AD and Ctl. **B)** Data from A) subdivided into the proportion of misincorporated bases on average. **C)** Analysis of jump rates at position 1374 of ND5 in the sequencing reads used in A) displays no significant alterations in the precuneus. **D)** Misincorporation rates at position 1374 of ND5 in the primary visual cortex exhibit a significant increase in AD patients. **E)** Data from D) subdivided into the proportion of misincorporated bases on average. **F)** Analysis of jump rates at position 1374 of ND5 in the sequencing reads used in D) shows no significant change between Ctl and AD in the primary visual cortex. **A)-F)** Raw data was extracted from the NCBI SRA (PRJNA720779) [427]. n= 5 Ctl, n= 5 AD, unpaired t-tests, **p<0.01, ns= not significant. Prim. Vis. Cx.=Primary Visual Cortex, T= Thymidine, G = Guanosine, C= Cytidine. One patient, carrying the G13708A single nucleotide polymorphism (SNP) has been excluded from the analysis (data points are labeled in red).

Comprehensive information on how this RNA-Seq study was performed can be found in Guennewig *et al.* [427] and section 3.1.8. In brief, five post-mortem brains from controls and

five from AD patients at Braak stage VI with a pathological diagnosis according to "ABC" criteria [461] were selected. Groups were matched for age, gender, APOE ε4 genotype and RNA-quality (RNA integrity number (RIN)). Next, RNA was extracted using TRIzol from frozen tissue of the precuneus and the primary visual cortex. After DNase I treatment and ribodepletion with RNase H, library preparation was conducted with the TruSeq Stranded Total RNA Sample Prep Kit (Illumina, USA) and the reverse transcriptase SuperScript II. Samples were sequenced in the Illumina HiSeq 2500 and uploaded to the NCBI Sequencing Read Archive[18]. Through this freely accessible platform, the data was then downloaded in our lab and the bioinformatics scripts (see section 3.2.6 & 4.1.3) were applied to determine m^1A^{1374} methylation levels via misincorporation and jump rates.

The analysis of m^1A-induced misincorporations at position 1374 of ND5 revealed no significant difference between AD patients and Ctl in the precuneus (Figure 4.30A). Of note, one patient displayed the G13708A single nucleotide polymorphism (SNP), which is among the defining SNPs of the Eurasian J haplogroup. This mutation is located two bases upstream of m^1A^{1374}, as position 1374 in ND5 equals position 13710 in the whole mtDNA. The G13708A SNP is known to prevent m^1A^{1374} methylation [312], and also shows a considerably lower mismatch rate in this data set (mean Ctl: 1.44%, mean AD patients: 1.53%, G13708A sample: 0.45%). Therefore, this individual has been excluded from the statistic analysis for both the precuneus and the primary visual cortex.

Table 4.6: Amount of misincorporated T [%], G [%] and C [%] in relation to the total amount of mismatch [%] at position 1374 of ND5. Data set from Figure 4.30.

Ratio $\frac{Base\ [\%]}{Mismatch\ [\%]}$	Precuneus, Ctl	Precuneus, AD	Prim. Vis. Cx., Ctl	Prim. Vis. Cx., AD
T	0.131	0.155	0.150	0.314
G	0.627	0.576	0.486	0.318
C	0.242	0.269	0.364	0.368

The division of misincorporated bases indicates that mainly G occurs at position 1374 in the sequencing reads, while T and C appear in lower proportions (Figure 4.30B und Table 4.6). This suggests that the reverse transcriptase used in this study preferentially incorporates C during the RT at the opposite site of m^1A. Besides, the mismatch composition remains unchanged between the Ctl and AD group.

Jump rates of the precuneus provide the same result as misincorporation rates. Again, no significant change is observed between Ctl and AD patients (Figure 4.30C). In summary, the data from the precuneus does not suggest that m^1A^{1374} methylation is elevated in Alzheimer's disease. However, evaluation of the primary visual cortex data yielded a different

[18] https://www.ncbi.nlm.nih.gov/sra

result. Here, m^1A-induced misincorporations are significantly elevated in AD patients in comparison to Ctl (Figure 4.30D). The mean value of Ctl is 1.13%, which rises to 1.55% in the AD group. Again, the individual carrying SNP G13708A showed a substantially lower value and was therefore excluded from the analysis. For the first time, the composition of misincorporated bases seems to be altered between two samples of the same sequencing run because in primary visual cortex samples of Ctl mainly G is found at position 1374, whereas the AD samples present an almost equal proportions of G, T and C in the sequencing reads (Figure 4.30E and Table 4.6).

In addition, jump rates show for the first time a different result that varies from mismatch rates because in the primary visual cortex no significant change between jump rates of AD and Ctl is detected (Figure 4.30F). However, it must be emphasized that the reverse transcriptase used in this study is obviously not prone to jumps in general, because the jump rates of all sample groups are extremely low. On average, they are at 0.02% (Ctl) and 0.03% (AD) in the precuneus and at 0.04% (Ctl) and 0.03% (AD) in the primary visual cortex. These values could also be the result of spontaneous nucleotide skipping events, therefore it can be suggested that m^1A does not evoke jumps during RT with the reverse transcriptase used in this study (SuperScript II). In consequence, misincorporation levels are more informative than jumps and more appropriate to assess of m^1A^{1374} methylation levels of ND5 in this study.

4.4.6 ND5 mRNA and protein levels in AD patients

The hypotheses (i) and (ii) were at least partially confirmed in AD patients. So the next step was to verify hypothesis (iii) and to examine whether ND5 protein expression might be altered in AD patients as it was observed in the HEK293 AD model. For this purpose, ND5 protein levels were investigated in the aforementioned frontal cortex tissue obtained from the NBB, and also mRNA levels were examined in the aforementioned RNA-Seq data sets to gain a comprehensive view of this protein. Unfortunately, Mathys *et al.* did not include mitochondrial encoded genes in their analysis, therefore this data set does not contain results for ND5. Yet the “Aging, Dementia and TBI Study” data set did provide FPKM values for ND5. Therefore ND5 mRNA expression was examined in this bulk RNA-Seq study, as it was done for TRMT10C, SDR5C1 and PRORP in the previous sections.

The “Aging, Dementia and TBI Study” data set yielded interesting results (Figure 4.31). The ND5 mRNA expression was significantly decreased in the hippocampus and the parietal cortex of AD patients. In the white matter of the parietal cortex and the temporal cortex a downward trend was also visible, however, these changes are not significant ($p= 0.13$ in PCx(WM) and $p= 0.29$ in TCx).

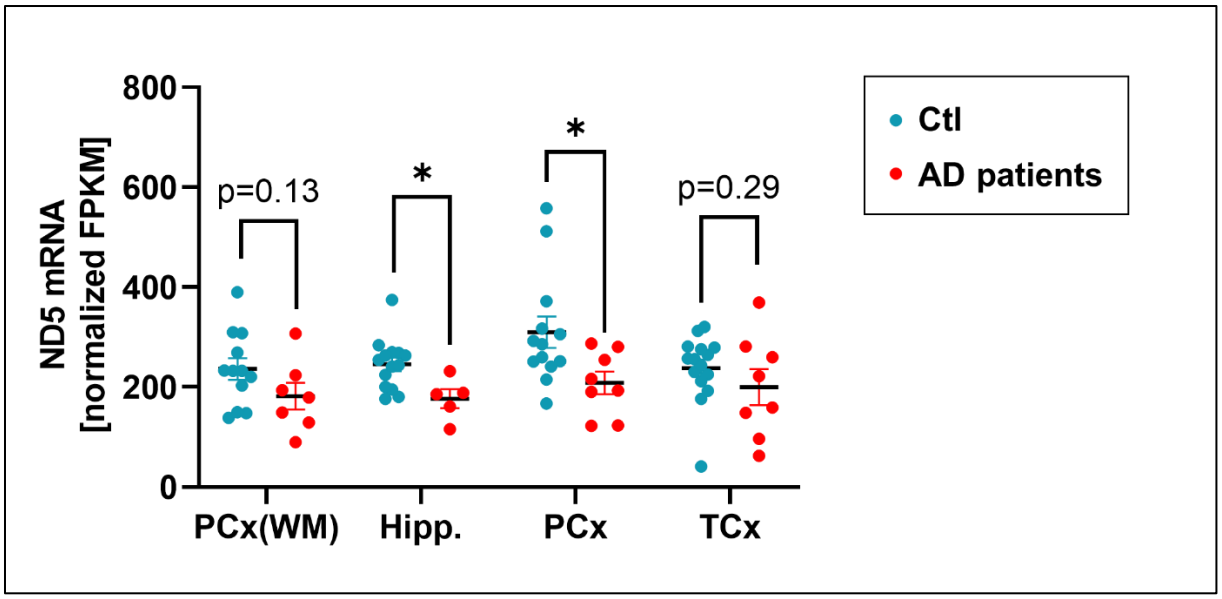

Figure 4.31: ND5 mRNA levels are significantly decreased in the hippocampus and the patietal cortex of AD patients. Normalized FPKM values were extracted from the "Aging, Dementia & TBI Study" data set [425]. AD & Ctl: Male individuals without TBI. Mean ± SEM, n= 13-15 Ctl, n= 5-8 AD, multiple unpaired t-tests, *p<0.05, ns= not significant. PCx(WM)= white matter of the parietal cortex, Hipp.= hippocampus, PCx= parietal cortex, TCx= temporal cortex.

Going one step further, ND5 protein levels should be determined in the frontal cortex tissue obtained from the NBB. Therefore, AD and Ctl samples were subjected to Western blot analysis for ND5. As in the previous blots for TRMT10C, SDR5C1 and PRORP GAPDH was used as reference enzyme.

In the first analysis, the Western blot did not show significant alterations in the ND5 protein expression between AD samples and the Ctl group (Figure 4.32A). Again, the AD patients displayed a relatively broad distribution varying from 18% to 167% in relation to the mean of Ctl. To determine whether this broad distribution might be caused by different disease stages among the AD patients, the data was subdivided according to Braak stages for both AD and Ctl. This division suggests a potential correlation between high Braak stages and lower ND5 protein levels (Figure 4.32B). At least, the mean values of each AD subgroup steadily fall from Braak 4 to 6. A similar pattern is visible in the Ctl group. Here, the mean value decreases from Braak stage 3 to 4, however, is nearly unchanged between Braak stage 1 and 2. This observation leads to the assumption that ND5 protein levels in the frontal cortex may decrease during the course of AD and are specifically reduced in late stages (Braak stages 5+6). To verify this assumption, a statistical unpaired t-test was performed between AD patients at Braak stage 5+6 and Ctl at Braak stage 0+2. Of note, this analysis indicates a tendential reduction (ns, p= 0.09) of the ND5 protein in AD patients at high Braak stages in comparison to Ctl.

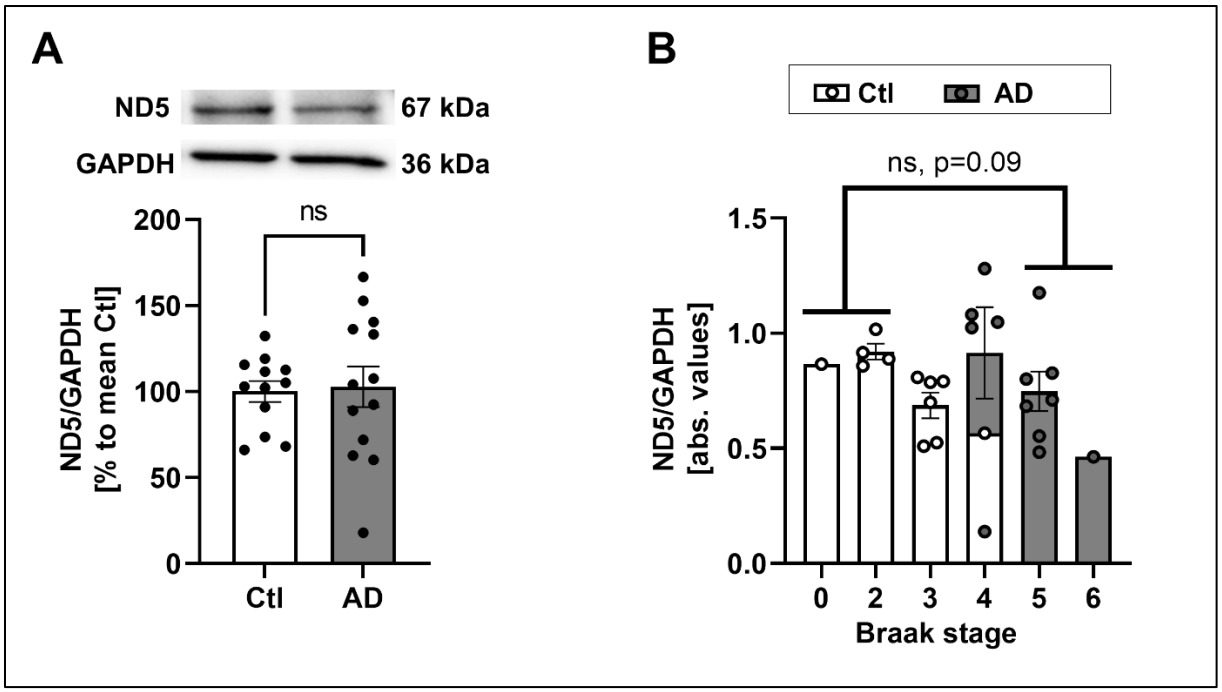

Figure 4.32: Comparing ND5 protein levels of AD patients with those of Ctl in the first analysis, no significant difference is detectable. A) Western blot of NBB frontal cortex samples does not show significant alterations between AD patients and Ctl. A representative membrane is displayed in the upper panel. Mean ± SEM, n= 12 Ctl and n= 13 AD, female and male individuals, unpaired t-tests, ns= not significant. **B)** Data from A) subdivided by Braak stages of both AD patients and Ctl. A tendential, nonsignificant (p= 0.09) decrease can be seen between Braak stage 5+6 (AD) and Braak stage 0+2 (Ctl). Grey-filled points represent values of AD patients, white-filled points represent those of Ctl. Superimposed scatter plot, Mean ± SEM, unpaired t-tests, ns= not significant.

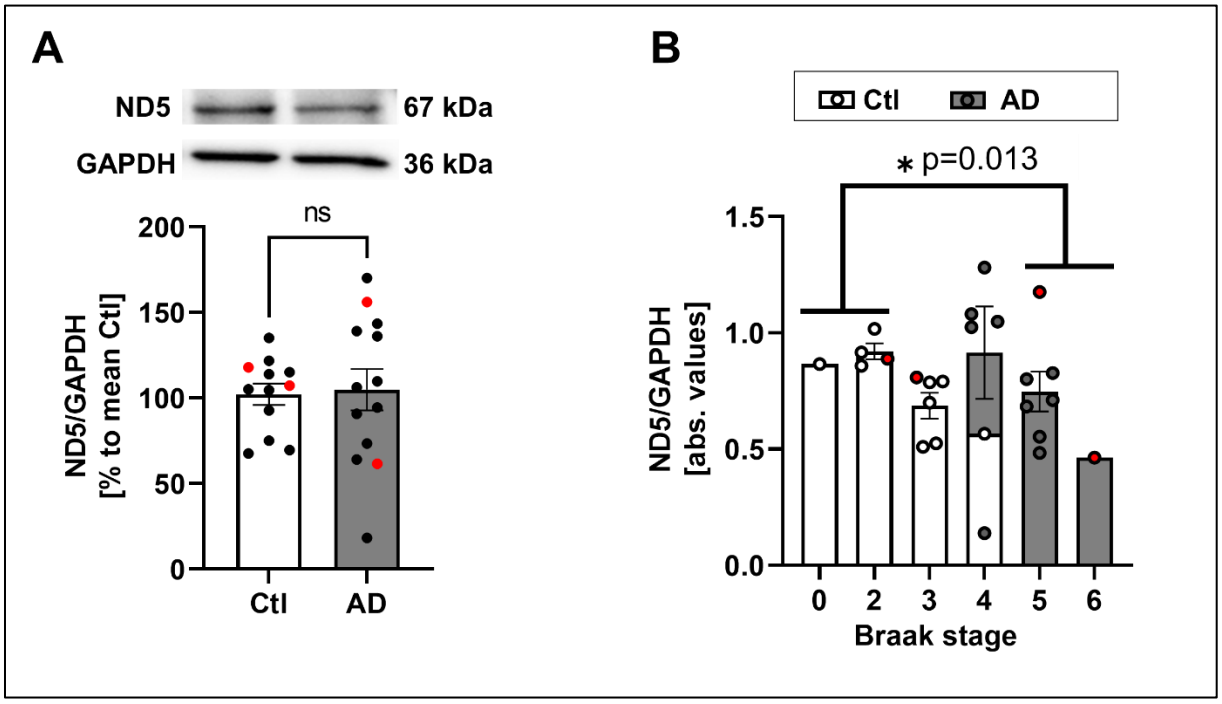

Figure 4.33: Reevaluation of Western blot data from Figure 4.32. After exclusion of G13708A SNP carriers, a significant decrease between AD patients at Braak stage 5+6 and Ctl at Braak stage 0+2 becomes apparent. A) ND5 Western blot does not show a significant alteration when comparing all AD patients versus Ctl. Data points from G13708A SNP carriers were blotted (highlighted in red), but not included in the statistical analysis. Mean ± SEM, n= 12 Ctl and n= 13 AD, female and male

individuals, unpaired t-tests, ns= not significant. **B)** Data from A) subdivided by Braak stages of both AD patients and Ctl. This division illustrates a significant diminution (p= 0.013) of ND5 protein in AD patients at Braak stage 5+6 in comparison to Ctl at Braak stage 0+2. Again, data points from G13708A SNP carriers were blotted (labeled in red), but not included in the statistical analysis. Grey-filled points represent values of AD patients, white-filled points represent those of Ctl. Superimposed scatter plot, Mean ± SEM, unpaired t-test, *p<0.05.

While writing this thesis, further investigations of our group have revealed that four individuals of the NBB cohort carry the G13708A SNP in the mRNA of ND5 two bases upstream of m^1A^{1374} (position 1374 in the mRNA of ND5 equals position 13710 in the mtDNA). As mentioned in section 4.4.5, G13708A SNP carriers presumably do not exhibit m^1A^{1374} methylation, as these individuals display dramatically reduced mismatch rates at position 1374. This interrelationship has already been observed by our group (see Figure 4.30) and Safra *et al.* [312]. In consequence, this mutation apparently prevents or at least impedes methylation of A^{1374} by TRMT10C. Since the aim of this work was to investigate whether m^1A^{1374} is capable of decreasing the synthesis of ND5 (see hypothesis (iii) in section 2), the G13708A SNP carriers are not suited to address this question. Therefore, the respective individuals, two in the Ctl and two in the AD group, were removed from the Western blot analysis. Comparing all AD patients to Ctl, this reevaluation still yields no significant change in the protein content of ND5 (Figure 4.32Figure 4.33A). However, interestingly, the comparison of AD patients at Braak stage 5+6 to Ctl at Braak stage 0+2 now results in a significant diminution (see Figure 4.33B). In other words, the trend observed in the overall evaluation was corroborated by the removal of SNP carriers. With a p-value of 0.013, this difference is now almost highly significant. That means the reevalution provides two pieces of information: First, it indicates that ND5 protein content declines in the late-stage of AD and, second, it suggests that m^1A^{1374} is involved in this reduction, strongly supporting hypothesis (iii). So in summary, it can be assumed by this data and the findings from section 4.2, that the upregulation of TRMT10C in AD leads to decreased ND5 protein levels (at least in Braak stage 5+6) via methylation of m^1A^{1374} in the mRNA of ND5.

5 Discussion

5.1 Enhanced TRMT10C mRNA and protein expression in different AD models and in AD patients

Over the past decade, numerous studies have linked TRMT10C to human diseases [403], [405], [407], [410], [462]. Especially in different types of cancer TRMT10C appears to play an important role. For example, in three subtypes of gynecological cancer a high number of *TRMT10C* mutations was found and increased mRNA expression was detected in comparison to healthy controls [405]. In addition, high TRMT10C mRNA levels correlated with poorer prognosis as measured by the overall survival rate. Besides, it is known that genetic mutations in *TRMT10C* can cause severe mitochondrial diseases. In one study, performed by Metodiev *et al.* [293], two patients harboring TRMT10C missense mutations were characterized. The affected patients displayed at birth hypotonia, feeding difficulties, lactate acidosis and deafness. Besides, the analysis of extracted fibroblasts revealed vastly decreased TRMT10C protein levels in conjunction with multiple respiratory chain deficiencies [293]. In a second study, progressive cognitive, motor impairments and brain atrophy were additionally found in an infant carrying a homozygous variant in *TRMT10C* [402]. In both studies, patients died at few months of age, highlighting the importance of TRMT10C for the human life.

In the context of AD, TRMT10C has not been mentioned until 2020, when Shafik *et al.* reported for the first time decreased protein and mRNA levels in an AD mouse model (5xFAD) [355]. However, only one animal model was investigated and no information about sex and age of these mice was stated. Besides, one recent study published in May 2023 reported elevated TRMT10C mRNA levels in pyramidal neurons of AD patients [463]. However, no further investigations, e.g. measuring the protein content of TRMT10C, have been conducted. Moreover, these results conflict with Shafik *et al.* [355]. Therefore, this work aimed to comprehensively investigate whether the mRNA and protein expression of TRMT10C is altered in relation to AD, according to hypothesis (i).

5.1.1 TRMT10C protein levels are consistently upregulated in AD model cells, mice and human AD cortex tissue

In HEK293 APPwt cells TRMT10C protein levels were dramatically increased in comparison to Ctl. Since these cells only differ in the abundance of APP due to the transfected

APPwt plasmid, the upregulation of TRMT10C must be caused by either increased APP or elevated APP-cleavage products. It was shown, that APPwt cells display 7x higher $A\beta_{1-40}$ levels [179], [216] than Ctl cells. As this and other Aβ peptides are known to exert numerous deleterious effects in cells [199], it is likely that they are directly or indirectly responsible for the the upregulation of TRMT10C. However, it must be considered that APP can be cleaved in multiple ways. Through the non-amyloidogenic pathway APP can be cleaved by the α-secretase resulting in the generation of sAPPα, p3 and CTFα fragments [61]. Through the amyloidogenic pathway which is initiated by the cleavage of β-secretase further APP-derived fragments are produced, namely sAPPβ , CTFβ and Aβ peptides of varying length [61], [464]. Except for $A\beta_{1-40}$, none of these fragments have been quantified in HEK293 APPwt and Ctl cells. However, an ~2.5 fold increased activity of the β-secretase has been measured in APPwt cells compared to Ctl [179]. Therefore, it can be assumed that TRMT10C overexpression is probably mediated by fragments derived from the amyloidogenic pathway, e.g. $A\beta_{1-40}$ or $A\beta_{1-42}$. To conclusively clarify whether these fragments induce the upregulation of TRMT10C an additional experiment is required. Thereby, cells (e.g. HEK293) would need to be treated with soluble or oligomeric Aβ peptides and afterwards TRMT10C levels would need to be checked via Western blot. Indeed, recent unpublished data of our group points to an upregulation of TRMT10C as consequence of treatment with oligomeric $A\beta_{40}$.

HEK293 APPwt cells represent a model for LOAD, thus the above mentioned finding represents a first hint for an elevation of TRMT10C in the context of AD. Likewise in HEK293 APPsw cells, the late-stage LOAD model, TRMT10C protein expression was significantly augmented in comparison to Ctl. As these cells diplay 10x higher $A\beta_{1-40}$ levels than APPwt and even 70x higher levels than Ctl [216], this again suggests that the TRMT10C upregulation is mediated directly or indirectly by Aβ peptides. Of note, TRMT10C levels are not significantly altered between APPwt and APPsw indicating that the expression of TRMT10C might have already reached a maximum in APPwt cells and does not correlate proportionally with the Aβ load.

In 5xFAD mice, TRMT10C protein levels were significantly increased in the hippocampus and the cortex in comparison to Wt mice. These findings are in line with the results obtained in HEK293 AD model cells and strongly support hypothesis (i), which states that TRMT10C levels are altered in AD. Importantly, the expression of TRMT10C was unchanged in the cerebellum which is devoid of amyloid plaques in 5xFAD mice [76]. In contrast, the hippocampus and cortex are strongly affected by amyloid pathology. As these brain regions showed high TRMT10C protein content, this again suggests a link between amyloid load or Aβ-peptides and the upregulation of TRMT10C.

The analysis of human frontal cortex tissue comfirmed the findings obtained in AD model cells and mice. Here, TRMT10C protein expression was also significantly increased in AD patients in comparison to Ctl. This augmentation seems to correlate with the disease progression and is also significant when only high Braak stages (5+6) are compared to healthy controls (Braak stages 0-3). In summary, the TRMT10C protein content was consistenly increased in APPwt and APPsw cells, 5xFAD mice, and in the frontal cortex of AD patients, validating hypothesis (i).

5.1.2 TRMT10C mRNA levels are increased specifically in neurons

While the analysis of proteins is by default performed from bulk preparations, RNAseq allows a comparatively simple cell type-specific analysis. For example, in the scRNA-Seq study from Mathys *et al.* [426] a small piece of tissue was excised from the prefrontal cortex, homogenized using a Wheaton Dounce tissue grinder, and filtered through a cell strainer. After the separation of nuclei by ultracentrifugation and library preparation with unique molecular identifiers (UMIs) to select single cells, the RNA sequencing was conducted. This approach allows the subsequent division of the obtained transcriptomes and their assignment to different cell types based on the expression of specific marker genes. In this way, Mathys *et al.* were able to study the mRNA expression of TRMT10C in six different brain cell types. The comparison of AD patients vs. Ctl in this data set revealed a significant increase solely in neurons and no changes in glia cells. This finding demonstrates that different brain cell types are differently involved in AD. This fact has already been proven by numerous other studies [465]–[467], pointing to the necessity of more cell-type specific investigations in the future.

Why TRMT10C mRNA is specifically raised in excitatory and inhibitory neurons of AD patients remains an open question. A higher Aβ load has not yet been clearly demonstrated in neurons. Quite the contrary, toxic Aβ conformers have been reported in astrocytes and extracellular fractions, which obviously allows Aβ to come into contact with all brain cell types [468]. However, certain cell types seem to be more susceptible to Aβ or other AD-related stressors, as a recent study has shown [469]. A second open question is why TRMT10C mRNA levels are decreased in the late-stage of AD in comparison to early-stage cases. On the one hand, this result is in line with a recent study published in May 2023, which also reported elevated TRMT10C mRNA levels in an early AD stage (Braak stage 0-3, pyramidal neurons) [463]. On the other hand, this result appears to be inconsistent with the findings of elevated TRMT10C protein levels in 5xFAD mice (42-55 weeks old) and AD cortex tissue (Braak stage 5+6) which both represent late stages of AD. One possibility for this contradiction is that mRNA and protein content do not match at this stage. The fact that mRNA and protein levels do not always correlate directly has yet been observed several times in the literature [455]–[457],

which might be caused by different turnovers of mRNA and proteins or by intracellular modulation of the translation process (e.g. via RNA modifications). Lastly, it is unfavorable for the assessment that Mathys *et al.* did not provide results of a direct comparison between late-stage AD and healthy controls.

As the “Aging, Dementia and TBI Study” data set was obtained from bulk tissue preparations the information content of this study is comparatively limited. However, the results revealed that TRMT10C mRNA is also elevated in the parietal cortex, in white matter preparations of the parietal cortex, and a nonsignificant tendency to increased levels was observed in the hippocampus and temporal cortex. All these brain regions are heavily affected from the AD pathology [412], [453]. Importantly, the patients studied had on average a Braak stage of 2.8, which indicates again that TRMT10C mRNA is upregulated rather early in the course of AD.

5.2 Enzymatic partner subunits of TRMT10C are differently affected in AD

As mentioned before, TRMT10C is the catalytical subunit of the mitochondrial methyltransferase that introduces m^1A and m^1G at position 9 of human mitochondrial tRNAs [329]. To exert its function it requires a tetramer of SDR5C1 as a scaffolding protein [329], [360], [470]. Since the chemical structure of adenosine is logically identical in tRNAs and mRNAs, the m^1A sites at position 9 in (mt)tRNA and at position 1374 in the ND5 mRNA only differ by the surrounding base sequence. Therefore, it is likely that SDR5C1 is also necessary for the methylation of m^1A^{1374} in ND5. However, a precise evidence in this case has not yet been provided in the literature. Nevertheless, it was important to investigate whether the expression of SDR5C1 is also altered in the context of AD to gain a comprehensive picture.

Unlike TRMT10C, SDR5C1 has been frequently linked to Alzheimer's disease. SDR5C1 is also known as 17β-hydroxysteroid dehydrogenase type 10 (HSD17B10), endoplasmic reticulum-associated amyloid-binding protein (ERAB) or amyloid binding alcohol dehydrogenase (ABAD). As the last two names illustrate, it was found that Aβ can directly bind to this protein [392], [471]. Furthermore, the toxic effect of Aβ was enhanced by overexpression of SDR5C1 and prevented by blocking SDR5C1 [394], [471]. Therefore, SDR5C1 inhibitors are discussed for the treatment of AD [391], [395], [396].

5.2.1 SDR5C1 is partly upregulated in AD models and human brain tissue

In HEK APPwt cells, SDR5C1 protein levels were significantly increased in comparison to Ctl. In APPsw cells, the augmentation was even more pronounced and the difference of APPsw was highly significant in comparison to both Ctl and APPwt. This clearly demonstrates that SDR5C1 is upregulated as a consequence of APP overexpression and/or elevated Aβ levels. At first glance, the results of SDR5C1 appear to be the same as those of TRMT10C. However, at the second glance, it can be seen that the SDR5C1 expression in APPsw is much stronger than in APPwt, which was not the case for TRMT10C. It seems that TRMT10C already reaches a maximum in the LOAD model APPwt, while SDR5C1 stil increases with the enormously high Aβ load in the late-stage LOAD model APPsw.

In 5xFAD mice, the expression of SDR5C1 was slightly different from that of TRMT10C. Whereas TRMT10C was upregulated in the hippocampus and cortex, SDR5C1 was only significantly elevated in the cortex of 5xFAD mice. However, in the hippocampus an upward trend was observed ($p= 0.31$, $n= 5$), which might become significant with a higher number of n. This is supported with a study performed by He *et al.* [472] in which increased levels of SDR5C1 were found in the hippocampus of 22-month-old 5xFAD mice. In contrast to this, SDR5C1 and TRMT10C were both unchanged in the cerebellum. Since no Aβ load was detected in this brain region of 5xFAD mice [76], these results again indicate that the upregulations in the hippocampus and cortex are likely a result of the Aβ burden in these regions.

In contradiction to this, SDR5C1 protein expression was unchanged in NBB frontal cortex tissue of AD patients in comparison to Ctl. So in this case, the behavior of SDR5C1 was clearly different from that of TRMT10C. Of note, another group found substantially elevated levels of SDR5C1 in the temporal lobe of AD patients as early as 1997 [471]. Especially in the area close to Aβ plaques, the neuronal SDR5C1 expression was increased. This again indicates that the upregulation of SDR5C1 is a cellular response to Aβ, respectively its oligomeric or fibrillar form. Why protein levels were not altered in the NBB frontal cortex tissue used in this thesis remains an open question.

However, the mRNA level of SDR5C1 did show a significant increase in the scRNA-Seq data set from Mathys *et al.* [426]. Here, SDR5C1 displayed exactly the same pattern as TRMT10C. In both cases, the mRNA was elevated in AD patients, but exclusively in excitatory and inhibitory neurons. Besides, the elevation was particularly pronounced in the early stage and disappeared comparing late versus early stage cases. In contrast, no significant change was found in any of the four brain regions studied in the “Aging, Dementia and TBI Study” data set. However, as mentioned earlier, a scRNA-Seq approach is more precise and reliable than a RNA-Seq approach performed with bulk preparations. Especially when regarding the fact

that the cell composition might cange due to atrophy in AD brains [473]. For these reasons, more weight should be given to the scRNA-Seq results.

In summary, the expression of SDR5C1 was partly increased in the AD models and AD patient samples used in this thesis. In those cases where the overexpression was absent (hippocampus of 5xFAD mice and cortex samples of AD patients), a counterexample was given by the literature. Therefore, it can be assumed that TRMT10C and SDR5C1 behave similarly in AD, but not entirely the same, which is probably related to the direct binding of Aβ to SDR5C1 [392], [471]. However, whether SDR5C1 is required for the m^1A^{1374} methylation process cannot be inferred from these experiments. To address this question a different experimental setup with recombinant proteins and a synthetic ND5 oligo would be needed. Besides it is important to mention that even if SDR5C1 protein levels would be unchanged in AD, this does enable to draw conclusion about its involvement in m^1A^{1374} methylation, because this protein could still be present in excess. Following this hypothesis, TRMT10C would serve as the limiting building block of the holoenzyme and the content of this protein would control the methylation level of m^1A^{1374} in the mRNA of ND5.

5.2.2 PRORP expression in largely unchanged in AD

In addition to methylating m^1A in (mt)tRNAs and the (mt)mRNA ND5, TRMT10C serves a third function as a subunit of the mitochondrial RNase P (mtRNase P) complex. Whereas the nuclear and bacterial RNase P are ribozymes, the mtRNase P comprises exclusively three protein subunits: TRMT10C alias MRPP1, SDR5C1 alias MRPP2 and PRORP alias MRPP3 [359], [360]. Since the human mitochondrial transcript contains mRNAs and rRNAs flanked by tRNAs, the mtRNase P is important to excise (mt)tRNAs at their 5'-ends thereby liberating all RNA species. In this case, PRORP is the catalytical subunit, while a subcomplex of TRMT10C and SDR5C1 is supposed to deliver the pre-tRNA substrate and activate PRORP through an induced-fit process [384], [474]. To assess whether the upregulation of TRMT10C might be associated with changes in PRORP expression, this protein was examined in all AD models and samples studied above. So far, in the literature, it has not yet been investigated whether the protein content of PRORP is altered in AD.

In HEK APPwt cells, PRORP protein levels were significantly decreased indicating that in comparison to TRMT10C, this protein displays an opposite behavior. Interestingly, this effect disappeared in APPsw cells, where the expression of PRORP was not significantly changed in comparison to Ctl. This result suggests that PRORP expression is diminished in an intermediate stage of AD (represented by APPwt), but no longer at the very late stage of LOAD (represented by APPsw). In addition, no significant change of PRORP was detected in the hippocampus, cortex and cerebellum of 5xFAD mice. Since these mice were 42-55 weeks old and 5xFAD mice at this age display very high levels of $A\beta_{40}$ and $A\beta_{42}$ [76], they can be

considered to represent a far advanced stage of AD. In this respect, the findings from 5xFAD mice and APPsw cells match very well.

In human tissue, a similar picture emerges. Here, no significant change in the protein level of PRORP was found when comparing AD (Braak stage 4-6) to Ctl. Besides, the expression does not seem to change during the course of the disease, because the mean values at Braak stage 4, 5 and 6 barely change. In this context, it fits very well that the mRNA expression of PRORP is unchanged in the “Aging, Dementia and TBI Study” data set [425] in any of the four investigated brain regions. Likewise, in the scRNA-Seq Study from Mathys *et al*. [426], apparently no significant alteration of PRORP mRNA was detected. The authors state that whenever no significant difference for a gene was found in AD patients, no FC value was listed in the freely accessible data table. This is the case for PRORP, reflecting the fact that no significant alteration was found in any of the six investigated brain cell types.

In summary, PRORP mRNA and protein expression was unchanged in several AD models and human AD patients. Only in HEK APPwt cells, the protein level of PRORP was significantly decreased. This discrepancy is possibily caused by the fact that cells behave differently from a whole organism.

5.2.3 Previously known role of mtRNase P and the m^1A^9 methylation in (mt)tRNAs in Alzheimer’s disease

As mentioned above, TRMT10C, SDR5C1 and PRORP form together the tripartite mtRNase P complex that cleaves (mt)tRNAs at their 5’-ends and a subcomplex of TRMT10C and SDR5C1 is sufficient to methylate (mt)tRNAs at position 9. Data from this thesis and previously published studies suggest that TRMT10C and SDR5C1, but not PRORP, are upregulated in AD models and AD patients (see section 5.1, 5.2.1 and 5.2.2). This raises the question of whether mtRNase P acitivity and the methylation of (mt)tRNAs are consequently altered in AD. Since this question cannot be answered by the experiments performed in this thesis, the literature was consulted. So until today, a systematic study of the involvement of mtRNase P in AD has not been carried out so far, though the direct binding of Aβ to SDR5C1 and the composition of mtRNase P are known for more than 13 years [359], [471]. Previous studies rather focused on other pathways of this multifunctional enzyme and their role in AD [389]. However, Vilardo *et al.* [475] have performed *in vitro* experiments to test the mtRNase P acitivity upon titration of Aβ. Using recombinant enzyme components they discovered that micromolar concentrations of monomeric or oligomerized Aβ inhibit the 5’-end processing of labeled (mt)$tRNA^{His}$ precursors. Besides, they observed that these concentrations prevent the methylation of (mt)$tRNA^{Ile}$ at position 9. It cannot be ruled out that Aβ blocks these two

processes by binding directly to SDR5C1, however, biochemical studies have shown that the Aβ binding to SDR5C1 occurs at nanomolar concentrations that are two orders of magnitude lower than those required to inhibit the processing and methylation activity [392]. Thus, the authors state that the inhibition of both enzyme activities is not mediated by the Aβ-SDR5C1 interaction, but might an unspecific effect. Furthermore, they question whether these micromolar concentrations are reached in mitochondria of AD patients. In conclusion, these *in vitro* experiments give a first hint that (mt)tRNA methylation and the mtRNase P are impaired by Aβ, but their implications for the pathogeneis of AD are questionable. Therefore, further invesigations in AD models and patients are needed.

Of note, two recent studies investigated m^1A^9 methylation levels *in vivo* in the context of AD and obtained opposite findings [355], [476]. Whereas Shafik *et al.* [355] detected significantly decreased m^1A^9 levels in four different (mt)tRNAs in the cortex 5xFAD mice, Silzer *et al.* [476] observed significantly increased m^1A^9 levels in eight (mt)tRNAs in RNA-Seq data obtained from the cerebellum of AD patients. One the one hand, the latter study agrees well with the results obtained in this thesis, as the observed upregulation of TRMT10C and SDR5C1 in AD models and patients potentially results in higher m^1A^9 methylation levels. On the other hand, this study was carried out with cerebellar tissue from AD patients, a region that is not tipically associated with the pathogenesis of AD. Therefore this data is not suitable for estimating the molecular processes that occur in severely affected brain regions, e.g. hippocampus and cortex. Though Shafik *et al.* did examine the cortex of 5xFAD mice, the applicability of these results to humans is also limited, because the human brain is more complex than any other organ relative to that found in lower mammals [477]. In summary, whether m^1A^9 in (mt)tRNA is up- or downregulated in AD remains an open question, but in fact there is evidence that the methylation levels are altered.

5.3 m^1A^{1374} levels are increased in AD model cells and human AD patients

TRMT10C protein levels were consistently upregulated in all AD models and the human tissue investigated in this thesis. As pointed out in hypothesis (ii), a plausible implication would be that m^1A^{1374} methylation in the ND5 mRNA is enhanced in these models and AD patients. To verify this assumption, the custom-designed m^1A^{1374} analysis method was performed with HEK APPwt, APPsw and Ctl cells. Besides, the method was adapted to the species mouse in order to explore the presence of an m^1A site in the murine ND5 mRNA. In a subsequent step, the bioinformatic scripts were applied to RNA-Seq data obtained from human AD patients.

5.3.1 Determining optimal reaction conditions to assess m^1A^{1374} methylation levels in ND5 mRNA

Several studies have previously demonstrated that m^1A-induced misincorporation during the reverse transcription process provides a reliable signal for the indirect determination of m^1A sites [312], [341], [439], [478]. Some of them used a m^1A-binding antibody to pre-enrich modified transcripts. However, further analysis revealed that some of the sites detected in this way were false-positives caused by the limited specificity of these antibodies [313], [314]. Even considering only studies performed without antibody pre-enrichment, the number of m^1A-methylated mRNA sites is highly variable. For instance, Safra *et al.* [312] discovered 14 m^1A sites in mRNA, 5 of which located on mitochondrial mRNAs, whereas Grozhik *et al.* [313] detected appreciable amounts of m^1A only in one mRNA: the mitochondrial ND5 transcript. Since this m^1A site at position 1374 of ND5 has already been confirmed by several independent groups [312], [313], [341], our analysis no longer required the use of a control to exclude false-positives. Instead, this thesis focused on achieving a reliable quantitative measurement of m^1A^{1374} methylation. In the literature, it has often been shown that the m^1A-induced misincorporation is not only suitable for the qualitative but also for the quantitative analysis of m^1A [355], [436]. This assumption is supported by the data obtained in this thesis. Even though the absolute values of misincoporation may vary between different experiments, the samples within the same run show an impressive reproducibility. For example, in Figure 4.11 Ctl samples treated with 1 µg/mL Tetracycline display almost the same misincorporation rates for all four biological replicates. For this reason, the relative abundance of misincorporations within one experiment is well comparable.

During the development of this m^1A^{1374} analysis method, several conditions were tested initially. Knowing that yields of misincorporation and reverse transcription arrest both depend heavily on reaction conditions and the reverse transcriptase, two different enzymes and two different RT buffers were examined. To be precise, the two reverse transcriptases EpiScript and SS-IV were each used once with a commercially available RT buffer containing 5 mM $MgCl_2$, and once with a custom-made RT buffer containing 5 mM $MnCl_2$ instead of $MgCl_2$. This experimental approach revealed that a Mn^{2+}-containing RT buffer significantly increases m^1A-induced mismatch and jump rates in comparison to an Mg^{2+}. This was true for both EpiScript and SS-IV. These findings confirmed for the first time in cellular material what Kristen *et al.* have already shown in *in vitro* experiments [437]. However, the amount of PCR amplicon product dramatically dropped by using Mn^{2+}, which made handling much more difficult when purifying the amplicon band. Besides, less amplicon product leads to lower read counts in the sequencing run, which could also affect the accuracy of the results. Therefore, a buffer containing Mg^{2+} was utilized in the main experiment. Given that only SS-IV showed appreciable

amounts of m^1A-induced jumps, this enzyme and not EpiScript was used as RT in the main experiment. In addition, it was shown by Werner *et al.* [302] and Kristen *et al.* [437] that SS-IV provides lower truncation rates than EpiScript, thus yielding more full-length product suitable for the RT-PCR and the following mismatch rate analysis.

5.3.2 m^1A-induced misincorporation is increased in HEK APPwt cells and the primary visual cortex of AD patients

Applying the optimized reaction conditions described above, the m^1A^{1374} analysis method was performed with total RNA from HEK293 APPwt, APPsw and Ctl cells. The results revealed a highly significant increase in the misincorporation rate of APPwt in comparison to Ctl. For the first time ever, this shows that m^1A^{1374} methylation levels are increased in a LOAD model and it provides the first link between AD and this m^1A site. Importantly, this elevation is also evident in the jump rate of these samples, representing a second independent parameter for m^1A. Furthermore, the augmentation is confirmed in mitochondrial extracts from these HEK cells, which were generated in order to pre-enrich mitochondrial RNAs and then subjected to the m^1A^{1374} analysis. Of note, misincorporation rates from mitochondrial extracts are in general on a higher level that those obtained from total RNA. For instance, total RNA samples of Ctl cells displayed misincorporation rates from 1.2-2.2% whereas the mitochondrial extracts of this cell line showed values of 5.0-6.4%. A similar shift can be observed in mitochondrial etracts of APPwt and APPsw cells. Since all samples were sequenced in the same run and both library preparation and bioinformatics followed the same procedure, these aspects cannot be the source of that difference. One possible explanation could be that the augmentation is not for technical reasons, but that m^1A methylation levels change physiologically when generating the mitochondrial extracts. During the isolation of mitochondria, the cells are stressed by homogenization step and the relatively long processing time. As previously shown by Li *et al.* [341], m^1A^{1374} can dynamically adapt to stressful conditions such as hypoxia and MitoBloCK-6 (a chemical compound that blocks the import of mitochondrial proteins). This dynamic reaction to harmful conditions was shown to appear already after a short time period. For example, after two hours of transcription arrest induced by Actinomycin D [312]. In all of these stress situations, m^1A^{1374} methylation levels of ND5 were increased, which is in line with our findings that stress conditions due to the isolation of mitochondria or Aβ lead to an increase of this methylation.

Interestingly, APPsw cells did not display an elevation of m^1A-induced misincorportions and jumps. Neither total RNA nor mitochondrial extracts showed a significant alteration in comparison to Ctl. In addition, both misincorporation and jump rates were significantly

decreased in comparison to APPwt cells. It is unclear why m^1A^{1374} is elevated in the intermediate LOAD model APPwt, but not in the late-stage LOAD model APPsw. However, one hypothesis is that the enormously high Aβ levels in these cells are sufficient to block the methyltransferase activity of the TRMT10C-SDR5C1 complex. As Vilardo *et al.* [475] demonstrated in 2013, a concentration of 5 µM $Aβ_{42}$ is able to inhibit the methyltransferase activity of a recombinant TRMT10C-SDR5C1 complex at position 9 of the (mt)$tRNA^{Ile}$. Though in this case a mitochondrial tRNA with m^1G at position 9 was investigated, it stands to reason that this also applies to the methylation of m^1A in mitochondrial mRNA. Yet, it is questionable whether this enormously high Aβ concentration is achieved in mitochondria of APPsw. On the one hand, only a concentration of 5 nM was detected when the extracellular concentration of $Aβ_{40}$ was measured for APPsw cells [216]. This is just one thousandth of the inhibitory concentration. On the other hand, it is difficult to assess the intracellular concentration of Aβ and in particular the one in mitochondria. In APPsw cells, this has never been measured and there is no universal formula that describes the ratio of intra- to extracellular or mitochondrial Aβ. However, it is known that Aβ accumulates inside cells and in particular in mitochondria [70], [479]–[481]. The authors of Vilardo *et al.* [475] doubt that the inhibitory concentration of 5 µM is reached *in vivo* in AD patients. However, APPsw cells are an artificial model exhibiting extremely high Aβ loads that might exceed the concentrations in human AD patients (extracellular $Aβ_{40}$ levels of APPsw are 10x higher than those of APPwt and 70x higher than those of Ctl). For this reason, it might still be possible that the inhibitory concentration in mitochondria of APPsw is reached or if not, is at least *in cellulo* sufficient to inhibit the methylation of m^1A^{1374}. A second hypothesis is that m^1A methylation levels are physiologically reduced in APPsw cells. Since the methylgroup can be dynamically installed, it can also be removed by a so far unknown eraser protein. This was also shown by Li *et al*. [341], when m^1A^{1374} methylation of ND5 dramatically dropped in HEK293T cells after 16 hours of serum starvation. Unfortunately, the authors of this publication did not provide an explanation of why m^1A methylation decreases after incubation with serum-free medium or a presumption about the purpose for cells. Likewise, for APPsw the reason for a downregulation of m^1A^{1374} is unclear. One suggestion would be that less m^1A is supposed to increase the synthesis of ND5 and the activity of Cpx I in the late stage of LOAD in order to compensate for the dramatic dysfunction of mitochondria at this stage.

Importantly, the results of the SRA data set [427] showed a similar pattern. In this RNA-Seq study, two brain regions from five AD patients at Braak stage 6 were compared to five age-, gender- and APOE ε4-matched non-demented controls. Here, m^1A-induced misincoporations at position 1374 of ND5 were significantly enhanced in the primary visual cortex of AD patients, but no significant alteration was observed in the second brain region investigated, the precuneus. In the primary visual cortex, the misincorporation rate marginally

increased from on average 1.1% in Ctl to 1.5% in AD patients, however, this difference accounts for +36% and was highly significant. This data shows for the first time that the methylation of m^1A^{1374} in ND5 is upregulated in human AD patients. Besides, this finding is in line with the result obtained in APPwt cells. In contrast, no significant alteration was detected in RNA-Seq data from the precuneus. This could be caused by the fact that in the patients studied the precuneus was moderately affected by disease pathology, whereas the primary visual cortex was mildly affected. In general, pathological changes occur earlier in the precuneus of AD patients than in the primary visual cortex, because this brain region is affected later in the course of the disease. As the authors of this study state, the comparison of these differentially affected brain areas may allow the temporal remodeling of disease progression [427]. This means that molecular signatures found in the primary visual cortex represent a change that occurs early in the destructive “cascade of AD”. This freely chosen term is intended to describe the process that causes neuronal loss in AD and is set in motion by a so far unknown trigger. Accordingly, the moderately affected precuneus represents a later time point in this cascade. This assumption is supported by the fact that Guennewig *et al.* [427] reported broader abnormalities in differential gene expression in the precuneus than in the primary visual cortex. Thus, the molecular mechanisms taking place in these two regions are very different. Accordingly, our results from the SRA data set show that m^1A^{1374} methylation is upregulated primarily early in the cascade and apparently decreases later in the pathological cascade of AD.

Furthermore, the analysis of the SRA data set [427] provided an additional insight into the relatively common G13708A SNP in ND5. The one patient carrying this SNP showed considerably lower misincorporation rates than the other AD patients and non-demented controls. In both the precuneus and the primary visual cortex this patient displayed a value below 0.5%. For comparison, lowest values of Ctl were 0.9% and in AD 1.3%. This indicates that stochiometires of m^1A^{1374} are extremely low in this patient and might even suggests that this adenosine base is not methylated at all. Because, when looking by way of example at the preceding position (C^{1373}), the mismatch rate is also on average 0.5% in AD patients (data not shown). That indicates that low misincorporation rates can also result from spontaneous errors during RT and PCR without any RNA modification in the original transcript. In line with this, Safra *et al.* [312] detected dramatically reduced misincorporation rates at position 1374 of ND5 in human ovary samples from individuals carrying the G13708A SNP in comparison to wild type samples. This SNP is among the defining SNPs of the Eurasian haplogroup J and located two bases upstream of the m^1A^{1374} site (position 1374 in the ND5 sequence equals position 13710 in the whole mtDNA sequence). Hence, the authors of Safra *et al.* [312] propose that the G13708A SNP reduces the ability of ND5 to undergo methylation, possibly because the

writer enzyme can no longer identify its target sequence. Interestingly, the halpogroup J displays an elevated risk of developing AD [482].

Moreover, one technical aspect about the SRA data set [427] should be mentioned. The group that generated this RNA-Seq data from AD patients and healthy controls used the RT SuperScript-II (SS-II) for library preparation (this information was received upon personal request). This enzyme apparently provides a different RT signature when it encounters m^1A in comparison to SS-IV, which was used in our in-house m^1A^{1374} analysis method applied on HEK293 cells. For this reason, the composition of misincorporated bases differs between the SRA data set and the data obtained from HEK293 cells. In the latter, where SS-IV was used, the mismatch at position 1374 consisted mainly of T and G in the sequenced reads. This implies that SS-IV lead to the incorporation of A and C, instead of normally T, at the complementary site of m^1A during the reverse transcription process. In contrast, the mismatch of the SRA data set at position 1374 comprises T, G and C in almost equal proportions indicating that SS-II incorporated A, C and G during the reverse transcription. In addition, mismatch rates are in general higher in the data generated with SS-IV than in the data generated with SS-II. For instance, mismatch rates for APPwt cells in our data set are 4.6-11.7% and AD patients showed mismatch rates of 1.4-1.8% in the SRA data set. Since this effect also occured in Ctl samples, but to a much lower extent, a physiological cause for these altered ranges cannot be ruled out. Besides, only SS-IV allows to assess m^1A methylation levels by the second parameter of jumps. Whereas jump rates generated with SS-IV were in the range of 0.5-6.5%, the data generated with SS-II displayed jump rates by a factor of 100 lower (0.00-0.05%). These values are extremely small and therefore not suitable for the quantitative evaluation of m^1A. To sum it all up, SS-IV provides higher mismatch and jump rates than SS-II and is therefore more appropriate for the quantitative analysis of m^1A. This conclusion is in accordance with Werner *et al.* [302]. In this publication SS-IV also showed the highest misincorporation and jump rates and, importantly, the lowest truncation rates in comparison to several other RTs. A low truncation rate is very important, because reads that are truncated during the RT cannot be amplified in the following PCR and consequently do not show up in the Illumina sequencing reads. On the one hand, this reduces the accuracy of the m^1A analysis method and, on the other hand, this leads to an underestimation of the obtained result. This fact must always be kept in mind when evaluating m^1A-induced misincorporations.

For the sake of completeness, it must be mentioned that m^1A^{1374} methylation levels were not studied in 5xFAD mice in this thesis. Since this modification site has only been reported in human-derived samples (cells and tissue) so far, the presence of an equivalent m^1A site in the species mouse had to be verified beforehand. Strikingly, the alignment of the human and murine ND5 sequence revealed an adenosine base at position 1374 that is in the same

sequence context as the human m^1A^{1374}. This was to be expected because all of the Cpx I core subunits are highly conserved in all organisms. So after adapting the RT and PCR primers to the ND5 sequence of mice, the m^1A^{1374} analysis method was applied to one exemplary mouse hippocampus (Wt, male, age: 27 weeks). This yielded vanishingly low values for the mismatch (0.019%) and jump rate (0.0006%). These values are in the area of spontaneous misincorporations and skipping events in this experiment set up, as demonstrated by evaluating position 1373 and 1375 in the same sequencing raw data. This fact points to the absence or at least a scarcity of m^1A^{1374} methylation in the species mouse. In order to completely reject or proof the presence of m^1A^{1374} in mice, the experiment would have to be repeated with a corresponding negative control (e.g. AlkB treatment or Dimroth rearrangement). Besides, it cannot be said on basis of this data, whether 5xFAD mice would display higher mismatch and jump rates than Wt mice.

Lastly, it should be mentioned that no results for m^1A^{1374} methylation of the NBB frontal cortex tissue are provided in this thesis. However, recent data of our group revealed a significantly elevated m^1A-induced mismatch rate at position 1374 in AD patients at high Braak stages (5+6) in comparison to Ctl. This data is expected to be published shortly in *Nucleic Acid Research* (current status: resubmitted) and is therefore not discussed at this point. Besides, m^1A^{1374} methylation of both the scRNA-Seq data set and the “Aging, Dementia and TBI study” data set is not presented in this thesis, because these two studies did not provide freely accessible sequencing raw data (fastq-files). These files are necessary to evaluate the mismatch rate at position 1374 in the mRNA of ND5. Therefore, unfortunately, neither in the data set of the "Aging, Dementia and TBI Study" nor in the scRNA-Seq from Mathys *et al.* study m^1A could be analyzed.

Nonetheless, the results of this thesis provide, for the first time, a link between the methylation of m^1A^{1374} in the ND5 mRNA and AD. In both the LOAD model APPwt and the primary visual cortex of AD patients increased levels of m^1A^{1374} were detected. These findings in combination with the observed elevation of TRMT10C in AD models and AD patients strongly support hypothesis (ii) and indicate that the upregulation of TRMT10C is accompanied by enhanced methylation of m^1A^{1374}.

5.3.3 Impact of m^1A^{1374} on the mitochondrial translation process

Although the m^1A^{1374} site in ND5 has been consistently reported in the literature [312], [313], [341], the effect of this methylation on the mitochondrial translation process has not been fully elucidated so far. However, there is some evidence that this m^1A-site may have a repressive effect on translation. For example, Safra *et al*. [312] performed polysome

fractionation experiments coupled with the ND5-specific analysis of m^1A-induced mismatch and detected higher misincorporation rates in the free mRNA and monosome fractions than in the light and heavy polysomal fractions. From this, the authors conclude that m^1A-containing mRNAs are inefficiently translated. Of note, they observed an altered behavior of cytosolic m^1A sites, which was also confirmed by Li *et al.* [341]. In the latter publication, ribosome profiling was additionally performed and compared to RNA-Seq data with regard to ND5. This comparison revealed that ribosomes are specifically enriched at the area -5 to -10 bases upstream of m^1A^{1374} indicating that this methylation leads to ribosome stalling.

Looking at the sequence of ND5, m^1A^{1374} is located at the third position of a GC**A** triplet coding for alanine (A458). Including the upstream and downstream codon-triplets the sequence is 5'-CUG GC**A** GCC-3'. Hence, the GUU CN**A** NNC motif, which was frequently found in cytosolic mRNAs prior to m^1A ([312], [341]), is not present in this case. As all of the four GCN triplets would code for alanine, the question about the impact of m^1A^{1374} on the synthesis of ND5 arises. In general, it seems obvious that the Watson-Crick disruptive nature of m^1A prevents the effective translation of modified codons. This assumption can be confidently applied to m^1A sites located in the first two nucleotides of a codon-triplet. At these two positions Watson-Crick base pairing is strictly monitored by the translating ribosomes. However, in the case of m^1A^{1374} the modified base is at the so-called "wobble" position, where nonstandard base-pairings are very common. Though the mitochondrial translation apparatus is considerably different from cytosolic ones, a productive nonstandard base pairing via the Hogsteen edge, remains a possible scenario [483]. In this cases, the triplet would still be decoded as alanine and m^1A would not affect the synthesis of ND5. In contrast, Hoernes *et al*. [338] demonstrated that m^1A at the third position of a codon-triplet indeed inhibits the translation process of the corresponding protein. In this publication, an artificial, modified transcripts coding for GFP was transfected into HEK293T cells. Afterwards the protein expression of GFP was determined by Western blot for cells transfected with mRNA modified at the first, second or third position of a selected AAA triplet. In all three preparations the GFP protein was not detected in the Western blot membrane indicating that m^1A, even at position 3, efficiently blocks the translation process. On the one hand, this finding refers to the cytosolic translation apparatus and is therefore of limited informative value for the mitochondrial translation process. On the other hand, these results suggest that m^1A might block translation not by inhibiting the binding of the complementary tRNA, but by other mechanisms, e.g. ribosomal scanning. As the methylation of m^1A adds a positive charge to the adenosine base, this positive charge might disturb the attachment of the intricate ribosome complex [484], [485]. However, the direct experimental proof of this hypothesis is very challenging, because mitoribosome preparations which would be needed for *in vitro* translation assays are very hard to access. Taken together, it is unlikely that the exact mechanism of m^1A on the mitochondrial

translation process will be revealed in the near future, but in general there is considerable evidence for a translation repression of the corresponding protein.

5.4 ND5 protein and mRNA levels are decreased in AD models and human AD patients

In light of the above findings, the question arose whether the elevation of TRMT10C and m^1A^{1374} methylation in AD models and patients is accompanied by a decreased expression of ND5. According to hypothesis (iii) and the results discussed in section 5.3.3, higher modification levels would impede the mitochondrial translation process, resulting in a lower ND5 protein content. To verify this, the ND5 protein expression was examined in all AD models mentioned so far. Besides, ND5 mRNA levels were studied in APPwt and APPsw cells, and in the "Aging, Dementia and TBI Study" data set to obtain a comprehensive picture.

5.4.1 ND5 protein levels are reduced in AD model cells, 5xFAD mice and human cortex tissue of patients at Braak stage 5+6

Strikingly, ND5 protein levels were significantly decreased in HEK293 APPwt and APPsw cells in comparison to Ctl. In case of APPwt, the decline was even highly significant. So in this LOAD model a decreased expression of ND5 coincides with elevated TRMT10C protein and m^1A^{1374} methylation levels. While this is no proof, it strongly suggests a causative relationship between the methylation of ND5 mRNA and reduced ND5 protein content, strongly supporting hypothesis (iii). In APPsw cells, the late-stage LOAD model, m^1A^{1374} levels were unchanged in comparison to Ctl. Therefore, the modification cannot be the cause for the reduction of ND5 in this cell line. Why the protein level has nevertheless fallen in APPsw cannot be said on basis of the data obtained in this thesis.

Significantly reduced ND5 protein levels were found in the hippocampus of 5xFAD mice. In the cortex, a marked reduction was also observed, but the difference was just not significant ($p=0.06$). Perhaps this would change with a higher number of n ($n > 5$). As shown in Oakley *et al.* [76], both brain regions are severely affected in this AD mouse model. Already at an age of 2 months, amyloid deposits are found in the cortex and subiculum, a connecting structure between the parahippocampal gyrus and the hippocampus. Especially the $A\beta_{42}$, but also the $A\beta_{40}$ load steadily increase with age and from 6 months on the hippocampus is also strongly affected. Regarding the experiment performed in this thesis, mice were dissected at an age of 42-55 weeks, which is equivalent to 10-12 months. At this age the presence of amyloid

depositis in the hippompus and cortex can be expected. This suggests that the reduction of ND5 likely results from the elevated Aβ burden or indirectly from Aβ-induced mechanisms. This assumption is supported by the finding of unaltered ND5 protein in the cerebellum. As stated by Oakley *et al.*, no amyloid deposits can be found in this brain region in 5xFAD mice [76]. It is reasonable to assume that the Aβ-induced decrease of ND5 protein is independent of m^1A^{1374} methylation, because mice eventually do not harbor an m^1A site in the mRNA of ND5. At least, this is suggested by the evaluation of one exemplary mouse hippocampus sample. Yet, further investigation of the m^1A modification landscape in the species mouse is needed.

At the first glance, the comparison of NBB frontal cortex samples from AD patients and healthy controls showed no significant alteration in the protein expression of ND5. But intriguingly, after all individuals were subdivided by their Braak stage, a possible correlation between high Braak stages and low ND5 protein levels became apparent. However, the comparison between AD at Braak stage 5+6 and Ctl at Braak stage 0+2 was initially not significant ($p=0.09$). As already mentioned in the section 4.4.6, further data of our group revealed that 4 out of 25 individuals of the NBB tissue donors carried the G13708A SNP in the mRNA of ND5. As it is known that G13708A SNP carriers contain no or scarce m^1A^{1374} modification, these individuals (2 in AD group, 2 in Ctl group) were removed from the analysis, because in this thesis, the effect of m^1A methylation on the ND5 protein levels was to be investigated. Strikingly, the reevalution revealed a significant decrease of ND5 between AD (Braak stage 5+6) and Ctl (Braak stage 0+2), confirming the trend observed in the first analysis. Of note, the fact that the ND5 diminution became significant only after removal of the SNP carriers confirms the involvement of m^1A^{1374}, according to hypothesis (iii). Only at Braak stage 5+6 neurofibrillary tangles are found throughout the entire cortex, whereas Braak stage 4 signifies that neurofibrillary tangles are observed exclusively in the transentorhinal and entorhinal cortex. That implies that the tau pathology has not yet reached the frontal cortex of patients at Braak stage 4. As NBB samples were prepared from the frontal cortex, it indeed makes sense to exclude patients with Braak stage 4. Interestingly, the cognitive decline of AD patients typically just starts at Braak stage 5 [454]. Nevertheless, it is important to stress that the common Braak classification (stages 1-4) relies on the distrubtion of neurofibrillary tangles and does not give any information about the amyloid burden. In fact, Braak *et al.* did also establish a classification based on Amyloid plaques (ABC staging [38]), but unfortunately no information about the ABC stage was given by the NBB. Another classification based on Aβ (e.g. Thal phases [486]) was also not consistently reported for all NBB samples. Therefore, the assessment of the AD stage in the NBB samples remained only possible on basis of the Braak stage classification (stage 1-6). Yet it is reasonable to assume that a greater burden of neurofibrillary tangles is paralleled by greater Aβ load because both increase during the course

of the disease. However, it must be noted that Aβ and tau do not spread in the same spatial and temporal manner throughout the brain [487]–[489]. That means, in this case it is not possible to say whether the decrease of ND5 directly correlates with increasing Aβ load in NBB samples. However, a link between elevated Aβ levels and the reduction of the ND5 protein has already been proven by the ND5 Western blots of APPwt cells and 5xFAD mice. For this reason, it is likely that the decrease of ND5 in the NBB AD patients is caused by Aβ and not by an alternative player (e.g. tau). In summary, the results of this thesis indicate that ND5 levels in the cortex of AD patients are reduced in the late stage of AD (Braak stages 5+6). This finding is in line, with the elevation of TRMT10C in AD patients at Braak stages 5+6. Additionally, recent data of our group showed m^1A^{1374} methylation is also increased in these AD subgroup (unpublished data), strongly supporting hypothesis (iii). About other brain regions, e.g. the hippocampus, no conclusion can be drawn based on this experiment, because different brain regions are affected differently during the course of AD [486].

Concerning the findings of ND5 in the frontal cortex tissue of AD patients, one more thing must be mentioned: Even the age-matched control partly displays advanced Braak stages. More precisely, all Ctl samples showed Braak stages in the range of 0 up to 4. This is due to the fact that neurofibrillary tangles, like amyloid plaques, can also be found in cognitively normal individuals [490]. For example, one study observed the presence of neurofibrillary tangles in brains of almost all individuals older than 70 years [491]. Why these aggregates lead or contribute to the development of AD in some individuals, while others remain cognitively normal is unclear. To ensure that the severe tau pathology in Ctl samples does not affect our evaluation, all Ctl subjects at Braak 4 were excluded in the final analysis when AD patients at Braak stages 5+6 were compared to Ctl.

5.4.2 Diminished expression of ND5 mRNA was detected in AD model cells and the human “Aging, Dementia and TBI Study” data set

To obtain a complete picture of ND5, the mRNA expression of this protein was also examined in the aforementioned AD models and in human data sets. Interestingly, in APPwt cells significantly decreased ND5 mRNA levels in comparison to Ctl were detected in qPCR measurements. In contrast, APPsw cells did not show a significant alteration compared to Ctl. However, a downward trend was apparent ($p=0.10$). Of note, protein levels of ND5 were significantly decreased in both of these cell lines. As ribosomes require mRNA for proteinbiosynthesis, lower mRNA expression is generally assumed to cause lower levels of the corresponding protein. So in the case of APPwt, this correlation seems to hold true and the lower protein content is most likely caused by the decreased mRNA level. Since elevated

m^1A^{1374} methylation was observed in this cell line, one can assume that this modification synergistically reduces protein levels of ND5. In the case of APPsw, the explanation for the reduction of ND5 protein is not that simple. As this cell line did not show higher m^1A^{1374} methylation than Ctl, the modification can not be responsible for the reduced protein content. Likewise, ND5 mRNA expression was only by trend (ns, p= 0.10) decreased in comparison to Ctl. However, as one mRNA molecule is transcribed simultaneously by several ribosomes (so-called polysome), this tendency of lower mRNA levels might already have a great impact on the corresponding protein expression. Besides, an accelerated degradation of mitochondrial proteins due to the enormous Aβ load in APPsw cells and the ensuing deleterious effects is conceivable. Nevertheless, these two aspects are only conjectures, an exact reason for the diminution of ND5 in APPsw cells cannot be given on basis of this data.

It is important to note that ND5 mRNA could not be examined in 5xFAD mice, because the qPCR TaqMan™ assay was not compatible with the mouse species. Besides, the scRNA-Seq data set from Mathys *et al.* [426] did not provide results for ND5, as mitochondrial genes were generally not considered. In addition, the ND5 mRNA expression was not investigated in the frontal cortex tissue from AD patients and age-matched Ctl, because the NBB samples have been stored for a very long time (up to 12 years). As mentioned previously, tissue freezing is known to compromise RNA integrity [282] and therefore no reliable mRNA quantification could have been performed with these samples. Lastly, the SRA data set from Guennewig *et al.* [427] was not suitable for the analysis of ND5 mRNA, because only 5 patients were studied, including one carrying the SNP G13708A. This number of n is likely too small to detect differences in human samples, especially because the one individual with the SNP G13708A might bias the result.

The only database that allowed a reliable evaluation of ND5 mRNA expression in human patients was the “Aging, Dementia and TBI Study” data set. Here, a significant diminution of this mRNA was detected in the hippocampus and parietal cortex of AD patients in comparison to Ctl. In the temporal cortex and white matter a tendency towards decreased levels was observed, however, this was not significant (p=013 PCx(WM), p=0.29 TCx). When regarding these results it must be kept in mind that if higher m^1A^{1374} levels would be present in the ND5 mRNA of AD patients, this would partly block the reverse transcription and would falsely suggest decreased mRNA levels, because trunced cDNA strands cannot be recorded in this experiment set up. This raises the question of whether the lowered mRNA levels of ND5 were actually existent in the sample or caused by enhanced methylation of m^1A^{1374}. This assumption could only be verified by analyzing the raw data of this data set and evaluating the mismatch rate at position 1374. But unfortunately, this data is not publicly available.

In summary, the data of this thesis shows that the protein expression of ND5 is consistently reduced in AD model cells, 5xFAD mice and frontal cortex tissue of AD patients at Braak stage 5+6. These findings strongly support hypothesis (iii), which states that elevated m^1A^{1374} modification, installed by TRMT10C, impedes the mitochondrial translation process and results in lower ND5 protein levels. Furthermore, ND5 mRNA was partly decreased in AD model cells and human patients. Whether the lower expression of ND5 mRNA is entirely or partly caused by increased m^1A^{1374} methylation cannot be said from these data. In general, a down regulation of Cpx I subunits has been reported several times in the literature [205], [206], among others in a recent meta-analysis where protein and mRNA levels were analyzed together [183].

5.5 Selective overexpression of TRMT10C enhances methylation of m^1A^{1374}, lowers ND5 protein levels and induces severe mitochondrial deficits

Although an elevation of TRMT10C and m^1A^{1374}, and a decrease in ND5 were detected in different AD models and patients, these results did not prove a causative relationship between these three findings. Therefore, it was crucial to investigate the downstream effects of TRMT10C overexpression to establish the link between the hypotheses (i)-(iv). For this purpose, a double-transfected HEK293-based cell system was chosen, which allows the selective overexpression of TRMT10C via incubation with the inducer Tetracycline. This customized cell line was designated as pTRMT10C cells. In parallel, once-transfected control cells (without the Tetracycline-inducible plasmid coding for TRMT10C) were studied to evaluate the effect of Tetracycline per se.

5.5.1 TRMT10C overexpression leads to elevated m^1A^{1374} methylation and decreased ND5 protein levels

In an inital experiment the optimal conditions for the Tetracycline-inducible pTRMT10C cell system were determined. Here, incubation with 0.1 µg/mL Tetracycline already evoked markedly increased TRMT10C protein levels, which were further enhanced in pTRMT10C cells after incubation with 1 µg/mL Tetracycline. Both concentrations were incubated for 24 h because this time was specified by the manufacturer. In Ctl cells, TRMT10C protein levels were relatively low and approximately equal to those in pTRMT10C cells without Tetracycline

addition. Furthermore, it was shown in this initial experiment that the pTRMT10C cell system functions efficiently, independent of the time between seeding and Tetracycline addition.

In the next step, m^1A-induced misincorporations and jumps at position 1374 of ND5 were analyzed in these two cell lines. Both parameters were significantly higher in pTRMT10C cells after incubation with 0.1 µg/mL and 1 µg/mL Tetracycline in comparison to untreated pTRMT10C cells. In contrast, both mismatch and jump rates remained unchanged in Ctl cells upon treatment with Tetracycline. These findings strongly confirm what has been proposed already in 2017: TRMT10C is the writer enzyme of m^1A^{1374} in ND5 [312]. In addition, the data suggests a correlation between these two factors, i.e. the higher the TRMT10C protein concentration the higher the m^1A^{1374} modification stoichiometry. However, this can only be estimated and is not supported by a statistical evaluation (Figure 4.11). Of note, the increased m^1A methylation could still be caused by an indirect effect of TRMT10C overexpression as a physiological response. Yet this can be ruled out with a high degree of probability, because Safra *et al.* [312] performed a control experiment with siRNA in HEK293T cells and found that misincorporation levels dramatically dropped. Thus, it can be assumed that TRMT10C is indeed the writer enzyme for this position and methylates m^1A^{1374} in the ND5 mRNA.

Furthermore, it is noticeable that the mismatch rates without Tetracycline are higher in pTRMT10C cells than in Ctl cells. This fact might suggest that the pTRMT10C cell system yet shows a low expression of TRMT10C in absence of the inducer and hence might be leaky. To test this assumption more closely, an additionally statistical test was performed between these two sample groups. The significant difference found in both misincorporation and jump rate suggests that this is not a coincidence. On the one hand, methylation level could just naturally differ between the two cell lines. On the other hand, the manufacturer stated that this Tetracycline-inducible system is not 100% leakproof in absence of the inducer. This obviously is the case for pTRMT10C cells and this fact should always be kept in mind when assessing the effects of TRMT10C overexpression in this cell system. In addition to the evaluation of effects derived from Tetracycline per se, this is one reason, why the results of pTRMT10C with Tetracycline always need to be compared to both pTRMT10C without Tetracycline and Ctl.

Concerning the analysis of m^1A-induced mismatch and jumps in pTRMT10C and Ctl cells it should further be mentioned that misincorporation rates are generally on a relatively low level. For example, the value for pTRMT10C cells untreated is 1.28% and rises to 2.85% upon Tetracycline treatment. Presuming that 2.85% of the mitochondrial ND5 mRNA is methylated instead of 1.28%, and conversely, 97.15% of these mRNAs instead of 98.72%, are present demethylated, this does not seem to have a major impact. However, it is important to note that a large number of ribosomes can bind to one individual mRNA strand to form multiple copies of a polypeptide simultaneously [492], [493]. This suggests that the effect of a single mRNA

strand being methylated is potentiated. Besides, the percentage of sequenced cDNAs showing misincorporation cannot be transferred to methylated mRNAs in a 1:1 ratio. The transferability of percent values is limited because on the one hand, the unique molecular identifiers (UMIs) in the RT primer sequence were not evaluated and, on the other hand, because m^1A-methylated strands that evoke a truncation of the newly synthesized cDNA strand cannot be amplified in the subsequent PCR and hence do not show up in the sequenced reads. Likewise, m^1A-methylated strands that result in the incorporation of the correct complementary base (Thymidine) during RT do not raise the mismatch rate. Importantly, both of these facts lead to an underestimation of the m^1A methylation level in the final analysis compared to the original sample.

The question of whether enhanced m^1A^{1374} methylation in pTRMT10C cells after Tetracycline-induced overexpression of TRMT10C is sufficient to alter protein levels of the corresponding protein was answered by means of Western blots. This method revealed significantly lower ND5 protein levels in pTRMT10C cells, when TRMT10C was overexpressed. When the effect of Tetracycline was subtracted, the difference became nearly highly significant ($p=0.014$). This finding is tremendously important, because it proves for the first time in the literature the repressive effect of the m^1A^{1374} methylation on the protein synthesis of ND5. As described in section 5.3.3, a repressive effect of this m^1A-site on translation has already been suggested by two different groups [312], [341]. However, in these publications, polysome fractionation experiments and Ribo-Seq were performed and possible alterations on protein level were not investigated. Only Hoernes *et al.* [338] found lower protein levels as a result of m^1A at position 3 of a codon triplet, but here a cytosolic, artificially modified transcript was used. Since differential effects for cytosolic and mitochondrial m^1A-sites have been posulated and mitoribosomes bight behave different from cytosolic ribosomes [312], [341], it is essential to assess each m^1A-site specifically. As already discussed in section 5.3.3, it is unlikely that the repressive effect of m^1A^{1374} on the mitochondrial translation is due to blockage of tRNA binding. Indeed, m^1A blocks the Watson-Crick base pairing, but at position 3 of a codon triplet (here: GC**A**) this is not necessarily required and all GCN triplets are coding for the same amino acid (alanine). Taken together, these findings indicate that m^1A^{1374} does inhibit the mitochondrial protein biosynthesis, but probably by disturbing the mitoribosome rather than by impeding tRNA binding. In any case, hypothesis (iii) was strongly supported by this experiment.

5.5.2 TRMT10C overexpression does not affect protein levels of SDR5C1 and PRORP

For methylation of mitochondrial tRNAs at position 9, TRMT10C requires an additional protein subunit, SDR5C1 [329]. Since (mt)tRNAs and (mt)mRNAs are nearly identical in their chemical structure, it stands to reason that SDR5C1 is also needed for methylation of m^1A^{1374} in the ND5 mRNA, even though the sequence around m^1A differs and the RNA secondary structure might play an additional role. As these two proteins work closely together and both TRMT10C and SDR5C1 were found to be upregulated in AD models and patients, a possible connection was investigated. More precisely, it was examined in the pTRMT10C cell system whether the selective overexpression of TRMT10C leads to an upregulation of SDR5C1. This assumption could not be confirmed, because pTRMT10C cells did not display significant changes in SDR5C1 protein after treatment with Tetracycline. Even when the result was offset against Ctl cells, no significant difference was observed. This indicates that the overexpression of TRMT10C alone does not lead to an increase of SDR5C1 protein and is in line with Metodiev *et al.* [293]. In this publication fibroblast cell lines derived from individuals harboring *TRMT10C* missense variants were investigated via Western blot. These fibroblasts showed markedly reduced protein levels of TRMT10C, whereas the protein expression of SDR5C1 was unchanged in comparison to control subjects. This result also suggests that the protein level of SDR5C1 is not affected by those of TRMT10C. Interestingly, a reverse effect has already been found in the literature [398]. In this publication, SDR5C1 protein levels were found to be reduced in fibroblast carrying the HSD17B10 mutation p.R130C, which was accompanied by a reduction in TRMT10C protein. In addition, in SDR5C1 knock-down cells TRMT10C protein content was diminished and the ectopic expression of SDR5C1 partly restored this defecit. These results strongly suggest that the protein level of SDR5C1 impacts the protein expression of TRMT10C. Therefore, it is more reasonable that the upregulation of TRMT10C in AD models and patients is caused by the elevation of SDR5C1 and not the other way around. In particular, since the neurotoxic Aβ protein is known to bind to SDR5C1 [392], it can be speculated that this may trigger a mechanism leading to the upregulation of TRMT10C in AD.

In conjunction with PRORP, TRMT10C and SDR5C1 form the tripartite mtRNase P complex that is responsible for the endonucleolytic release of tRNA 5'-ends from mitochondrial primary transcripts, a vital step in mitochondrial RNA maturation [187]. For this reason, it was aimed to investigate whether TRMT10C overexpression has an impact on PRORP protein content. Yet, this was not the case because PRORP expression in pTRMT10C cells remained unchanged after incubation with Tetracycline. There was also no significant difference when compared to the control cell line. Thus, it can be concluded that TRMT10C protein levels do not alter the protein expression of PRORP. This matches well with the findings obtained in

HEK293 APPsw cells, 5xFAD mice and AD patients, in which PRORP protein levels were unchanged despite of the upregulation of TRMT10C. Although a significant downregulation of PRORP was detected in APPwt cells, it is unlikely that this is a regulatory consequence of TRMT10C. Also, in the literature, only a reverse effect has been observed, viz. that decreased PRORP alters TRMT10C protein levels [386]. According to the author of this recent study, fibroblasts from patients with bi-allelic variants in *PRORP* exhibited lower PRORP and TRMT10C protein levels than control subjects indicating a regulatory effect of PRORP on TRMT10C. However, it must be mentioned that the depicted Western blot membrane in this publication does no clearly prove this assertion and no statistical test was performed to verify this claim. So in summary, there is no firm evidence that the regulation of PRORP and TRMT10C are related.

Although in the pTRMT10C model system overexpression of TRMT10C did not affect protein levels of SDR5C1 and PRORP, the question of whether the sole elevation of TRMT10C leads to an alteration of the mtRNase P activity remained open. For this reason, the amount of (mt)tRNAs was determined in pTRMT10C cells after addition of Tetracycline. Here, (mt)tRNAs were hybridized with specific, fluorescently-labeled oligos and related to cytosolic tRNAs (also detected by fluorescently-labeled oligos). This ratio was not significantly altered in both pTRMT10C and Ctl cells after Tetracycline-treatment. Assuming that an altered cleavage acitivity of mtRNase P would directly affect the total amount of (mt)tRNAs, the overexpression of TRMT10C does not seem to have any impact on the mtRNase P. However, this conclusion must be taken with a grain of salt. Because in the case at hand, the upregulation of TRMT10C would be expected to increase the mtRNase P activity. This enhanced activity may not be reflected in (mt)tRNA levels, if all of the pre-tRNAs have already been entirely excised from the precursor transcript. This means that, conversely, only a reduced acitivity of mtRNase P can be detected with this experimental setup. And hence, only a decreased, but not an increased activity of mtRNase P can be excluded in pTRMT10C cells. This is particularly important because Holzmann *et al.* [359] detected an elevated mtRNase P cleavage activity in HEK cells overexpressing TRMT10C. Here, the specific effect on (mt)pre-tRNA^{Tyr} was investigated using mitochondrial extracts, SDS-PAGE and silver staining. So in summary, it is unclear whether the upregulation of TRMT10C alone *in vivo* leads to an enhanced mtRNase P acitivity or not, and a more suitable experiment setup is needed. Also, with respect to our findings in AD models and patients, it is not possible to say whether the activity of mtRNase P is altered or not.

5.5.3 TRMT10C overexpression results in an impairment of the mitochondrial respiration and a decrease of the MMP

ND5 is one of the 14 core subunits of Cpx I, which are considered essential for the catalysis of electron transfer from NADH to Ubiquinone and for generation of the proton-motive force [494]. Among these core subunits, which are all conserved from bacteria to humans, ND5 plays a special role. It is located at the most distal end of the membrane-embedded arm of Cpx I that translocates protons from the matrix into the intermembrane space [144], [154]. The energy for this process is provided by the redox reaction of Ubiquinone to Ubiquinol, which occurs at the interface between the membrane and the peripheral arm of Cpx I. Importantly, ND5 contains a long amphiphatic α-helix spanning from the most distal part of the membrane-arm to the junction with the peripheral arm. It is assumed that the conformational changes at this junction drive the long amphiphatic α-helix of ND5 in a piston-like motion, thereby moving the antiporter-like subunits ND4, ND2 and ND4L in the membrane-arm, which results in the translocation of protons [155]. Using site-directed mutagenesis in *E.coli,* it was shown that mutations in NuoL (homolog of ND5 in bacteria) lead to a substantial loss of the proton pumping efficiency of Cpx I [156]. In addition, mutations in ND5 are known to cause severe mitochondriopathies, such as Leber's hereditary optic neuropathy (LHON), Leigh syndrome (LS) and a syndrome consisting of mitochondrial encephalomyopathy, lactic acidosis, and strokelike episodes (MELAS) [159], [162], [163], [170]. These findings highlight the importance of ND5 and suggest that the disruption of ND5 protein biosynthesis by m^1A^{1374} may have detrimental effects on Cpx I activity and the overall mitochondrial respiration.

For this reason, it was investigated whether increased m^1A^{1374} methylation may lead to a decreased Cpx I activity by lowering the ND5 protein content, as postulated in hypothesis (iv). Since Cpx I is the first enzyme and rate-limiting step of the ETC, this decrease would be reflected in an overall decline of the mitochondrial respiration. Therefore, the oxygen consumption of pTRMT10C and Ctl cells, both treated with 1 µg/mL Tetracycline, was measured in both a Seahorse XFe 96 analyzer and the OROBOROS oxygraph-2k in order to verify hypothesis (iv). Strikingly, the results of the Seahorse XFe 96 analyzer revealed a significant reduction of the Basal respiration in pTRMT10C cells, which was almost highly significant ($p=0.019$, nested analysis). This indicates that overexpression of TRMT10C and the concomitant increase of m^1A^{1374} methylation, indeed results in an impairment of the respiratory chain. Regarding the ATP-linked turnover a similar picture emerges, as the oxygen consumption after Oligomycin addition was on average lower in pTRMT10C cells than in Ctl. This reduction was just not significant ($p=0.057$, nested analysis, $n=3$), but might have reached significance with a higher n-number. Interestingly, the ETS capacity was not significantly altered between pTRMT10C and Ctl. However, the values of this parameter varied widely

between Day 1, 2 and 3. Therefore, it might be that the ETS capacity values were affected by technical issues. This presumption is very likely because the second measurement in the OROBOROS oxygraph-2k showed a clear reduction of the ETS Capacity in pTRMT10C cells ($p=0.011$, $n=8$). Of note, the non-mitochondrial respiration was not altered between pTRMT10C and Ctl cells. This parameter reflects the amount of O_2 that is consumed by cells apart from the respiratory chain, e.g. in enzymatic reactions that use oxygen as a reactant. The fact that the non-mitochondrial respiration is unchanged in pTRMT10C cells proves that the observed effect in the Basal respiration and ETS capacity is indeed attributable to the respiratory chain and not to other cellular changes.

The measurement in the OROBOROS oxygraph-2k provided slightly different results. Here, the Basal respiration and ATP-linked turnover was not significantly altered between pTRMT10C and Ctl cells, but the ETS capacity displayed significantly lower values in pTRMT10C cells. Yet, the non-mitochondrial respiration was unchanged between pTRMT10C and Ctl, exactly as it was observed in the Seahorse XFe 96 analyzer. So in summary, neither method seems to be entirely accurate and in addition, the results of an oxygen-consumption measurement in cells might change due to environmental conditions, e.g. cell growth status or daily temperature fluctuations. Nevertheless, a significant decrease was found in pTRMT10C cells in both Basal respiration and ETS capacity, strongly suggesting that TRMT10C overexpression leads to a severe impairment of the respiratory chain via methylation of m^1A^{1374} and the reduction of ND5. Thus, in the pTRMT10C cell model, a causal chain could be demonstrated that is initiated by the upregulation of TRMT10C and ends in the decline of the mitochondrial respiration, ultimately linking hypotheses (i)-(iv). Hypothesis (iv), which states that an impairment of ND5 causes dysfunction of Cpx I, is also supported by external studies. For example, Zhang *et al.* [163] and Singh *et al.* [175] showed that mutations in ND5 lead to a reduction of Cpx I activity. Apparently, not only the activity of this complex but also the sheer amount of ND5 protein and the enzyme complex is diminished as a consequence of this mutation [163].

The findings obtained with the oxygen electrode measurements are in line with former studies of our group investigating the mitochondrial respiration in HEK293 APPwt and APPsw cells. As mentioned earlier, these two cell lines exhibited significantly elevated TRMT10C protein levels and were found to display various mitochondrial deficiencies, among others a reduced respiratory control ratio and decreased ATP levels [179], [210], [441]. In this respect, it can be assumed that, at least in the LOAD model APPwt, the upregulation of TRMT10C causes or enhances mitochondrial dysfuction via m^1A^{1374} methylation and the ensuing reduction of ND5. Of course, it should be noted that the neurotoxic Aβ peptide, which is abundantly produced in these cells, has additional deleterious effects on mitochondria and the

whole cell an therefore causes mitochondrial impariments per se [70], [199], [495], [496]. However, the here newly discribed mechanism obviously seems to contribute to mitochondrial dysfunction and offers for the first time an explanation for the Cpx I impairment that has been observed in numerous times in both AD models and patients [182], [183], [202], [210], [497].

Next to the impairment of the mitochondrial respiration, a decreased MMP was also observed in pTRMT10C cells in comparison to Ctl. Since the MMP is built up by the proton-pumping activity of Cpx I-IV, this also indicates an impaired function of the ETC upon overexpression of TRMT10C. Besides, a rapid reduction of the MMP takes place as an early event in the apoptotic pathway [133] and may therefore indicate that these cells are undergoing increased apoptosis. These findings align well with former studies in HEK293 APPwt cells, where a decreased MMP was also observed [179], [216]. Likewise, in brains of AD patients a reduced MMP was reported, interstingly, also in lymphocytes (reviewed in [102]).

In conclusion, the experiments performed in pTRMT10C cells clearly demonstrate a causative relationship between the hypotheses (i)-(iv). Besides this thesis provides considerable evidence that this mechanism initiated by the elevation of TRMT10C is implicated in the pathogenesis of AD. According to our hypotheses, the initial upregulation of TRMT10C leads to increased methylation of m^1A^{1374} and an attenuated synthesis of ND5, which ultimately results in an impairment of Cpx I and the mitochondrial respiratory chain. This mechanism is particularly important because a reduction in the mitochondrial function can trigger apoptosis, causing neuronal death and cognitive decline in AD [71], [102], [498]. At this point, however, it is unclear why exactly this mechanism is initiated in AD, although the models studied in this thesis suggest a direct or indirect downstream effect of Aβ. Recent unpublished data of our group also suggests an upregulation of TRMT10C as a consequence of elevated ROS levels. Moreover, it is not entirely clear whether the TRMT10C-induced downregulation of Cpx I is in fact a pathological mechanism or whether it may be part of a protective mechanism that counterbalances deleterious events and mitochondrial dysfunction in AD. Since Cpx I is one of the major source of mitochondrial ROS and highly elevated ROS levels were found in brains of AD patients, both assumptions are conceivable [212], [499]. Considering that APP and Aβ are known to block the mitochondrial TIM/TOM complex, which inhibits the import of nuclear-encoded proteins, TRMT10C and m^1A^{1374} could also serve to fine-tune the interplay of nuclear and mitochondrial encoded Cpx I subunits [500], [501]. Since it is well known that RNA modifications play multiple roles in post-transciptional gene regulation pathways, this hypothesis is particularly interesting and requires further investigation [280], [306], [502].

6 Conclusion and Outlook

In this thesis, the potential involvement of m^1A^{1374} in the mitochondrial mRNA ND5 and its corresponding writer enzyme TRMT10C within the pathophysiology of AD was investigated. In addition, it was examined whether m^1A^{1374} is able to decrease protein levels of ND5, thus leading to an impairment of Cpx I and a reduced mitochondrial respiration. As this thesis focused on m^1A, it is embedded within the highly competitive and dynamic research area of RNA modifications. As a variety of RNA modifications has been discovered over the last decades, the question of their biological functions has emerged and a growing number of studies suggests that RNA modifications are essential players in both physiological and pathophysiological processes. Also in the case of AD, decreased neuronal levels of m^6A were observed in AD brains along with a reduced expression of its writer enzyme METTL3, which was associated with increased neuronal death, synaptic dysfunction and memory deficits [345]. However, the role of m^1A mRNA methylation in the context of AD and for the mitochondrial function under physiological conditions, has not yet been investigated and is therefore of great interest.

Regarding the hypotheses postulated in section 2, the following conclusions can be drawn:

(i) **The expression of writer enzyme TRMT10C is upregulated in AD**. Enhanced protein expression was observed in AD model cells and mice, both characterized by elevated Aβ levels, and in frontal cortex tissue of human AD patients. Besides, increased TRMT10C mRNA levels were detected specifically in neurons and this upregulation was particularly pronounced in the early stage of AD.

(ii) **m^1A^{1374} methylation is correlated with TRMT10C protein levels**. The Tetracycline-induced overexpression of TRMT10C in pTRMT10C cells revealed higher m^1A^{1374} levels with increasing Tetracycline-concentrations. In addition, elevated m^1A^{1374} methylation was detected in APPwt cells and the mildly affected primary visual cortex of AD patients. However, no significant alteration was observed in APPsw cells and the moderately affected precuneus, pointing to a stage-dependent involvement in AD.

(iii) **ND5 protein levels are diminished as a consequence of m^1A^{1374} methylation.** Decreased ND5 protein levels were measured in pTRMT10C and HEK APPwt cells, both displaying elevated m^1A^{1374} methylation in the mRNA of ND5. While the reduction of ND5 in HEK APPwt cells could be caused by alternative Aβ-induced mechanisms, the selective overexpression of TRMT10C in pTRMT10C cells suggests a direct causative relationship between TRMT10C, m^1A^{1374} and ND5.

(iv) Reduced levels of ND5 decrease the basal mitochondrial respiration by lowering the activity of Cpx I. Measurements of pTRMT10C cells with an oxygen electrode revealed a significantly reduced basal mitochondrial respiration and a decreased MMP as a consequence of TRMT10C overexpression. This decline of the respiratory chain is most likely caused by decreased levels of ND5 and the consecutive impairment of Cpx I.

The data of this thesis clearly demonstrates that TRMT10C is upregulated within the context of AD. Besides, these results independently confirm that TRMT10C incorporates m^1A^{1374} in the mRNA of ND5, which was recently postulated by Safra *et al.* [312]. Moreover, this thesis shows that enhanced m^1A^{1374} methylation results in decreased ND5 protein levels, although the exact mechanism of this translational repression remains unclear. Since increased m^1A^{1374} levels were already reported in light polysomal fractions [312], an impaired binding of the mitoribosome or a disruption of the translation elongation process can be suspected. Moreover, this thesis provides first evidence that a reduction of ND5 due to m^1A^{1374} is able to induce severe mitochondrial defecits by an impairment of Cpx I. A reduced acitivity of Cpx I due to mutations or depletion of ND5 has already been reported numerous times in the literature [156], [159], [169], [170], [418], [503]–[505]. There are even hints that mutations in ND5 may result in a enhanced generation of ROS, an aspect that is of particular importance with regard to AD [175].

However, a few questions still remain unanswered. For example, it is unclear whether TRMT10C requires an additional enzymatic partner protein or is able to catalyze m^1A^{1374} methylation as a stand alone enzyme. As SDR5C1 is indispensable for m^1A^9 methylation in (mt)tRNAs, one can assume that it is also needed for the methylation of m^1A^{1374} in ND5. However, to prove this assumption biochemical experiments are imperative. In addition, it is not conclusively resolved to what extent the activity of mtRNase P is affected by the upregulation of TRMT10C. Though the ratio of mitochondrial to cytosolic tRNAs was not altered in our experiments, Holzmann *et al.* obtained opposite results [359]. In this case, a more accurate method might be beneficial to detect minor differences. Furthermore, the question remains why APPsw cells show an upregulation of TRMT10C but no alteration of m^1A^{1374}. Although extremely high concentrations of Aβ were shown to inhibit the methyltransferase activity of TRMT10C *in vitro*, this inhibitory concentration is unlikely to be reached in APPsw cells. As elevated m^1A^{1374} levels were also observed in the mildly affected primary visual cortex but not in the moderately affected precuneus of AD pateints, a stage-depent activation of this mechanism is conceivable. Lastly, it is uncertain whether the upregulation of TRMT10C and m^1A^{1374}, and the ensuing effect on ND5 is a harmful downstream effect of Aβ or might be part of counteracting mechanisms, in order to compensate for the elevated ROS generation

observed in AD. Recent unpublished data of our group indicates an upregulation of TRMT10C in consequence of Aβ and H_2O_2 treatment in cells, and TRMT10C levels in HEK293 APPwt cells were lowered by incubation with Vitamin C, a common antioxidant. Therefore it is reasonable to assume that TRMT10C is upregulated by mitochondrial ROS, thus leading to mitochondrial dysfunction in AD.

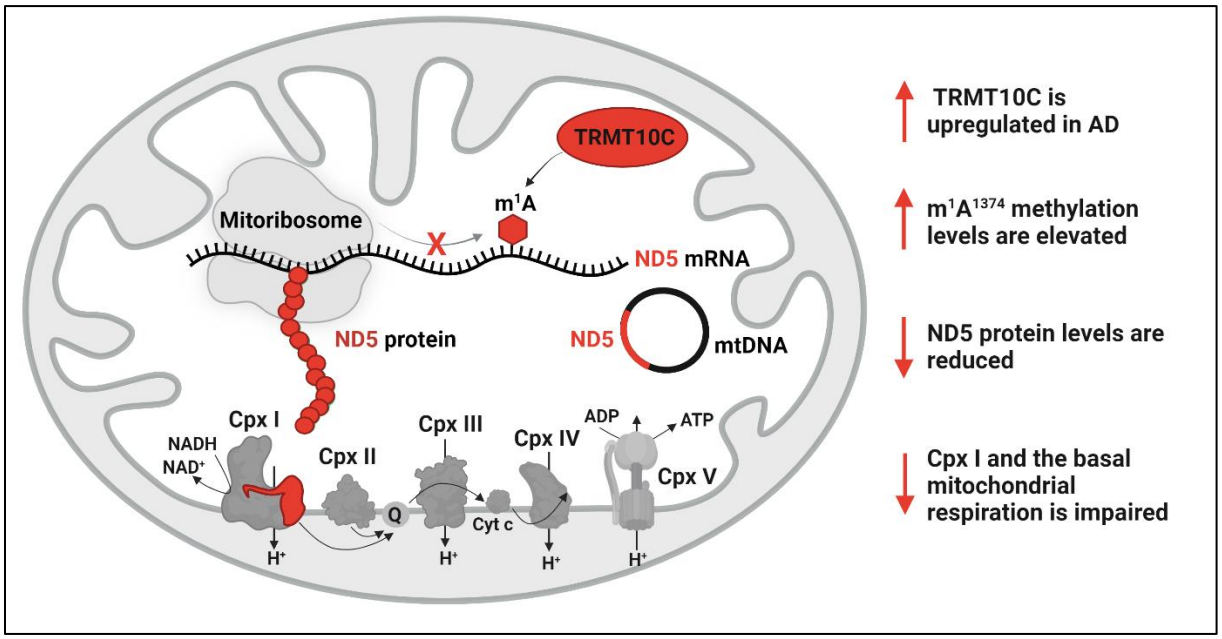

Figure 6.1: Graphical abstract of the main findings obtained in this thesis. Simplified illustration in analogy to the hypotheses (i)-(iv) postulated in section 2**.** TRMT10C protein and mRNA expression were upregulated in AD models and human patients. m^1A^{1374} methylation was partly enhanced in AD (elevation was observed in APPwt cells and the primary visual cortex of AD patients). ND5 protein levels were reduced in HEK APPwt cells, frontal cortex samples of AD patients with high Braak stages and cells overexpressing TRMT10C. Basal mitochondrial respiration was reduced in pTRMT10C cells after incubation with Tetracycline. This impaired function of the respiratory chain is most likely caused by an impaired activity of Cpx I due the reduction of the ND5 protein.

With regard to AD, this newly identified mechanism offers a plausible explanation for the impaired activity of Cpx I that has been observed in AD models and brains of AD patients. One possible hypothesis is that this mechanism might down-tune mitochondrial function under physiological conditions and is dysregulated in the pathophysiology of AD. As mitochondrial dysfunction represents an early and possibly causative event in AD, these findings are of great importance and provide a new and potential target for the treatment of AD. Specific examples for the development of new drug candidates would be a TRMT10C inhibitor or siRNA against TRMT10C mRNA. Interestingly, a reduced basal respiration rate and a decreased MMP were also reported in lymphocytes of AD patients [217], therefore m^1A^{1374} may also provide potential to establish a new biomarker to detect AD in blood samples. Although all these ideas require further research, and a TRMT10C inhibitor may need to be combined with other drugs, this work certainly takes us a small step closer to deciphering the complex pathogenesis of AD.

Bibliography

[1] A. Alzheimer, “Über eine eigenartige Erkrankung der Hirnrinde,” *Allg. Zeitschrift für Psychiatr. und Psych. Medizin*, vol. 64, pp. 145–148, 1907.

[2] M. W. Bondi, E. C. Edmonds, and D. P. Salmon, “Alzheimer’s Disease: Past, Present and Future,” *J. Int. Neurospsychological Soc.*, vol. 23, no. 9–10, pp. 818–831, 2017.

[3] A. Alzheimer, “über eigenartige Krankheitsfälle des späteren Alters,” *Zeitschrift für die gesamte Neurol. und Psychiatr.*, vol. 4, no. 1, pp. 356–385, 1911.

[4] X. X. Zhang, Y. Tian, Z. T. Wang, Y. H. Ma, L. Tan, and J. T. Yu, “The Epidemiology of Alzheimer’s Disease Modifiable Risk Factors and Prevention,” *J. Prev. Alzheimer’s Dis.*, vol. 8, no. 3, pp. 313–321, 2021.

[5] A. Association, “2020 Alzheimer’s disease facts and figures,” *Alzheimer’s Dement.*, vol. 16, no. 3, pp. 391–460, 2020.

[6] K. M. Langa *et al.*, “a Comparison of the Prevalence of Dementia in the United States in 2000 and 2012,” *Innov. Aging*, vol. 1, no. suppl_1, pp. 933–933, 2017.

[7] K. M. Sheffield and M. K. Peek, “Changes in the prevalence of cognitive impairment among older Americans, 1993-2004: Overall trends and differences by race/ethnicity,” *Am. J. Epidemiol.*, vol. 174, no. 3, pp. 274–283, 2011.

[8] Y. T. Wu *et al.*, “The changing prevalence and incidence of dementia over time-current evidence,” *Nat. Rev. Neurol.*, vol. 13, no. 6, pp. 327–339, 2017.

[9] W. A. Rocca *et al.*, “Trends in the incidence and prevalence of Alzheimer’s disease, dementia, and cognitive impairment in the United States,” *Alzheimer’s Dement.*, vol. 7, no. 1, pp. 80–93, 2011.

[10] C. Qiu, E. von Strauss, L. Bäckman, B. Winblad, and L. Fratiglioni, “Twenty-year changes in dementia occurrence suggest decreasing incidence in central Stockholm, Sweden,” *Neurology*, vol. 80, no. 20, pp. 1888 LP – 1894, May 2013.

[11] E. M. C. Schrijvers, B. F. J. Verhaaren, P. J. Koudstaal, A. Hofman, M. A. Ikram, and M. M. B. Breteler, “Is dementia incidence declining?,” *Neurology*, vol. 78, no. 19, pp. 1456 LP – 1463, May 2012.

[12] F. E. Matthews *et al.*, “A two-decade comparison of prevalence of dementia in individuals aged 65 years and older from three geographical areas of England: Results of the cognitive function and ageing study i and II,” *Lancet*, vol. 382, no. 9902, pp. 1405–1412, 2013.

[13] J. O. Cerasuolo *et al.*, “Population-based stroke and dementia incidence trends: Age and sex variations,” *Alzheimer’s Dement.*, vol. 13, no. 10, pp. 1081–1088, 2017.

[14] E. M. Crimmins, Y. Saito, J. K. Kim, Y. S. Zhang, I. Sasson, and M. D. Hayward, “Educational Differences in the Prevalence of Dementia and Life Expectancy with Dementia: Changes from 2000 to 2010,” *Journals Gerontol. - Ser. B Psychol. Sci. Soc. Sci.*, vol. 73, pp. S20–S28, 2018.

[15] J. C. Seidell, “Obesity, insulin resistance and diabetes - A worldwide epidemic,” *Br. J. Nutr.*, vol. 83, no. SUPPL. 1, pp. 5–8, 2000.

[16] C. P. Ferri and K. S. Jacob, “Dementia in low-income and middle-income countries: Different realities mandate tailored solutions,” *PLoS Med.*, vol. 14, no. 3, pp. 2–5, 2017.

[17] L. E. Hebert, J. Weuve, P. A. Scherr, and D. A. Evans, “Alzheimer disease in the United States (2010–2050) estimated using the 2010 census,” *Neurology*, vol. 80, no. 19, pp. 1778–1783, 2013..

[18] D. M. Holtzman, J. Herz, and G. Bu, “Apolipoprotein E and apolipoprotein E receptors: Normal biology and roles in Alzheimer disease,” *Cold Spring Harb. Perspect. Med.*, vol. 2, no. 3, pp. 1–24, 2012.

[19] Daniel M. Michaelson, “APOE e4, the most prevalent yet understudied risk factor Alzheimer’s disease,” *Alzheimer*, vol. 10, no. 6, 2014.

[20] A. Ward *et al.*, “Prevalence of Apolipoprotein E4 genotype and homozygotes (APOE e4/4) among patients diagnosed with alzheimer’s disease: A systematic review and meta-analysis,” *Neuroepidemiology*, vol. 38, no. 1, pp. 1–17, 2012.

[21] R. C. Green *et al.*, “Risk of Dementia Among White and African American Relatives of Patients With Alzheimer Disease,” *JAMA*, vol. 287, no. 3, pp. 329–336, Jan. 2002.

[22] C. T. Loy, P. R. Schofield, A. M. Turner, and J. B. Kwok, “Genetics of dementia,” *Lancet*, vol. 9919, 2014.

[23] F. J. Wolters *et al.*, “Parental family history of dementia in relation to subclinical brain disease and dementia risk,” *Neurology*, vol. 88, no. 17, pp. 1642 LP – 1649, Apr. 2017.

[24] R. S. Vest and C. J. Pike, “Gender, sex steroid hormones, and Alzheimer’s disease,” *Horm. Behav.*, vol. 63, no. 2, pp. 301–307, 2013.

[25] C. Borrás, J. Gambini, R. López-Grueso, F. V. Pallardó, and J. Viña, “Direct antioxidant and protective effect of estradiol on isolated mitochondria,” *Biochim. Biophys. Acta - Mol. Basis Dis.*, vol. 1802, no. 1, pp. 205–211, 2010.

[26] M. Baumgart, H. M. Snyder, M. C. Carrillo, S. Fazio, H. Kim, and H. Johns, “Summary of the evidence on modifiable risk factors for cognitive decline and dementia: A population-based perspective,” *Alzheimer’s Dement.*, vol. 11, no. 6, pp. 718–726, 2015.

[27] D. G. Blazer, K. Yaffe, and C. Liverman, *Committee on the Public Health Dimensions of Cognitive Aging; Board on Health Sciences Policy; Institute of Medicine. Cognitive Aging: Progress in Understanding and Opportunities for Action.* Washington (DC), 2015.

[28] A. Grimm, K. Friedland, and A. Eckert, “Mitochondrial dysfunction: the missing link between aging and sporadic Alzheimer’s disease,” *Biogerontology*, vol. 17, no. 2, pp. 281–296, 2016.

[29] S. Jayadev, “Genetics of Alzheimer Disease.,” *Continuum (Minneap. Minn).*, vol. 28, no. 3, pp. 852–871, Jun. 2022.

[30] C. Reitz and R. Mayeux, “Alzheimer disease: Epidemiology, diagnostic criteria, risk factors and biomarkers,” *Biochem. Pharmacol.*, vol. 88, no. 4, pp. 640–651, 2014.

[31] E. L. Ashby, J. S. Miners, S. Kumar, J. Walter, S. Love, and P. G. Kehoe, “Investigation of Aß phosphorylated at serine 8 (pAß) in Alzheimer’s disease, dementia with Lewy bodies and vascular dementia,” *Neurophathology Apllied Neurobiol.*, 2014.

[32] D. Van Dam and P. P. De Deyn, “Drug discovery in dementia: The role of rodent models,” *Nat. Rev. Drug Discov.*, vol. 5, no. 11, pp. 956–970, 2006.

[33] R. A. Sperling *et al.*, “Toward defining the preclinical stages of Alzheimer’s disease: Recommendations from the National Institute on Aging-Alzheimer’s Association workgroups on diagnostic guidelines for Alzheimer’s disease,” *Alzheimer’s Dement.*, vol. 7, no. 3, pp. 280–292, 2011.

[34] M. S. Albert *et al.*, “The diagnosis of mild cognitive impairment due to Alzheimer’s

disease: Recommendations from the National Institute on Aging- Alzheimer's Association workgroups on diagnostic guidelines for Alzheimer's disease," *Alzheimer's Dement.*, vol. 27, no. 3, pp. 270–279, 2011.

[35] G. McKhann *et al.*, "the diagnosis of dementia due to Alzheimer's disease," *Alzheimers Dement*, vol. 7, no. 3, pp. 263–269, 2012.

[36] C. R. Jack *et al.*, "Prevalence of Biologically vs Clinically Defined Alzheimer Spectrum Entities Using the National Institute on Aging-Alzheimer's Association Research Framework," *JAMA Neurol.*, vol. 76, no. 10, pp. 1174–1183, 2019.

[37] L. Vermunt *et al.*, "Duration of Preclinical, Prodromal and Dementia Alzheimer Disease Stages in Relation to Age, Sex, and APOE genotype," *Physiol. Behav.*, vol. 176, no. 1, pp. 139–148, 2018.

[38] H. Braak and E. Braak, "Neuropathological stageing of Alzheimer-related changes," *Acta Neuropatholigca*, vol. 82, pp. 239–259, 1991.

[39] D. A. Bennett *et al.*, "Neuropathology of older persons without cognitive impairment from two community-based studies," *Neurology*, vol. 66, no. 12, pp. 1837 LP – 1844, Jun. 2006.

[40] R. C. Petersen *et al.*, "Practice guideline update summary: Mild cognitive impairment report of theguideline development, dissemination, and implementation," *Neurology*, vol. 90, no. 3, pp. 126–135, 2018.

[41] L. Yue *et al.*, "Asymmetry of hippocampus and amygdala defect in subjective cognitive decline among the community dwelling Chinese," *Front. Psychiatry*, vol. 9, no. JUN, pp. 1–11, 2018.

[42] A. J. Mitchell and M. Shiri-Feshki, "Rate of progression of mild cognitive impairment to dementia - Meta-analysis of 41 robust inception cohort studies," *Acta Psychiatr. Scand.*, vol. 119, no. 4, pp. 252–265, 2009.

[43] P. Müller, M. Stiebler, S. Schwarck, A. Haghikia, and E. Düzel, "Physical activity, aging and brain health," *Dtsch. Z. Sportmed.*, vol. 72, no. 7, pp. 327–334, 2021.

[44] K. A. Jellinger, "Neuropathology of the Alzheimer's continuum: an update," *Free Neuropathol.*, vol. 1, pp. 1–34, 2020.

[45] U. C. Müller, T. Deller, and M. Korte, "Not just amyloid: Physiological functions of the amyloid precursor protein family," *Nat. Rev. Neurosci.*, vol. 18, no. 5, pp. 281–298, 2017.

[46] T. A. Bayer *et al.*, "Key Factors in Alzheimer's Disease, ß-amyloid Precursor protein processing, metabolism and intraneuronal transport," *Brain Pathol.*, vol. 11, pp. 1–11, 2001.

[47] D. J. Selkoe, "Alzheimer's disease: Genes, proteins, and therapy," *Physiol. Rev.*, vol. 81, no. 2001, p. 4110, 2001.

[48] H. K. Anandatheerthavarada, G. Biswas, M. A. Robin, and N. G. Avadhani, "Mitochondrial targeting and a novel transmembrane arrest of Alzheimer's amyloid precursor protein impairs mitochondrial function in neuronal cells," *J. Cell Biol.*, vol. 161, no. 1, pp. 41–54, 2003.

[49] R. W. Y. Choy, Z. Cheng, and R. Schekman, "Amyloid precursor protein (APP) traffics from the cell surface via endosomes for amyloid β (Aβ) production in the trans-Golgi network," *Proc. Natl. Acad. Sci. U. S. A.*, vol. 109, no. 30, pp. 2077–2082, 2012.

[50] H. A. R. De Silva, A. Jen, C. Wickenden, L. S. Jen, S. L. Wilkinson, and A. J. Patel, "Cell-specific expression of β-amyloid precursor protein isoform mRNAs and proteins in neurons and astrocytes," *Mol. Brain Res.*, vol. 47, no. 1–2, pp. 147–156, 1997.

[51] M. Gralle and S. T. Ferreira, “Structure and functions of the human amyloid precursor protein: The whole is more than the sum of its parts,” *Prog. Neurobiol.*, vol. 82, no. 1, pp. 11–32, 2007.

[52] E. Kojro and F. Fahrenholz, “The Non-Amyloidogenic Pathway: Structure and Function of α-Secretases,” in *Alzheimer’s Disease: Cellular and Molecular Aspects of Amyloid β*, J. R. Harris and F. Fahrenholz, Eds. Boston, MA: Springer US, 2005, pp. 105–127.

[53] G. F. Chen *et al.*, “Amyloid beta: Structure, biology and structure-based therapeutic development,” *Acta Pharmacol. Sin.*, vol. 38, no. 9, pp. 1205–1235, 2017.

[54] H. S. Hoe, H. K. Lee, and D. T. S. Pak, “The upside of APP at synapses,” *CNS Neurosci. Ther.*, vol. 18, no. 1, pp. 47–56, 2012.

[55] T. L. Young-Pearse, A. C. Chen, R. Chang, C. Marquez, and D. J. Selkoe, “Secreted APP regulates the function of full-length APP in neurite outgrowth through interaction with integrin beta1,” *Neural Dev.*, vol. 3, no. 1, 2008.

[56] N. Gakhar-Koppole *et al.*, “Activity requires soluble amyloid precursor protein alpha to promote neurite outgrwoth in neural stem cell-derived neurons via activation of the MAPK pathway,” *Eur. J. Neurosci.*, vol. 28, no. 5, pp. 871–882, 2008.

[57] J. Morales-Corraliza *et al.*, “In vivo turnover of tau and APP metabolites in the brains of wild-type and Tg2576 mice: Greater stability of sAPP in the β-amyloid depositing mice,” *PLoS One*, vol. 4, no. 9, pp. 1–8, 2009.

[58] S. E. Hoey, R. J. Williams, and M. S. Perkinton, “Synaptic NMDA receptor activation stimulates α-secretase amyloid precursor protein processing and inhibits amyloid-β Production,” *J. Neurosci.*, vol. 29, no. 14, pp. 4442–4460, 2009.

[59] J. Prox *et al.*, “Postnatal disruption of the disintegrin/metalloproteinase ADAM10 in brain causes epileptic seizures, learning deficits, altered spine morphology, and defective synaptic functions,” *J. Neurosci.*, vol. 33, no. 32, pp. 12915–12928, 2013.

[60] S. Weber and P. Saftig, “Ectodomain shedding and ADAMs in development,” *Dev.*, vol. 139, no. 20, pp. 3693–3709, 2012.

[61] H. Hampel *et al.*, “The ß-Secretase BACE1 in Alzheimer’s disease,” *Biol. Psychiatry*, vol. 89, no. 8, pp. 745–756, 2021.

[62] X. Zhang, Y. Li, H. Xu, and Y. W. Zhang, “The γ-secretase complex: From structure to function,” *Front. Cell. Neurosci.*, vol. 8, no. DEC, pp. 1–10, 2014.

[63] J. Hardy and G. Higgins, “Alzheimer’ s Disease : The Amyloid Cascade Hypothesis,” *Science (80-.).*, vol. 256, no. 6, pp. 184–185, 1992.

[64] Y. F. Shea, L. W. Chu, A. O. K. Chan, J. Ha, Y. Li, and Y. Q. Song, “A systematic review of familial Alzheimer’s disease: Differences in presentation of clinical features among three mutated genes and potential ethnic differences,” *J. Formos. Med. Assoc.*, vol. 115, no. 2, pp. 67–75, 2016.

[65] M. McCarron, P. McCallion, E. Reilly, P. Dunne, R. Carroll, and N. Mulryan, “A prospective 20-year longitudinal follow-up of dementia in persons with Down syndrome,” *J. Intellect. Disabil. Res.*, vol. 61, no. 9, pp. 843–852, 2017.

[66] B. O’Nuallain *et al.*, “Amyloid β-protein dimers rapidly form stable synaptotoxic protofibrils,” *J. Neurosci.*, vol. 30, no. 43, pp. 14411–14419, 2010.

[67] L. Mucke and D. J. Selkoe, “Neurotoxicity of amyloid β-protein: Synaptic and network dysfunction,” *Cold Spring Harb. Perspect. Med.*, vol. 2, no. 7, pp. 1–18, 2012.

[68] S. T. Ferreira, M. V. Lourenco, M. M. Oliveira, and F. G. De Felice, “Soluble amyloid-β

oligomers as synaptotoxins leading to cognitive impairment in Alzheimer's disease," *Front. Cell. Neurosci.*, vol. 9, no. MAY, pp. 1–17, 2015.

[69] S. T. Ferreira and W. L. Klein, "The Aß oligomer hypothesis for synapse failure and memory loss in Alzheimer's disease," *Neurobiol. Learn. Mem.*, vol. 96, no. 4, pp. 529–543, 2011.

[70] F. M. LaFerla, K. N. Green, and S. Oddo, "Intracellular amyloid-β in Alzheimer's disease," *Nat. Rev. Neurosci.*, vol. 8, no. 7, pp. 499–509, 2007.

[71] K. Friedland-Leuner, C. Stockburger, I. Denzer, G. P. Eckert, and W. E. Müller, "Mitochondrial Dysfunction: Cause and Consequence of Alzheimer's Disease," *Prog. Mol. Biol. Transl. Sci.*, vol. 127, pp. 183–210, 2014.

[72] J. M. Craft, M. D. Watterson, and L. J. Van Eldnik, "Human amyloid ß-induced neuroinflammation is an early event in neurodegeneration," *Glia*, vol. 53, no. 4, pp. 484–90, 2005.

[73] E. Jamasbi, J. Wade, F. Separovic, and M. Hossain, "Amyloid Beta (Aß) Peptide and Factors that Play Important Roles in Alzheimer's Disease," *Curr. Med. Chem.*, vol. 23, no. 9, pp. 884–892, 2016.

[74] M. Westwood and A. D. G. Lawson, "Opportunities for conformation-selective antibodies in amyloid-related diseases," *Antibodies*, vol. 4, no. 3, pp. 170–196, 2015.

[75] D. Puzzo, L. Lee, A. Palmeri, G. Calabrese, and O. Arancio, "Behvioral assays with mouse models of Alzheimer's disease, practical considerations and guidelines," *Biochem. Pharmacol.*, vol. 88, no. 4, pp. 450–467, 2014.

[76] H. Oakley *et al.*, "Intraneuronal β-amyloid aggregates, neurodegeneration, and neuron loss in transgenic mice with five familial Alzheimer's disease mutations: Potential factors in amyloid plaque formation," *J. Neurosci.*, vol. 26, no. 40, pp. 10129–10140, 2006.

[77] S. Schemmert *et al.*, "Aβ Oligomer Elimination Restores Cognition in Transgenic Alzheimer's Mice with Full-blown Pathology," *Mol. Neurobiol.*, vol. 56, no. 3, pp. 2211–2223, 2019..

[78] J. Moreth, C. Mavoungou, and K. Schindowski, "Passive anti-amyloid immunotherapy in Alzheimer's disease: What are the most promising targets?," *Immun. Ageing*, vol. 10, no. 1, pp. 1–9, 2013.

[79] R. Katzman *et al.*, "Clinical, pathological, and Neurochemical Changes in Dementia: A Subgroup with preserved Mental Status and Numerous Neocortical Plaques," *Petrochemical Equip.*, vol. 37, no. 4, pp. 51–58, 2008.

[80] P. Delaère, C. Duyckaerts, C. Masters, K. Beyreuther, F. Piette, and J.-J. Hauw, "Large amounts of neocortical βA4 deposits without neuritic plaques nor tangles in a psychometrically assessed, non-demented person," *Neurosci. Lett.*, vol. 116, no. 1–2, pp. 87–93, 1990.

[81] V. L. Villemagne *et al.*, "Longitudinal assessment of Aβ and cognition in aging and Alzheimer disease," *Ann. Neurol.*, vol. 69, no. 1, pp. 181–192, 2011.

[82] D. W. Dickson *et al.*, "Identification of normal and pathological aging in prospectively studied nondemented elderly humans," *Neurobiol. Aging*, vol. 13, no. 1, pp. 179–189, 1992.

[83] H. J. Aizenstein *et al.*, "Frequent amyloid deposition without significant cognitive impairment among the elderly," *Arch. Neurol.*, vol. 65, no. 11, pp. 1509–1517, 2008.

[84] G. K. Gouras, T. T. Olsson, and O. Hansson, "β-amyloid Peptides and Amyloid Plaques in Alzheimer's Disease," *Neurotherapeutics*, vol. 12, no. 1, pp. 3–11, 2015.

[85] E. Drummond and T. Wisniewski, “ALzheimer’s disease, experimental models and reality,” *Acta Neuropathol.*, vol. 133, no. 2, 2017.

[86] K. Scearce-Levie, P. E. Sanchez, and J. W. Lewcock, “Leveraging preclinical models for the development of Alzheimer disease therapeutics,” *Nat. Rev. Drug Discov.*, vol. 19, no. 7, pp. 447–462, 2020.

[87] M. Rapoport, H. N. Dawson, L. I. Binder, M. P. Vitek, and A. Ferreira, “Tau is essential to β-amyloid-induced neurotoxicity,” *Proc. Natl. Acad. Sci. U. S. A.*, vol. 99, no. 9, pp. 6364–6369, 2002,.

[88] E. D. Roberson *et al.*, “Reducing endogenous Tau ameliorates amyloid ß-induced deficits in an Alzheimer’s disease mouse model,” *Science (80-.).*, vol. 316, no. May, pp. 750–754, 2007.

[89] K. Leroy *et al.*, “Lack of tau proteins rescues neuronal cell death and decreases amyloidogenic processing of APP in APP/PS1 mice,” *Am. J. Pathol.*, vol. 181, no. 6, pp. 1928–1940, 2012.

[90] J. Lewis *et al.*, “Enhanced neurofibrillary degeneration in transgenic mice expressing mutant tau and APP,” *Science (80-.).*, vol. 293, no. 5534, pp. 1487–1491, 2001.

[91] E. M. Ribé *et al.*, “Accelerated amyloid deposition, neurofibrillary degeneration and neuronal loss in double mutant APP/tau transgenic mice,” *Neurobiol. Dis.*, vol. 20, no. 3, pp. 814–822, 2005.

[92] L. M. Ittner and J. Götz, “Amyloid-β and tau — a toxic pas de deux in Alzheimer’s disease,” *Nat. Rev. Neurosci.*, vol. 12, no. 2, pp. 67–72, 2011.

[93] G. S. Bloom, “Amyloid-β and tau: The trigger and bullet in Alzheimer disease pathogenesis,” *JAMA Neurol.*, vol. 71, no. 4, pp. 505–508, 2014.

[94] J. L. Price, P. B. Davis, J. C. Morris, and D. L. White, “The distribution of tangles, plaques and related immunohistochemical markers in healthy aging and Alzheimer’s disease,” *Neurobiol. Aging*, vol. 12, no. 4, pp. 295–312, 1991.

[95] B. Schönheit, R. Zarski, and T. G. Ohm, “Spatial and temporal relationships between plaques and tangles in Alzheimer-pathology,” *Neurobiol. Aging*, vol. 25, no. 6, pp. 697–711, 2004.

[96] J. A. R. Nicoll *et al.*, “Persistent neuropathological effects 14 years following amyloid-β immunization in Alzheimer’s disease,” *Brain*, vol. 142, no. 7, pp. 2113–2126, 2019.

[97] D. Ferreira, L.-O. Wahlund, and E. Westman, “The heterogeneity within Alzheimer’s disease,” *Aging (Albany. NY).*, vol. 10, no. 11, pp. 3058–3060, 2018.

[98] J. W. Vogel *et al.*, “Four distinct trajectories of tau deposition identified in Alzheimer’s disease,” *Nat. Med.*, vol. 27, no. 5, pp. 871–881, 2021.

[99] R. La Joie *et al.*, “Association of APOE4 and Clinical Variability in Alzheimer Disease With the Pattern of Tau- and Amyloid-PET,” *Neurology*, vol. 96, no. 5, pp. e650–e661, 2021.

[100] M. Dani, D. J. Brooks, and P. Edison, “Suspected non Alzheimer’s pathology – Is it non-Alzheimer’s or non-amyloid?,” *Ageing Res. Rev.*, vol. 36, pp. 20–31, 2017.

[101] S. Schreiber *et al.*, “Alzheimer disease signature neurodegeneration and APOE genotype in mild cognitive impairment with suspected non-Alzheimer disease pathophysiology,” *JAMA Neurol.*, vol. 74, no. 6, pp. 650–659, 2017.

[102] M. Jörg, J. E. Plehn, K. Friedland, and W. E. Müller, “Mitochondrial Dysfunction as a Causative Factor in Alzheimer’s Disease-Spectrum Disorders: Lymphocytes as a

Window to the Brain," *Curr. Alzheimer Res.*, vol. 18, no. 10, pp. 733–752, 2021.

[103] E. P. Bulthuis, M. J. W. Adjobo-Hermans, P. H. G. M. Willems, and W. J. H. Koopman, "Mitochondrial Morphofunction in Mammalian Cells," *Antioxidants Redox Signal.*, vol. 30, no. 18, pp. 2066–2109, 2019.

[104] L. Ernster and G. Schatz, "Mitochondria: A Historical Review," *J. Cell Biol.*, vol. 91, no. 3, 1981.

[105] L. Dard, W. Blanchard, C. Hubert, D. Lacombe, and R. Rossignol, *Mitochondrial functions and rare diseases*, vol. 71. 2020.

[106] J. Marín-García and M. J. Goldenthal, "The mitochondrial organelle and the heart," *Rev. Esp. Cardiol.*, vol. 55, no. 12, pp. 1293–1310, 2002.

[107] M. M. Anastacio *et al.*, "Relationship between mitochondrial matrix volume and cellular volume in response to stress and the role of atp-sensitive potassium channel," *Circulation*, vol. 128, no. SUPPL.1, pp. 1–12, 2013.

[108] L. Wiemerslage and D. Lee, "Quantification of mitochondrial morphology in neurites of dopaminergic neurons using multiple parameters," *J. Neurosci. Methods*, vol. 262, pp. 56–65, 2016.

[109] W. Kühlbrandt, "Structure and function of mitochondrial membrane protein complexes," *BMC Biol.*, vol. 13, no. 1, pp. 1–11, 2015.

[110] C. T. Campbell, J. E. Kolesar, and B. A. Kaufman, "Mitochondrial transcription factor A regulates mitochondrial transcription initiation, DNA packaging, and genome copy number," *Biochim. Biophys. Acta*, vol. 1819, no. 9–10, pp. 921–929, 2012.

[111] Y. Zhang *et al.*, "High copy number of mitochondrial DNA (mtDNA) predicts good prognosis in glioma patients.," *Am. J. Cancer Res.*, vol. 5, no. 3, pp. 1207–16, 2015.

[112] A. J. Roger, S. A. Muñoz-Gómez, and R. Kamikawa, "The Origin and Diversification of Mitochondria," *Curr. Biol.*, vol. 27, no. 21, pp. R1177–R1192, 2017.

[113] J. W. Taanman, "The mitochondrial genome: Structure, transcription, translation and replication," *Biochim. Biophys. Acta - Bioenerg.*, vol. 1410, no. 2, pp. 103–123, 1999.

[114] A. Amorim, T. Fernandes, and N. Taveira, "Mitochondrial DNA in human identification: A review," *PeerJ*, vol. 7, 2019.

[115] B. M. Hällberg and N. G. Larsson, "Making proteins in the powerhouse," *Cell Metab.*, vol. 20, no. 2, pp. 226–240, 2014.

[116] S. Anderson *et al.*, "Sequence and organization of the human mitochondrial genome," *Nature*, vol. 290, no. April, pp. 1–18, 1981.

[117] E. Jemt *et al.*, "Regulation of DNA replication at the end of the mitochondrial D-loop involves the helicase TWINKLE and a conserved sequence element," *Nucleic Acids Res.*, vol. 43, no. 19, pp. 9262–9275, 2015..

[118] B. Kruse, N. Narasimhan, and G. Attardi, "Termination of transcription in human mitochondria: Identification and purification of a DNA binding protei factor that promotes termination," *Cell*, vol. 58, no. 2, 1989.

[119] M. Terzioglu *et al.*, "MTERF1 Binds mtDNA to prevent transcriptional interference at the light-strand promoter but is dispensable for rRNA gene transcription regulation," *Cell Metab.*, vol. 17, no. 4, pp. 618–626, 2013.

[120] O. Pellegrini, J. Nezzar, A. Marchfelder, H. Putzer, and C. Condon, "Endonucleolytic processing of CCA-less tRNA precursors by RNase Z in Bacillus subtilis," *EMBO J.*, vol.

22, no. 17, pp. 4534–4543, 2003.

[121] D. Ojala, J. Montoya, and G. Attardi, “tRNA punctuation model of RNA processing in human mitochondria,” *Nature*, vol. 290, pp. 470–474, 1981.

[122] R. J. Temperley, M. Wydro, R. N. Lightowlers, and Z. M. Chrzanowska-Lightowlers, “Human mitochondrial mRNAs-like members of all families, similar but different,” *Biochim. Biophys. Acta - Bioenerg.*, vol. 1797, no. 6–7, pp. 1081–1085, 2010.

[123] T. Nagaike, T. Suzuki, T. Katoh, and T. Ueda, “Human mitochondrial mRNAs are stabilized with polyadenylation regulated by mitochondria-specific poly(A) polymerase and polynucleotide phosphorylase,” *J. Biol. Chem.*, vol. 280, no. 20, pp. 19721–19727, 2005.

[124] B. J. Greber *et al.*, “Architecture of the large subunit of the mammalian mitochondrial ribosome,” *Nature*, vol. 505, no. 7484, pp. 515–519, 2014.

[125] B. J. Greber *et al.*, “The complete structure of the large subunit of the mammalian mitochondrial ribosome,” *Nature*, vol. 515, no. 7526, pp. 283–286, 2014.

[126] M. T. Bohnsack and K. E. Sloan, “The mitochondrial epitranscriptome: the roles of RNA modifications in mitochondrial translation and human disease,” *Cell. Mol. Life Sci.*, vol. 75, no. 2, pp. 241–260, 2018.

[127] K. Watanabe, “Unique features of animal mitochondrial translation systems: The non-universal genetic code, unusual features of the translational apparatus and their relevance to human mitochondrial diseases,” *Proc. Japan Acad. Ser. B Phys. Biol. Sci.*, vol. 86, no. 1, pp. 11–39, 2010.

[128] I. Vercellino and L. A. Sazanov, “The assembly, regulation and function of the mitochondrial respiratory chain,” *Nat. Rev. Mol. Cell Biol.*, vol. 23, no. 2, pp. 141–161, 2022.

[129] O. Biner, T. Schick, A. A. Ganguin, and C. Von Ballmoos, “Towards a synthetic mitochondrion,” *Chimia (Aarau).*, vol. 72, no. 5, pp. 291–296, 2018.

[130] P. R. Rich and A. Maréchal, “The mitochondrial respiratory chain,” *Essays Biochem.*, vol. 47, pp. 1–23, 2010.

[131] A. Osyczka, C. C. Moser, and L. P. Dutton, “Fixing the Q cycle,” *Trends Biochem. Sci.*, vol. 30, no. 4, pp. P176-182, 2005.

[132] D. Nolfi-Donegan, A. Braganza, and S. Shiva, “Mitochondrial electron transport chain: Oxidative phosphorylation, oxidant production, and methods of measurement,” *Redox Biol.*, vol. 37, p. 101674, 2020.

[133] D. R. Green and J. C. Reed, “Mitochondria and Apoptosis,” *Science (80-.).*, vol. 281, no. 5381, pp. 1309–1312, 1998.

[134] F. J. Bock and S. W. G. Tait, “Mitochondria as multifaceted regulators of cell death,” *Nat. Rev. Mol. Cell Biol.*, 2019.

[135] M. Circu and T. Tee Aw, “Reactive oxygen species, cellular redox systems and apoptosis,” *Free Radic Biol Med.*, vol. 48, no. 6, pp. 749–762, 2010.

[136] R. B. Hamanaka and N. S. Chandel, “Mitochondrial reactive oxygen species regulate cellular signaling and dictate biological outcomes,” *Trends Biochem. Sci.*, vol. 35, no. 9, pp. 505–513, 2010.

[137] J. Nunnari and A. Suomalainen, “Mitochondria: In Sickness and in Health,” *Cell*, vol. 148, no. 6, pp. 1145–1159, 2012, doi: 10.1016/j.cell.2012.02.035.Mitochondria.

[138] G. S. Shadel and T. L. Horvath, “Mitochondrial ROS Signaling in Organismal Homeostasis,” *Cell*, vol. 163, no. 3, pp. 560–569, 2015.

[139] R. Lill and U. Mühlenhoff, “Maturation of iron-sulfur proteins in eukaryotes: Mechanisms, connected processes, and diseases,” *Annu. Rev. Biochem.*, vol. 77, pp. 669–700, 2008.

[140] S. Missiroli, I. Genovese, M. Perrone, B. Vezzani, V. A. M. Vitto, and C. Giorgi, “The role of mitochondria in inflammation: From cancer to neurodegenerative disorders,” *J. Clin. Med.*, vol. 9, no. 3, 2020.

[141] M. Iino, “Spatiotemporal dynamics of Ca2+ signaling and its physiological roles,” *Proc. Japan Acad. Ser. B Phys. Biol. Sci.*, vol. 86, no. 3, pp. 244–256, 2010.

[142] M. Brini, T. Calì, D. Ottolini, and E. Carafoli, “Neuronal calcium signaling: Function and dysfunction,” *Cell. Mol. Life Sci.*, vol. 71, no. 15, pp. 2787–2814, 2014.

[143] L. Sharma, J. Lu, and Y. Bai, “Mitochondrial Respiratory Complex I, structure, function and implication in human diseases,” *Physiol. Behav.*, vol. 176, no. 1, pp. 139–148, 2016.

[144] J. M. Berrisford, R. Baradaran, and L. A. Sazanov, “Structure of bacterial respiratory complex i,” *Biochim. Biophys. Acta - Bioenerg.*, vol. 1857, no. 7, pp. 892–901, 2016.

[145] J. Friedman, L. Mourokh, and M. Vittadello, “Mechanism of proton pumping in complex i of the mitochondrial respiratory chain,” *Quantum Reports*, vol. 3, no. 3, pp. 425–434, 2021.

[146] M. Mimaki, X. Wang, M. McKenzie, D. R. Thorburn, and M. T. Ryan, “Understanding mitochondrial complex I assembly in health and disease,” *Biochim. Biophys. Acta - Bioenerg.*, vol. 1817, no. 6, pp. 851–862, 2012.

[147] D. A. Stroud *et al.*, “Accessory subunits are integral for assembly and function of human mitochondrial complex i,” *Nature*, vol. 538, no. 7623, pp. 123–126, 2016.

[148] J. Hirst, “Why does mitochondrial complex I have so many subunits?,” *Biochem. J.*, vol. 437, no. 2, pp. 3–5, 2011.

[149] J. Carroll, I. M. Fearnley, J. M. Skehel, R. J. Shannon, J. Hirst, and J. E. Walker, “Bovine complex I is a complex of 45 different subunits,” *J. Biol. Chem.*, vol. 281, no. 43, pp. 32724–32727, 2006.

[150] L. A. Sazanov, “A giant molecular proton pump: Structure and mechanism of respiratory complex I,” *Nat. Rev. Mol. Cell Biol.*, vol. 16, no. 6, pp. 375–388, 2015.

[151] J. A. Birrell, K. Morina, H. R. Bridges, T. Friedrich, and J. Hirst, “Investigating the function of [2Fe-2S] cluster N1a, the off-pathway cluster in complex I, by manipulating its reduction potential,” *Biochem. J.*, vol. 456, no. 1, pp. 139–146, 2013.

[152] T. Pohl *et al.*, “Iron-sulfur Cluster N7 of the NADH:Ubiquinone Oxidoreductase (complex I) is essential for stability but not involved in electron transfer,” pp. 6588–6596, 2007.

[153] P. Hinchliffe and L. A. Sazanov, “Organization of iron-sulfur clusters in respiratory complex I,” *Science (80-.).*, vol. 309, no. 5735, pp. 771–774, 2005.

[154] A. N. A. Agip *et al.*, “Cryo-em structures of complex i from mouse heart mitochondria in two biochemically defined states,” *Nat. Struct. Mol. Biol.*, vol. 25, no. 7, pp. 548–556, 2018.

[155] R. G. Efremov, R. Baradaran, and L. A. Sazanov, “The architecture of respiratory complex I,” *Nature*, vol. 465, no. 7297, pp. 441–445, 2010.

[156] G. Belevich, J. Knuuti, M. I. Verkhovsky, M. Wikström, and M. Verkhovskaya, “Probing the mechanistic role of the long α-helix in subunit L of respiratory Complex I from

Escherichia coli by site-directed mutagenesis," *Mol. Microbiol.*, vol. 82, no. 5, pp. 1086–1095, 2011.

[157] F. Hoeser *et al.*, "Respiratory complex I with charge symmetry in the membrane arm pumps protons," *Proc. Natl. Acad. Sci. U. S. A.*, vol. 119, no. 27, pp. 1–10, 2022.

[158] A. Di Luca, A. P. Gamiz-Hernandez, and V. R. I. Kaila, "Symmetry-related proton transfer pathways in respiratory complex I," *Proc. Natl. Acad. Sci. U. S. A.*, vol. 114, no. 31, pp. E6314–E6321, 2017.

[159] S. Shanske *et al.*, "The G13513A Mutation in the ND5 Gene of Mitochondrial DNA as a Common Cause of MELAS or Leigh Syndrome," vol. 65, no. 3, pp. 368–372, 2008.

[160] D. R. Thorburn, J. Rahman, and S. Rahman, "Mitochondrial DNA-Associated Leigh Syndrome and NARP.," in *GeneReviews*, M. P. Adam, D. B. Everman, G. M. Mirzaa, R. A. Pagon, S. E. Wallace, L. J. H. Bean, K. W. Gripp, and A. Amemiya, Eds. Seattle (WA), 2017.

[161] J. Finsterer, "Mitochondriopathies," *Eur. J. Neurol.*, vol. 11, no. 3, pp. 16–186, 2004.

[162] V. Mayorov, V. Biousse, N. J. Newman, and M. D. Brown, "The role of the ND5 gene in LHON: Characterization of a new, heteroplasmic LHON mutation," *Ann. Neurol.*, vol. 58, no. 5, pp. 807–811, 2005.

[163] J. Zhang *et al.*, "Leber's hereditary optic neuropathy (LHON)-associated ND5 12338T > C mutation altered the assembly and function of complex I, apoptosis and mitophagy," *Hum. Mol. Genet.*, vol. 27, no. 11, pp. 1999–2011, 2018.

[164] S. G. Pavlakis, P. C. Phillips, S. DiMauro, D. De Vivo, and L. P. Rowland, "Mitochondrial myopathy, encephalopathy, lactic acidosis, and strokelike episodes: A distinctive clinical syndrome," *Ann. Neurol.*, vol. 16, no. 4, pp. 481–488, 1984.

[165] L. M. Seed, A. Dean, D. Krishnakumar, P. Phyu, R. Horvath, and P. D. Harijan, "Molecular and neurological features of MELAS syndrome in paediatric patients: A case series and review of the literature," *Mol. Genet. Genomic Med.*, vol. 10, no. 7, pp. 1–13, 2022.

[166] N. Manwaring *et al.*, "Population prevalence of the MELAS A3243G mutation," *Mitochondrion*, vol. 7, no. 3, pp. 230–233, 2007.

[167] E. A. Shoubridge, "Mitochondrial DNA diseases: Histological and cellular studies," *J. Bioenerg. Biomembr.*, vol. 26, no. 3, pp. 301–310, 1994.

[168] C. B. Park and N. G. Larsson, "Mitochondrial DNA mutations in disease and aging," *J. Cell Biol.*, vol. 193, no. 5, pp. 809–818, 2011.

[169] E. Malfatti *et al.*, "Novel mutations of ND genes in complex I deficiency associated with mitochondrial encephalopathy," *Brain*, vol. 130, no. 7, pp. 1894–1904, 2007.

[170] A. B. Naini *et al.*, "Novel Mitochondrial DNA ND5 Mutation in a Patient With Clinical Features of MELAS and MERRF," *Arch Neurol*, vol. 62, pp. 473–476, 2005.

[171] D. B. Zorov, M. Juhaszova, and S. J. Sollott, "Mitochondrial reactive oxygen species (ROS) and ROS-induced ROS release," *Physiol. Rev.*, vol. 94, no. 3, pp. 909–950, Jul. 2014.

[172] M. P. Murphy, "How mitochondria produce reactive oxygen species," *Biochem. J.*, vol. 417, no. 1, pp. 1–13, 2008.

[173] J. Hirst, M. S. King, and K. R. Pryde, "The production of reactive oxygen species by complex I," *Biochem. Soc. Trans.*, vol. 36, no. 5, pp. 976–980, Sep. 2008.

[174] R. Fato, C. Bergamini, S. Leoni, P. Strocchi, and G. Lenaz, “Generation of reactive oxygen species by mitochondrial complex I: Implications in neurodegeneration,” *Neurochem. Res.*, vol. 33, no. 12, pp. 2487–2501, 2008.

[175] R. K. Singh, S. Saini, D. Verma, P. Kalaiarasan, and R. N. K. Bamezai, “Mitochondrial ND5 mutation mediated elevated ROS regulates apoptotic pathway epigenetically in a P53 dependent manner for generating pro-cancerous phenotypes,” *Mitochondrion*, vol. 35, no. April, pp. 35–43, 2017.

[176] D. Pignataro *et al.*, “A missense MT-ND5 mutation in differentiated Parkinson Disease cytoplasmic hybrid induces ROS-dependent DNA Damage Response amplified by DROSHA,” *Sci. Rep.*, vol. 7, no. 1, pp. 1–14, 2017.

[177] Y. Kushnareva, A. N. Murphy, and A. Andreyev, “Complex I-mediated reactive oxygen species generation: Modulation by cytochrome c and NAD(P)+ oxidation-reduction state,” *Biochem. J.*, vol. 368, no. 2, pp. 545–553, 2002.

[178] A. Singh, R. Kukreti, L. Saso, and S. Kukreti, “Oxidative stress: A key modulator in neurodegenerative diseases,” *Molecules*, vol. 24, no. 8, pp. 1–20, 2019.

[179] K. Leuner *et al.*, “Mitochondrion-derived reactive oxygen species lead to enhanced amyloid beta formation,” *Antioxidants Redox Signal.*, vol. 16, no. 12, pp. 1421–1433, 2012.

[180] E. Tamagno *et al.*, “Oxidative stress activates a positive feedback between the gamma- and beta-secretase cleavages of the beta-amyloid precursor protein,” *J. Neurochem.*, vol. 104, no. 3, pp. 683–695, 2008.

[181] E. Llanos-González *et al.*, “Interplay Between Mitochondrial Oxidative Disorders and Proteostasis in Alzheimer’s Disease,” *Front. Neurosci.*, vol. 13, no. January, pp. 1–10, 2020.

[182] T. Terada *et al.*, “Mitochondrial complex I abnormalities is associated with tau and clinical symptoms in mild Alzheimer’s disease,” *Mol. Neurodegener.*, vol. 16, no. 1, pp. 1–12, 2021.

[183] L. Holper, D. Ben-Shachar, and J. Mann, “Multivariate meta-analyses of mitochondrial complex I and IV in major depressive disorder, bipolar disorder, schizophrenia, Alzheimer disease, and Parkinson disease,” *Neuropsychopharmacology*, vol. 44, no. 5, pp. 837–849, 2019.

[184] L. Zhang *et al.*, “Modulation of Mitochondrial Complex I Activity Averts Cognitive Decline in Multiple Animal Models of Familial Alzheimer’s Disease,” *EBioMedicine*, vol. 2, no. 4, pp. 294–305, 2015.

[185] E. Trushina, S. Trushin, and M. F. Hasan, “Mitochondrial complex I as a therapeutic target for Alzheimer’s disease,” *Acta Pharm. Sin. B*, vol. 12, no. 2, pp. 483–495, 2022.

[186] A. Stojakovic *et al.*, “Partial inhibition of mitochondrial complex I ameliorates Alzheimer’s disease pathology and cognition in APP/PS1 female mice,” *Commun. Biol.*, vol. 4, no. 1, 2021.

[187] J. Holzmann and W. Rossmanith, “tRNA recognition, processing, and disease: Hypotheses around an unorthodox type of RNase P in human mitochondria,” *Mitochondrion*, vol. 9, no. 4, pp. 284–288, 2009.

[188] W. Wang, F. Zhao, X. Ma, G. Perry, and X. Zhu, “Mitochondria dysfunction in the pathogenesis of Alzheimer’s disease: Recent advances,” *Mol. Neurodegener.*, vol. 15, no. 1, pp. 1–22, 2020.

[189] A. Misrani, S. Tabassum, and L. Yang, “Mitochondrial Dysfunction and Oxidative Stress

in Alzheimer's Disease," *Front. Aging Neurosci.*, vol. 13, no. February, pp. 1–20, 2021.

[190] L. Mosconi, A. Pupi, and M. J. De Leon, "Brain Glucose Hypometabolism and oxidative Stress in Preclinical Alzheimer's disease," *Ann. N. Y. Acad. Sci.*, vol. 1147, no. 1, pp. 180–195, 2008.

[191] G. E. Gibson, K. F. R. Sheu, and J. P. Blass, "Abnormalities of mitochondrial enzymes in Alzheimer disease," *J. Neural Transm.*, vol. 105, no. 8–9, pp. 855–870, 1998.

[192] M. Héroux, V. L. Raghavendra Rao, J. Lavoie, J. S. Richardson, and R. F. Butterworth, "Alterations of thiamine phosphorylation and of thiamine-dependent enzymes in Alzheimer's disease," *Metab. Brain Dis.*, vol. 11, no. 1, pp. 81–88, 1996.

[193] K. Ishii, H. Kitagaki, M. Kono, and E. Mon, "Decreased Medial Temporal Oxygen Metabolism in Alzheimer's Disease Shown by PET," *J. Nucl. Med.*, vol. 37, no. 7, pp. 1159–1165, 1995.

[194] H. Tohgi *et al.*, "Cerebral blood flow and oxygen metabolism in senile dementia of Alzheimer's type and vascular dementia with deep white matter changes," *Neuroradiology*, vol. 40, no. 3, pp. 131–137, 1998.

[195] W. D. Parker, J. P. BA, C. M. Filley, and B. K. Kleinschmidt-DeMasters, "Electron transport chain defects in Alzheimer's disease brain," *Neurology*, vol. 44, no. 6, pp. 1090 LP – 1090, Jun. 1994.

[196] S. M. Bell *et al.*, "Mitochondrial dysfunction in Alzheimer's disease: A biomarker of the future?," *Biomedicines*, vol. 9, no. 1, pp. 1–26, 2021.

[197] I. Maurer, S. Zierz, and H.-J. Möller, "A selective defect of cytochrome c oxidase is present in brain of Alzheimer disease patients," *Neurobiol. Aging*, vol. 21, no. 3, pp. 455–462, 2000.

[198] L. F. Hernandez-Zimbron *et al.*, "Amyloid-β peptide binds to cytochrome C oxidase subunit 1," *PLoS One*, vol. 7, no. 8, pp. 29–31, 2012.

[199] P. Picone, D. Nuzzo, D. Giacomazza, and M. Di Carlo, "β-Amyloid Peptide: the Cell Compartment Multi-faceted Interaction in Alzheimer's Disease," *Neurotox. Res.*, vol. 37, no. 2, pp. 250–263, 2020.

[200] T. Terada *et al.*, "Mitochondrial complex-I abnormalities underlie neurodegeneration and cognitive decline in Alzheimer's disease," *Eur. J. Neurol.*, vol. 29, no. 5, pp. 1324–1334, 2022.

[201] R. Derungs *et al.*, "Genetic ablation of the p66 Shc adaptor protein reverses cognitive deficits and improves mitochondrial function in an APP transgenic mouse model of Alzheimer's disease," *Mol. Psychiatry*, vol. 22, no. 4, pp. 605–614, 2017.

[202] V. Rhein *et al.*, "Amyloid-β and tau synergistically impair the oxidative phosphorylation system in triple transgenic Alzheimer's disease mice," *Proc. Natl. Acad. Sci. U. S. A.*, vol. 106, no. 47, pp. 20057–20062, 2009.

[203] V. Sorrentino *et al.*, "Enhancing mitochondrial proteostasis reduces amyloid-β proteotoxicity," *Nature*, vol. 552, no. 7684, pp. 187–193, 2017.

[204] B. Minjarez *et al.*, "Identification of proteins that are differentially expressed in brains with Alzheimer's disease using iTRAQ labeling and tandem mass spectrometry," *J. Proteomics*, vol. 139, pp. 103–121, 2016.

[205] M. Manczak, B. S. Park, Y. Jung, and P. H. Reddy, "Differential Expression of Oxidative Phosphorylation Genes in Patients with Alzheimer's Disease: Implications for Early Mitochondrial Dysfunction and Oxidative Damage," *NeuroMolecular Med.*, vol. 5, no. 2, pp. 147–162, 2004.

[206] R. Fukuyama, K. Hatanpää, S. I. Rapoport, and K. Chandrasekaran, “Gene expression of ND4, a subunit of complex I of oxidative phosphorylation in mitochondria, is decreased in temporal cortex of brains of Alzheimer’s disease patients,” *Brain Res.*, vol. 713, no. 1–2, pp. 290–293, 1996.

[207] D. Mastroeni *et al.*, “Nuclear but not mitochondrial-encoded oxidative phosphorylation genes are altered in aging, mild cognitive impairment, and ALzheimer’s disease,” *Alzheimer’s Dementiad Dement.*, vol. 13, no. 5, pp. 510–519, 2016.

[208] W. S. Liang *et al.*, “Alzheimer’s disease is associated with reduced expression of energy metabolism genes in posterior cingulate neurons,” *Proc. Natl. Acad. Sci. U. S. A.*, vol. 105, no. 11, pp. 4441–4446, 2008.

[209] D. C. David *et al.*, “Proteomic and functional analyses reveal a mitochondrial dysfunction in P301L tau transgenic mice,” *J. Biol. Chem.*, vol. 280, no. 25, pp. 23802–23814, 2005.

[210] S. H. Eckert, J. Eckmann, K. Renner, G. P. Eckert, K. Leuner, and W. E. Muller, “Dimebon ameliorates amyloid-β induced impairments of mitochondrial form and function,” *J. Alzheimer’s Dis.*, vol. 31, no. 1, pp. 21–32, 2012.

[211] C. S. Casley, J. M. Land, M. A. Sharpe, J. B. Clark, M. R. Duchen, and L. Canevari, “β-Amyloid fragment 25-35 causes mitochondrial dysfunction in primary cortical neurons,” *Neurobiol. Dis.*, vol. 10, no. 3, pp. 258–267, 2002.

[212] A. Bobba, G. Amadoro, D. Valenti, V. Corsetti, R. Lassandro, and A. Atlante, “Mitochondrial respiratory chain Complexes I and IV are impaired by β-amyloid via direct interaction and through Complex I-dependent ROS production, respectively,” *Mitochondrion*, vol. 13, no. 4, pp. 298–311, 2013.

[213] A. M. Aleardi *et al.*, “Gradual alteration of mitochondrial structure and function by β-amyloids: Importance of membrane viscosity changes, energy deprivation, reactive oxygen species production, and cytochrome c release,” *J. Bioenerg. Biomembr.*, vol. 37, no. 4, pp. 207–225, 2005.

[214] S. M. Cardoso, S. Santos, R. H. Swerdlow, and C. R. Oliveira, “Functional mitochondria are required for amyloid β-mediated neurotoxicity,” *FASEB J.*, vol. 15, no. 8, pp. 1439–1441, 2001.

[215] M. E. Munguia, T. Govezensky, R. Martinez, K. Manoutcharian, and G. Gevorkian, “Identification of amyloid-beta 1-42 binding protein fragments by screening of a human brain cDNA library,” *Neurosci. Lett.*, vol. 397, no. 1–2, pp. 79–82, 2006.

[216] U. Keil *et al.*, “Amyloid β-induced changes in nitric oxide production and mitochondrial activity lead to apoptosis,” *J. Biol. Chem.*, vol. 279, no. 48, pp. 50310–50320, 2004.

[217] K. Leuner *et al.*, “Peripheral mitochondrial dysfunction in Alzheimer’s disease: Focus on lymphocytes,” *Mol. Neurobiol.*, vol. 46, no. 1, pp. 194–204, 2012.

[218] K. Leuner *et al.*, “Enhanced apoptosis, oxidative stress and mitochondrial dysfunction in lymphocytes as potential biomarkers for Alzheimer’s disease,” *J. Neural Transm.*, no. 72, pp. 207–215, 2007.

[219] S. Hauptmann *et al.*, “Mitochondrial dysfunction: An early event in Alzheimer pathology accumulates with age in AD transgenic mice,” *Neurobiol. Aging*, vol. 30, no. 10, pp. 1574–1586, 2009.

[220] X. Wang *et al.*, “Amyloid-β overproduction causes abnormal mitochondrial dynamics via differential modulation of mitochondrial fission/fusion proteins,” *Proc. Natl. Acad. Sci. U. S. A.*, vol. 105, no. 49, pp. 19318–19323, 2008.

[221] X. Wang *et al.*, “Impaired balance of mitochondrial fission and fusion in Alzheimer’s

disease," *J. Neurosci.*, vol. 29, no. 28, pp. 9090–9103, 2009.

[222] P. H. Reddy, "Defective Autophagy and Mitophagy in Alzheimer ' s Disease," 2019.

[223] J. A. Pradeepkiran and P. Hemachandra Reddy, "Defective mitophagy in Alzheimer's disease," *Ageing Res. Rev.*, vol. 64, pp. 1–38, 2020.

[224] K. Iijima-Ando, S. A. Hearn, C. Shenton, A. Gatt, L. Zhao, and K. Iijima, "Mitochondrial mislocalization underlies aβ42-induced neuronal dysfunction in a drosophila model of alzheimer's disease," *PLoS One*, vol. 4, no. 12, 2009.

[225] W. Qin *et al.*, "PGC-1α expression decreases in the Alzheimer disease brain as a function of dementia," *Arch. Neurol.*, vol. 66, no. 3, pp. 352–361, 2009.

[226] R. Ventura-Clapier, A. Garnier, and V. Veksler, "Transcriptional control of mitochondrial biogenesis: The central role of PGC-1α," *Cardiovasc. Res.*, vol. 79, no. 2, pp. 208–217, 2008.

[227] L. Devi, B. M. Prabhu, D. F. Galati, N. G. Avadhani, and H. K. Anandatheerthavarada, "Accumulation of amyloid precursor protein in the mitochondrial import channels of human Alzheimer's disease brain is associated with mitochondrial dysfunction," *J. Neurosci.*, vol. 26, no. 35, pp. 9057–9068, 2006.

[228] C. A. Hansson Petersen *et al.*, "The amyloid β-peptide is imported into mitochondria via the TOM import machinery and localized to mitochondrial cristae," *Proc. Natl. Acad. Sci. U. S. A.*, vol. 105, no. 35, pp. 13145–13150, 2008.

[229] N. Alikhani *et al.*, "Decreased Proteolytic Activity of the Mitochondrial Amyloid-β Degrading Enzyme, PreP Peptidasome, in Alzheimer's Disease Brain Mitochondria," *J. Alzheimer's Dis.*, vol. 27, pp. 75–87, 2011.

[230] A. Falkevall *et al.*, "Degradation of the amyloid β-protein by the novel mitochondrial peptidasome, PreP," *J. Biol. Chem.*, vol. 281, no. 39, pp. 29096–29104, 2006.

[231] A. C. Rice, P. M. Keeney, N. K. Algarzae, A. C. Ladd, R. R. Thomas, and J. P. Bennett Jr., "Mitochondrial DNA Copy Numbers in Pyramidal Neurons are Decreased and Mitochondrial Biogenesis Transcriptome Signaling is Disrupted in Alzheimer's Disease Hippocampi," *J. Alzheimer's Dis.*, vol. 40, pp. 319–330, 2014..

[232] M. A. Lovell, S. Soman, and M. A. Bradley, "Oxidatively modified nucleic acids in preclinical Alzheimer's disease (PCAD) brain," *Mech. Ageing Dev.*, vol. 132, no. 8–9, pp. 443–448, 2011.

[233] M. Blanch, J. L. Mosquera, B. Ansoleaga, I. Ferrer, and M. Barrachina, "Altered mitochondrial DNA methylation pattern in Alzheimer disease-related pathology and in Parkinson disease," *Am. J. Pathol.*, vol. 186, no. 2, pp. 385–397, 2016.

[234] A. Stoccoro, G. Siciliano, L. Migliore, and F. Coppedè, "Decreased Methylation of the Mitochondrial D-Loop Region in Late-Onset Alzheimer's Disease," *J. Alzheimer's Dis.*, no. 59, pp. 559–564, 2017.

[235] G. Cenini and W. Voos, "Mitochondria as potential targets in Alzheimer disease therapy: An update," *Front. Pharmacol.*, vol. 10, no. JULY, pp. 1–20, 2019.

[236] H. M. Wilkins, I. W. Weidling, Y. Ji, and R. H. Swerdlow, "Mitochondria-derived damage-associated molecular patterns in neurodegeneration," *Front. Immunol.*, vol. 8, no. APR, pp. 1–12, 2017.

[237] A. Eckert, K. Schmitt, and J. Götz, "Mitochondrial dysfunction - The beginning of the end in Alzheimer's disease? Separate and synergistic modes of tau and amyloid-toxicity," *Alzheimer's Res. Ther.*, vol. 3, no. 3, 2011.

[238] R. H. Swerdlow, “Mitochondria and Mitochondrial Cascades in Alzheimer’s Disease,” *J. Alzheimer’s Dis.*, vol. 62, no. 3, pp. 1403–1416, 2018.

[239] X. Wang, W. Wang, L. Li, G. Perry, H. Lee, and X. Zhu, “Oxidative stress and mitochondrial dysfunction in Alzheimer’s disease,” *Biochim. Biophys. Acta*, vol. 1842, no. 8, pp. 1240–1247, 2014.

[240] S. Miwa *et al.*, “Low abundance of the matrix arm of complex I in mitochondria predicts longevity in mice,” *Nat. Commun.*, vol. 5, no. May, 2014.

[241] R. H. Swerdlow, S. Koppel, I. Weidling, C. Hayley, Y. Ji, and H. M. Wilkins, “Mitochondria, Cybrids, Aging, and Alzheimer’s Disease,” *Prog. Mol. Biol. Transl. Sci.*, vol. 146, pp. 259–302, 2017.

[242] D. Harman, “Aging: A Theory Based on Free Radical and Radiation Chemistry,” *J. Gerontol.*, vol. 11, no. 3, pp. 298–300, Jul. 1956.

[243] A. Grimm and A. Eckert, “Brain aging and neurodegeneration: from a mitochondrial point of view,” *J. Neurochem.*, vol. 143, no. 4, pp. 418–431, 2017.

[244] K. Leuner, W. E. Müller, and A. S. Reichert, “From mitochondrial dysfunction to amyloid beta formation: Novel insights into the pathogenesis of Alzheimer’s disease,” *Mol. Neurobiol.*, vol. 48, pp. 186–193, 2012.

[245] A. Bratic and N.-G. Larsson, “The role of mitochondria in aging,” *J. Clin. Invest.*, vol. 123, no. 3, pp. 951–957, 2013.

[246] R. Stefanatos and A. Sanz, “Mitochondrial complex I: A central regulator of the aging process,” *Cell Cycle*, vol. 10, no. 10, pp. 1528–1532, 2011..

[247] C. Venkateshappa, G. Harish, A. Mahadevan, M. M. Srinivas Bharath, and S. K. Shankar, “Elevated oxidative stress and decreased antioxidant function in the human hippocampus and frontal cortex with increasing age: Implications for neurodegeneration in Alzheimer’s disease,” *Neurochem. Res.*, vol. 37, no. 8, pp. 1601–1614, 2012.

[248] K. Leuner *et al.*, “Mitochondrial dysfunction: The first domino in brain aging and Alzheimer’s disease?,” *Antioxidants Redox Signal.*, vol. 9, no. 10, pp. 1659–1675, 2007.

[249] R. H. Swerdlow and S. M. Khan, “A ‘mitochondrial cascade hypothesis’ for sporadic Alzheimer’s disease,” *Med. Hypotheses*, vol. 63, no. 1, pp. 8–20, 2004.

[250] S. S. Bassett, D. Avramopoulos, and D. Fallin, “Evidence for parent of origin effect in late-onset Alzheimer disease,” *Am. J. Med. Genet.*, vol. 114, no. 6, pp. 679–686, 2002.

[251] S. D. Edland, J. M. Silverman, E. R. Peskind, D. Tsuang, E. Wijsman, and J. C. Morris, “Increased risk of dementia in mothers of Alzheimer’s disease cases,” *Neurology*, vol. 47, no. 1, pp. 254 LP – 256, Jul. 1996.

[252] L. Mosconi, V. Berti, R. H. Swerdlow, A. Pupi, R. Duara, and M. de Leon, “Maternal transmission of Alzheimer’s disease: Prodromal metabolic phenotype and the search for genes,” *Hum. Genomics*, vol. 4, no. 3, pp. 170–193, 2010.

[253] R. Egensberger, S. Kösel, N. M. Schnopp, P. Mehraein, and M. B. Graeber, “Association of the mitochondrial tRNA(A4336G) mutation with Alzheimer’s and Parkinson’s disease,” vol. 23, no. 4, pp. 315–321, 1997.

[254] M. Mancuso *et al.*, “May mitochondrial eve and mitochondrial haplogroups play a role in neurodegeneration and alzheimer’s disease?,” *Int. J. Alzheimers. Dis.*, vol. 2011, p. 11, 2011.

[255] A. Maruszak, J. A. Canter, M. Styczyńska, C. Żekanowski, and M. Barcikowska, “Mitochondrial haplogroup H and Alzheimer’s disease—Is there a connection?,”

Neurobiol. Aging, vol. 30, no. 11, pp. 1749–1755, 2009.

[256] A. Lakatos *et al.*, “Association between mitochondrial DNA variations and Alzheimer’s disease in the ADNI cohort,” *Neurobiol. Aging*, vol. 31, no. 8, pp. 1355–1363, 2010.

[257] S. M. Cardoso, I. Santana, R. H. Swerdlow, and C. R. Oliveira, “Mitochondria dysfunction of Alzheimer’s disease cybrids enhances Aβ toxicity,” *J. Neurochem.*, vol. 89, no. 6, pp. 1417–1426, 2004.

[258] D. F. Silva *et al.*, “Bioenergetic flux, mitochondrial mass and mitochondrial morphology dynamics in AD and MCI cybrid cell lines,” *Hum. Mol. Genet.*, vol. 22, no. 19, pp. 3931–3946, 2013.

[259] Y. Michikawa, F. Mazzucchelli, N. Bresolin, G. Scarlato, and G. Attardi, “Aging-dependent large accumulation of point mutations in the human mtDNA control region for replication,” *Science (80-.).*, vol. 286, no. 5440, pp. 774–779, 1999.

[260] M. T. Lin, D. K. Simon, C. H. Ahn, L. M. Kim, and M. Flint Beal, “High aggregate burden of somatic mtDNA point mutations in aging and Alzheimer’s disease brain,” *Hum. Mol. Genet.*, vol. 11, no. 2, pp. 133–145, 2002.

[261] Y. Joh and W.-S. Choi, “Mitochondrial Complex I Inhibition Accelerates Amyloid Toxicity,” *Dev. Reprod.*, vol. 21, no. 4, pp. 417–424, 2017.

[262] D. Gabuzda, J. Busciglio, L. B. Chen, P. Matsudaira, and B. A. Yankner, “Inhibition of energy metabolism alters the processing of amyloid precursor protein and induces a potentially amyloidogenic derivative,” *J. Biol. Chem.*, vol. 269, no. 18, pp. 13623–13628, 1994.

[263] R. H. Swerdlow and S. J. B. T.-I. R. of N. Kish, “Mitochondria in Alzheimer’s disease,” *Int. Rev. Neurobiol.*, vol. 53, pp. 341–385, 2002.

[264] J. P. Blass, A. C. Baker, L. W. Wen Ko, and R. S. Black, “Induction of Alzheimer Antigens by an Uncoupler of Oxidative Phosphorylation,” *Arch. Neurol.*, vol. 47, no. 8, pp. 864–869, 1990.

[265] T. Szabados, C. Dul, K. Majtényi, J. Hargitai, Z. Pénzes, and R. Urbanics, “A chronic Alzheimer’s model evoked by mitochondrial poison sodium azide for pharmacological investigations,” *Behav. Brain Res.*, vol. 154, no. 1, pp. 31–40, 2004.

[266] A. Eckert *et al.*, “Oligomeric and fibrillar species of β-amyloid (Aβ42) both impair mitochondrial function in P301L tau transgenic mice,” *J. Mol. Med.*, vol. 86, no. 11, pp. 1255–1267, 2008.

[267] Y. Cheng and F. Bai, “The association of tau with mitochondrial dysfunction in Alzheimer’s disease,” *Front. Neurosci.*, vol. 12, no. MAR, pp. 2014–2019, 2018.

[268] C. Stockburger, S. H. Eckert, G. P. Eckert, K. Friedland, and W. E. Müller, “Mitochondrial Function, Dynamics, and Permeability Transition: A Complex Love Triangle as A Possible Target for the Treatment of Brain Aging and Alzheimer’s Disease,” *J. Alzheimer’s Dis.*, vol. 64, no. s1, pp. S455–S467, 2018.

[269] M. Guglielmotto *et al.*, “The up-regulation of BACE1 mediated by hypoxia and ischemic injury: Role of oxidative stress and HIF1α,” *J. Neurochem.*, vol. 108, no. 4, pp. 1045–1056, 2009.

[270] M. Kaido *et al.*, “Alzheimer-type pathology in a patient with mitochondrial myopathy, encephalopathy, lactic acidosis and stroke-like episodes (MELAS),” *Acta Neuropathol.*, vol. 92, no. 3, pp. 312–318, 1996.

[271] T. Carell *et al.*, “Structure and Function of Noncanonical Nucleobases,” vol. 51, no. 29, pp. 7110–7131, 2012.

[272] Y. Zhang, L. Lu, and X. Li, “Detection technologies for RNA modifications,” *Exp. Mol. Med.*, vol. 54, no. 10, pp. 1601–1616, 2022.

[273] V. F. Reichle, D. P. Petrov, V. Weber, K. Jung, and S. Kellner, “NAIL-MS reveals the repair of 2-methylthiocytidine by AlkB in E. coli,” *Nat. Commun.*, vol. 10, no. 1, 2019.

[274] B. Il Kang *et al.*, “Identification of 2-methylthio cyclic N6-threonylcarbamoyladenosine (ms2ct6A) as a novel RNA modification at position 37 of tRNAs,” *Nucleic Acids Res.*, vol. 45, no. 4, pp. 2124–2136, 2017.

[275] Y. Sugio, R. Yamagami, N. Shigi, and H. Hori, “A selective and sensitive detection system for 4-thiouridine modification in RNA,” *RNA*, 2022.

[276] P. A. Limbach, P. F. Crain, and J. A. Mccloskey, “Summary: The modified nucleosides of RNA,” *Nucleic Acids Res.*, vol. 22, no. 12, pp. 2183–2196, 1994.

[277] Y. Motorin and M. Helm, “RNA nucleotide methylation: 2021 update,” *Wiley Interdiscip. Rev. RNA*, vol. 13, no. 1, pp. 1–37, 2022.

[278] X. Yang *et al.*, “N6-methyladenine modification in noncoding RNAs and its function in cancer,” *Biomark. Res.*, vol. 8, no. 1, pp. 1–12, 2020.

[279] M. Helm *et al.*, “The presence of modified nucleotides is required for cloverleaf folding of a human mitochondrial tRNA,” *Nucleic Acids Res.*, vol. 26, no. 7, pp. 1636–1643, 1998.

[280] I. A. Roundtree, M. E. Evans, T. Pan, and C. He, “Dynamic RNA Modifications in Gene Expression Regulation,” *Cell*, vol. 169, no. 7, pp. 1187–1200, 2017.

[281] M. Taoka *et al.*, “Landscape of the complete RNA chemical modifications in the human 80S ribosome,” *Nucleic Acids Res.*, vol. 46, no. 18, pp. 9289–9298, 2018.

[282] F. Richter *et al.*, “RNA marker modifications reveal the necessity for rigorous preparation protocols to avoid artifacts in epitranscriptomic analysis,” *Nucleic Acids Res.*, vol. 50, no. 8, pp. 4201–4215, 2021.

[283] M. Helm, R. Giegé, and C. Florentz, “A Watson-Crick base-pair-disrupting methyl group (m1A9) is sufficient for cloverleaf folding of human mitochondrial tRNA(Lys),” *Biochemistry*, vol. 38, no. 40, pp. 13338–13346, 1999.

[284] K. E. Sloan, A. S. Warda, S. Sharma, K. D. Entian, D. L. J. Lafontaine, and M. T. Bohnsack, “Tuning the ribosome: The influence of rRNA modification on eukaryotic ribosome biogenesis and function,” *RNA Biol.*, vol. 14, no. 9, pp. 1138–1152, 2017.

[285] L.-S. Zhang *et al.*, “Transcriptome-wide mapping of internal N7-methylguanosine methylome in mammalian messenger RNA,” *Mol. Cell*, vol. 74, no. 6, pp. 1304–1316, 2019.

[286] H. Shen *et al.*, “TET-mediated 5-methylcytosine oxidation in tRNA promotes translation,” *J. Biol. Chem.*, vol. 296, p. 100087, 2021.

[287] N. Jonkhout, J. Tran, M. A. Smith, N. Schonrock, J. S. Mattick, and E. M. Novoa, “The RNA modification landscape in human disease,” *RNA*, vol. 23, no. 12, pp. 1754–1769, 2017.

[288] B. S. Zhao, I. A. Roundtree, and C. He, “Post-transcriptional gene regulation by mRNA modfications,” *Nat Rev Mol Cell Biol.*, vol. 176, no. 1, pp. 100–106, 2017.

[289] H. Chen *et al.*, “Research Progress for RNA Modifications in Physiological and Pathological Angiogenesis,” *Front. Genet.*, vol. 13, no. July, pp. 1–14, 2022.

[290] Z. Yang *et al.*, “RNA Modifications Meet Tumors,” *Cancer Manag. Res.*, vol. 14, no.

November, pp. 3223–3243, 2022.

[291] X. Zhang *et al.*, “RNA Modifications in Gastrointestinal Cancer : Current Status and Future Perspectives,” *Biomedicines*, vol. 10, no. 1918, pp. 1–15, 2022.

[292] L. Cui *et al.*, “RNA modifications: importance in immune cell biology and related diseases,” *Signal Transduct. Target. Ther.*, no. June, 2022.

[293] M. D. Metodiev *et al.*, “Recessive Mutations in TRMT10C Cause Defects in Mitochondrial RNA Processing and Multiple Respiratory Chain Deficiencies,” *Am. J. Hum. Genet.*, vol. 98, no. 5, pp. 993–1000, 2016.

[294] D. Gillis, A. Krishnamohan, B. Yaacov, A. Shaag, J. E. Jackman, and O. Elpeleg, “TRMT10A dysfunction is associated with abnormalities in glucose homeostasis, short stature and microcephaly,” *J. Med. Genet.*, vol. 51, no. 9, pp. 581–586, 2014.

[295] D. B. Dunn, “The occurrence of 1-methyladenine in ribunucleic acid,” *Biochim. Bioph*, vol. 46, no. 1, pp. 198–200, 1959.

[296] D. B. Dunn, “isolation of 1-methyladenylic acid and 7-methylguanylic acid from ribonucleic acid,” in *Biochemical Journal*, 1963, vol. 86, no. 3, p. 14.

[297] C. Zhang and G. Jia, “Reversible RNA Modification N1-methyladenosine (m1A) in mRNA and tRNA,” *Genomics, Proteomics Bioinforma.*, vol. 16, no. 3, pp. 155–161, 2018.

[298] J. B. Macon and R. Wolfenden, “1-Methyladenosine. Dimroth Rearrangement and Reversible Reduction,” *Biochemistry*, vol. 7, no. 10, pp. 3453–3458, 1968.

[299] H. Zhou *et al.*, “m1A and m1G disrupt A-RNA structure through the intrinsic instability of Hoogsteen base pairs,” *Nat. Struct. Mol. Biol.*, vol. 23, no. 9, pp. 803–810, 2016.

[300] J. C. Delaney and J. M. Essigmann, “Mutagenesis, genotoxicity, and repair of 1-methyladenine, 3-alkylcytosines, 1-methylguanine, and 3-methylthymine in alkB Escherichia coli,” *Proc. Natl. Acad. Sci. U. S. A.*, vol. 101, no. 39, pp. 14051–14056, 2004.

[301] X. Zhang, A. E. Cozen, Y. Liu, Q. Chen, and T. M. Lowe, “Small RNA Modifications: Integral to Function and Disease,” *Trends Mol. Med.*, vol. 22, no. 12, pp. 1025–1034, 2016.

[302] S. Werner *et al.*, “Machine learning of reverse transcription signatures of variegated polymerases allows mapping and discrimination of methylated purines in limited transcriptomes.,” *Nucleic Acids Res.*, vol. 48, no. 7, pp. 3734–3746, 2020.

[303] S. Oerum, C. Dégut, P. Barraud, and C. Tisné, “m1A post-transcriptional modification in tRNAs,” *Biomolecules*, vol. 7, no. 1, pp. 1–15, 2017.

[304] H. Shima and K. Igarashi, “N 1-methyladenosine (m1A) RNA modification: the key to ribosome control,” *J. Biochem.*, pp. 1–5, 2020.

[305] V. A. Arzumanian, G. V. Dolgalev, I. Y. Kurbatov, O. I. Kiseleva, and E. V. Poverennaya, “Epitranscriptome: Review of Top 25 Most-Studied RNA Modifications,” *Int. J. Mol. Sci.*, vol. 23, no. 22, p. 13851, 2022.

[306] H. Jin, C. Huo, T. Zhou, and S. Xie, “m1A RNA Modification in Gene Expression Regulation,” *Genes (Basel).*, vol. 13, no. 5, p. 910, 2022.

[307] T. Suzuki *et al.*, “Complete chemical structures of human mitochondrial tRNAs,” *Nat. Commun.*, vol. 11, no. 1, pp. 1–15, 2020.

[308] S. Sharma *et al.*, “A single N1-methyladenosine on the large ribosomal subunit rRNA

impacts locally its structure and the translation of key metabolic enzymes," *Sci. Rep.*, vol. 8, no. 1, pp. 1–16, 2018.

[309] D. Bar-Yaacov *et al.*, "Mitochondrial 16S rRNA Is Methylated by tRNA Methyltransferase TRMT61B in All Vertebrates," *PLoS Biol.*, vol. 14, no. 9, pp. 1–21, 2016.

[310] X. Li *et al.*, "Transcriptome-wide mapping reveals reversible and dynamic N1-methyladenosine methylome," *Nat. Chem. Biol.*, vol. 12, no. 5, pp. 311–316, 2016.

[311] D. Dominissini *et al.*, "The dynamic N1-methyladenosine methylome in eukaryotic messenger RNA," *Nature*, vol. 530, 2016.

[312] M. Safra *et al.*, "The m1A landscape on cytosolic and mitochondrial mRNA at single-base resolution," *Nature*, vol. 551, pp. 251–257, 2017.

[313] A. V. Grozhik, A. O. Olarerin-George, M. Sindelar, X. Li, S. S. Gross, and S. R. Jaffrey, "Antibody cross-reactivity accounts for widespread appearance of m1A in 5'UTRs," *Nat. Commun.*, vol. 10, no. 1, pp. 1–13, 2019.

[314] M. Helm, F. Lyko, and Y. Motorin, "Limited antibody specificity compromises epitranscriptomic analyses," *Nat. Commun.*, vol. 10, no. 1, pp. 9–11, 2019.

[315] F. Voigts-Hoffmann *et al.*, "A methyl group controls conformational equilibrium in human mitochondrial tRNALys," *J. Am. Chem. Soc.*, vol. 129, no. 44, pp. 13382–13383, 2007.

[316] N. Horie *et al.*, "Two tRNA Species from an Extreme Thermophile, Thermus thermophilus HB8: Effect of 2-Thiolation of Ribothymidine on the Thermostability of tRNA†," *Biochemistry*, vol. 24, no. 21, pp. 5711–5715, 1985.

[317] J. Wei *et al.*, "Differential m6A, m6Am, and m1A Demethylation Mediated by FTO in Cell Nucleus and Cytoplasm," *Mol Cell.*, vol. 71, no. 6, pp. 973–985, 2018.

[318] C. T. Y. Chan, M. Dyavaiah, M. S. DeMott, K. Taghizadeh, P. C. Dedon, and T. J. Begley, "A quantitative systems approach reveals dynamic control of tRNA modifications during cellular stress," *PLoS Genet.*, vol. 6, no. 12, pp. 1–9, 2010.

[319] J. Anderson *et al.*, "The essential Gcd10p-Gcd14p nuclear complex 15 required for 1-methyladenosine modification and maturation of initiator methionyl-tRNA," *Genes Dev.*, vol. 12, no. 23, pp. 3650–3662, 1998.

[320] J. Anderson, L. Phan, and A. G. Hinnebusch, "The Gcd10p/Gcd14p complex is the essential two-subunit tRNA(1-methyladenosine) methyltransferase of Saccharomyces cerevisiae," *Proc. Natl. Acad. Sci. U. S. A.*, vol. 97, no. 10, pp. 5173–5178, 2000.

[321] S. Ozanick, A. Krecic, J. Andersland, and J. T. Anderson, "The bipartite structure of the tRNA m1A58 methyltransferase from S. cerevisiae is conserved in humans," *RNA*, vol. 11, no. 8, pp. 1281–1290, 2005.

[322] B. Xu, D. Liu, Z. Wang, R. Tian, and Y. Zuo, "Multi-substrate selectivity based on key loops and non-homologous domains: new insight into ALKBH family," *Cell. Mol. Life Sci.*, vol. 78, no. 1, pp. 129–141, 2021.

[323] S. Sharma, P. Watzinger, P. Kötter, and K. D. Entian, "Identification of a novel methyltransferase, Bmt2, responsible for the N-1-methyl-adenosine base modification of 25S rRNA in Saccharomyces cerevisiae," *Nucleic Acids Res.*, vol. 41, no. 10, pp. 5428–5443, 2013.

[324] T. Waku *et al.*, "NML-mediated rRNA base methylation links ribosomal subunit formation to cell proliferation in a p53-dependent manner," *J. Cell Sci.*, vol. 129, no. 12, pp. 2382–2393, 2016.

[325] Q. Zheng *et al.*, "Cytoplasmic m1A reader YTHDF3 inhibits trophoblast invasion by

downregulation of m1A-methylated IGF1R," *Cell Discov.*, vol. 6, no. 1, pp. 1–12, 2020.

[326] S. Xie *et al.*, "Programmable RNA N1-Methyladenosine Demethylation by a Cas13d-Directed Demethylase," *Angew. Chemie - Int. Ed.*, vol. 60, no. 36, pp. 19592–19597, 2021.

[327] X. Dai, T. Wang, G. Gonzalez, and Y. Wang, "Identification of YTH Domain-Containing Proteins as the Readers for N1-Methyladenosine in RNA," *Anal. Chem.*, vol. 90, no. 11, pp. 6380–6384, 2018.

[328] K. W. Seo and R. E. Kleiner, "YTHDF2 Recognition of N1-Methyladenosine (m1A)-Modified RNA Is Associated with Transcript Destabilization," *ACS Chem. Biol.*, vol. 15, no. 1, pp. 132–139, 2020.

[329] E. Vilardo, C. Nachbagauer, A. Buzet, A. Taschner, J. Holzmann, and W. Rossmanith, "A subcomplex of human mitochondrial RNase P is a bifunctional methyltransferase-extensive moonlighting in mitochondrial tRNA biogenesis," *Nucleic Acids Res.*, vol. 40, no. 22, pp. 11583–11593, 2012.

[330] T. Chujo and T. Suzuki, "Trmt61B is a methyltransferase responsible for 1-methyladenosine at position 58 of human mitochondrial tRNAs," *Rna*, vol. 18, no. 12, pp. 2269–2276, 2012.

[331] L. Kawarada, T. Suzuki, T. Ohira, S. Hirata, K. Miyauchi, and T. Suzuki, "ALKBH1 is an RNA dioxygenase responsible for cytoplasmic and mitochondrial tRNA modifications," *Nucleic Acids Res.*, vol. 45, no. 12, pp. 7401–7415, 2017.

[332] L. S. Zhang *et al.*, "ALKBH7-mediated demethylation regulates mitochondrial polycistronic RNA processing," *Nat. Cell Biol.*, vol. 23, no. 7, pp. 684–691, 2021.

[333] C. Legrand *et al.*, "Statistically robust methylation calling for wholetranscriptome bisulfite sequencing reveals distinct methylation patterns for mouse RNAs," *Genome Res.*, vol. 27, no. 9, pp. 1589–1596, 2017.

[334] S. Zaccara, R. J. Ries, and S. R. Jaffrey, "Reading, writing and erasing mRNA methylation," *Nat. Rev. Mol. Cell Biol.*, vol. 20, no. 10, pp. 608–624, 2019.

[335] M. Xue *et al.*, "MFAP2, upregulated by m1A methylation, promotes colorectal cancer invasiveness via CLK3," *Cancer Med.*, vol. 00, no. December, pp. 1–12, 2022.

[336] Y. Wu, Z. Chen, G. Xie, H. Zhang, and Z. Wang, "RNA m1A methylation regulates glycolysis of cancer cells through modulating ATP5D," *PNAS*, vol. 119, no. 28, pp. 1–12, 2022.

[337] E. N. Thomas, K. Q. Kim, E. P. McHugh, T. Marcinkiewicz, and H. S. Zaher, "Alkylative damage of mRNA leads to ribosome stalling and rescue by trans translation in bacteria," *Elife*, vol. 9, pp. 1–24, 2020.

[338] T. P. Hoernes *et al.*, "Eukaryotic translation elongation is modulated by single natural nucleotide derivatives in the coding sequences of mRNAs," *Genes (Basel).*, vol. 10, no. 2, pp. 1–12, 2019.

[339] W. Kuang *et al.*, "ALKBH3-dependent m1A demethylation of Aurora A mRNA inhibits ciliogenesis," *Cell Discov.*, vol. 8, no. 1, 2022.

[340] H. H. Woo and S. K. Chambers, "Human ALKBH3-induced m1A demethylation increases the CSF-1 mRNA stability in breast and ovarian cancer cells," *Biochim. Biophys. Acta - Gene Regul. Mech.*, vol. 1862, no. 1, pp. 35–46, 2019.

[341] X. Li *et al.*, "Base-Resolution Mapping Reveals Distinct m1A Methylome in Nuclear- and Mitochondrial-Encoded Transcripts," *Mol. Cell*, vol. 68, no. 5, pp. 993–1005, 2017.

[342] S. Schwartz, “m1A within cytoplasmic mRNAs at single nucleotide resolution: A reconciled transcriptome-wide map,” *RNA*, vol. 24, no. 11, pp. 1427–1436, 2018.

[343] M. Alriquet *et al.*, “The protective role of m1A during stress-induced granulation,” *J. Mol. Cell Biol.*, vol. 0, no. 0, pp. 1–11, 2020.

[344] Z. Jiapaer *et al.*, “Regulation and roles of RNA modifications in aging-related diseases,” *Aging Cell*, vol. 21, no. 7, 2022.

[345] F. Zhao *et al.*, “METTL3-dependent RNA m6A dysregulation contributes to neurodegeneration in Alzheimer’s disease through aberrant cell cycle events,” *Mol. Neurodegener.*, vol. 16, no. 1, pp. 1–25, 2021.

[346] Y. Hu, J. Chen, and Y. Wang, “FTO alleviates Aß 1-40 induced retinal pigment epithelium degeneration via PKA / CREB signaling pathway,” *Res. Sq.*, vol. 10, pp. 1–27, 2020.

[347] R. Zhang, Y. Zhang, F. Guo, S. Li, and H. Cui, “RNA N6-Methyladenosine Modifications and Its Roles in Alzheimer’s Disease,” *Front. Cell. Neurosci.*, vol. 16, no. March, pp. 1–14, 2022.

[348] H. Huang, J. Camats-Perna, R. Medeiros, V. Anggono, and J. Widagdo, “Altered expression of the m6A methyltransferase METTL3 in Alzheimer’s disease,” *eNeuro*, vol. 7, no. 5, pp. 1–10, 2020, doi: 10.1523/ENEURO.0125-20.2020.

[349] H. Li *et al.*, “FTO is involved in Alzheimer’s disease by targeting TSC1-mTOR-Tau signaling,” *Biochem. Biophys. Res. Commun.*, vol. 498, no. 1, pp. 234–239, 2018.

[350] A. M. Shafik *et al.*, “N6-methyladenosine dynamics in neurodevelopment and aging, and its potential role in Alzheimer’s disease,” *Genome Biol.*, vol. 22, no. 1, pp. 1–19, 2021.

[351] Z. Cockova, O. Honc, P. Telensky, M. J. Olsen, and J. Novotny, “Streptozotocin-Induced Astrocyte Mitochondrial Dysfunction Is Ameliorated by FTO Inhibitor MO-I-500,” *ACS Chem. Neurosci.*, vol. 12, no. 20, pp. 3818–3828, Oct. 2021.

[352] T. Zhao, X. Li, D. Sun, and Z. Zhang, “Oxidative stress: One potential factor for arsenite-induced increase of N6-methyladenosine in human keratinocytes,” *Environ. Toxicol. Pharmacol.*, vol. 69, pp. 95–103, 2019.

[353] Y. Fu and X. Zhuang, “m6A-binding YTHDF proteins promote stress granule formation,” *Nat. Chem. Biol.*, vol. 16, no. 9, pp. 955–963, 2020.

[354] I. Livneh, S. Moshitch-Moshkovitz, N. Amariglio, G. Rechavi, and D. Dominissini, “The m6A epitranscriptome: transcriptome plasticity in brain development and function,” *Nat. Rev. Neurosci.*, vol. 21, no. January, 2019.

[355] A. M. Shafik, H. Zhou, J. Lim, B. Dickinson, and P. Jin, “Dysregulated mitochondrial and cytosolic tRNA m1A methylation in Alzheimer’s disease,” *Hum. Mol. Genet.*, vol. 00, no. 00, pp. 1–8, 2022.

[356] S. Sekar and W. Liang, “Alzheimer’s disease is associated with altered expression of genes involved in immune response and mitochondrial processes in astrocytes,” *Bone*, vol. 23, no. 1, pp. 1–7, 2008.

[357] X. Zhang *et al.*, “Small RNA modifications in Alzheimer’s disease,” *Neurobiol. Dis.*, vol. 145, no. August, p. 105058, 2020.

[358] K. Khermesh *et al.*, “Reduced levels of protein recoding by A-to-I RNA editing in Alzheimer’s disease,” *RNA*, vol. 22, no. 2, pp. 290–302, 2016.

[359] J. Holzmann, P. Frank, E. Löffler, K. L. Bennett, C. Gerner, and W. Rossmanith, “RNase P without RNA: Identification and Functional Reconstitution of the Human Mitochondrial

tRNA Processing Enzyme," *Cell*, vol. 135, no. 3, pp. 462–474, 2008.

[360] A. Bhatta, C. Dienemann, P. Cramer, and H. S. Hillen, "Structural basis of RNA processing by human mitochondrial RNase P," *Nat. Struct. Mol. Biol.*, vol. 28, no. 9, pp. 713–723, 2021.

[361] S. R. Bacman, P. A. Gammage, M. Minczuk, and C. T. Moraes, "Chapter 19 - Manipulation of mitochondrial genes and mtDNA heteroplasmy," in *Mitochondria, 3rd Edition*, vol. 155, L. A. Pon and E. A. B. T.-M. in C. B. Schon, Eds. Academic Press, 2020, pp. 441–487.

[362] S. Oerum *et al.*, "Structural insight into the human mitochondrial tRNA purine N1-methyltransferase and ribonuclease P complexes," *J. Biol. Chem.*, vol. 293, no. 33, pp. 12862–12876, 2018.

[363] L. Reinhard, S. Sridhara, and B. M. Hällberg, "The MRPP1/MRPP2 complex is a tRNA-maturation platform in human mitochondria," *Nucleic Acids Res.*, vol. 45, no. 21, pp. 12469–12480, 2017.

[364] L. K. Brzezniak, M. Bijata, R. J. Szczesny, and P. P. Stepien, "Involvement of human ELAC2 gene product in 3′ end processing of mitochondrial tRNAs," *RNA Biol.*, vol. 8, no. 4, pp. 616–626, 2011,.

[365] V. Anantharaman, E. V Koonin, and L. Aravind, "SPOUT: a class of methyltransferases that includes spoU and trmD RNA methylase superfamilies, and novel superfamilies of predicted prokaryotic RNA methylases," *J. Mol. Microbiol. Biotechnol.*, vol. 4, no. 1, pp. 71–75, 2002.

[366] H. Hori, "Transfer RNA methyltransferases with a SpoU-TrmD (SPOUT) fold and their modified nucleosides in tRNA," *Biomolecules*, vol. 7, no. 1, pp. 1–24, 2017.

[367] K. L. Tkaczuk, S. Dunin-Horkawicz, E. Purta, and J. M. Bujnicki, "Structural and evolutionary bioinformatics of the SPOUT superfamily of methyltransferases," *BMC Bioinformatics*, vol. 8, 2007.

[368] M. A. Kurowski, J. M. Sasin, M. Feder, J. Debski, and J. M. Bujnicki, "Characterization of the cofactor-binding site in the SPOUT-fold methyltransferases by computational docking of S-adenosylmethionine to three crystal structures," *BMC Bioinformatics*, vol. 4, pp. 1–11, 2003.

[369] B. Van Laer *et al.*, "Structural and functional insights into tRNA binding and adenosine N1-methylation by an archaeal Trm10 homologue," *Nucleic Acids Res.*, vol. 44, no. 2, pp. 940–953, 2016.

[370] Z. Shao *et al.*, "Crystal structure of tRNA m1G9 methyltransferase Trm10: Insight into the catalytic mechanism and recognition of tRNA substrate," *Nucleic Acids Res.*, vol. 42, no. 1, pp. 509–525, 2014.

[371] W. Swinehart, J. C. Henderson, and J. E. Jackman, "tRNA substrate recognition by the yeast m1G9 methyltransferase," *RNA*, vol. 19, no. 8, pp. 9–10, 2013.

[372] E. Vilardo, F. Amman, U. Toth, A. Kotter, M. Helm, and W. Rossmanith, "Functional characterization of the human tRNA methyltransferases TRMT10A and TRMT10B," *Nucleic Acids Res.*, vol. 48, no. 11, pp. 6157–6169, 2020.

[373] W. E. Swinehart and J. E. Jackman, "Diversity in mechanism and function of tRNA methyltransferases," *RNA Biol.*, vol. 12, no. 4, pp. 398–411, 2015.

[374] J. E. Jackman, R. K. Montange, H. S. Malik, and E. M. Phizicky, "Identification of the yeast gene encoding the tRNA m1G methyltransferase responsible for modification at position 9," *RNA*, vol. 9, no. 5, pp. 574–585, 2003.

[375] M. Igoillo-Esteve *et al.*, “tRNA Methyltransferase Homolog Gene TRMT10A Mutation in Young Onset Diabetes and Primary Microcephaly in Humans,” *PLoS Genet.*, vol. 9, no. 10, 2013.

[376] A. Zung, M. Kori, E. Burundukov, T. Ben-Yosef, Y. Tatoor, and E. Granot, “Homozygous deletion of TRMT10A as part of a contiguous gene deletion in a syndrome of failure to thrive, delayed puberty, intellectual disability and diabetes mellitus,” *Am. J. Med. Genet. Part A*, vol. 167, no. 12, pp. 3167–3173, 2015.

[377] M. Narayanan *et al.*, “Case Report: Compound heterozygous nonsense mutations in TRMT10A are associated with microcephaly, delayed development, and periventricular white matter hyperintensities,” *F1000Research*, vol. 4, no. 0, 2015.

[378] T. W. Yew, L. McCreight, K. Colclough, S. Ellard, and E. R. Pearson, “tRNA methyltransferase homologue gene TRMT10A mutation in young adult-onset diabetes with intellectual disability, microcephaly and epilepsy,” *Diabet. Med.*, vol. 33, no. 9, pp. e21–e25, 2016.

[379] H. J. Ahn, H. W. Kim, H. J. Yoon, B. Il Lee, S. W. Suh, and J. K. Yang, “Crystal structure of tRNA (m1G37) methyltransferase: Insights into tRNA recognition,” *EMBO J.*, vol. 22, no. 11, pp. 2593–2603, 2003,.

[380] P. A. Elkins *et al.*, “Insights into Catalysis by a Knotted TrmD tRNA Methyltransferase,” *J. Mol. Biol.*, vol. 333, no. 5, pp. 931–949, 2003.

[381] A. R. D’Souza and M. Minczuk, “Mitochondrial transcription and translation: overview,” *Essays Biochem.*, vol. 62, no. 3, pp. 309–320, 2018.

[382] B. P. Klemm *et al.*, “The diversity of ribonuclease P: Protein and RNA catalysts with analogous biological functions,” *Biomolecules*, vol. 6, no. 2, 2016.

[383] A. Karasik, C. A. Fierke, and M. Koutmos, “Interplay between substrate recognition, 5’ end tRNA processing and methylation activity of human mitochondrial RNase P,” *RNA*, vol. 25, pp. 1646–1660, 2019.

[384] L. Reinhard, S. Sridhara, and B. M. Hällberg, “Structure of the nuclease subunit of human mitochondrial RNase P,” *Nucleic Acids Res.*, vol. 43, no. 11, pp. 5664–5672, 2015.

[385] W. Rossmanith and R. M. Karwan, “Characterization of Human Mitochondrial RNase P: Novel Aspects in tRNA Processing,” *Biochem. Biophys. Res. Commun.*, vol. 247, no. 2, pp. 234–241, 1998.

[386] I. Hochberg *et al.*, “Bi-allelic variants in the mitochondrial RNase P subunit PRORP cause mitochondrial tRNA processing defects and pleiotropic multisystem presentations,” *Am. J. Hum. Genet.*, vol. 108, no. 11, pp. 2195–2204, 2021.

[387] A. Sen, A. Karasik, A. Shanmuganathan, E. Mirkovic, M. Koutmos, and R. T. Cox, “Loss of the mitochondrial protein-only ribonuclease P complex causes aberrant tRNA processing and lethality in Drosophila,” *Nucleic Acids Res.*, vol. 44, no. 13, pp. 6409–6422, 2016.

[388] S. Y. Yang, X. Y. He, and D. Miller, “Hydroxysteroid (17β) dehydrogenase X in human health and disease,” *Mol. Cell. Endocrinol.*, vol. 343, no. 1–2, pp. 1–6, 2011.

[389] S. Y. Yang, X. Y. He, C. Isaacs, C. Dobkin, D. Miller, and M. Philipp, “Roles of 17β-hydroxysteroid dehydrogenase type 10 in neurodegenerative disorders,” *J. Steroid Biochem. Mol. Biol.*, vol. 143, pp. 460–472, 2014.

[390] X. Y. He, J. Wegiel, and S. Y. Yang, “Intracellular oxidation of allopregnanolone by human brain type 10 17beta-hydroxysteroid dehydrogenase,” *Brain Res.*, vol. 1040, no.

1–2, pp. 29–35, 2005.

[391] A. Morsy and P. C. Trippier, “Amyloid-Binding Alcohol Dehydrogenase (ABAD) Inhibitors for the Treatment of Alzheimer’s Disease,” *J. Med. Chem.*, vol. 62, no. 9, pp. 4252–4264, 2019.

[392] J. W. Lustbader *et al.*, “ABAD Directly Links Aβ to Mitochondrial Toxicity in Alzheimer’s Disease,” *Science (80-.).*, vol. 304, no. 5669, pp. 448–452, 2004.

[393] S. Du Yan *et al.*, “Role of ERAB/L-3-hydroxyacyl-coenzyme A dehydrogenase type II activity in Aβ-induced cytotoxicity,” *J. Biol. Chem.*, vol. 274, no. 4, pp. 2145–2156, 1999.

[394] Y. A. Lim *et al.*, “Inhibition of the mitochondrial enzyme ABAD restores the amyloid-β-mediated deregulation of estradiol,” *PLoS One*, vol. 6, no. 12, 2011.

[395] J. Xie, R. Liang, Y. Wang, J. Huang, X. Cao, and B. Niu, “Progress in Target Drug Molecules for Alzheimer’s Disease,” *Curr. Top. Med. Chem.*, vol. 20, no. 1, pp. 4–36, 2019,.

[396] Z. Fišar *et al.*, “Effects of novel 17β-hydroxysteroid dehydrogenase type 10 inhibitors on mitochondrial respiration,” *Toxicol. Lett.*, vol. 339, pp. 12–19, 2021.

[397] K. Valaasani *et al.*, “Identification of Human ABAD Inhibitors for Rescuing Aβ-Mediated Mitochondrial Dysfunction,” *Curr. Alzheimer Res.*, vol. 11, no. 2, pp. 128–136, 2014.

[398] A. J. Deutschmann *et al.*, “Mutation or knock-down of 17β-hydroxysteroid dehydrogenase type 10 cause loss of MRPP1 and impaired processing of mitochondrial heavy strand transcripts,” *Hum. Mol. Genet.*, vol. 23, no. 13, pp. 3618–3628, 2014.

[399] S. Oerum *et al.*, “Novel patient missense mutations in the HSD17B10 gene affect dehydrogenase and mitochondrial tRNA modification functions of the encoded protein,” *Biochim. Biophys. Acta - Mol. Basis Dis.*, vol. 1863, no. 12, pp. 3294–3302, 2017.

[400] J. Zschocke, “HSD10 disease: clinical consequences of mutations in the HSD17B10 gene.” pp. 81–89, 2012.

[401] M. J. Falk *et al.*, “A novel HSD17B10 mutation impairing the activities of the mitochondrial Rnase P complex causes X-linked intractable epilepsy and neurodevelopmental regression,” *RNA Biol.*, vol. 13, no. 5, pp. 477–485, 2016.

[402] C. G. Camelo *et al.*, “Severe progressive brain involvement in a patient with TRMT10C mutation,” *Arq. Neuropsiquiatr.*, vol. 79, no. 3, pp. 259–260, 2021.

[403] P. Song *et al.*, “RNA modification writers influence tumor microenvironment in gastric cancer and prospects of targeted drug therapy,” *J. Bioinforma. omputational Biol.*, vol. 20, no. 2, pp. 1–24, 2022.

[404] B. Zhou *et al.*, “RNA modification writer expression profiles predict clinical outcomes and guide neoadjuvant immunotherapy in non-small cell lung cancer,” *eBioMedicine*, vol. 84, p. 104268, 2022.

[405] Q. Wang, Q. Zhang, Y. Huang, and J. Zhang, “m1A Regulator TRMT10C Predicts Poorer Survival and Contributes to Malignant Behavior in Gynecological Cancers,” *DNA Cell Biol.*, vol. 39, no. 10, pp. 1–12, 2020,.

[406] D. Shao *et al.*, “An m6A/m5C/m1A/m7G-Related Long Non-coding RNA Signature to Predict Prognosis and Immune Features of Glioma,” *Front. Genet.*, vol. 13, no. May, pp. 1–15, 2022.

[407] L. Gao, R. Chen, M. Sugimoto, M. Mizuta, Y. Kishimoto, and K. Omori, “The impact of m1A methylation modification patterns on tumor immune microenvironment and prognosis in oral squamous cell carcinoma,” *Int. J. Mol. Sci.*, vol. 22, no. 19, 2021.

[408] Q. Shi, C. Xue, X. Yuan, Y. He, and Z. Yu, “Gene signatures and prognostic values of m1A-related regulatory genes in hepatocellular carcinoma,” *Sci. Rep.*, vol. 10, no. 1, pp. 1–13, 2020.

[409] M. Mao, Q. Chu, Y. Lou, P. Lv, and L. Wang, “RNA N1-methyladenosine regulator-mediated methylation modification patterns and heterogeneous signatures in glioma,” *Front. Immnology*, no. July, pp. 1–15, 2022.

[410] S. Mao, Z. Chen, Y. Wu, H. Xiong, and X. Yuan, “Crosstalk of Eight Types of RNA Modification Regulators Defines Tumor Microenvironments, Cancer Hallmarks, and Prognosis of Lung Adenocarcinoma,” *J. Oncol.*, vol. 19, 2022.

[411] M. Saoji, A. Sen, and R. T. Cox, “Loss of individual mitochondrial ribonuclease P complex proteins differentially affects mitochondrial trna processing in vivo,” *Int. J. Mol. Sci.*, vol. 22, no. 11, 2021.

[412] L. C. Walker, *Amyloid beta plaques*, vol. 1, no. 31. 2020.

[413] N. N. Naseri, H. Wang, J. Guo, M. Sharma, and L. Wenjie, “The complexity of tau in Alzheimer’s disease,” *Neurosci. Lett.*, pp. 183–194, 2019.

[414] S. Asher and R. Priefer, “Alzheimer’s disease failed clinical trials,” *Life Sci.*, vol. 306, pp. 24–32, 2022.

[415] E. Karran and B. De Strooper, “The amyloid hypothesis in Alzheimer disease: new insights from new therapeutics,” *Nat. Rev. Drug Discov.*, vol. 21, no. 4, pp. 306–318, 2022.

[416] A. Zainab, “The mechanism of action of the controversial drug; aducanumab and the story behind its speedy approval,” *J. Pakistan Medicial Assoc.*, vol. 72, no. 5, p. 2022, 2022.

[417] G. Monzio Compagnoni, A. Di Fonzo, S. Corti, G. P. Comi, N. Bresolin, and E. Masliah, *The Role of Mitochondria in Neurodegenerative Diseases: the Lesson from Alzheimer’s Disease and Parkinson’s Disease*, vol. 57, no. 7. 2020.

[418] P. Corona *et al.*, “A Novel mtDNA Mutation in the ND5 Subunit of Complex I in Two MELAS patients,” *Ann. Neurol.*, vol. 49, no. 1, pp. 106–110, 2001.

[419] A. V. Grozhik and S. R. Jaffrey, “Shrinking maps of RNA modifications,” *Nature*, vol. 551, no. 7679, pp. 174–176, 2017.

[420] F. L. Graham, J. Smiley, W. C. Russell, and R. Nairn, “Characteristics of a human cell line transformed by DNA from human adenovirus type 5,” *J. Gen. Virol.*, vol. 36, no. 1, pp. 59–72, 1977.

[421] Y. C. Lin *et al.*, “Genome dynamics of the human embryonic kidney 293 lineage in response to cell biology manipulations,” *Nat. Commun.*, vol. 5, no. 11, 2014.

[422] A. Eckert *et al.*, “Elevated vulnerability to oxidative stress-induced cell death and activation of caspase-3 by the Swedish amyloid precursor protein mutation.pdf,” *J. Neurosci. Res.*, vol. 64, pp. 183–192, 2001.

[423] C. Brandscheid *et al.*, “Altered Gut Microbiome Composition and Tryptic Activity of the 5xFAD Alzheimer’s Mouse Model.,” *J. Alzheimers. Dis.*, vol. 56, no. 2, pp. 775–788, 2017.

[424] T. J. Montine, J. A. Sonnen, K. S. Montine, P. K. Crane, and E. B. Larson, “Adult Changes in Thought study: dementia is an individually varying convergent syndrome with prevalent clinically silent diseases that may be modified by some commonly used therapeutics.,” *Curr. Alzheimer Res.*, vol. 9, no. 6, pp. 718–23, 2012.

[425] J. A. Miller *et al.*, “Neuropathological and transcriptomic characteristics of the aged brain,” *Elife*, vol. 6, pp. 1–26, 2017.

[426] H. Mathys *et al.*, “Single-cell transcriptomic analysis of Alzheimer’s disease,” *Nature*, vol. 570, no. 7761, pp. 332–337, 2019.

[427] B. Guennewig *et al.*, “Defining early changes in Alzheimer’s disease from RNA sequencing of brain regions differentially affected by pathology,” *Sci. Rep.*, vol. 11, no. 1, pp. 1–15, 2021.

[428] A. M. Bolger, M. Lohse, and B. Usadel, “Trimmomatic: A flexible trimmer for Illumina sequence data,” *Bioinformatics*, vol. 30, no. 15, pp. 2114–2120, 2014.

[429] B. Langmead and S. L. Salzberg, “Fast gapped-read alignment with Bowtie 2,” *Nat. Methods*, vol. 9, no. 4, pp. 357–359, 2012.

[430] H. Li *et al.*, “The Sequence Alignment/Map format and SAMtools,” *Bioinformatics*, vol. 25, no. 16, pp. 2078–2079, 2009.

[431] J. T. Robinson *et al.*, “Integrative Genome Viewer,” *Nat. Biotechnol.*, vol. 29, no. 1, pp. 24–6, 2011.

[432] N. R. Sims and M. F. Anderson, “Isolation of mitochondria from rat brain using Percoll density gradient centrifugation,” *Nat. Protoc.*, vol. 3, no. 7, pp. 1228–1239, 2008.

[433] B. Ewing and P. Green, “Base-calling of automated sequencer traces using phred. II. Error probabilities,” *Genome Res. Ewing, B. Green, P. Base-calling Autom. Seq. traces using phred. II. Error Probab. Genome Res. 8, 186–194 (1998).*, vol. 8, no. 3, pp. 186–194, 1998.

[434] M. Waskom, “Seaborn: Statistical Data Visualization,” *J. Open Source Softw.*, vol. 6, no. 60, p. 3021, 2021.

[435] D. J. Selkoe *et al.*, “Beta-amyloid precursor protein of Alzheimer disease occurs as 110- to 135-kilodalton membrane-associated proteins in neural and nonneural tissues.,” *Proc. Natl. Acad. Sci.*, vol. 85, no. 19, pp. 7341–7345, 1988.

[436] H. Zhou and Y. Z. Wei Huang, Xiaoyan Lei, Geert Ridder, John Strauss, “Evolution of a Reverse Transcriptase to Map N1-Methyladenosine in Human mRNA,” *Physiol. Behav.*, vol. 176, no. 5, pp. 139–148, 2020.

[437] M. Kristen *et al.*, “Manganese ions individually alter the reverse transcription signature of modified ribonucleosides,” *Genes (Basel).*, vol. 11, no. 8, pp. 1–12, 2020.

[438] L. Schmidt *et al.*, “Graphical workflow system for modification calling by machine learning of reverse transcription signatures,” *Front. Genet.*, vol. 10, no. SEP, 2019.

[439] R. Hauenschild *et al.*, “The reverse transcription signature of N-1-methyladenosine in RNA-Seq is sequence dependent,” *Nucleic Acids Res.*, vol. 43, no. 20, pp. 9950–9964, 2015.

[440] D. Osorio and J. J. Cai, “Systematic determination of the mitochondrial proportion in human and mice tissues for single-cell RNA-sequencing data quality control,” *Bioinformatics*, vol. 37, no. 7, pp. 963–967, 2021.

[441] S. H. Eckert, J. Gaca, N. Kolesova, K. Friedland, G. P. Eckert, and W. E. Muller, “Mitochondrial pharmacology of dimebon (latrepirdine) calls for a new look at its possible therapeutic potential in alzheimer’s disease,” *Aging Dis.*, vol. 9, no. 4, pp. 729–744, 2018.

[442] C. Stockburger, C. Kurz, K. A. Koch, S. H. Eckert, K. Leuner, and W. E. Müller, “Improvement of mitochondrial function and dynamics by the metabolic enhancer

piracetam," *Biochem. Soc. Trans.*, vol. 41, no. 5, pp. 1331–1334, 2013.

[443] I. A. Chatzispyrou, N. M. Held, L. Mouchiroud, J. Auwerx, and R. H. Houtkooper, "Tetracycline antibiotics impair mitochondrial function and its experimental use confounds research," *Cancer Res.*, vol. 75, no. 21, pp. 4446–4449, 2015.

[444] R. H. Houtkooper *et al.*, "Mitonuclear protein imbalance as a conxerved longevity mechanism," *Nature*, vol. 497, no. 7450, pp. 451–457, 2013.

[445] D. Moechars *et al.*, "Early phenotypic changes in transgenic mice that overexpress different mutants of amyloid precursor protein in brain," *J. Biol. Chem.*, vol. 274, no. 10, pp. 6483–6492, 1999.

[446] S. Forner *et al.*, "Systematic phenotyping and characterization of the 5xFAD mouse model of Alzheimer's disease," *Sci. Data*, vol. 8, no. 1, pp. 1–16, 2021.

[447] N. A. Xiao *et al.*, "Reduction of glucose metabolism in olfactory bulb is an earlier Alzheimer's disease-related biomarker in 5XFAD mice," *Chin. Med. J. (Engl).*, vol. 128, no. 16, pp. 2220–2227, 2015.

[448] R. Kimura and M. Ohno, "Impairments in remote memory stabilization precede hippocampal synaptic and cognitive failures in 5XFAD Alzheimer mouse model," *Neurobiol. Dis.*, vol. 33, no. 2, pp. 229–235, 2009.

[449] M. Dos Santos Guilherme, N. M. Stoye, S. Rose-John, C. Garbers, A. Fellgiebel, and K. Endres, "The synthetic retinoid acitretin increases IL-6 in the central nervous system of Alzheimer disease model mice and human patients," *Front. Aging Neurosci.*, vol. 10, no. JUL, pp. 1–7, 201.

[450] L. Wang *et al.*, "Synaptosomal mitochondrial dysfunction in 5xFAD mouse model of Alzheimer's disease," *PLoS One*, vol. 11, no. 3, pp. 1–18, 2016.

[451] J. V. Andersen *et al.*, "Hippocampal disruptions of synaptic and astrocyte metabolism are primary events of early amyloid pathology in the 5xFAD mouse model of Alzheimer's disease," *Cell Death Dis.*, vol. 12, no. 11, p. 954, 2021.

[452] N. Sharma, R. Banerjee, and R. L. Davis, "Early Mitochondrial Defects in the 5xFAD mouse model of Alzheimer's Disease," *Res. Sq.*, 2022.

[453] G. Coughlan, J. Laczó, J. Hort, A. M. Minihane, and M. Hornberger, "Spatial navigation deficits — Overlooked cognitive marker for preclinical Alzheimer disease?," *Nat. Rev. Neurol.*, vol. 14, no. 8, pp. 496–506, 2018.

[454] A. J. Ehrenberg *et al.*, "Neuropathologic Correlates of Psychiatric Symptoms in Alzheimer's Disease," *J. Alzheimer's Dis.*, vol. 66, no. 1, pp. 115–126, 2018.

[455] C. Vogel and E. M. Marcotte, "Insights into the regulation of protein abundance from proteomic and transcriptomic analyses," *Nat. Rev. Genet.*, vol. 13, no. 4, pp. 227–232, 2012.

[456] R. de Sousa Abreu, L. O. Penalva, E. M. Marcotte, and C. Vogel, "Global signature of protein and mRNA expression levels," *Mol. Biosyst.*, vol. 5, no. 12, pp. 1512–1526, 2009.

[457] A. Koussounadis, S. P. Langdon, I. H. Um, D. J. Harrison, and V. A. Smith, "Relationship between differentially expressed mRNA and mRNA-protein correlations in a xenograft model system," *Sci. Rep.*, vol. 5, no. June, pp. 1–9, 2015.

[458] A. E. Cavanna and M. R. Trimble, "The precuneus: A review of its functional anatomy and behavioural correlates," *Brain*, vol. 129, no. 3, pp. 564–583, 2006.

[459] S. Brodt, D. Pöhlchen, V. L. Flanagin, S. Glasauer, S. Gais, and M. Schönauer, "Rapid

and independent memory formation in the parietal cortex," *Proc. Natl. Acad. Sci. U. S. A.*, vol. 113, no. 46, pp. 13251–13256, 2016.

[460] L. Zhaoping, "A new framework for understanding vision from the perspective of the primary visual cortex," *Curr. Opin. Neurobiol.*, vol. 58, no. Box 1, pp. 1–10, 2019.

[461] T. J. Montine *et al.*, "National institute on aging-Alzheimer's association guidelines for the neuropathologic assessment of Alzheimer's disease: A practical approach," *Acta Neuropathol.*, vol. 123, no. 1, pp. 1–11, 2012.

[462] Q. Lin, H. Ni, Z. Zheng, J. Zhong, and H. Nie, "Cross-talk of four types of RNA modification writers defines the immune microenvironment in severe asthma," *Ann. N. Y. Acad. Sci.*, pp. 1–11, 2022.

[463] Z. Qi *et al.*, "N1-Methyladenosine modification of mRNA regulates neuronal gene expression and oxygen glucose deprivation / reoxygenation induction," *CDDpress*, vol. 159, no. 1, 2023.

[464] V. H. Finder and R. Glockshuber, "Amyloid-β aggregation," *Neurodegener. Dis.*, vol. 4, no. 1, pp. 13–27, 2007.

[465] S. F. Lau, H. Cao, A. K. Y. Fu, and N. Y. Ip, "Single-nucleus transcriptome analysis reveals dysregulation of angiogenic endothelial cells and neuroprotective glia in Alzheimer's disease," *Proc. Natl. Acad. Sci. U. S. A.*, vol. 117, no. 41, pp. 25800–25809, 2020.

[466] A. Grubman *et al.*, "A single-cell atlas of entorhinal cortex from individuals with Alzheimer's disease reveals cell-type-specific gene expression regulation.," *Nat. Neurosci.*, vol. 22, no. December, 2019.

[467] X. L. Wang and L. Li, "Cell type-specific potential pathogenic genes and functional pathways in Alzheimer's Disease," *BMC Neurol.*, vol. 21, no. 1, pp. 1–18, 2021.

[468] Y. Kageyama *et al.*, "Amyloid β toxic conformer has dynamic localization in the human inferior parietal cortex in absence of amyloid plaques," *Sci. Rep.*, vol. 8, no. 1, pp. 1–17, 2018.

[469] C. R. Muratore *et al.*, "Cell-type Dependent Alzheimer's Disease Phenotypes: Probing the Biology of Selective Neuronal Vulnerability," *Stem Cell Reports*, 2017.

[470] E. Vilardo and W. Rossmanith, "Molecular insights into HSD10 disease: Impact of SDR5C1 mutations on the human mitochondrial RNase P complex," *Nucleic Acids Res.*, vol. 43, no. 10, pp. 5112–5119, 2015.

[471] S. Du Yan *et al.*, "An intracellular protein that binds amyloid-β peptide and mediates neurotoxicity in Alzheimer's disease," *Nature*, vol. 389, no. 6652, pp. 689–695, 1997.

[472] X. Y. He *et al.*, "Abundant type 10 17β-hydroxysteroid dehydrogenase in the hippocampus of mouse Alzheimer's disease model," *Mol. Brain Res.*, vol. 99, no. 1, pp. 46–53, 2002.

[473] T. S. Johnson *et al.*, "Combinatorial analyses reveal cellular composition changes have different impacts on transcriptomic changes of cell type specific genes in Alzheimer's Disease," *Sci. Rep.*, vol. 11, no. 1, pp. 1–19, 2021.

[474] F. Li, X. Liu, W. Zhou, X. Yang, and Y. Shen, "Auto-inhibitory mechanism of the human mitochondrial RNase P protein complex," *Sci. Rep.*, vol. 5, pp. 1–7, 2015.

[475] E. Vilardo and W. Rossmanith, "The Amyloid-β-SDR5C1(ABAD) Interaction Does Not Mediate a Specific Inhibition of Mitochondrial RNase P," *PLoS One*, vol. 8, no. 6, pp. 6–11, 2013.

[476] T. K. Silzer, G. A. Pathak, and N. R. Phillips, “Mitochondrial tRNA methylation in Alzheimer’s disease and progressive supranuclear palsy,” *BMC Med. Genomics*, vol. 13, no. 1, pp. 1–12, 2020.

[477] R. D. Hodge *et al.*, “Conserved cell types with divergent features in human versus mouse cortex,” *Nature*, vol. 573, no. 7772, pp. 61–68, 2019.

[478] L. Tserovski, V. Marchand, R. Hauenschild, F. Blanloeil-Oillo, M. Helm, and Y. Motorin, “High-throughput sequencing for 1-methyladenosine (m1A) mapping in RNA,” *Methods*, vol. 107, pp. 110–121, 2016.

[479] C. Wild-Bode *et al.*, “Intracellular Generation and Accumulation of Amyloid β-peptide terminating at Amino Acid 42,” *J. Biol. Chem.*, vol. 272, no. 26, pp. 16085–16088, 1997.

[480] M. Manczak, T. S. Anekonda, E. Henson, B. S. Park, J. Quinn, and P. Hemachandra Reddy, “Mitochondria are a direct site of Aβ accumulation in AD neurons; implications for free radical generation and oxidative damage.pdf,” *Hum. Mol. Genet.*, vol. 15, no. 9, pp. 1437–1449, 2006.

[481] J. Frackowiak *et al.*, “Secretion and accumulation of Alzheimer’s β-protein by cultured vascular smooth muscle cells from old and young dogs,” *Brain Res.*, vol. 676, no. 1, pp. 225–230, 1995.

[482] R. H. Swerdlow *et al.*, “Exploratory analysis of mtDNA haplogroups in two Alzheimer’s longitudinal cohorts,” *Alzheimer’s Dement.*, vol. 16, no. 8, pp. 1164–1172, 2020.

[483] B. Sathyamoorthy *et al.*, “Insights into Watson-Crick/Hoogsteen breathing dynamics and damage repair from the solution structure and dynamic ensemble of DNA duplexes containing m1A,” *Nucleic Acids Res.*, vol. 45, no. 9, pp. 5586–5601, 2017.

[484] S. Klinge and J. L. Woolford, “Ribosome assembly coming into focus,” *Nat. Rev. Mol. Cell Biol.*, vol. 20, no. 2, pp. 116–131, 2019.

[485] T. Budkevich *et al.*, “Structure and dynamics of the mammlian ribsomoal pre-translocation complex,” *Mol. Cell*, vol. 44, no. 2, pp. 214–224, 2011.

[486] D. R. Thal, U. Rüb, M. Orantes, and H. Braak, “Phases of Aß-deposition in the human brain and its relevance for the development of AD,” *Neurology*, vol. 58, no. 12, pp. 1791–800, 2002.

[487] P. V. Arriagada, J. H. Growdon, E. T. Hedley-Whyte, and B. T. Hyman, “Neurofibrillary tangles but not senile plaques parallel duration and severity of Alzheimer’s disease,” *Neurology*, vol. 42, no. 3, pp. 631–639, 1992.

[488] H. Braak and E. Braak, “The human entorhinal cortex: normal morphology and lamina-specific pathology in various diseases,” *Neurosci. Res.*, vol. 15, no. 1–2, pp. 6–31, 1992.

[489] S. E. Arnold, B. T. Hyman, J. Flory, A. R. Damasio, and G. W. Van Hoesen, “The Topographical and Neuroanatomical Distribution of Neurofibrillary Tangles and Neuritic Plaques in the Cerebral Cortex of Patients with Alzheimer’s Disease,” *Cereb. Cortex*, vol. 1, no. 1, pp. 103–116, Jan. 1991.

[490] J. Ziontz *et al.*, “Tau pathology in cognitively normal older adults,” *Alzheimer’s Dement. Diagnosis, Assess. Dis. Monit.*, vol. 11, pp. 637–645, 2019.

[491] C. Bouras, P. R. Hof, P. Giannakopoulos, J. P. Michel, and J. H. Morrison, “Regional distribution of neurofibrillary tangles and senile plaques in the cerebral cortex of elderly patients: A quantitative evaluation of a one-year autopsy population from a geriatric hospital,” *Cereb. Cortex*, vol. 4, no. 2, pp. 138–150, 1994.

[492] Q. Daoming and K. Fredrick, “Chapter Eight - Analysis of Polysomes from Bacteria,” *Methods Enzymol.*, vol. 530, pp. 159–172, 2013.

[493] H. Yoshikawa *et al.*, “Efficient analysis of mammalian polysomes in cells and tissues using ribo mega-SEC,” *Elife*, vol. 7, pp. 1–26, 2018.

[494] J. Hirst, J. Carroll, I. M. Fearnley, R. J. Shannon, and J. E. Walker, “The nuclear encoded subunits of complex I from bovine heart mitochondria,” *Biochim. Biophys. Acta - Bioenerg.*, vol. 1604, no. 3, pp. 135–150, 2003.

[495] H. K. Anandatheerthavarada and L. Devi, “Amyloid precursor protein and mitochondrial dysfunction in Alzheimer’s disease,” *Neuroscientist*, vol. 13, no. 6, pp. 626–638, 2007.

[496] J. Pozueta, R. Lefort, and M. L. Shelanski, “Synaptic changes in Alzheimer’s disease and its models,” *Neuroscience*, vol. 251, pp. 51–65, 2013.

[497] J. Han *et al.*, “Alzheimer’s disease-causing presenilin-1 mutations have deleterious effects on mitochondrial function,” *Theranostics*, vol. 11, no. 18, pp. 8855–8873, 2021.

[498] M. Obulesu and M. J. Lakshmi, “Apoptosis in Alzheimer’s Disease: An Understanding of the Physiology, Pathology and Therapeutic Avenues,” *Neurochem. Res.*, vol. 39, no. 12, pp. 2301–2312, 2014.

[499] J. Hirst, “Mitochondrial complex i,” *Annu. Rev. Biochem.*, vol. 82, pp. 551–575, 2013.

[500] A. Bogorodskiy *et al.*, “Neurodegenerative and Cardiovascular Diseases,” *Cells*, pp. 1–22, 2021.

[501] W. K. Gottschalk *et al.*, “Journal of Parkinson’s disease & Alzheimer’s disease,” *J. Park. Dis. Alzheimer’s Dis.*, vol. 1, no. 1, pp. 1–25, 2014.

[502] Raquel García-Vilchez; Ana Sevilla; Sandra Blanco, “Post-transcriptional regulation by cytosine-5 methylation of RNA.” Biochimica et Biophysica Acta (BBA) - Gene Regulatory Mechanisms, pp. 240–252, 2019.

[503] M. Chol *et al.*, “The mitochondrial DNA G13513A MELAS mutation in the NADH dehydrogenase 5 gene is a frequent cause of Leigh-like syndrome with isolated complex I deficiency,” *J. Med. Genet.*, vol. 40, no. 3, pp. 188–191, 2003.

[504] P. Cardol, L. Boutaffala, S. Memmi, B. Devreese, R. F. Matagne, and C. Remacle, “In Chlamydomonas, the loss of ND5 subunit prevents the assembly of whole mitochondrial complex I and leads to the formation of a low abundant 700 kDa subcomplex,” *Biochim. Biophys. Acta - Bioenerg.*, vol. 1777, no. 4, pp. 388–396, 2008.

[505] E. Nakamaru-Ogiso, M. C. Kao, H. Chen, S. C. Sinha, T. Yagi, and T. Ohnishi, “The membrane subunit NuoL(ND5) is involved in the indirect proton pumping mechanism of Escherichia coli complex I,” *J. Biol. Chem.*, vol. 285, no. 50, pp. 39070–39078, 2010.

Figures and Tables

All figures were created with biorender.com (premium account including publication license).

Nomenclature

Table 6.1: List of Abbreviations used in this thesis.

Abbreviation	Description	Further information
ND5	NADH-Dehydrogenase subunit 5	NADH-Ubiquinone Oxidoreductase Chain 5
RNA	Ribonucleic acid	
mRNA	Messenger RNA	
tRNA	Transfer RNA	
(mt)tRNA	Mitochondrial tRNA	
(mt)mRNA	Mitochondrial mRNA	
rRNA	Ribosomal RNA	
m^1A	N^1-methyladenosine	In this work, m^1A always refers to RNA modification (not DNA).
AD	Alzheimer‘s Disease	
Aβ	Amyloid β	
TRMT10C	tRNA Methyltransferase 10 homolog C	MRPP1; RG9MTD1
SDR5C1	Short Chain Dehydrogenase/ Reductase Family 5C, Member 1	MRPP2; ERAB; ABAD; HSD17B10; MHBD; HADH2
PRORP	Protein Only RNase P Catalytic subunit	MRPP3; KIAA0391
mtRNase P	Mitochondrial RNase P	
ATP	Adenosine triphosphate	
NADH	Nicotinamide adenine dinucleotide	
ROS	Reactive Oxygen Species	
SNP	Single Nucleotide Polymorphism	
RNA-Seq	RNA sequencing	
scRNA-Seq	Single-cell RNA sequencing	
HEK	Human Embryonic Kidney cells	
APP	Amyloid Precursor Protein	
APPwt	HEK 293, stabily transfected with a plasmid coding for the human wild-type APP gene	
APPsw	HEK 293, stabily transfected with a plasmid coding for the human APP gene including the Swedish (K670M/N671L) mutation	
Ctl	Respective control	
DMEM	Dulbecco’s Modified Eagle’s Medium	
FCS	Fetal Calf Serum	
TetR	Tetracycline Repressor protein	
$TetO_2$	2x Tet operator binding sequence	
pTRMT10C	T-Rex™ cells, stabily transfected with a plasmid coding for TRMT10C (tetracycline-inducable expression)	
FAD	Familial Alzheimer’s Disease	

LOAD	Late-onset Alzheimer's Disease	
Wt	Wild type	
TBI	Traumatic Brain Injury	
FPKM	Fragments per kilobase per million mapped fragments	
FC	Fold Change	
padj.	Adjusted p-value	
NCBI	National Center for Biotechnology Information	
SRA	Sequence Read Archive	
NBB	Netherlands Brain Bank	
CERAD	Consortium to Establish a Registry for Alzheimer's Disease	
SD	Standard Deviation	
SEM	Standard Error of the Mean	
n.s.	Not significant	
p-value	Probability value	
PBS	Phosphate buffered saline	
WB	Western Blot	
RIPA	Radio-immunoprecipitation Assay buffer	
SDS	Sodium Dodecyl Sulfate	
PMSF	Phenylmethylsulfonylfluorid	
BSA	Bovine Serum Albumin	
TBST	Tris buffered saline with Tween®	
L	Liter	
mL	Milliliter	
µL	Microliter	
µg	Microgram	
µM	Micromolar	
GAPDH	Glyceraldehyde-3-Phosphate Dehydrogenase	
IB	Isolation Buffer	
EGTA	Ethylene glycol-bis(2-aminoethylether)-N,N,N′,N′-tetraacetic acid	
g	Gravitational force	
min	Minutes	
DTT	Dithiothreitol	
SS-IV	SuperScript™ IV	
RT	Reverse Transcription/ Reverse Transcriptase	
PCR	Polymerase Chain Reaction	
DNA	Deoxyribonucleic acid	
mtDNA	Mitochondrial DNA	
cDNA	Complementary DNA	
BAM	Binary Alignment Map	
PAGE	Polyacrylamide Gel Electrophoresis	
h	Hours	
oligo	Oligonucleotide	
FAM	Fluorescein amidite	
TMRM	Tetramethylrhodamine methyl ester	

CO_2	Carbon dioxide	
FCCP	Carbonyl cyanide-p-trifluoromethoxyphenylhydrazone	
OCR	Oxygen Consumption Rate	
MMP	Mitochondrial Membrane Potential	
ETS	Electron Transport System	
Tetra	Tetracycline	
LS	Leigh-Syndrome	
LHON	Leber's hereditary optic neuropathy	
MELAS	Mitochondrial encephalomyopathy, lactic acidosis and strokelike episodes	
RRF	Ragged-red fibres	
yW	Wybutosine	
Q	Queuosine	
m^5C	5-methylcytidine	
m^6A	6-methyladenosine	
Am	2'-O-methyladenosine	
s^4U	4-thiouridine	
m^7G	7-methylguanosine	
W	Watt	

List of Publications

Curriculum Vitae